学位申請論文

後藤忠徳

Study on the Electrical Resistivity Structure around the Seismogenic Zone in the Crust

By Tadanori Goto

Kyoto University

Mar., 1997

Abstract

We studied the electrical resistivity structure around the seismogenic zone in the upper crust to identify the relationship between the resistivity structure and the seismicity. We carried out the magnetotelluric soundings at two different seismogenic regions in Japan. One is the Atotsugawa region, central Japan, where a lot of micro-earthquakes have actively occurred along the Atotsugawa fault. Additionally, as compared with the other areas along the fault, the central part of the Atotsugawa fault shows low seismicity, possibly where the 1858 Hida earthquake(M7.0) occurred. Another is the Ebino region on the foot of the Kirishima volcanoes, Kyushu district, Japan. The 1968 Ebino earthquake swarm including the largest earthquake with M6.1 occurred in this region. The resistivity structure may give us important information on physical property around the seismogenic zone in association with the occurrence of the earthquakes in these regions.

Before constructing the resistivity model, the directions of strike of the resistivity structure at each site were precisely determined to eliminate the local effect of the resistivity anomaly very near the surface which is called the galvanic distortion. Then, the two-dimensional models of the resistivity were constructed around each surveying area with the inverse method. The effect of the near-surface resistivity anomaly, called the static shift, was also corrected through the inverse process.

In the Atotsugawa region, a clearly different structure between the low-seismicity and the high-seismicity part along the fault is found. A resistive layer more than 2000 Ω m is widely spread beneath the low-seismicity part, underlain at 3-7 km in depth beneath the moderately conductive surface. A conductive layer also underlies broadly beneath 10 km in depth. On the other hand, there is no horizontally spreading resistive layer beneath the high-seismicity part. But the fault makes a boundary between a northern resistive zone and a southern conductive zone, although this southern zone shows a relatively higher resistivity than that of the low-seismicity part of the fault.

To explain both the features of the resistivity structure and the heterogeneity of the seismicity along the Atotsugawa fault, we consider that the existence of fluid is probably concerned with the occurrence of the earthquakes. Beneath the western part of the Atotsugawa fault, fluid may upwell from the deep interior of the crust through the fault, and may cause the high-seismicity and the relatively resistive lower crust. On the other hand, upwelling fluid may be trapped beneath the resistive layer across the central part of the Atotsugawa fault, causing the conductive lower crust and the low-seismicity along the fault.

In the Ebino region, the hypocentral area of the 1968 Ebino earthquake swarm was recognized as a highly resistive zone. This result is not harmony with the previous studies in which it has been pointed out that the seismically active zone is often found in the low resistivity zone. We consider that the supply of fluid into the seismogenic zone was stopped already.

Acknowledgments

The author is deeply grateful to Professor N. Sumitomo for his continuous advice and encouragement throughout this investigation. Special acknowledgment goes to Dr. N. Oshiman for his valuable suggestions and critical reading of this manuscript.

The author thanks Drs. Y. Tanaka and T. Iemori for their valuable comments. He also thanks Drs. K. Ito and K. Watanabe for the valuable discussion on the seismicity around the survey area. He is also grateful to Drs. H. Utada, Y. Sasai and T. Kagiyama of Earthquake Research Institute, Univ. of Tokyo for their valuable discussion. He also thanks to Drs. S. Yamaguchi of Kobe Univ. and I. Shiozaki of Tottori Univ. for their valuable comments. The Research Group for Crustal Resistivity Structure (RGCRS) kindly allows him to use the MT data in the Ebino region. The author's special acknowledgment goes to RGCRS. He also thanks to Drs. T. Uchida and Y. Ogawa of Geological Survey of Japan for providing their inversion code for MT data.

The author greatly thanks Messrs. H. Wada and Y. Wada for their kind assists for the field work in the Atotsugawa region. In addition, the author wishes to express his sincere thanks to Messrs. S. Sakanaka, M. Ichiki, T. Kasaya, K. Tanimoto, Y. Kobayashi, F. Hori, M. Amita, Shimoyama and Mses. Y. Hori and K. Goto for their great assists for the field work in the Atotsugawa region.

Contents

1. Introduction

The purposes of this study are first to investigate the resistivity structure around the seismogenic zone in the crust, secondly to confirm the relationship between the resistivity structure and the seismicity, and finally to constrain the major cause of the occurrence of earthquakes. In this chapter, we briefly review the previous studies concerning the relationship between the resistivity structure and the seismogenic zone in the crust .

The electrical conductivity or the resistivity, which is reciprocal of conductivity, is one of the important parameters for investigations of the earth 's interior because the resistivity is strongly affected by the temperature (Kariya and Shankland, 1983), pore fluid in rocks(e.g. Olhoeft, 1981), partial melting (Waff, 1974) and rock composition. Among them, the effect of pore fluid on conductivity is significant. The relation between conductivity and porosity is expressed by the Archie's law (Archie, 1942) which is often an appropriate first - order model for the total conductivity of a medium:

$$\sigma_m = \sigma_f \eta^m$$

where σ_m and σ_f are the conductivity of the bulk medium and of the fluid included in pores respectively, and η is the porosity. The value of m is experimentally determined between 1 and 2. Thus, one of the important factors controlling the bulk resistivity is the resistivity and the content of fluid. The resistivity is highly sensitive to very small changes in such minor constituents of the rocks. In addition, the resistivity in the crust varies over 7 order of the magnitude. Some examples of the resistivity for typical rocks are indicated in Fig. 1-1 after Haak and Hutton(1986). This magnitude range is the widest of any physical parameters in the earth's interior and enable us to

analyze the deep resistivity structure of the earth's crust, although the electromagnetic field is basically diffusive and the resolution of the resistivity structure decreases toward deeper parts in the crust.

The resistivity structure of the crust may produce important information of the causes of the earthquakes because the resistivity is sensitive the state of water or temperature, or both, that have crucial effects on controlling the mechanical property on rocks. In recent several decades, the electromagnetic (EM) surveys have revealed the resistivity structure in the crust. Many researchers have adopted the DC resistivity sounding, the magnetotelluric (MT) sounding, the geomagnetic depth sounding (GDS) and so on to identify the resistivity structure. And the resistivity structure in the seismogenic zone have been studied since 1980's in the world. In Japan, Electromagnetic Research Group for the Active Fault (ERGAF) investigated the resistivity structure around active faults (ERGAF, 1982, 1983; Yukutake, 1985) using DC resistivity measurements and MT soundings. The sounding depth of those DC and MT soundings were limited to only a few km, however, they found that remarkably low resistivity zones often accompany the active fault. One of the results is indicated in Handa and Sumitomo(1985) as shown in Fig. 1-2. They studied the Yamasaki fault and the Hanaori fault, those of the most active faults in Japan, using the ELF-MT soundings. They found the low resistivity zone developing in the width of about 1-2km along these faults and the resistivity is smaller in magnitude by one order than the surrounding area. They concluded that the low resistivity zone is possibly due to existence of water involved in the fracture zones which were formed by fault movements. ERGAF(1983) also suggested that a width of the low resistivity zone will represent an activity of the active fault. Recently, Ogawa (1994) reported that the remarkably conductive anomaly ($< 1\,\Omega\,m$) exists at 500m in depth below the Kita-Izu fault system which may correspond to a fracture

zone.

Similar low resistivity zones along active faults were also recognized in other countries. Pous et al.(1995) derived the resistivity structure image around the North Pyrenean zone on the basis of the wide-band MT soundings. They found the low resistivity zone penetrating from the surface to a depth of 20km along the major fault zones. Jones et al. (1992) carried out the MT soundings across the Fraser River fault. They inferred the existence of the narrow low resistivity zone with a width of about a few km beneath the Fraser River fault. Jones et al.(1992) found the low $\delta\ ^{13}C$ along the Fraser River fault and concluded that the low resistivity zone is due to organic carbon or graphite formed by the upwelling of water deeply penetrating in the fault zone. It is important, anyway, that fluid in the fracture zone possibly relates to the fault activity.

Late in the 1980's, the electromagnetic soundings have revealed large-scale resistivity structures including the seismogenic depth. The preliminary result in Japan was reported in Research Group for Crustal Resistivity Structure (RGCRS,1983). RGCRS(1983) carried out MT soundings across the northern Honsyu and estimated the one-dimensional resistivity structure (Fig. 1-3). They found that a low resistivity layer of 60 Ω m underlies a resistive layer. The depth to this low resistivity layer was estimated to be 18km , which coincided with the depth of the Conrad discontinuity determined by the seismic refraction experiments(Yoshii and Asano, 1972). Takagi et al.(1977) showed that the earthquakes mostly occur in the upper crust and very few in the lower crust. In this case, the conductive lower crust is characterized by low seismic activity. Such feature of the lower crust is often observed. Utada(1987) identified some typical characteristics of the large-scale conductivity structure in the subduction zone across the northeast

and the central Japan using the two-dimensional direct inversion. The resistivity models proposed by Utada(1987) are shown in Fig. 1-4. He pointed out the existence of the lower crustal conductor beneath central Japan. Such a high conductive lower crust also has been found in many regions over the world (Jones , 1987; 1992). For example, beneath the Vancouver island, Canada, Kurtz et al.(1986) indicated a highly conductive zone at the depth of about 20-30km. The other example is found in the northern Europe (Korja et al., 1989). Since the earthquakes in the earth's crust have been found to occur mainly in the depth shallower than 15-20km, although the cutoff depth varies regionally (Sibson, 1984), it is recognized basically that the upper crust is electrically resistive and seismically active and responds to stress elastically with brittle fractures, and that the lower crust is conductive and aseismic and shows ductile response to stress (see Fig.1-5).

It is noteworthy that these lower crust conductors are often accompanied with seismic reflectors (Jones, 1987). In the case of the Vancouver island, Green et al.(1980) revealed strong acoustic reflections from the corresponding depth of the high conductive zone. The conductive layer found in northern Europe by Korja et al.(1989) also accompanies the seismic reflector (Behrens et al., 1989). Kurtz et al.(1986) suggested that such conductive layer could be interpreted by trapped saline fluids in a rock matrix of porosity 1.6 - 3.6%. Similarly, Gough (1986) explained these characteristics by saline water, which is interconnected as film-like shape in the lower crust. Thus, the correspondence between the conductive zone and the seismic reflectors in the lower crust is generally found in many regions and is characterized by the existence of fluid in the lower crust(Jones, 1987). In contrast there exist some exceptions. Jiracek et al.(1983, 1987) carried out the EM surveys in the Rio Grande rift. They found that the conductive zone

below 10km depth in Rio Grande rift exists. However, they reported that this conductor was not found in the other area along this rift where many micro-earthquakes occurred and strong seismic reflectors were found. They presented the hypothesis that the ductile cap overlies the conductive zone to trap water, but this cap may be disturbed by magma injection possibly corresponding to the seismogenic zone and reflectors, and release water. Anyway, the existence of fluid in the lower crust is significant to consider the difference between the brittle upper crust and the ductile lower crust.

The spatial distributions of the seismicity in the upper crust is not laterally uniform but heterogeneous in general. As the case of the correspondence is recognized between the conductive layer and low seismicity in the lower crust, the resistivity structure in the upper crust will also give valuable information or constrains on mechanical properties of rocks. Recently, in 1990's, many studies on the relationship of the resistivity structure and the seismicity have been presented. Most of these studies were based on the broad-band MT measurements. In Japan, Shiozaki (1993) studied the two-dimensional resistivity structure across the Shikoku district (Fig. 1-6). He found that a large zone of low resistivity in the upper crust extending from the depth of the nearly surface to about 20km. Shiozaki (1993) concluded that this conductive zone is characterized by low seismicity. Fujita (1994) investigated the two-dimensional resistivity structure across the Kii peninsula(Fig. 1-7). He concluded that the low resistivity body extends in the middle crust from a few km to 20km in depth, which coincides with the aseismic zone. He suggested that the low resistivity body may be due to the accretionary metamorphic sediments. These studies show the correlation between the low resistivity and the aseismic zone. On the other hand, Ogawa et al.(1994) constructed the two-dimensional resistivity model around the Hidaka mountains, Hokkaido(Fig.1-8). He found

the low resistivity zone at the depth ranging from 5km to about 20km beneath the Hidaka main thrust where micro-earthquakes occurred. He concluded that the low resistivity zone might comprise a trapped sedimentary block by the ancient plate motion. Kanda et al.(1996) studied the low resistivity zone in the northern part of Miyagi prefecture, Northeastern Japan where seismic activity is very high. They carried out the time domain electro-magnetic (TDEM) experiment and constructed 1-dimensional resistivity models at each site. They revealed the correlation between the low resistivity layer and the high seismicity zone. In the same area as Kanda et al.(1996) studied, Ichiki et al.(1997) constructed 2-dimensional resistivity model by using MT sounding data(Fig. 1-9). They found a similar correlation to that is pointed out by Kanda(1996). Additionally, they reported that the resistive layer overlies the seismic zone. Yamaguchi(1996, pers. comm.) found that micro-earthquakes concentrates in low resistivity regions in the west side of the Hanaori fault, Kinki district. Those results imply that the low resistivity relates to the high seismicity zone. In Canada, Kurtz et al.(1992) investigated the resistivity structure around the Miramichi earthquake zone in north-central New Brunswick where four earthquakes occurred in 1982 with magnitudes ranging from 5.0 to 5.7. They carried out the MT measurement and found that the crustal resistivity in the Miramichi earthquake zone is considerably high as compared with those in other regions in eastern North America. However, the high value is typical for the Precambrian Shield and they concluded that the resistivity structure directly associated with the Miramichi earthquakes was unable to be identified. In US, Eberhart-Phillips et al.(1990) reported the preliminary 2-dimensional resistivity model and 3-dimensional seismic velocity model of the Loma Prieta earthquake region near the San Andreas fault (Fig. 1-10). They identified that the main shock and most of after shocks of the Loma Prieta earthquakes in 1989 occurred in the high-resistivity and high-velocity zone sandwiched between the San Andreas fault

and the Sargent fault. In India, Gupta et al.(1996) conducted geophysical measurements on the hypocentral zone of the Latur earthquake, 1993. They constructed 1-dimensional resistivity models at each site and concluded that the low resistivity layer, corresponding to the low velocity zone, underlies the focal region.

Thus, the relationship between the resistivity structure and the seismic activity in the upper crust is very complicated. However, in some of those resistivity model, the static effects(Jones, 1988) was not considered well, which distorts the obtained model illegally. Moreover, the sensitivity and the resolution of the model were not presented in those models. Additionally, these studies were based on the only one profile of the EM survey and did not enable us to make an enough comparison between the constructed resistivity model and the horizontally heterogeneous seismicity. So, in order to identify the detailed relationship between the resistivity structure and the seismicity, it becomes essential to investigate the resistivity structure in various regions and to get enough sounding depth up to the seismogenic area where the seismic activity and other geophysical characteristics are well studied.

By the way, there are many causes controlling occurrences of earthquakes. Sibson (1984) pointed out that the factors affecting the cutoff depth of the earthquakes are so many as crustal composition, geometry and mode of faulting, fluid pressure, water content, strain rate and geothermal gradient. In particular, Ito (1993) pointed out that the thermal structure of the crust strongly controls the cutoff depth. On the other hand, recently, much interest have been focused on the upwelling of the fluid from a deep interior of the Earth's crust as one of the causes of the occurrence of the earthquakes. It has been argued as one of seismogenic models that fluid makes an important role in the occurrence of earthquakes (Sibson et al.,1988 ; Rice,

1992 ; Byerlee, 1990, Blanpied et al., 1992). The basic concept is the reduction of the frictional strength of the fault by the highly pressurized fluid. If the frictional strength of the fault may be approximated by Coulomb-Mohr criterion, the increase of the fluid pressure decreases the frictional strength and make the fault to be "weaken". Sibson et al.(1988) suggested that the overpressured fluid below the seismogenic zone is expelled upward through the fault zone during the process of an earthquake rupture as shown in Fig.1-11. Rice's (1992) model was considered of the San Andreas fault in which a high fluid pressure has taken into consideration in the fault zone. Byerlee (1990) noted that pore pressure gradient has a threshold under which zero flow of fluid is provided. In Byerlee's model, both the source under the fault zone and the continual replenishment of the overpressured fluid is not required. Basing upon the experimental results, Blanpied et al. (1992) proposed the compaction creep which yields the rapid sealing of the faults and produces high pore pressure. The large deep fluid source is not required in the Blanpied 's model.

In addition, some notable phenomena have been so far observed to support the significance of the pressurized fluid which is responsible for the occurrence of earthquakes. One is the artificially induced earthquake of which occurrences are controlled with the water injection at Rangely, Colorado(Raleigh et al, 1976) and the reservoir induced seismicity(Simpson et al., 1988). The other is observed as the natural earthquake swarms. In the Matsuhiro earthquake swarm which occurred in 1965 in central Japan, a large amount of fluid eruption was observed on the surface. The source of this fluid is inferred as that arose from in the deep interior of the crust on the basis of the $^{4}He/^{3}He$ ratio (Wakita et al., 1978). The time variation of the geomagnetic total force preceded the Matsushiro earthquake swarm is considered to be caused by the upwelling of a large amount of fluid from the

lower crust (Sasai, 1994). In addition, the spreading of the several earthquake swarms infers a correlation between earthquake swarms and fluid(e.g. Tanaka, 1990).

If fluid is concerned with a seismogenic zone along faults or a hypocentral zone of an earthquake swarm, then the resistivity should be low there. Therefore, the resistivity structure produces important information on the occurrence of the earthquakes, especially the relationship between the seismogenic zone and the fluid. However, the knowledge of deep resistivity structures of the fault is a very few, and the detailed resistivity structure around the hypocentral area of the earthquake swarm have not been made clear. So, in this thesis, we studied about the resistivity structure around the seismogenic zone in two different seismogenic regions. One is the Atotsugawa region, located in the northern Gifu prefecture, central Japan. The Atotsugawa fault is one of the most active fault in Japan, where the high seismic activity is recognized. The heterogeneity of the seismicity was clearly recognized along the Atotsugawa fault (Mikumo et al., 1988; Wada et al., 1995; 1996) We selected two profiles of the MT soundings to cross sections of the fault where the seismicity is different from each other. Another area studied in the thesis is the Ebino region located on the foot of the Kirishima Volcanoes, in the southern Kyushu, Japan. In this area, the Ebino earthquake swarm , accompanied with the largest one of M6.1, occurred in 1968 -1969. We took four profiles near and away from the region where epicenters of the Ebino earthquake swarm concentrated. In this thesis, we construct the two-dimensional resistivity models along these profiles. After that, we interpret the resistivity structures and discuss the relationship between those structures and the seismicity around two regions, respectively. Finally, we propose a probably significant factor to consider the occurrence of the earthquakes.

Fig. 1-1 An example of the resistivity for several kind of rocks (after Haak and Hutton, 1986)

Fig. 1-2 The resistivity structure across the Yamasaki fault obtained by Handa and Sumitomo(1985)

Fig. 1-3 (a) The distribution of the earthquakes in the northern Honsyu together with the seismic velocity structure(after Takagi et al., 1977)

(b) The preliminary result of the resistivity structure across the northern Honsyu (Research Group for Crustal Resistivity Structure ,1983). RGCRS carried out MT soundings and estimated the 1-dimensional resistivity structure.

Fig. 1-4 The conductivity structure across the northeast and the central Japan by Utada(1987)

Fig. 1-5 Schematic model for the crust presented by Gough (1986) . UC and LC means the upper crust and the lower crust. Shaded zone implies the existence of fluid.

Fig. 1-6 The two-dimensional resistivity structure across the Shikoku district obtained by Shiozaki (1993)

Fig. 1-7(Upper) The two-dimensional resistivity structure across the Kii obtained by Fujita (1994)

Fig. 1-8(Lower) The two-dimensional resistivity model around the Hidaka mountains, Hokkaido(Ogawa et al., 1994)

Fig. 1-9 The two-dimensional resistivity model in the northern part of Miyagi prefecture, Northeastern Japan (after Ichiki et al., 1997)

Fig. 1-10(Upper) The preliminary two-dimensional resistivity model of the Loma Prieta earthquake region near the San Andreas fault (Eberhart-Phillips et al.,1990)

Fig. 1-11(Lower) The seismogenic model presented by Sibson et al.(1988)

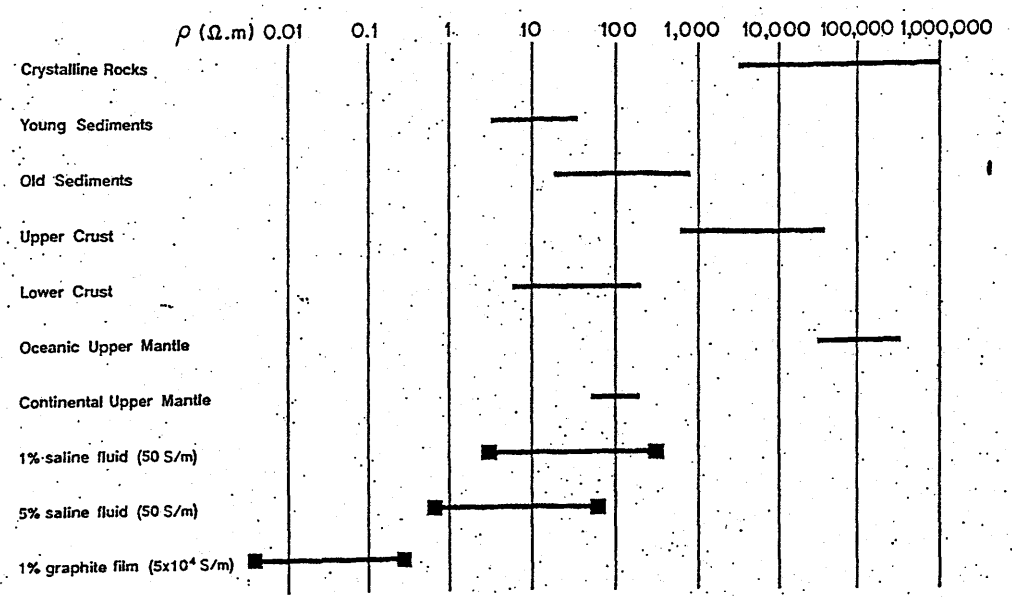
ρ (Ω.m) 0.01
0.1
1
10
100
1,000
10,000
100,000
1,000,000
Crystalline Rocks
Young Sediments
Old Sediments
Upper Crust
Lower Crust
Oceanic Upper Mantle
Continental Upper Mantle
1% saline fluid (50 S/m)
5% saline fluid (50 S/m)
1% graphite film (5x10⁴ S/m)

Fig. 1-1

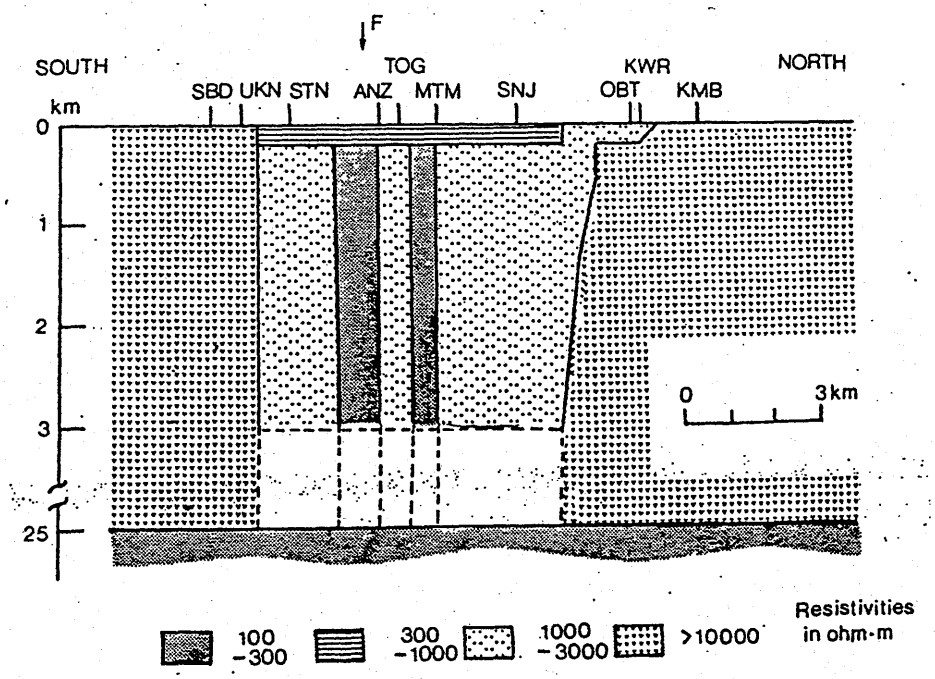
F
SOUTH
NORTH
SBD
UKN
STN
TOG
ANZ
MTM
SNJ
KWR
OBT
KMB
km
0
1
2
3
25
0
3km
100
-300
300
-1000
1000
-3000
>10000
Resistivities
in ohm-m

Fig. 1-2

(a)

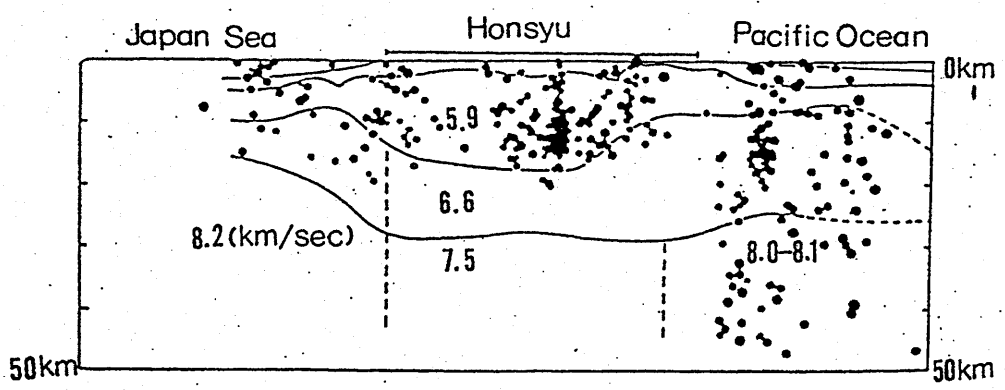
Japan Sea
Honsyu
Pacific Ocean
0km
5.9
6.6
8.2(km/sec)
7.5
8.0–8.1
50km
50km

(b)

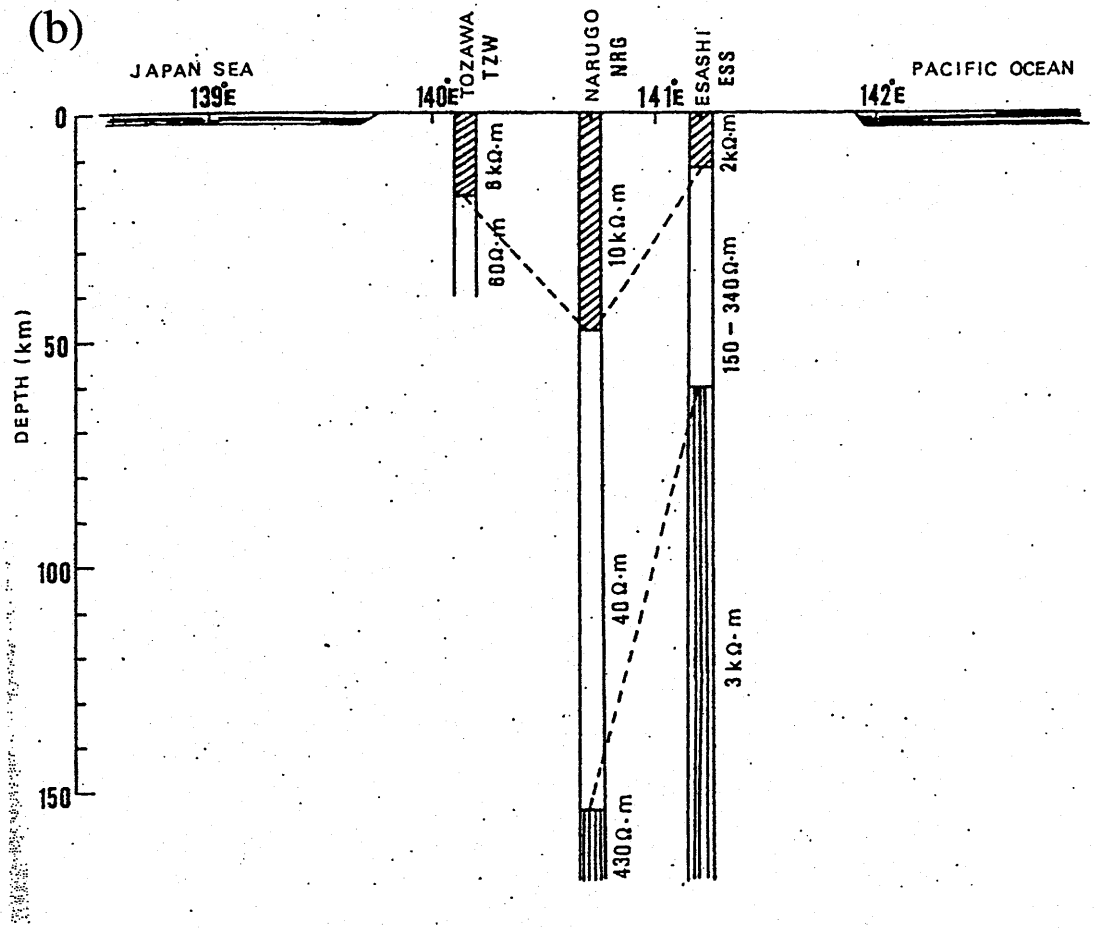
JAPAN SEA
139°E
140°E
TOZAWA
TZW
NARUGO
NRG
141°E
ESASHI
ESS
142°E
PACIFIC OCEAN
DEPTH (km)
0
50
100
150
8kΩ·m
60Ω·m
10kΩ·m
2kΩ·m
150 – 340Ω·m
40Ω·m
3kΩ·m
430Ω·m

Fig. 1-3

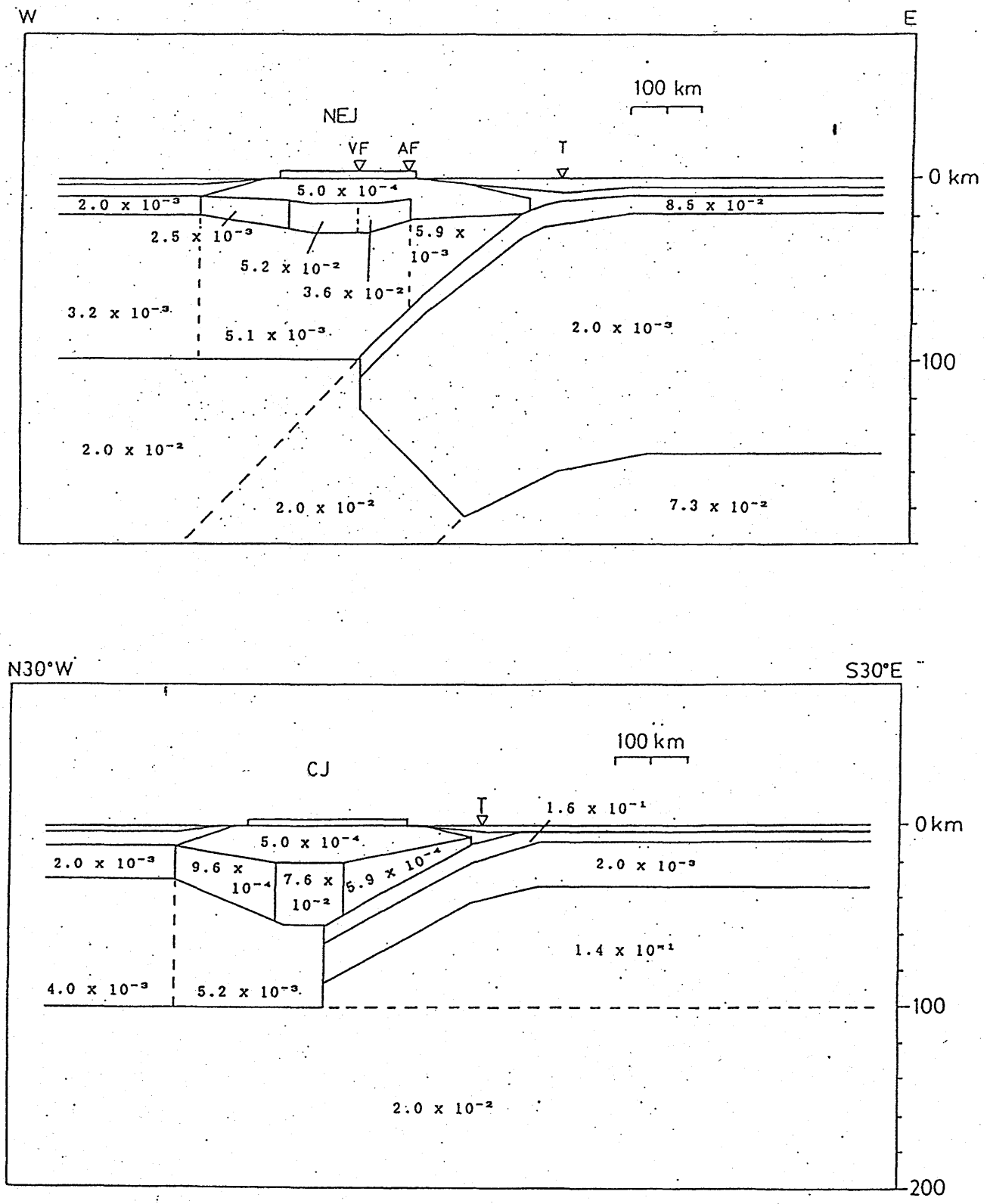
W
E
100 km
NEJ
VF
AF
T
0 km
100
5.0 x 10⁻⁴
2.0 x 10⁻³
2.5 x 10⁻³
5.2 x 10⁻²
3.6 x 10⁻²
5.9 x 10⁻³
8.5 x 10⁻²
3.2 x 10⁻³
5.1 x 10⁻³
2.0 x 10⁻³
2.0 x 10⁻²
2.0 x 10⁻²
7.3 x 10⁻²
N30°W
S30°E
100 km
CJ
T
1.6 x 10⁻¹
0 km
5.0 x 10⁻⁴
2.0 x 10⁻³
9.6 x 10⁻⁴
7.6 x 10⁻²
5.9 x 10⁻⁴
2.0 x 10⁻³
1.4 x 10⁻¹
4.0 x 10⁻³
5.2 x 10⁻³
100
2.0 x 10⁻²
200

Fig. 1-4

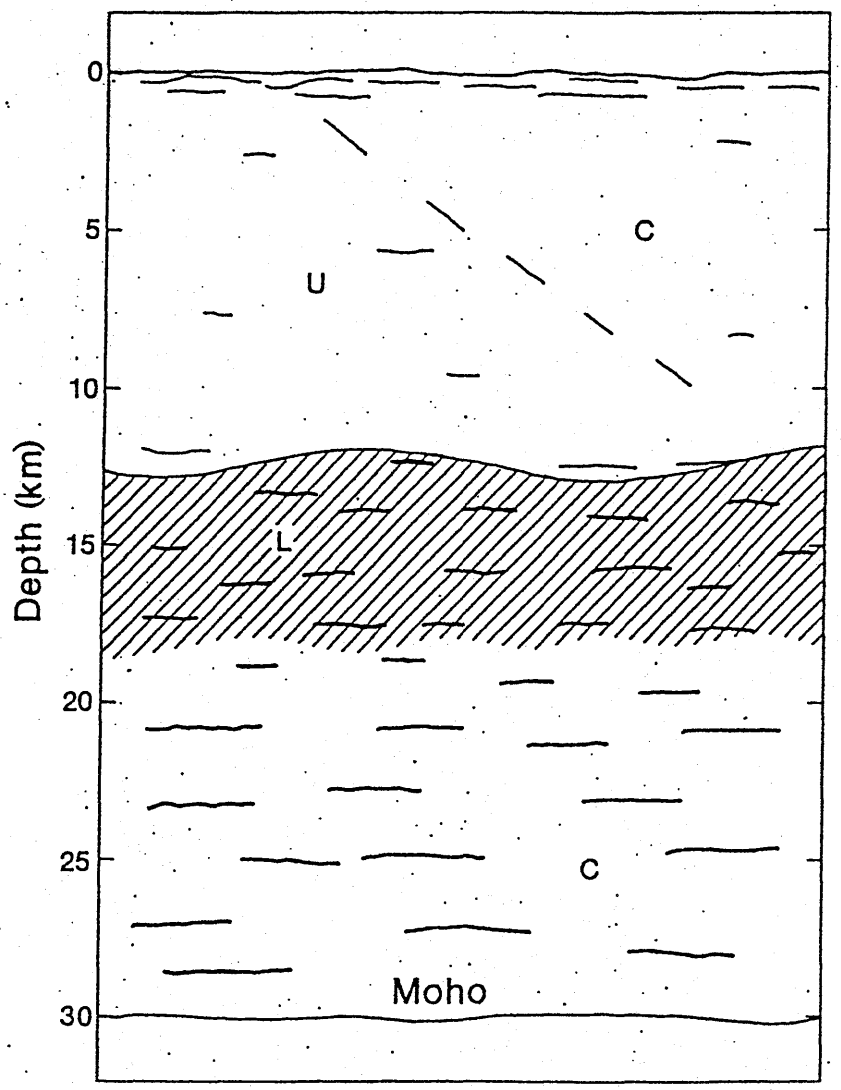

Fig. 1-5

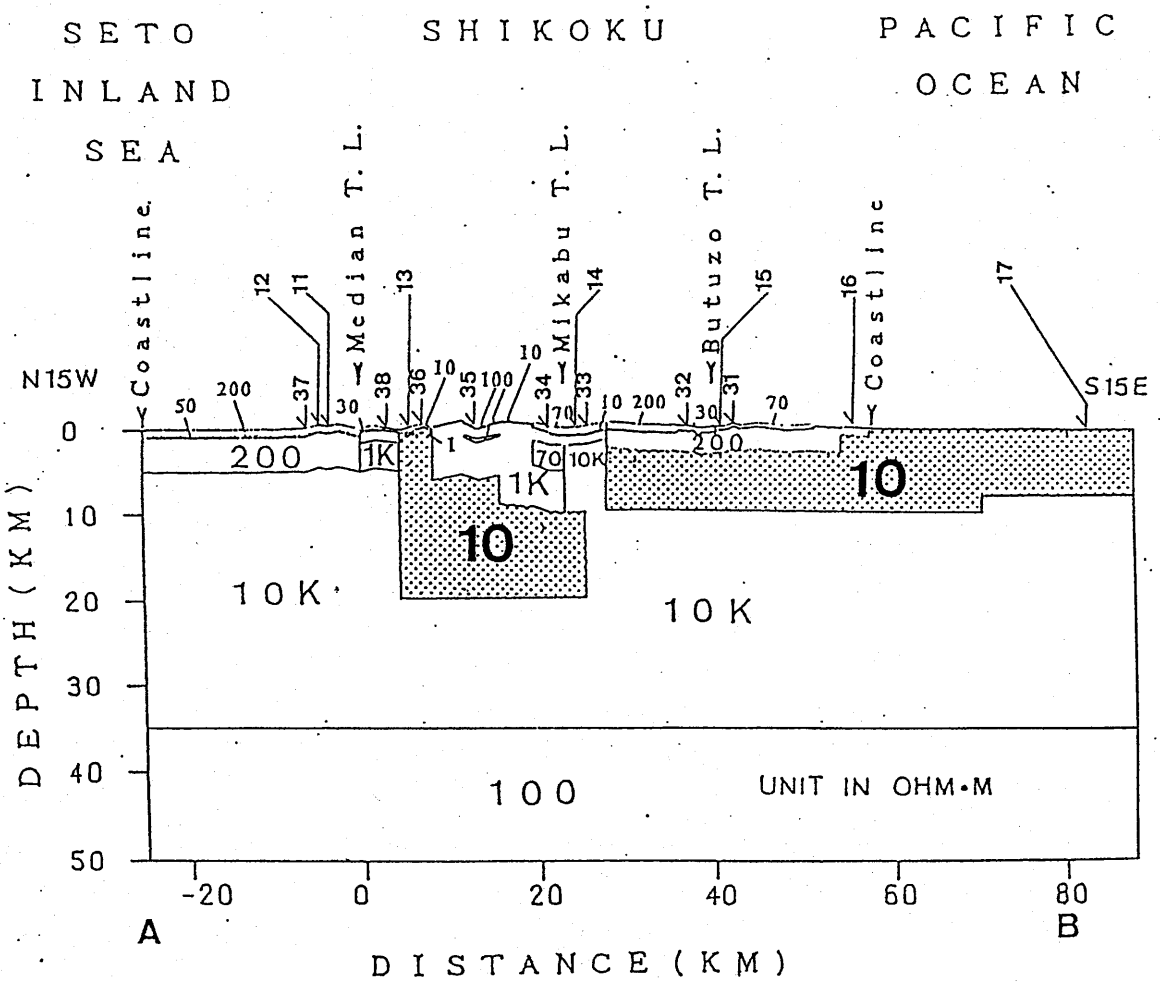
SETO
INLAND
SEA
SHIKOKU
PACIFIC
OCEAN
Coastline
Median T. L.
Mikabu T. L.
Butuzo T. L.
Coastline
N15W
S15E
DEPTH (KM)
DISTANCE (KM)
A
B
200
1K
10
10K
100
UNIT IN OHM•M

Fig. 1-6

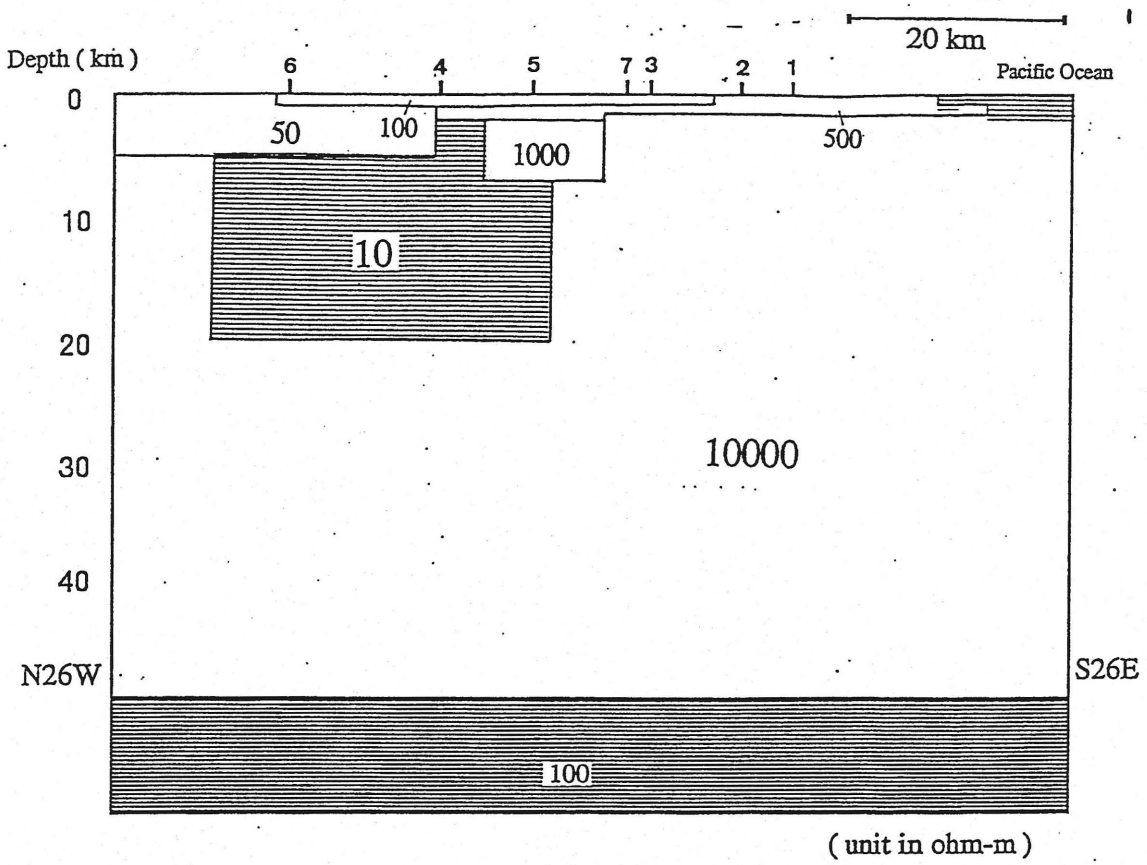
20 km
Depth (km)
6
4
5
7
3
2
1
Pacific Ocean
0
50
100
1000
500
10
20
10000
30
40
N26W
S26E
100
(unit in ohm-m)

Fig. 1-7

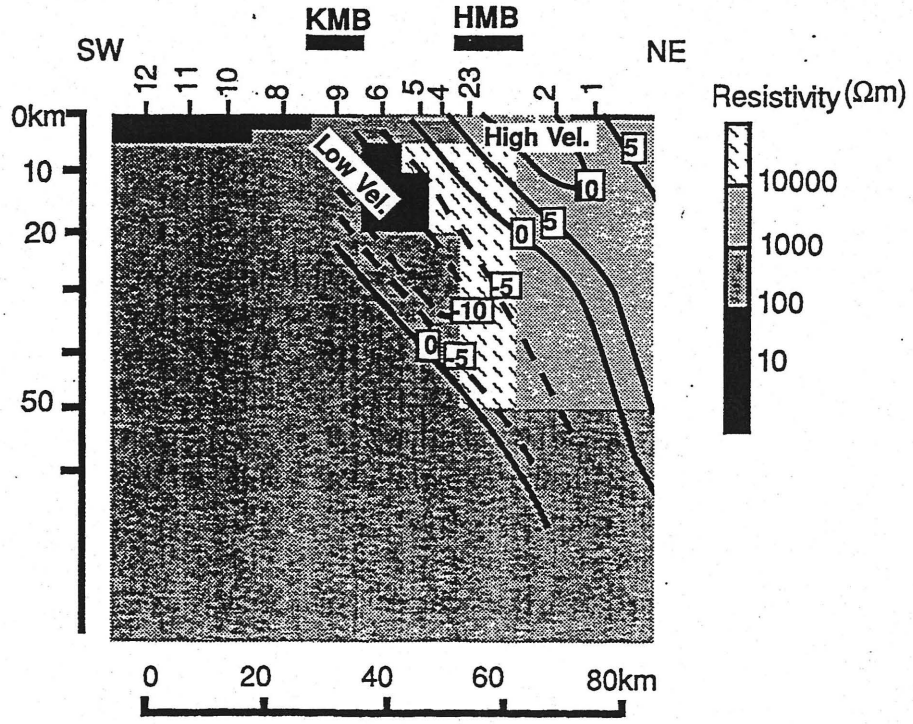
KMB
HMB
SW
NE
12
11
10
8
9
6
5
4
3
2
1
0km
10
20
50
Low Vel.
High Vel.
5
10
0
5
-5
-10
0
-5
Resistivity (Ωm)
10000
1000
100
10
0
20
40
60
80km

Fig. 1-8

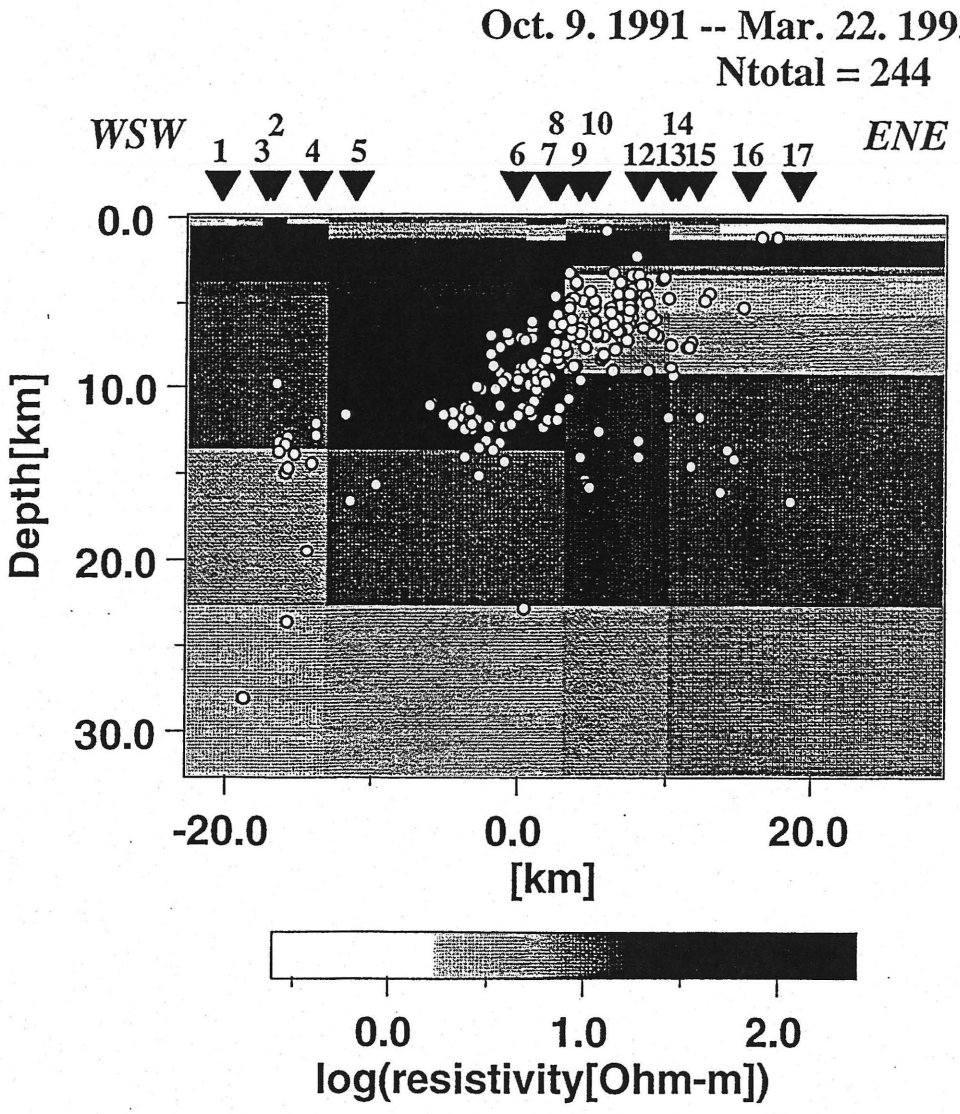
Oct. 9. 1991 -- Mar. 22. 1993
Ntotal = 244
WSW
ENE
1 2 3 4 5 6 7 8 9 10 12 13 14 15 16 17
0.0
10.0
20.0
30.0
Depth[km]
-20.0
0.0
20.0
[km]
0.0
1.0
2.0
log(resistivity[Ohm-m])

Fig. 1-9

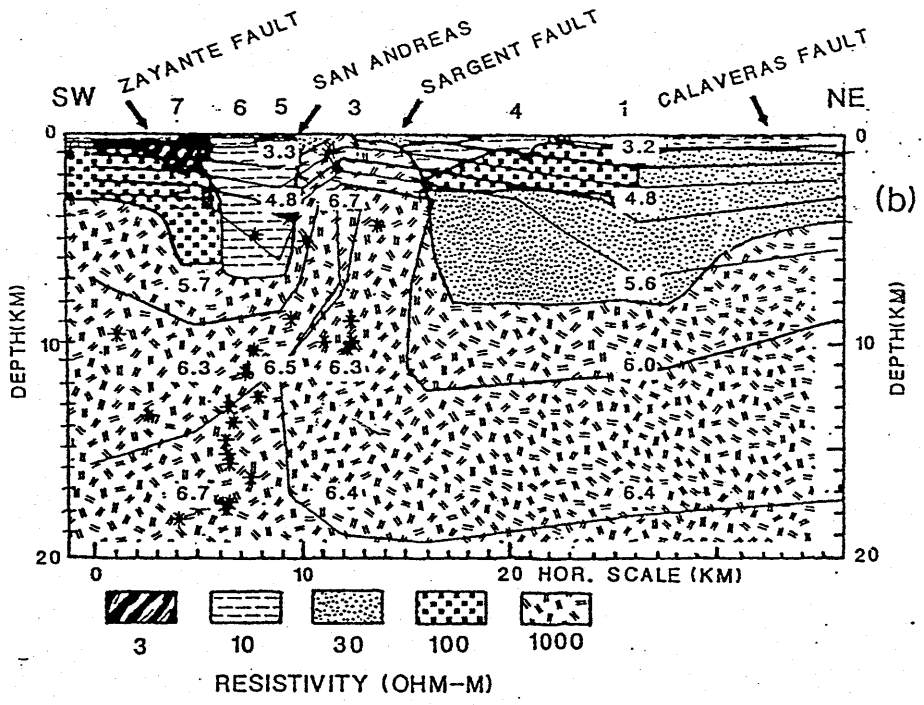

Fig. 1-10

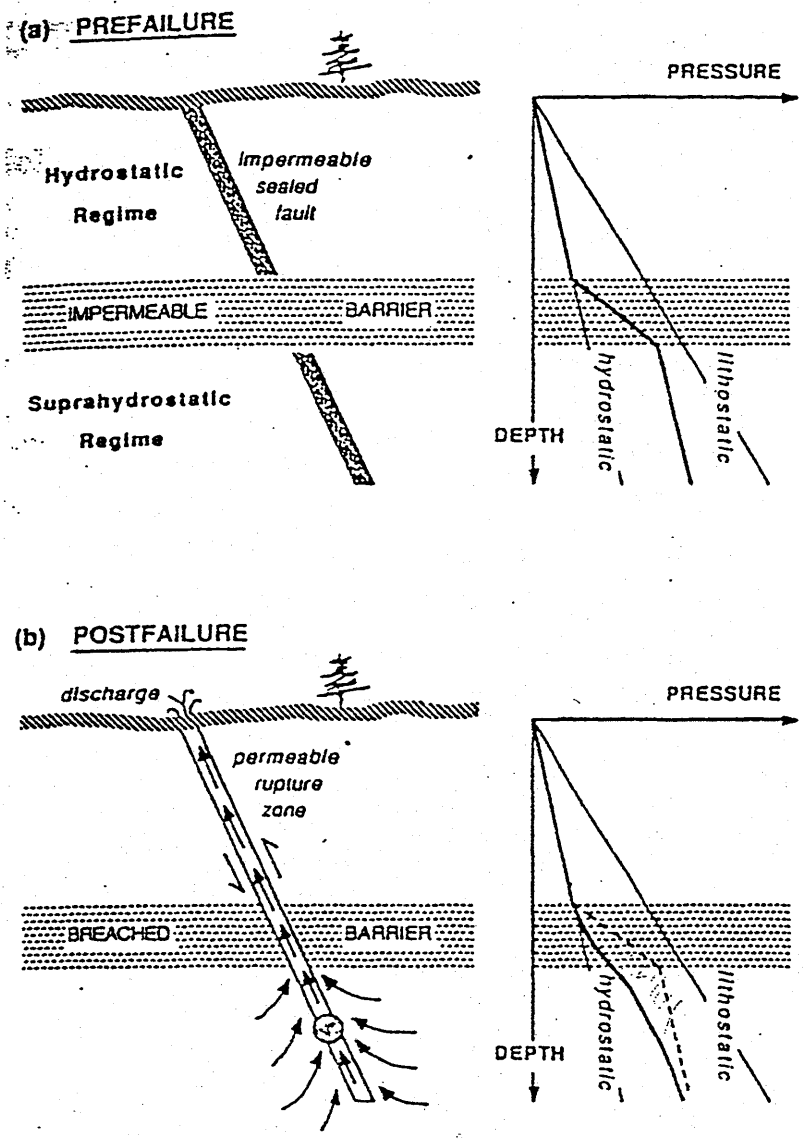

Fig. 1-11

2. Theory

We use the magnetotelluric (MT) method in order to investigate the resistivity structures. The MT method is one of the geophysical surveys which determine the resistivity under the ground by using, in general, the natural fluctuations of the magnetic fields and the induced electric fields within the earth's interior. In the MT method, the relationship between the resistivity(ρ) of the earth's material, and amplitudes of the magnetic and the electric fields (H and E) is expressed in the following equation,

$$\rho \propto \frac{E^2}{H^2}.$$

We review the basic equations of the MT method and the procedures to analyze the resistivity structure in this section. In this chapter, the cordinate axis is taken as shown in Fig. 2-1.

2. 1. Induction equation

Temporal variations of the magnetic field induce the electric current in the ground, which is called the telluric current. The magnetotelluric method uses this natural fluctuations of the magnetic and electric fields, and give us information of the resistivity within the earth's interior. The MT method is based on the Maxwell's equation for the electromagnetic induction as follows.

$$rot\mathbf{E} = -\frac{\partial \mathbf{B}}{\partial t} \qquad (2.1.1)$$

$$rot\mathbf{H} = \mathbf{j} + \frac{\partial \mathbf{D}}{\partial t} \qquad (2.1.2)$$

$$div\mathbf{D} = q \qquad (2.1.3)$$

$$div\mathbf{B} = 0 \qquad (2.1.4)$$

where $\mathbf{E,H,D,B,j}$ and q denote the electric field, the magnetic field, the electric flux density, the magnetic flux density, the current density and the electric charge density. Additionally, following equations are defined;

$$\mathbf{D} = \varepsilon\mathbf{E} \qquad (2.1.5)$$

$$\mathbf{B} = \mu\mathbf{H} \qquad (2.1.6)$$

$$\mathbf{j} = \sigma\mathbf{E} \qquad (2.1.7)$$

where ε, μ and σ are the dielectric constant, the magnetic permeability and the electrical conductivity. The equation (2. 1. 7) is the Ohm's law.

Using above equations and assuming the electric and the magnetic fields vary depending upon the angular frequency ω, equation(2. 1. 1)-(2. 1. 4) are rewritten as

$$rot\mathbf{E} = -i\omega\mu\mathbf{H} \qquad (2.1.8)$$

$$rot\mathbf{H} = \sigma\mathbf{E} + i\omega\varepsilon\mathbf{E} \qquad (2.1.9)$$

$$div\mathbf{E} = \frac{q}{\varepsilon} \qquad (2.1.10)$$

$$div\mathbf{H} = 0. \qquad (2.1.11)$$

Since the ε and μ vary little in the earth's crust as compared with the conductivity, we assume that ε and μ have the values in vacuum, i.e.,

$$\varepsilon = \frac{1}{36\pi} \cdot 10^{-9} (F/M) \qquad (2.1.12)$$

$$\mu = 4\pi \cdot 10^{-7} (N/A^2). \qquad (2.1.13)$$

In eq.(2. 1. 2) and (2. 1. 9), the first and the second term are called conduction current and displacement current. The ratio of the first and the second term is

$$\left(\frac{\partial \mathbf{D}}{\partial t}\right) / \mathbf{j} = \frac{\omega\varepsilon}{\mu} \approx \frac{f}{2\sigma} 10^{-10} \qquad (2.1.14)$$

In case of the MT method, $\sigma > 10^{-5}$ (S/m) and $f < 10^{4}$ (Hz), the ratio is smaller than 0.05 and we can neglect the second term. Then, we can present the following induction eq.(2. 1. 8) and (2. 1. 9) as

$$\nabla^2 \mathbf{E} + i\omega\mu\sigma\mathbf{E} = 0 \qquad (2.1.15)$$

$$\nabla^2 \mathbf{H} + i\omega\mu\sigma\mathbf{H} = 0 \qquad (2.1.16)$$

2. 2. Uniform earth

First, we assume the uniform conductivity earth. To solve the induction equation, the horizontal magnetic fields are assumed to be uniform everywhere on the earth, i. e.,

$$\frac{\partial}{\partial x} = \frac{\partial}{\partial y} = 0 \qquad (2.2.1)$$

This is called the plane wave assumption. Here, the electric field and the magnetic field are assumed to have only the north and the east components, respectively, i. e.,

$$\mathbf{E} = (E_x, 0, 0), \quad \mathbf{H} = (0, H_y, 0) \qquad (2.2.2)$$

The boundary conditions are assumed as follows,

$$E_x = H_y = 0 \text{ at } Z=\infty,$$

$$E_x = E_x(0) \text{ and } H_y = H_y(0) \text{ at Z=0} \qquad (2.2.3)$$

where z means a depth (downward positive).

Then eq. (2. 1. 15) and (2. 1. 16) are rewritten as

$$\frac{\partial^2 E_x}{\partial^2 z} + k^2 E_x = 0 \qquad (2.2.4)$$

$$\frac{\partial^2 H_y}{\partial^2 z} + k^2 H_y = 0 \qquad (2.2.5)$$

where $k=(i\,\sigma\,\mu\,\omega)^{1/2}$

The general solution of eq.(2. 2. 4) is

$$E_x = (Ae^{ikz} + Be^{-ikz})e^{-i\omega t} \qquad (2.2.6)$$

where A, B is arbitrary constant, t is the time and z is the depth.

The solution for Hy is lead by substituting eq.(2. 2. 6) to eq.(2. 1. 8), which is

$$H_y = \frac{k}{\omega\mu}(Ae^{ikz} - Be^{-ikz})e^{-i\omega t} \qquad (2.2.7)$$

Substituting the boundary conditions to eq.(2. 2. 6) and (2. 2. 7) , following equations are obtained;

$$E_x = E_x(0) \cdot e^{ikz} e^{-i\omega t} \qquad (2.2.8)$$

$$H_y = \frac{k}{\omega\mu} E_x(0) \cdot e^{ikz} e^{-i\omega t} \qquad (2.2.9)$$

Eq. (2. 2. 8) and (2. 2. 9) shows that the ratio of *Ex* and *Hy* on the surface does not include arbitrary constants such as

$$Z_{xy} = \frac{E_x(0)}{H_y(0)} = \frac{\omega\mu}{k} = (\frac{\omega\mu}{\sigma})^{1/2} \cdot e^{-i\pi/4} = (\frac{2\pi\omega\mu f}{\sigma})^{1/2} \qquad (2.2.10)$$

where f is the frequency of the oscillation of the electromagnetic field which is equivalent to $\omega/2\pi$. Zxy is called an impedance. The resistivity (reciprocal of conductivity σ) , ρ , is derived from the impedance in a uniform earth, i. e.

$$\rho = \frac{1}{\sigma} = \mathrm{Real}\left(\frac{1}{2\pi\mu f}\left|Z_{xy}\right|^2\right) = \frac{1}{2\pi\mu f}\frac{\left|E_x(0)\right|^2}{\left|H_y(0)\right|^2} \qquad (2.2.11)$$

Since Zxy is observable, the resistivity of the earth is directly calculated from observed Zxy in the uniform case.

In this case, the impedance phase, simply called the "phase" as usual, is 45 degrees,

$$\phi = -\arg(Z_{xy}) = \frac{\pi}{4} \qquad (2.2.12)$$

In general, the exploration depth is approximately given as the skin depth δ

$$\delta = \left(\frac{2}{\sigma\omega\mu}\right)^{1/2} \approx 0.5\sqrt{\rho T} \qquad (2.2.13)$$

where T is the period of fluctuations of the electromagnetic field. Substituting eq.(2. 2. 13) to eq.(2. 2. 8) and (2. 2. 9), it is found that the magnetic and electric fields decay by 1/e of the surface values at the skin depth. Therefore, it is considered that the impedance of the electromagnetic field at high frequencies reflect the resistivity structure of shallow parts, and the impedance at lower frequencies reflect the resistivity structure of the deeper part of the earth.

2. 3. One-dimensional resistivity structure

The theoretical impedance can be calculated from an arbitrary 1-dimensional (1-D) layered resistivity structure (Cagniard 1953, Kaufman and Keller, 1981). In the 1-D case, eq.(2. 2. 4) and (2. 2. 5) are applied to each layer and general solutions of the electromagnetic fields are the same as eq.(2. 2. 6) and (2. 2. 7). The boundary condsions are that the magnetic and the electric fields become zero at $z= \infty$ and $z= 0$. The boundary conditions at each boundary of layers are defined such that the electromagnetic field is continuous across the boundary. Assuming these boundary conditions, the impedance on the surface of n-layered medium(Fig. 2-2), Zxy, is lead by a recurrence formula such as

$$Z_{xy} = Z_n = \frac{\omega\mu}{k_1}\coth\left(-ik_1h_1 + \coth\frac{k_1}{\omega\mu}Z_{n-1}\right) \qquad (2.3.1)$$

$$Z_{n-1} = \frac{\omega\mu}{k_2}\coth\left(-ik_2h_2 + \coth\frac{k_2}{\omega\mu}Z_{n-2}\right)$$

$$Z_{n-2} = \frac{\omega\mu}{k_3}\coth\left(-ik_3h_3 + \coth\frac{k_3}{\omega\mu}Z_{n-3}\right)$$

$$\vdots$$

$$Z_1 = \frac{\omega\mu}{k_n}.$$

The eq.(2. 3. 1) shows that, as different from the uniform case, the resistivity in the earth was not directly calculate from the observed impedance. However, the calculated resistivity from the observed impedance by eq. (2. 2. 11) shows the information of the resistivity struture. This calculated resistivity is defined as apparent resistivity (expressed as ρ_a as usual). In addition, the phase calculated from the observed impedanceby eq.(2. 2. 12) also indicate the charactristics of the resistivity structure.

An Example of the apparent resistivity and the phase on a 1-D resistivity structure is shown in Fig. 2-3. To simplify, two-layered resistivity structure is dealt here. If the h_1, σ_1 and σ_2 means the thickness of the first layer, the conductivity of the first and second layer respectively, the impedance obtained on the surface is

$$Z_{xy} = Z_1 \frac{1 + K_{12} e^{2ik_1 h_1}}{1 - K_{12} e^{2ik_1 h_1}} \qquad (2.3.2)$$

where

$$Z_1 = \frac{\omega\mu}{k_1}, \quad K_{12} = \frac{k_1 - k_2}{k_1 + k_2}, \qquad (2.3.3)$$

$$k_1 = (i\sigma_1\omega\mu)^{1/2}, \quad k_2 = (i\sigma_2\omega\mu)^{1/2} \qquad (2.3.4)$$

In Fig. 2-3, note that apparent resistivity vary gradually with decreasing the frequency, although the resistivity of the structure changes discontinuously. I also refer that the impedance phase become more than 45 degrees if the conductive layer underlies the resistive surface, and less than 45 degrees if resistive one undelies the conductive one. On the basis of eq.(2.3.2), if the second layer is a perfect conductor,

$$\phi \to \frac{\pi}{2} \qquad (2.3.5)$$

with decreasing the frequency. Otherwise, if the second layer is a insulator,

$$\phi \to 0 \qquad (2.3.6)$$

with decreasing the frequency. Thus, in general, a high phase (> 45 degrees) is responsible to a conductive underlying layer, and a low phase (< 45 degrees) is responsible to a resistive one.

2. 4. Two-dimensional resistivity structure

Next, the electromagnetic induction on a two-dimensional resistivity structure such as in Fig. 2-4 is considered. In the two-dimensional case, the basic equation for the induction problem is also eq.(2. 1. 15) and (2. 1. 16). It is assumed that the x axis as the strike of the structure, derivatives with respect to x are zero. Under this condition, the induction equation in eq.(2. 1. 15) and (2. 1. 16) are rewritten as six formulas with six components of the magnetic and the electric fields, that is, H = (H_x, H_y, H_z) and E = (E_x, E_y, E_z). Those six equations are decoupled into two modes; one consists of H_x, E_y, E_z and another consists of H_y, H_z, E_x . The former is called TM mode or B-polarization, and the later is called TE mode or E-polarization (Fig.2-5). The formulas for the TM mode are presented as follows,

$$\frac{\partial}{\partial y}\left(\frac{1}{\sigma}\frac{\partial H_x}{\partial y}\right)+\frac{\partial}{\partial z}\left(\frac{1}{\sigma}\frac{\partial H_x}{\partial z}\right)-i\omega\mu H_x=0 \qquad (2.4.1)$$

$$E_y=\frac{1}{\sigma}\frac{\partial H_x}{\partial z}, \quad E_z=\frac{-1}{\sigma}\frac{\partial H_x}{\partial y} \qquad (2.4.2)$$

And the formulas for the TE mode are

$$\frac{\partial}{\partial y}\left(\frac{1}{i\omega\mu}\frac{\partial E_x}{\partial y}\right)+\frac{\partial}{\partial z}\left(\frac{1}{i\omega\mu}\frac{\partial E_x}{\partial z}\right)-\sigma E_x=0 \qquad (2.4.3)$$

$$H_y=\frac{1}{i\omega\mu}\frac{\partial E_x}{\partial z}, \quad H_z=\frac{-1}{i\omega\mu}\frac{\partial E_x}{\partial y} \qquad (2.4.4)$$

In 2-dimensional and 3-dimensional cases, the observed impedance is expressed as not a scaler but a tensor type. That is, .

$$\begin{pmatrix}E_x\\E_y\end{pmatrix}=\begin{pmatrix}Z_{xx} & Z_{xy}\\Z_{yx} & Z_{yy}\end{pmatrix}\begin{pmatrix}H_x\\H_y\end{pmatrix} \quad \text{or} \quad \mathbf{E}=\mathbf{ZH} \qquad (2.4.5)$$

where Zxx and Zyy is zero in this cordinate,

In the TM mode, the apparent resistivity and the phase is defined as

$$\rho_{xy} = \frac{1}{\omega\mu}\left|Z_{xy}\right|^2 = \frac{1}{\omega\mu}\left|\frac{E_y}{H_x}\right|^2 \qquad (2.4.6)$$

$$\phi_{xy} = -\arg\left(Z_{xy}\right) = -\arg\left(\frac{E_y}{H_x}\right) \qquad (2.4.7)$$

And the TE mode the apparent resistivity, phase and the tipper, which is also one of the observed response, is defined as

$$\rho_{yx} = \frac{1}{\omega\mu}\left|Z_{yx}\right|^2 = \frac{1}{\omega\mu}\left|\frac{E_x}{H_y}\right|^2 \qquad (2.4.8)$$

$$\phi_{yx} = \pi - \arg\left(Z_{yx}\right) = \pi - \arg\left(\frac{E_x}{H_y}\right) \qquad (2.4.9)$$

$$Tipper = \frac{H_z}{H_y} \qquad (2.4.10)$$

Note that the value of ϕ_{yx} is replaced by π - ϕ because ϕ_{yx} ranges from 180 to 270 degrees.

These response functions are analytically solved on some simple 2-dimensional structures (d'Erceville and Kunetz, 1962; Gayer, 1972; Weaver et al., 1985, 1986) However, in general, these response functions are calculated by using the numerical method. Most commom schemes are base on the finite difference method (Pascoe and Jones, 1972) and the finite element method (Reddy and Rankin, 1973; Rodi, 1976). In this thesis, I adpoted the FEM and briefly explain it.

The equation (2. 4. 1) and (2. 4. 3) is rewritten as follows,

$$\left[\frac{\partial}{\partial y}\left(h\frac{\partial}{\partial y}\right)+\frac{\partial}{\partial z}\left(h\frac{\partial}{\partial z}\right)+\lambda\right]u=0 \qquad (2.4.11)$$

where $u=E_x$, $h=\frac{1}{i\omega\mu}$, $\lambda=\sigma$ for the TM mode(2. 4. 12)

and $u=H_x$, $h=\frac{1}{\sigma}$, $\lambda=i\omega\mu$ for the TE model.(2. 4. 13)

Since the other fields in eq. (2. 4. 2) (2. 4. 4) can be obtained from u, we solve the partial differential equation in eq.(2. 4. 11). Here, the left side of eq. (2. 4. 11) is drawn as R(u; y, z), which is satisfied to be zero over the entire region. This is written with using the weight function δw in order to obtain an accurate solution as follows:

$$\int_s R(u;y,z)\cdot\delta w ds=0 \qquad (2.4.14)$$

In FEM, the resistivity model is constructed by triangular or rectangular elements and u is interpolated in each element by the discreate values at the nodes of a element. Then, eq. (2. 4. 14) is rewritten as

$$\sum_{e=1}^{E}\int_{Se}\left[h\left(\frac{\partial u}{\partial y}\frac{\partial\delta u}{\partial y}+\frac{\partial u}{\partial z}\frac{\partial\delta u}{\partial z}\right)+\lambda u\cdot\delta u\right]ds=0 \qquad (2.4.15)$$

where E is the total number of elements, $\int_{Se} ds$ denotes the areal integral in the e'th element and δw is assumed as δu . Eq.(2. 4. 15) is called the Galerkin equation. Since the derivatives in eq.(2. 4. 15) are simply derived as linear terms composed of the field *u* at the nodes and geometric constants, the following equation is finally obtained,

$$K(\omega,\sigma,r)\cdot u = b .$$

Here, *K* is a matrix determined from the frequency (ω), the conductivity of each element(σ) and the location of each node(*r*). *b* is the boundary conditions as follow (see Fig. 2-6 also) :

for the TM mode,

$H_x = 1$ on the surface and (2. 4. 16)

$\frac{\partial H_x}{\partial n} = 0$ at y=ymax, y=ymin and z=bottom of the model (2. 4. 17)

and for the TE mode,

$E_x = 0$ on the top of the air layer and (2. 4. 18)

$\frac{\partial E_x}{\partial n} = 0$ at y=ymax, y=ymin and z=bottom of the model (2. 4. 19)

2. 5. Tensor impedance

As described in eq.(2. 4. 5), tensor impedance is generally used as the electromagnetic response function. In addition, the tipper (geomagnetic transfer function) is also used as observed response. The tensor impedance (Z) and the tipper (T) is expressed by the observed magnetic(H) and electric field (E) as follows:

$$\mathbf{E} = \mathbf{Z}\mathbf{H} \quad \text{and} \quad H_z = \mathbf{T}\mathbf{H}, \tag{2.5.1}$$

where

$$\mathbf{E} = \begin{pmatrix} E_x \\ E_y \end{pmatrix}, \mathbf{H} = \begin{pmatrix} H_x \\ H_y \end{pmatrix}, \mathbf{Z} = \begin{pmatrix} Z_{xx} & Z_{xy} \\ Z_{yx} & Z_{yy} \end{pmatrix}, \mathbf{T} = \begin{pmatrix} T_x & T_y \end{pmatrix} \tag{2.5.2}$$

After Vozoff (1972), the impedance tensor and tipper is derived from the following equations

$$Z_{xx} = \frac{\langle E_x H_x^* \rangle \langle H_y H_y^* \rangle - \langle E_x H_y^* \rangle \langle H_y H_x^* \rangle}{\langle H_x H_x^* \rangle \langle H_y H_y^* \rangle - \langle H_x H_y^* \rangle \langle H_y H_x^* \rangle}$$

$$Z_{xy} = \frac{\langle E_x H_y^* \rangle \langle H_x H_x^* \rangle - \langle E_x H_x^* \rangle \langle H_x H_y^* \rangle}{\langle H_x H_x^* \rangle \langle H_y H_y^* \rangle - \langle H_x H_y^* \rangle \langle H_y H_x^* \rangle}$$

$$Z_{yx} = \frac{\langle E_y H_x^* \rangle \langle H_y H_y^* \rangle - \langle E_y H_y^* \rangle \langle H_y H_x^* \rangle}{\langle H_x H_x^* \rangle \langle H_y H_y^* \rangle - \langle H_x H_y^* \rangle \langle H_y H_x^* \rangle}$$

$$Z_{yy} = \frac{\langle E_y H_y^* \rangle \langle H_x H_x^* \rangle - \langle E_y H_x^* \rangle \langle H_x H_y^* \rangle}{\langle H_x H_x^* \rangle \langle H_y H_y^* \rangle - \langle H_x H_y^* \rangle \langle H_y H_x^* \rangle} \tag{2.5.3}$$

and

$$T_x = \frac{\langle H_z H_x^* \rangle \langle H_y H_y^* \rangle - \langle H_z H_y^* \rangle \langle H_y H_x^* \rangle}{\langle H_x H_x^* \rangle \langle H_y H_y^* \rangle - \langle H_x H_y^* \rangle \langle H_y H_x^* \rangle}$$

$$T_y = \frac{\langle H_z H_y^* \rangle \langle H_x H_x^* \rangle - \langle H_z H_x^* \rangle \langle H_x H_y^* \rangle}{\langle H_x H_x^* \rangle \langle H_y H_y^* \rangle - \langle H_x H_y^* \rangle \langle H_y H_x^* \rangle} \tag{2.5.4}$$

where $\langle AB^* \rangle$ means the cross-power obtained from field A and conjugate of B . If the magnetic field at the site far from the analyzed one are used as Hx* and Hy*, the bias error of impedance due to the auto-power of the magnetic field is diminished. Then, the acculacy of the impedance becoe more high. This processing is called the remote reference method (Gamble et al., 1979).

The remote reference method also is effective if both magnetic and electric fields contain the correlated noise such as made by leakage current from DC railway.

The impedance tensor produces the apparent resistivity, phase as described in eq. (2. 4. 6) - (2. 4. 9), and additionally other parameters involving the imformation of the resistivity sturucture. In this thesis, I use the skewness which shows the 3-dimensional heterogeity of the sturucture as follows.

$$skewness = \left| \frac{Z_{xx} + Z_{yy}}{Z_{xy} - Z_{yx}} \right| \qquad (2.\ 5.\ 5)$$

In the 1- or 2-dimensional resistivity strucutre , skewness equals to zero. The 3-dimensional structure shows larger skewness value. After the 3-dimensional calculation after Reddy et al.(1977), It is generally accepted that the 3-dimensional structure shows skewness more than about 0.2.

The transfer function is used to indicate the horizontall heterogenity of the resistivity structure. Here, the induction arrow is usually applied (Schmucker, 1970). The induction vector have a length of L and an angle θ (clockwise rotation from north) ,

$$L = \left(real(T_x)^2 + real(T_y)^2 \right)$$
$$\theta = \arctan\left(real(T_y) / real(T_x) \right) \qquad (2.\ 5.\ 6)$$

and show the qualitative distance and the direction to the conductive zone. In eq.(2. 5. 6), only the real induction arrow is shown. If you replace the operator real() to imag(), then imaginaly induction arrow is obtained. However, only the real induction arrow is dealt in this thesis.

2. 6. Static shift

The MT meshod suffers from some problems in relation to near surface inhomogeneith of the resistivity sturucture. The static effect , or static shift is one of the significant problem, which is near surface resistivity anomaly.

The mechanizm of the static shift is briefly explained. If the horizontally heterogeniety of the resistivity is there, the electrical charge is generated near the boundary because the current density across the horizontal heterogeniety is continuous. Now, I consider the case that the heterogeniety scale is enough small as compared to the skin depth. In this case, the electrical field due to the charge is expressed only the scaler potential because such small-scale charge can not generate the secondary field (deGroot-Hedlin, 1991). So, the electric field due to this small heterogeniety near the surface, Es, is approximately written as

$$E_s = k_s E_p \qquad (2.6.1)$$

where Ep is the primary electric field and ks is a constant independent of the frequency. Since the charge can not make secondary field, the magnetic field is not affected. As a result, the calculated apparent resistivity from Ep+Es are biased on the logarithmic plot with DC like by 2log(1+Ks).

The method of the correction of the static shift used previous studies were reviewed in Jiracek(1990) and Ogawa(1992). There are several method for the correction by

(1) using the known resistivity or boundary based on logging data or other

geophysical and geological studies (Jones, 1988),

(2) using the resistivity soundings based on the observation of the magnetic fields only (Sternberg et al., 1988; Takakura, 1993; Mitsuhata and Ogawa, 1994),

(3) using the spatial filtering of the apparent resistivity (called EMAP after Torres-Verdin and Bostick, 1992),

(4) including the shallow resistivity structure in the 2- of 3-dimensional resistivity model derived by other electrical soundings (Ogawa and Uchida, 1987),

(5) averaging the TE apparent resistivity at the lowest frequency(used in Jones et al., 1992) and

(6)using the inversion method detectable both the resistivity model and the factor of the static shift (deGroot-Hedlin, 1991, 1995,; Ogawa , 1996)

There are many attempt for the correction, however, these method are still problematic. The methods of 1 - 4 needs some of the additional informations. As compared with these method, the method 5 is the convinient way. But the method 5 is also problematic because the resonse in the TE mode is strongly affected 3-dimensional heterogeneity of the resistivity structure described later, and apparent resistivity at the lower frequecy have a large error. The most reliable method is 6, but the one more hyper-parameter is necessary to balance the fittness and the roughness of the static-shift factor in the inversion scheme. It prevent to search the suitable model quickly. Moreover, if the surface resistivity is partly known and is able to contain the model, the method 7 needs some additional hyper-parameter.

In this thesis, I propose a new and a simple removing method of the static

shift by using the inverse algorithm. This method is similar to the combinations of the method 4 and 6. The detail is presented in the next chapter.

2. 6. Galvanic distortion and its correction

In eq. (2. 5. 2), both Zxx and Zyy equal to zero in the case of the 1- or 2-dimensional resistivity structure. So, the impedance tensor on the 2-dimensional earth is written as

$$Z_{2d} = \begin{pmatrix} 0 & Z_{xy} \\ Z_{yx} & 0 \end{pmatrix} \qquad (2.7.1)$$

where Z_{2d} is the impedance on 2-dimensional structure. In the 1-dimensional case, Zyx = -Zxy.

If the observed cordinate is rotated θ which was taken positive from the north with clockwise rotations, the observed impedance is rotated to Z' as

$$Z' = R(\theta)^{-1} Z_{2d} R(\theta) \qquad (2.7.2)$$

where R(θ) is a rotation matrix with θ , and R(θ)$^{-1}$ is the transposed matrix of R(θ). In 2-dimensional case, since the diagonal and off-diagonal component of the observed impedance tensor become minimun and maximum respectively when is parallel to the strike of the 2-dimensional resistivity structure, the strike angle θ is estimated from the following equation (Swift, 1967):

$$\theta = \frac{1}{4}\arctan\left[\frac{\left(Z_{xx}-Z_{yy}\right)\left(Z_{xy}+Z_{yx}\right)^{*}+\left(Z_{xy}+Z_{yx}\right)\left(Z_{xx}-Z_{yy}\right)^{*}}{\left|Z_{xx}-Z_{yy}\right|^{2}-\left|Z_{xy}+Z_{yx}\right|^{2}}\right] \qquad (2.7.3)$$

θ is called the principle axis or the strike direction.

Recently, It is well known that the near-surface and 3-dimensional heterogeniety give misleading of the strike directions by the conventional analyses in eq.(2. 7. 3). Of cource, such heterogeniety also distorts the apparent resistivity and the phase for the analyses of the 1- or 2-dimensional structure. This effect is called the galvanic distortion. If such heterogeneity exists on the 2-dimensional resistivity structure and small as compared with the skin depth, the effect of the galvanic distortion is expressed by scaler matrix(C) and the observed impedance is expressed as

$$Z' = R(\theta)^{-1} C Z_{2d} R(\theta)$$
$$C = \begin{pmatrix} a & b \\ c & d \end{pmatrix} \qquad (2.7.4)$$

Additionally, the distortion matrix C is decomposed to accumulation of 4 basical matrix (Groom and Bailey, 1989). This decomposition can be written as the product such as

$$C = \begin{pmatrix} 1 & -t \\ -t & 1 \end{pmatrix} \begin{pmatrix} 1 & e \\ e & 1 \end{pmatrix} g \begin{pmatrix} 1+s & 0 \\ 0 & 1-s \end{pmatrix} \qquad (2.7.5)$$

where t, e, g, s is real constants called the twist, the shear, the site gain and the anisotropy (Groom and Bailey, 1989). The physical meaning of these parameter is that the combination of t and e express the current channeling to the arbitrary direction, and g and s present the static shift factor of Zxy and Zyx. The decomposition based on eq. (2. 7. 5) is called the Groom-Bailey decomposition. To decompose the observed impedance to the near-surface distrotion and regional 2-dimensional induction, the least square method is applied since the eq.(2. 7. 5) is linear. In fact, since 7 decomposed parameters is not stably detected from 8 observed parameter at 1 frequency, some decomposed parameters such as the strike direction, the twist or the shear are

usually fixed in the regard to the frequency. Or the constrain is sometimes added that the decomposed paramters vary smoothly in the regard to the frequency (Ogawa and Mitsuhata, 1994).

Some more simple way to detect the strike direction not affected by the galvanic distortion are presented. One is the method using the phase difference between the components of the observed impedance (Chakridi et al., 1992). Eq.(2. 7. 4) is rewritten in

$$Z' = R(\theta)^{-1}\begin{pmatrix} bZ_{yx} & aZ_{xy} \\ dZ_{yx} & cZ_{xy} \end{pmatrix}R(\theta) \qquad (2.\ 7.\ 6)$$

This equation means that ,if the observed cordinate is same as one for the 2-dimensional structure, the component of the impedance in right and left column have same phase, respectively. In the other words, the phase difference in the column component of the observed impedance takes the minimum value when the rotation direction is parallel to the strike of the 2-dimensional structure. This feature is written as

$$\left|\arctan\left(\frac{imag\left[Z_{xx}' / Z_{yx}'\right]}{real\left[Z_{xx}' / Z_{yx}'\right]}\right)\right| = \min \qquad (2.\ 7.\ 7)$$

or

$$\left|\arctan\left(\frac{imag\left[Z_{xy}' / Z_{yy}'\right]}{real\left[Z_{xy}' / Z_{yy}'\right]}\right)\right| = \min \qquad (2.\ 7.\ 8)$$

where Zij' is the observed component of the impedance. Note that eq.(2. 7. 7) and (2. 7. 8) include the ambiguity of 180 and 90 degrees.

The other way is the use of the invariant forms of the observed impedance (Jones, 1992). This forms does not varied by the rotational operator and have been well used for the 1-dimensional analysis. Following form, called "

determinant average" is constant against the arbitrary distrotion matrix:

$$Z_D = (Z_{xx}Z_{yy} - Z_{xy}Z_{yx})^{1/2} \qquad (2.7.9)$$

Note that these decomposition or reduction of the distortions is effective only in the case that the heterogeniety is small and the regional structure is 2-dimensional. If the resistivity structure is fully 3-dimensional, these analysis is not valid sometimes.

Fig. 2-1 The coordinate axis considered in this thesis

Fig. 2-2 The resistivity structure of n-layered medium. σ means the conductivity of the each layer and h means the thickness.

Fig. 2-3 Theoretical electromagnetic responses after Kaufman and Keller (1981). h1, σ 1 and σ 2 means the thickness of the first layer, the conductivity of the first and second layer, respectively. normalized frequency is $\lambda_1 = 2\pi\ \delta_1$ where δ_1 is the skin depth for the surface layer.

Fig. 2-4 An example of a two-dimensional resistivity structure

Fig. 2-5. The TM mode(Upper) and the TE mode(Lower)

Fig. 2-6 The boundary conditions in the calculation for the two-dimensional resistivity structure

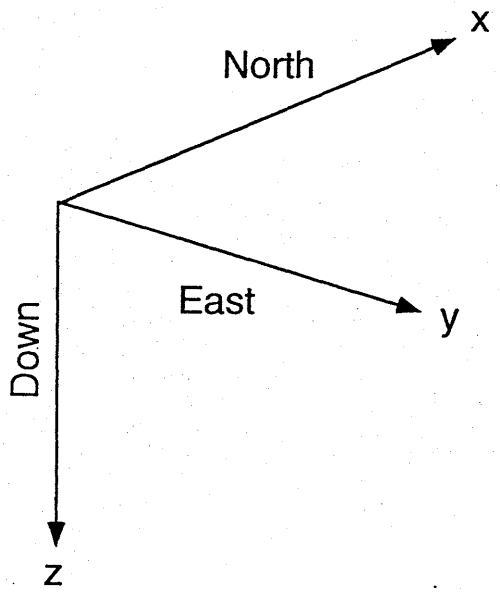

Fig. 2-1

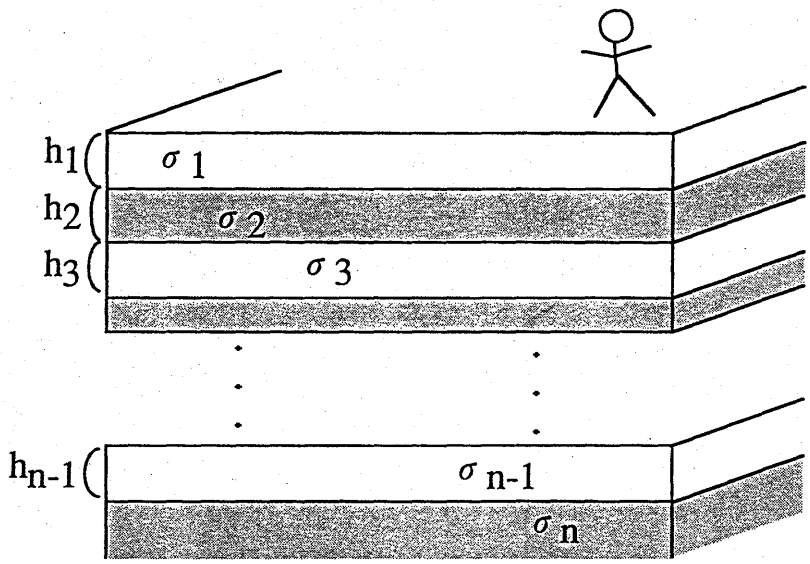

Fig. 2-2

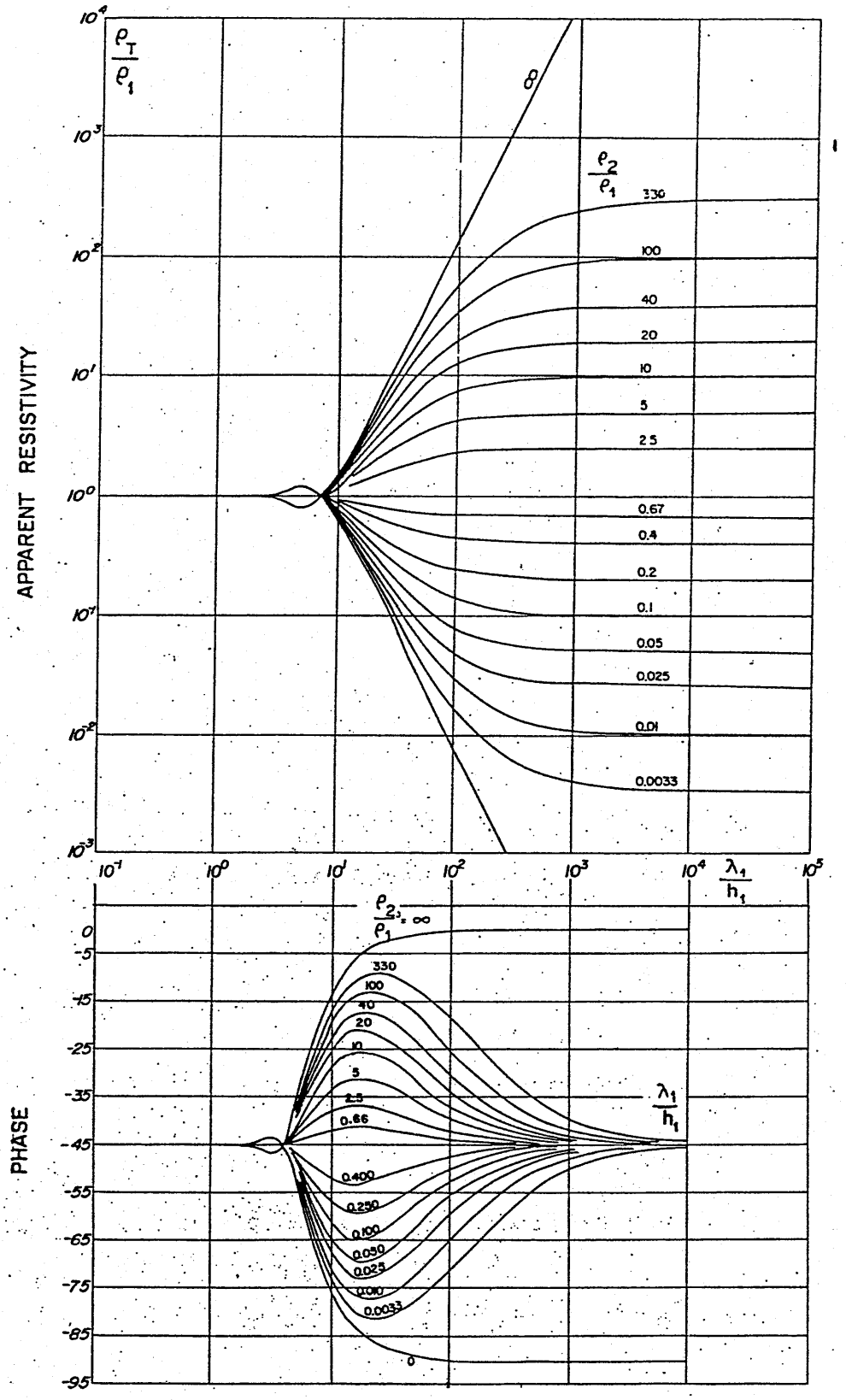
APPARENT RESISTIVITY
$\frac{\rho_T}{\rho_1}$
θ
$\frac{\rho_2}{\rho_1}$
330
100
40
20
10
5
2.5
0.67
0.4
0.2
0.1
0.05
0.025
0.01
0.0033
$\frac{\lambda_1}{h_1}$
PHASE
$\frac{\rho_2}{\rho_1}=\infty$
330
100
40
20
10
5
2.5
0.66
0.400
0.250
0.100
0.050
0.025
0.010
0.0033
0
$\frac{\lambda_1}{h_1}$

Fig. 2-3

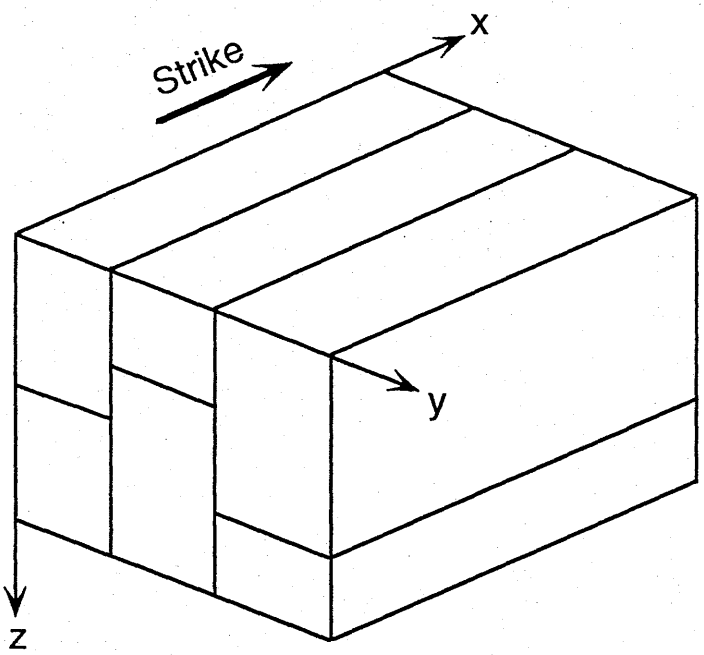

Fig. 2-4

TM mode

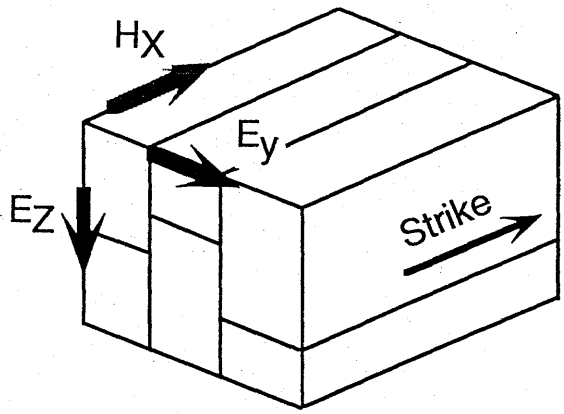

TE mode

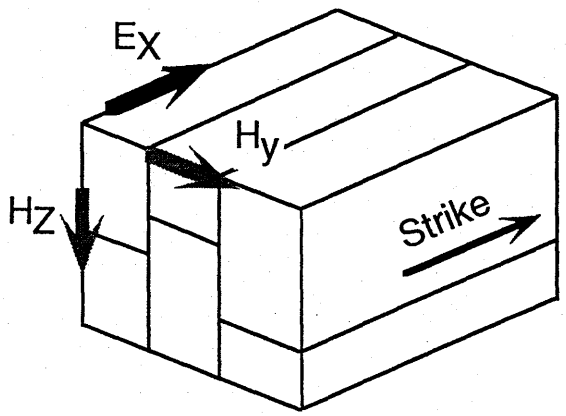

Fig. 2-5

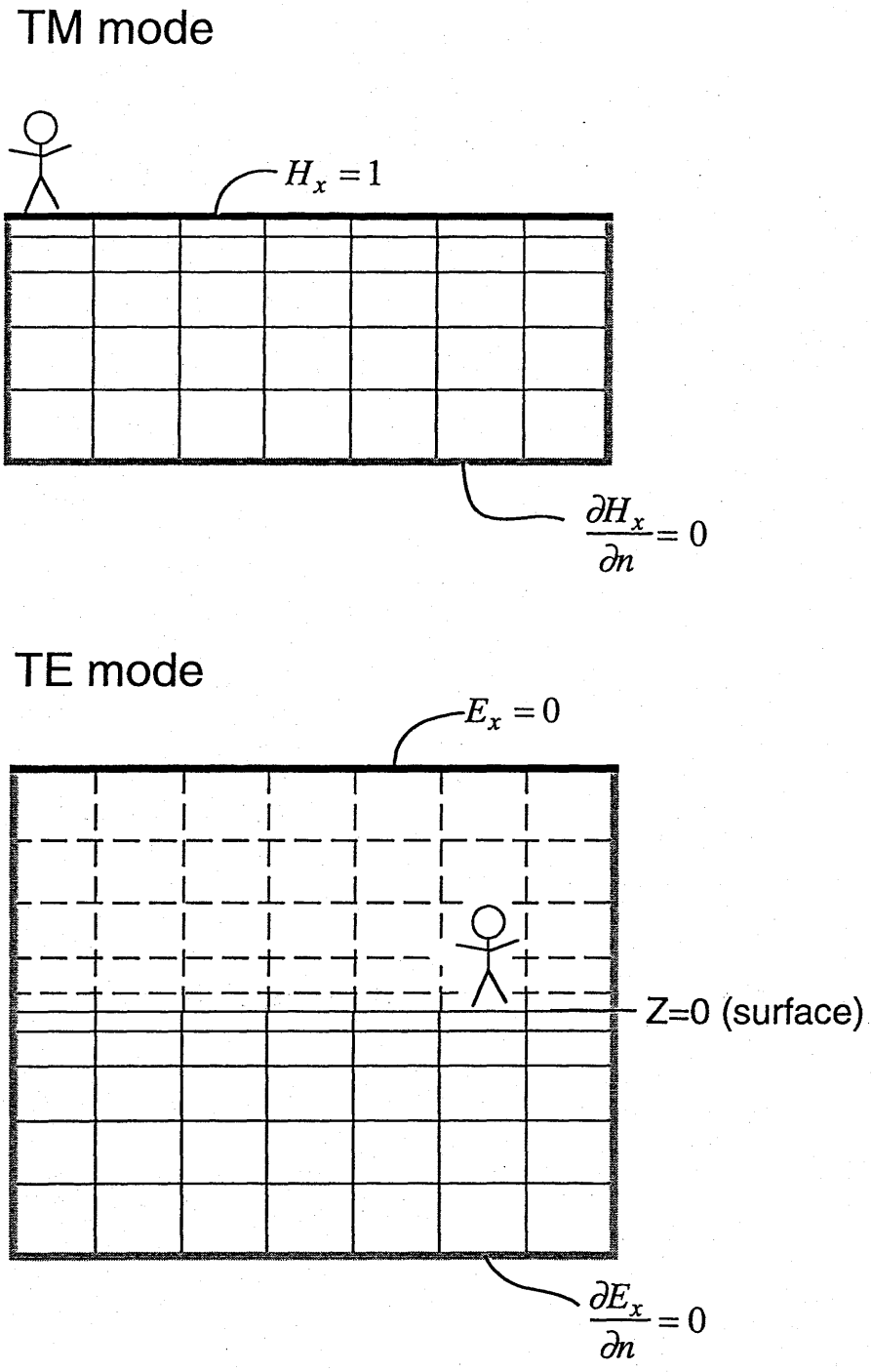
TM mode
$H_x = 1$
$\frac{\partial H_x}{\partial n} = 0$
TE mode
$E_x = 0$
Z=0 (surface)
$\frac{\partial E_x}{\partial n} = 0$

Fig. 2-6

3. Method for MT data acquisition, processing and modeling

3. 1. Instruments for the MT sounding

The MT data was acquired with the Phoenix V5-based MT system manufactured by Phoenix Geophysics Ltd. This V5 system covers a wide frequency band ranging from 384Hz to 0.00055Hz. The 40 frequencies selected in the measurement were summarized in Table. 3-1 with the sampling rates. The hardware configuration was shown in Fig. 3-1. The V5 MT system equipped magnetic sensors and electrodes. Magnetic fields for the three components (north, east and vertical) were observed by using three induction coils. Chopper amplifiers were mounted inside the coils. The two components (north and east) of the electric field were observed by using two pairs of electrodes of Pb-PbCl2 type with a separation of about 50 - 100m. Since the magnetic and the electric signals are extremely low level, they are amplified, notch-filtered and band-pass-filtered in the sensor processor (SPV5) located close to the sensors. Then, the output signals from the SPV5 are transmitted to the main processor (V5). The V5 is separated from SPV5 more than 50m for the reduction of the noise generated in V5 itself. The transmitted signals are notch-filtered and digitized by a 16 bit A/D converter in V5. A 32 bit central processing unit installed in V5 enables the real-time data processing on site. Although results of the real-time data processing are not used in the main analysis, they are useful to check the data quality in site. A large RAM board with 40M byte is also installed and the time series data are recorded on it. About 20M byte is spent for recording thorough one night.

3. 2. Data analysis

We analyzed the observed time series data and obtained the electromagnetic responses in the laboratory. Time series data processing followed the cascade decimation (Wight and Bostick, 1980). The observed data was divided every 32 points for one data unit. These data units were calculated with DFT, and Fourier components of 8-th and 6-th harmonics frequencies were stored. After that, the time series data were decimated every two data point and filtered to make the data units for lower frequencies. The procedure of the cascade decimation increases the number of stacking at higher frequencies(> 1Hz) and yields more stable electromagnetic responses.

We adopted the remote reference processing (Gamble et a., 1979) for removing unwanted noises in measurements. In this study, two or more V5 MT systems were arranged and synchronously operated in the area surveyed. The synchronized clock is connected to the all V5 MT system. It enables us to acquire the synchronized data. When we analyzed the data of one site, the data of another site were selected as the reference field used in eq. (2. 5. 3). The analyzed site and the remote site were separated with the distance as long as 2km at least. The remote reference method gives the smooth MT parameters in regard to the frequency and reduce the bias noise to the MT parameters. Thus, we obtained the cross powers of various pairs of the magnetic and the electric fields, and determined the apparent resistivity, the impedance phase and other MT parameters.

3. 3. Strike detection

It is important to determine the strike direction of the resistivity structure in order to analyze the two-dimensional resistivity structure beneath the target area. To avoid galvanic distortions, we adopted the method after Chakridi et al.(1992) to estimate the strike direction, described in the chapter 2. We rotated the impedance tensor every 5 degrees to search the rotation angle at which the phase differences in eq.(2. 7. 7) and (2. 7. 8) become minimum, and we estimated the strike direction at each frequency at each site. Although the method of the strike detection after Chakridi et al. is effective on the two-dimensional resistivity structure, the calculated strike direction is not stable on the one-dimensional earth because the phase difference in eq.(2. 7. 7) and (2. 7. 8) is very small at all rotation angles. So, we also adopted the similar method of the strike detection to that described in Jones and Groom (1993, eq.10 and 11). They described that the following phase difference also becomes the minimum value at the rotation angle parallel or perpendicular to the strike of the resistivity structure.

$$\left|\arctan\left(\frac{imag\left[(Z_{xx}' + Z_{xy}')/(Z_{yx}' + Z_{yy}')\right]}{real\left[(Z_{xx}' + Z_{xy}')/(Z_{yx}' + Z_{yy}')\right]}\right)\right| = \min \qquad (3.3.1)$$

or

$$\left|\arctan\left(\frac{imag\left[(Z_{xx}' - Z_{xy}')/(Z_{yx}' - Z_{yy}')\right]}{real\left[(Z_{xx}' - Z_{xy}')/(Z_{yx}' - Z_{yy}')\right]}\right)\right| = \min \qquad (3.3.2)$$

The denominator in these equations becomes not zero on the one-dimensional resistivity structure and is robust to a one-dimensional resistivity structure. We, after all, adopted the method which gives a smaller standard

deviation of the strike at each site.

3. 4. Static-shift correction and two-dimensional resistivity modeling

We developed a simple and effective method for the correction of the static shift effect in this thesis. After Ogawa(1992), the static shift to the apparent resistivity in the TM mode is expressed by using the two-dimensional resistivity model. In the method, we corrected the static-shift factor for the TM apparent resistivity (see Chapter 2) by including the effect of static shift to the surface layer of the two-dimensional resistivity model. The method of our static shift correction is very simple as follows. Here, we used the inversion algorithm developed by Uchida and Ogawa(1993). First, we exclude the surficial resistivity block just beneath the site in calculation of the smoothness. Secondly, we assume the surface layer in the model obtained in this first inversion makes the static shift effect. We calculate the 'true' apparent resistivity from the model which is obtained by the first inversion, in which however only the surface layer is removed. The resistivity value of the surface layer is substituted from the underlying second layer. Thirdly, we assume that the difference between this calculated and the observed apparent resistivity curve is due to the effect of the static shift. Thus, we determined the magnitude of the static-shift effects.

To check the ability of the our method for the static-shift correction, the synthetic data were used. We prepared the model including underlying resistive and conductive prisms (Fig. 3-3) and calculated responses from this model. The calculated responses were appended the gaussian noise of 3%

and the static shift. The magnitude of the static shift at sites with even and odd number was 1 or -1 respectively, in logarithmic unit of the resistivity. We regard this calculated response as the 'observed' one and applied the correcting method of the static shift described above. The result of the static-shift correction is shown in Fig. 3-4 to Fig. 3-7. First, Fig.3-4 is the model obtained by the inversion without the static-shift correction together with the model from the data appended no static shift for the comparison. The model in Fig. 3-4(b) is very similar to original one (Fig. 3-3). However, it is obvious that the model in Fig. 3-4(a) is strongly disturbed by the static shift. Secondly, the model obtained by the first inversion in our method is shown in Fig.3-5. The obtained model in Fig. 3-5 is more similar to that in Fig. 3-4(b). In addition, the surface layer of the model in Fig. 3-5 show the high and low resistivity anomaly corresponding to the appended static shift. The calculated responses from the model in Fig. 3-5 without the surface layer were shown in Fig. 3-6 together with the observed data. The difference between the calculated and observed response roughly coincide with the magnitude of the appended static shift to the site. Thus, the model obtained by the first inversion is useful to estimate the approximate magnitude of the static shift. Finally, the most suitable model was obtained by the second inversion using the data which is removed the predicted static shift. The most suitable model was shown in Fig. 3-7. It is obvious that the model in Fig. 3-7 is quite similar to that in Fig. 3-4(b), and that the our method for the static-shift correction is very effective. However, both the resistive and the conductive prism is suitable model in Fig. 3-7 is resolved more deeply and more resistive than the original one (Fig. 3-7(b)). The reason is possibly that the number of sites appended the positive static shift is greater than that appended the negative one. In one-dimensional case, it is well known that the positive static shift

causes the both resistivities and depths of layers in the obtained model to be greater than the true model. A similar effect was found in the two-dimensional case here. We conclude that the average value of the static shift of the whole site can not be corrected by our method and there remains the effect shifting whole resistivity and depth of the obtained two-dimensional model with DC like. As similar to the one-dimensional case, if a site is there where the resistivity in the shallow depth is investigated and we fix it as the surface resistivity beneath this site in the inversion, the average static shift in the whole site will be corrected. It is confirmed in the field data in the Atotsugawa region described the later chapter.

After we checked the validity of a two-dimensional structural analysis and corrected the static shift, we estimated the resistivity models by using the two-dimensional least square inversion with the smoothness constraint developed by Uchida(1993). In inversion, we used the least square method with the smoothness constraint with the iterative process. Some initial models with 1-1000 ohm-m uniform were tested. As a result, we found that the most suitabe models obtained from these various initial models are very simialr. In this thesis, the initial model for the inversion was determined as the uniform earth with resistivity of 1000 ohm-m. The inversion was executed very stably in each profile, and usually about ten times of iterations for each profile were sufficient to reach a suitable convergence. We adopted most suitable model with the least ABIC during ten iterations.

3. 5. Sensitivity of the model

We checked the sensitivity of the model. The schematical concept is

shown in Fig. 3-8. The sensitivity in this thesis is defined as the maximum variation of the apparent resistivity or the phase when a resistivity value of one resistivity block increases 1 order. This maximum change is normalized by corresponding observed errors. Although the sensitivity is relative, the qualitative resolution of the resistivity of each block can be obtained from the sensitivity. Let us consider a resistivity block whose sensitivity is 5. The sensitivity of 5 means that the maximum variation of the response is 5 times as large as the observed error when the resistivity of this block is increased by one order of magnitude. On the other word, the maximum variation of the responses is as same as the observed error when the resistivity of this block is changed by Log(1/5) of its magnitude. That is, the model with variation of the resistivity of this blocks smaller than Log(1/5) provides as similar fitness of the observed to the calculated apparent resistivity and phase as the most suitable model. Thus, the resolution of logarithmic resistivity of each block is qualitatively given by the reciprocal of the sensitivity if the residual between the observed and calculated response from this model is smaller than the observed error.

As an example, the sensitivity for the two prism model is shown in Fig. 3-9(a). In general, the depth of the top of a conductive zone is well resolved in the MT method. And it is also accepted that the depth of the top of the resistive zone is more difficult to detect than the conductive one. This feature is theoretically checked in one-dimensional resistivity structure. In Fig. 3-9 (b), such feature of the resolution is well expressed: the sensitivity of the top of the conductive zone is high, while it is low in the resistive layer. On the other hand, the sensitivity is low at the bottom of the conductive zone, while the sensitivity seems rather high at the bottom of the resistive zone. Thus,

although the sensitivity is no more relative and qualitative, this is useful for the approximate criterion for the resolution of the model.

Table. 3-1 The frequency table for the V5 MT system

Fig. 3-1 The schematic view of the hardware configuration of the Phoenix V5-based MT system

Fig. 3-2 Schematic diagram for the method of static shift correction in this study

Fig. 3-3 The resistivity model with two buried resistive and conductive prisms to check the ability of the our method for the static-shift correction

Fig.3-4 (a) The most suitable resistivity model obtained by the inversion using the data set including static shift.
(b) The most suitable resistivity model obtained by the inversion using the data set without static shift

Fig.3-5 The resistivity model obtained by the first process of the inversion to correct the static shift

Fig. 3-6 The calculated responses from the model in Fig. 3-5(dashed curves) and the calculated one from the model without the upper most layer only(solid curves). Circles: observed values.

Fig. 3-7 (a)The finally obtained resistivity model by the our method for the static correction.
(b) same as Fig.3-4(b)

BAND	F#	F(Hz),(50 Hz)	F(Hz),(60Hz)	Range	Level	S-Rate(50)	SR(60)
1	1	320.0	384.0	Hi	3	2560	3072
	2	240.0	288.0				
2	3	160.0	192.0				
	4	120.0	144.0				
3	5	80.0	96.0				
	6	60.0	72.0				
4	7	40.0	48.0	Hi	4	320	384
	8	30.0	36.0				
5	9	20.0	24.0				
	10	15.0	18.0				
6	11	10.0	12.0				
	12	7.50	9.00				
7	13	6.00		Low	5	24	24
	14	4.50					
8	15	3.00					
	16	2.25					
9	17	1.50					
	18	1.12					
10	19	0.750					
	20	0.5625					
11	21	0.3750					
	22	0.28125					
12	23	0.18750					
	24	0.14063					
13	25	0.09375	(10.7 sec)				
	26	0.07031	(14.2 sec)				
14	27	0.04688	(21.3 sec)				
	28	0.03516	(28.4 sec)				
15	29	0.02344	(42.7 sec)				
	30	0.01758	(56.9 sec)				
16	31	0.01172	(85.3 sec)				
	32	0.00879	(113.8 sec)				
17	33	0.00586	(170.7 sec)				
	34	0.00439	(227.6 sec)				
18	35	0.00293	(341.3 sec)				
	36	0.00220	(455.1 sec)				
19	37	0.00146	(682.7 sec)				
	38	0.00110	(910.2 sec)				
20	39	0.00073	(1365 sec)				
	40	0.00055	(1820 sec)				

Table. 3-1

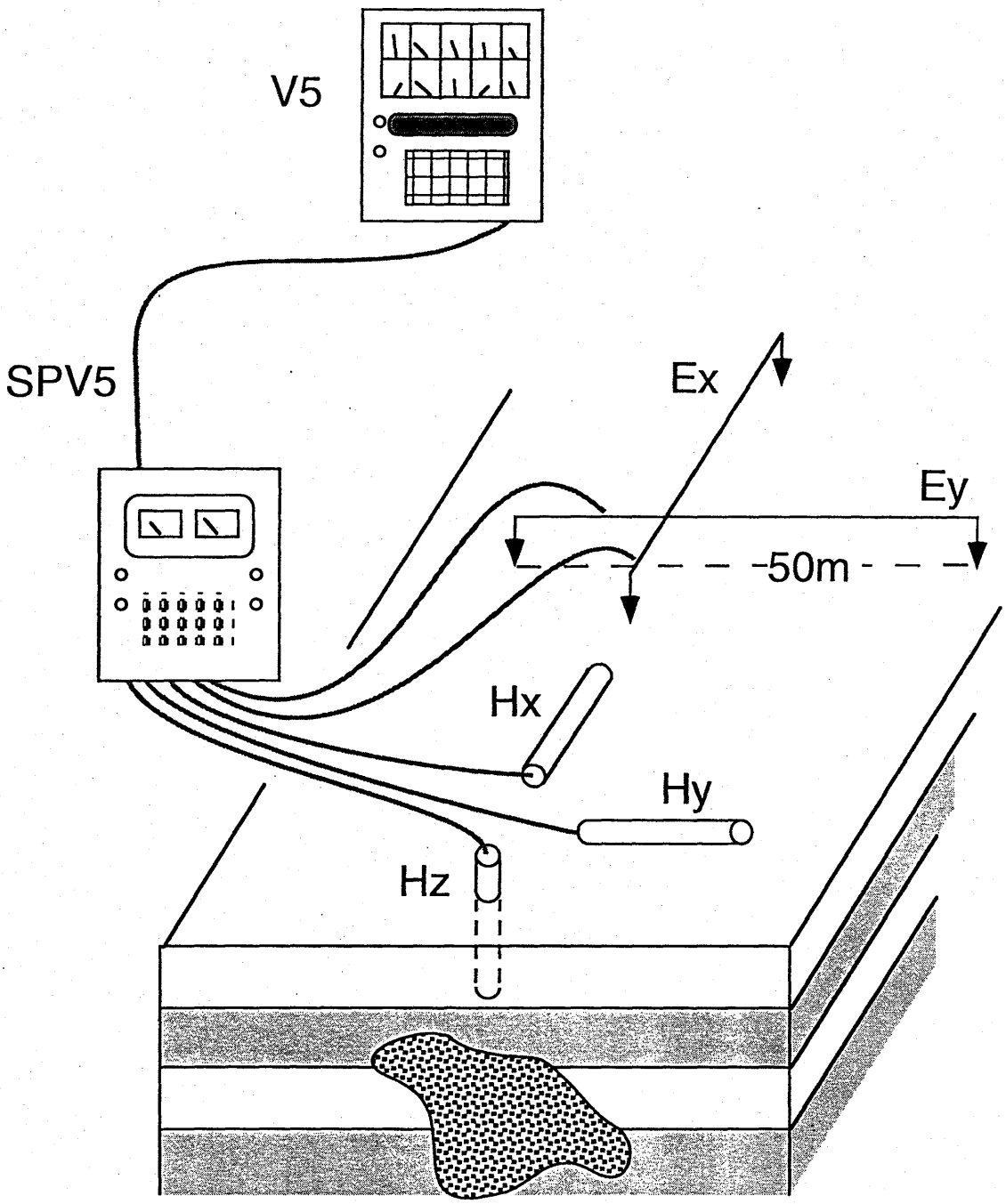

Fig. 3-1

(1) The resistivity model obtained by the inversion method for the TM mode

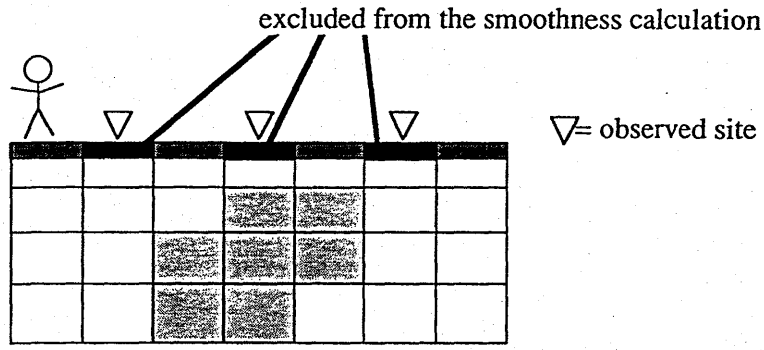

(2) The resistivity model same as (1), but removed the surface layer

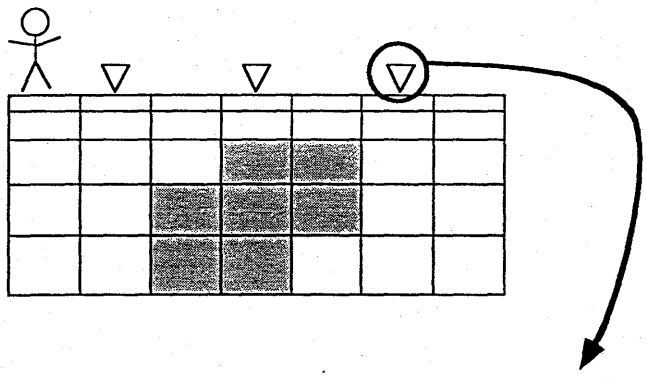

(3) The observed TM apparent resistivity and calculated one from the model (2)

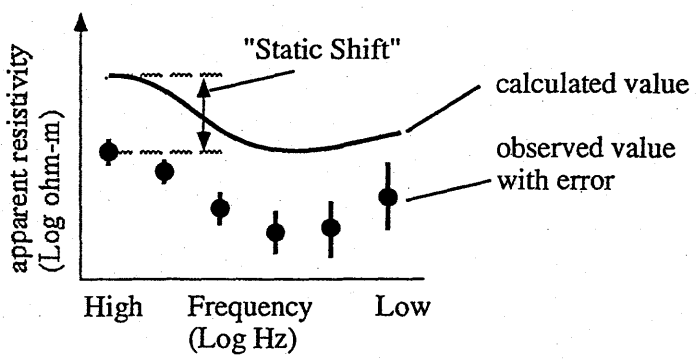

Fig. 3-2

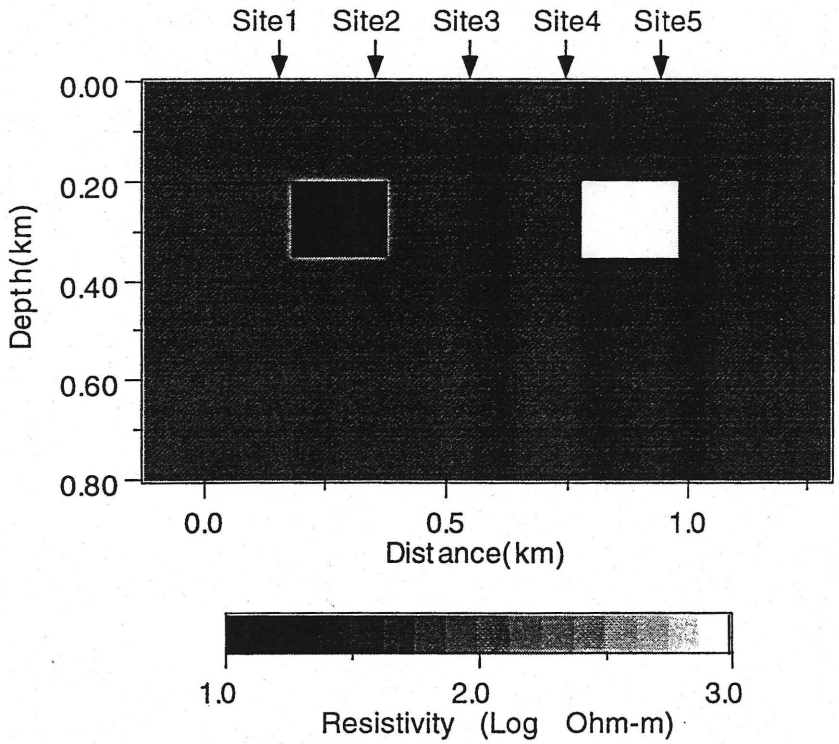
Site1
Site2
Site3
Site4
Site5
0.00
0.20
0.40
0.60
0.80
Depth(km)
0.0
0.5
1.0
Distance(km)
1.0
2.0
3.0
Resistivity (Log Ohm-m)

Fig. 3-3

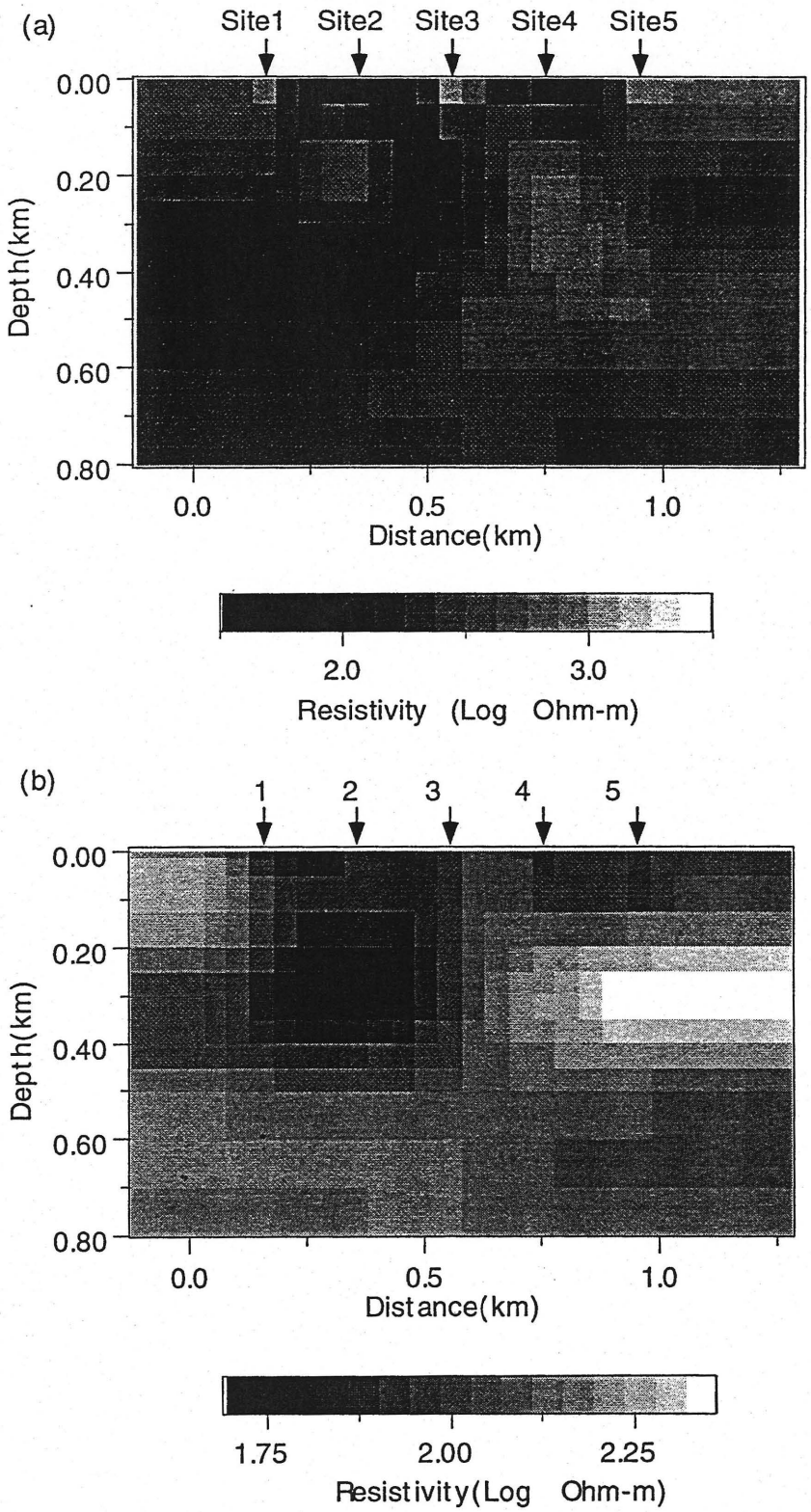
(a)
Site1
Site2
Site3
Site4
Site5
0.00
0.20
0.40
0.60
0.80
Depth(km)
0.0
0.5
1.0
Distance(km)
2.0
3.0
Resistivity (Log Ohm-m)
(b)
1
2
3
4
5
0.00
0.20
0.40
0.60
0.80
Depth(km)
0.0
0.5
1.0
Distance(km)
1.75
2.00
2.25
Resistivity(Log Ohm-m)

Fig.3-4

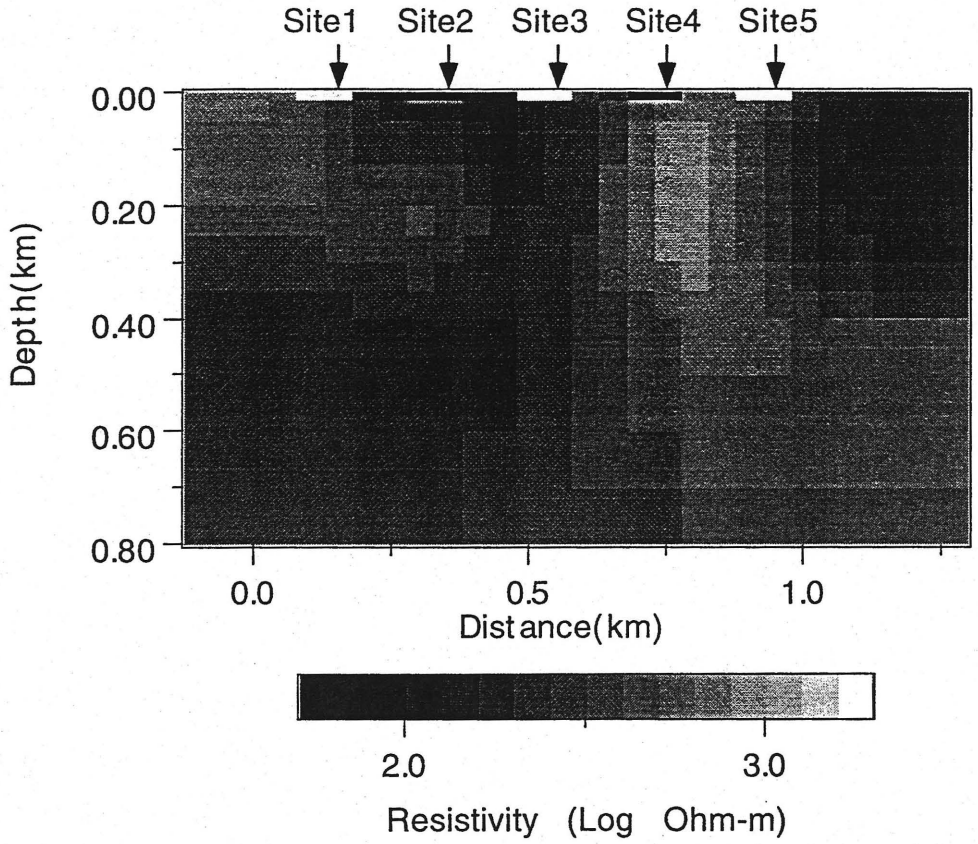
Site1
Site2
Site3
Site4
Site5
0.00
0.20
0.40
0.60
0.80
Depth(km)
0.0
0.5
1.0
Distance(km)
2.0
3.0
Resistivity (Log Ohm-m)

Fig.3-5

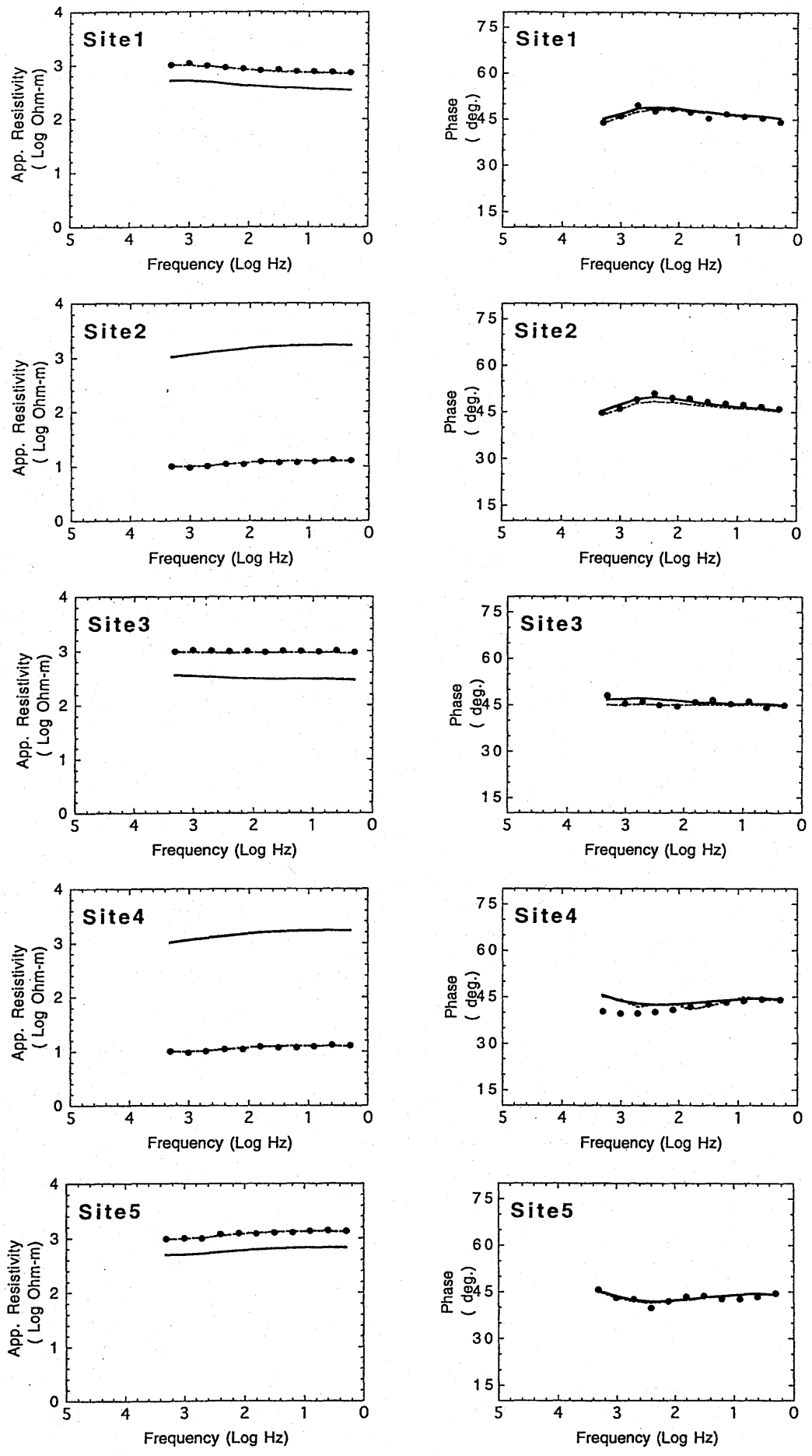
Site1
App. Resistivity (Log Ohm-m)
Frequency (Log Hz)
Site1
Phase (deg.)
Frequency (Log Hz)
Site2
App. Resistivity (Log Ohm-m)
Frequency (Log Hz)
Site2
Phase (deg.)
Frequency (Log Hz)
Site3
App. Resistivity (Log Ohm-m)
Frequency (Log Hz)
Site3
Phase (deg.)
Frequency (Log Hz)
Site4
App. Resistivity (Log Ohm-m)
Frequency (Log Hz)
Site4
Phase (deg.)
Frequency (Log Hz)
Site5
App. Resistivity (Log Ohm-m)
Frequency (Log Hz)
Site5
Phase (deg.)
Frequency (Log Hz)

Fig. 3-6

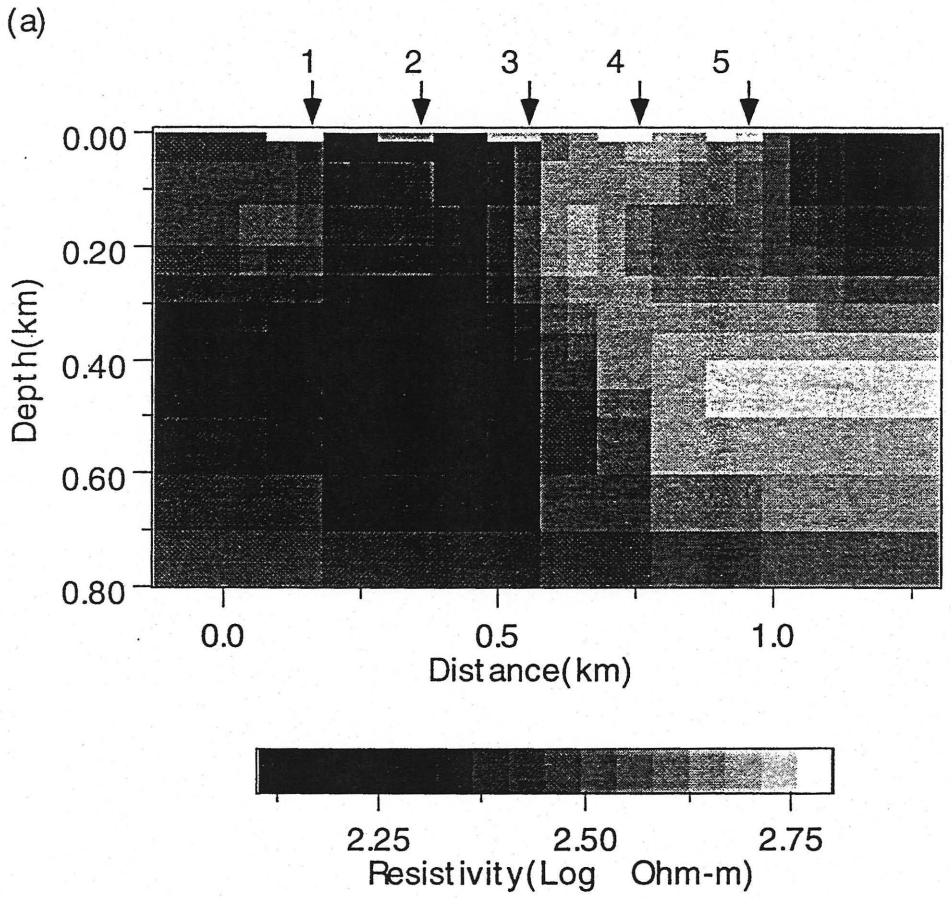
(a)
1
2
3
4
5
0.00
0.20
0.40
0.60
0.80
Depth(km)
0.0
0.5
1.0
Distance(km)
2.25
2.50
2.75
Resistivity(Log Ohm-m)

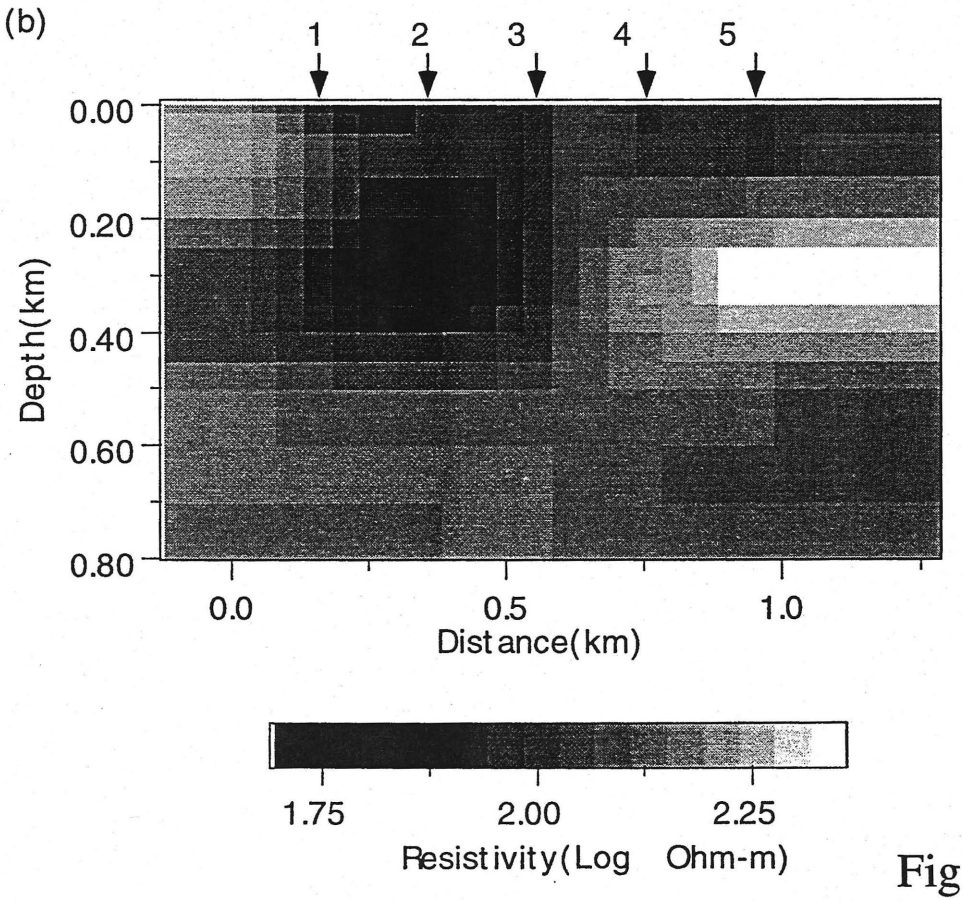
(b)
1
2
3
4
5
0.00
0.20
0.40
0.60
0.80
Depth(km)
0.0
0.5
1.0
Distance(km)
1.75
2.00
2.25
Resistivity(Log Ohm-m)

Fig. 3-7

Observed data Q_{mn} with an error w_{mn}
at site# m, frequency# n

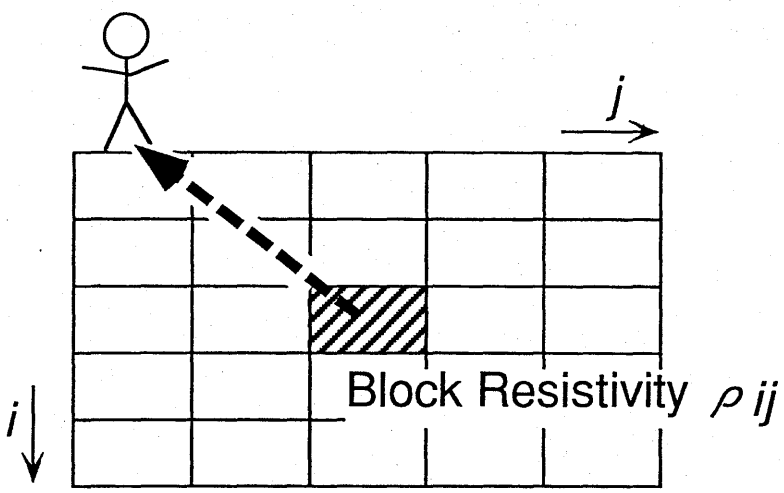

$$\text{Sensitivity} = \max\left(\frac{\partial Q_{mn} / \partial \log(\rho_{ij})}{w_{mn}}\right)$$

Q: logarithmical apparent resistivity or phase

w: standard error of Q

Fig. 3-8

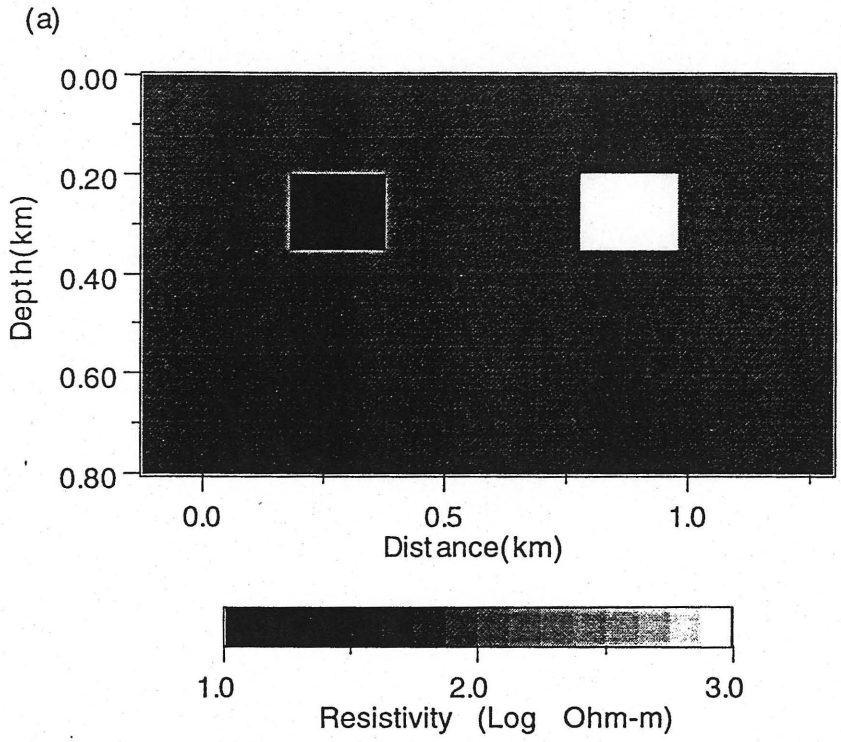
(a)
0.00
0.20
0.40
0.60
0.80
Depth(km)
0.0
0.5
1.0
Distance(km)
1.0
2.0
3.0
Resistivity (Log Ohm-m)

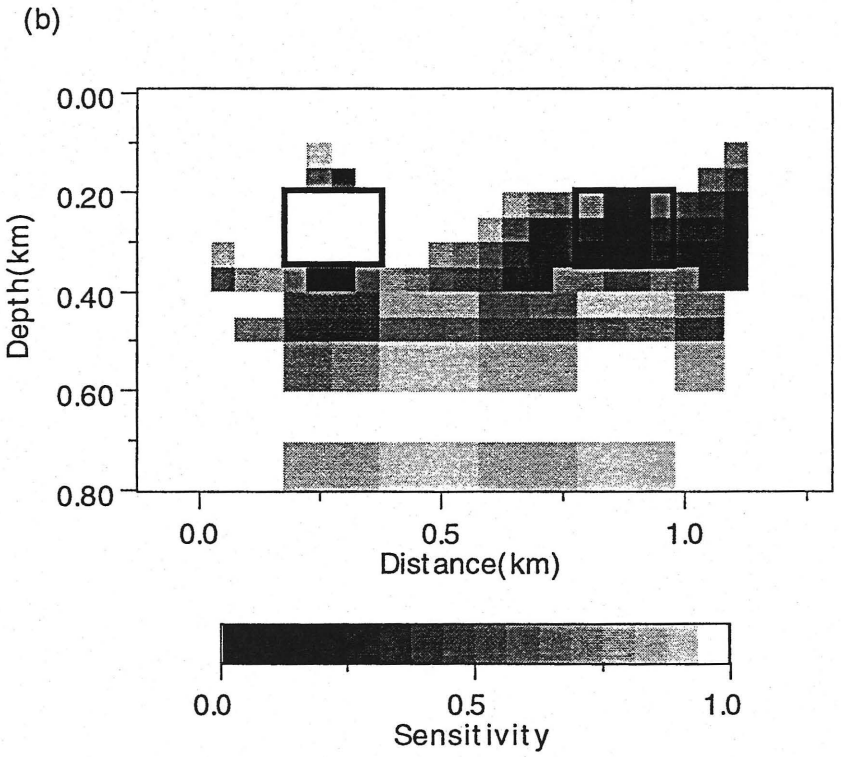
(b)
0.00
0.20
0.40
0.60
0.80
Depth(km)
0.0
0.5
1.0
Distance(km)
0.0
0.5
1.0
Sensitivity

Fig. 3-9

4. Observations and modeling in the Atotsugawa region

4. 1. The Atotsugawa fault

The Atotsugawa fault, which runs and extends longer than 60km in central Japan(Fig. 4-1), is one of the most active faults in Japan (Research Group for Active Faults, 1991). The Atotsugawa fault is a strike-slip fault with a right lateral displacement(Matsuda, 1966; Togo et al., 1983; Okada et al., 1983). According to geological studies, the average rate of displacement is estimated as being more than 1m / 10^3 years. The strike of the fault trace is approximately N60E. The fault plane stands vertically ($90^\circ \pm 10^\circ$) near the surface. The Atotsugawa fault began to move in the latest Tertiary (Matsuda, 1966).

The topographical offset of 3km is found along the fault, which may be regarded as seismic displacements accumulated by repeated large earthquakes since late Tertiary. Mikumo et al.(1988) suggested that large earthquakes have occurred in Quaternary period about 1000 times, and the interval of successive large earthquakes would be about 1000-2000 years. The trenching survey across the Atotsugawa fault (Research Group for Excavation of the Atotsugawa fault, 1983) supported their suggestion of the recurrence interval of large earthquakes. The latest large earthquake of M=7.0 in the Atotsugawa region occurred in 1858, named the Ansei Hida earthquake (Yamazawa, 1929 ; Mikumo et al., 1988).

The seismicity along the Atotsugawa fault is very clearly recognized. The distribution of epicenters around the Atotsugawa region is shown in Fig.4-1.

In Fig. 4-1, two lineaments of epicenters coincide with the Atotsugawa and Ushikubi faults. On the other hand, the seismicity in the adjacent zone, southern side, of these faults is remarkably low. Additionally, the spatial heterogeneity of the seismic activity along the Atotsugawa fault is also clearly recognized (Mikumo et al, 1988, Wada et al, 1996). In the central part of the Atotsugawa fault, the seismicity is rather low as compared with the eastern and the western part of the fault. Mikumo et al.(1988) suggested that the high seismicity at the eastern and western part of the fault may be due to postseismic stress concentration after the 1858 Hida earthquake.

In this area, several geophysical surveys were conducted and showed the discontinuity of the properties of rocks around the Atotsugawa fault. Okubo et al. (1988) constructed the density model based on the gravity data. They found small changes in the gravity anomaly along the fault and concluded that these are due to small density difference around the fault. Okubo et al. (1989) estimated the distribution of the depth of the Curie point isotherm in Japan. It is recognized that the depth of the Curie point isotherm gradually changes around the Atotsugawa fault. Additionally, Hirahara et al. (1986) revealed the three-dimensional seismic velocity structure in central Japan. They showed that the seismic velocity changed at the western part of the Atotsugawa fault. These geophysical studies help us to interpret our resistivity structure inferred from MT soundings.

4. 2. Observation in the Atotsugawa region

We observed natural fluctuations of the electric and magnetic fields around the Atotsugawa region. Observations were carried out in June and August in

1994, and August in 1995. Total number of observation sites is 19. Locations of the sites were shown in Fig. 4-2. We arranged these sites along the two survey lines as shown in Fig. 4-2. The survey line AA' runs across the seismically active portion of the Atotsugawa fault through Kawai village, Gifu prefecture. The survey line BB' runs across the aseismic portion of the Atotsugawa fault through Kamioka city, Gifu prefecture. We used two V5 MT systems and recorded two components of the electric field and three components of the magnetic field at each site for about three days. The total number of stacked cross power is about 20,000 around 1Hz and about 100 around 0.01Hz. The V5 systems worked with the synchronized clocks and were separately set up at least 20km apart, acquiring time series data at the same time. The simultaneous time series data at two sites were used in the remote reference processing each other.

At the northern sites along the survey line BB' , the observed data were disturbed by cultural noise of a rectangular shape. The apparent resistivity and the impedance phase were biased by this noise. An example of the biased apparent resistivity is shown in the upper panel of Fig. 4-3. The apparent resistivity becomes linearly larger below the frequency range of 1Hz. The source of the noise is possibly due to Toyama Local Railway which is operated by DC electricity and just runs about 7km north from the observation site 11, because the time when the noises is observed is from 5: 00AM to 10:30PM and it accords with the operating time of the railway. Then, we analyzed the time series data obtained during the night time, i.e. from 10:30PM to 5:00AM at observation sites 11, 12, 13 and 14. An example of the selectively stacked apparent resistivity is shown in the lower panel of Fig. 4-3. We recognize that the selective stacking resulted in fairly

increasing the quality of the estimated MT parameters.

We checked an effectiveness of the remote reference processing using data of a very far remote station. Although the remote site is separated about 20km from the analyzed site in the Atotsugawa region, the distance of separation may not be so sufficient that artificial noises such as that from DC railway are effectively reduced. So we checked the availability of the remote reference by using the time series data obtained in August, 1995 at the Mineyama observatory of Disaster Prevention Research Institute, Kyoto University. The Mineyama observatory is located at northern Kyoto prefecture and about 200km west far from the Atotsugawa region. The data at Mineyama was collected by another V5 MT system synchronized with the V5 MT systems set up in the Atotsugawa region. Two type of the apparent resistivity calculated with the remote reference method for Site 11 were shown in Fig. 4-4 for example. One was obtained with using data set at Mineyama and another was obtained with using data set at Site 4 as a remote reference data set. Since the two curves of the apparent resistivity are very similar, we can conclude that a remote site separating about 20km from an analyzed site is sufficient in the Atotsugawa region.

We carried out an AMT (audio-magnetotelluric) measurement at observation site 14 to investigate the shallow resistivity structure near the Atotsugawa fault. V5 MT system was also used for the AMT sounding. The covered frequency for the AMT sounding ranges from 10kHz to about 1Hz. The system installs a high sampling A/D converter (500kHz) and three induction coils were replaced with shorter ones, which is more sensitive for the frequency band in the AMT sounding The observed magnetic and electric

fields were processed with the technique of the Cascade decimation (Wight and Bostick, 1980) on the site. Then, calculated cross powers and MT parameters were stored. Time series data of the AMT sounding are not stored, so the remote reference processing was not carried out in the AMT sounding.

For the procedure of modeling, we have to reject poor quality impedances. In the following procedure, we used impedances of a small error, which is represented by percentage error of the apparent resistivity less then 100% and a error of the phase less than 30 degrees. We also checked the data quality using the multiple coherency (Fig.4-10). The majority of multiple coherency was greater than 0.8, and impedances with a high quality were selected during the frequency range between 400Hz and about 0.01Hz.

4. 3. Strike direction and induction arrow

The strike directions were calculated with the method of Chakridi et al. (1992). The distribution of the strike direction was averaged in the whole frequencies at each site , and is shown in Fig. 4-5. The strike tends to NNW-SSE or ENE-WSW direction approximately. The average strikes at 1-0.01Hz along the profiles AA' and BB' are N10W and N45W, respectively. The frequency dependence of the strike is shown in Fig. 4-6 with a rose diagram. The strike is not stable at a frequency range of 10 - 1Hz. This means that the three-dimensional inhomogeneity exists at shallow depths. However, the strike is stable at a frequency range from 1 - 0.01Hz. The sounding depth at a frequency of 1Hz is greater than 10km considering the

skin depth and the averaged apparent resistivity at that frequency. We infer that the strike of NNW-SSE or ENE-WSW is the regional strike of a resistivity structure of the crust.

The induction arrows are also calculated around the Atotsugawa region. The distributions at some representative frequencies are shown in Fig. 4-7. The average directions along each profile are also shown in the figure. Generally, the induction arrows around the Atotsugawa region tends to the NNW-SSE direction.

The skewness is small around the target area, especially along the profile BB'. The skewness along the BB' is lower than 0.3 (see Fig.4-10) Then, we consider that the resistivity structure beneath the profile BB' is approximately two-dimensional. The skewness along the profile AA' is lower than 0.4 except for Site 8, which is larger than along the BB'. It is inferred from the skewness that the three-dimensional inhomogeneity of the resistivity exists beneath the profile AA'. However, the distribution of the strike shows a stable direction at the frequency of 1 - 0.01Hz, especially at Site 8. It is judged that the 3-D inhomogeneity may exist near the surface or a shallow depth, and that the resistivity structure along the AA' is also regionally two-dimensional. Considering the coincidence of the strikes, the induction arrows and the geological strike, the regional strike of the resistivity structure is regarded being N30W along the both profiles.

4. 4. The apparent resistivity and the phase

The observed apparent resistivity and the impedance phase along the profiles AA' and BB' are shown in Fig. 4-8 and 4-9. Note again that the impedance phase is called "phase" simply. In these figures, N30W is taken as the x axis of the coordinate system and N60W as the y axis. Both the apparent resistivities, ρ_{xy} and ρ_{yx}, do not have the same value but show splitting at higher frequencies. This splitting of the apparent resistivity curve implies the existence of the static-shift effect.

The apparent resistivity and the phase changes sharply near the Atotsugawa fault. At the northern sites of the fault (Sites 4, 5, 6, 8, and 2), increasing of the apparent resistivity is clearly recognized in both ρ_{xy} and ρ_{yx} with decreasing of the frequency. On the other hand, the apparent resistivity decreases as the frequency increases at the southern sites of the fault (Sites 9, 3, 1, and 19). Since the averaged strike directions at Sites 6, 2, 9, 1 and 3 are similar with each other, the rotation of the impedance does not affect this sharp change of the apparent resistivity. The phase values also show the different feature between the northern and southern areas of the Atotsugawa fault. The phases of the both axes (ϕ_{xy} and ϕ_{yx}) at the northern sites of the fault show phase values smaller than 45 degrees at the frequency higher than 1Hz. The phases at the southern sites show values higher than 45 degrees at the corresponding frequency. These sharp changes of both the apparent resistivity and the phase near the Atotsugawa fault imply that the resistivity of the underlying layer beneath the surface is high in the northern area of the Atotsugawa fault and low in the southern area. In other word, the Atotsugawa fault seems to be a resistivity boundary.

On the contrary of the profile AA', the apparent resistivities and the phases

along the BB' are very similar with each other. The apparent resistivities at all sites along BB' increase around a frequency of 10Hz and decrease around 0.1Hz. Similarly, the phase at all sites along BB' decreases around 10Hz and increases around 0.1Hz. This feature may indicates that the underlying resistivity layer widely spread beneath the profile BB'. Additionally, it is noteworthy that a very high value of the phase ($\approx$60 degrees for ϕ_{xy}, and $\approx$ 75 degrees for ϕ_{yx}) around a frequency of 0.1Hz is found at the southern sites of the Atotsugawa fault (Sites 15, 17 and 18).

The apparent resistivity and the phase obtained by the AMT sounding at Site 14 on the profile BB' is shown in Fig. 4-11. The apparent resistivity is about 130 Ω m at the frequency of 10kHz, which is a similar value at the highest frequency of the MT sounding. These responses are used for the static-shift correction in the following process of modeling.

4. 5. Modeling for the Atotsugawa profiles

We construct the two-dimensional(2-D) resistivity structure models beneath the profiles AA' and BB'. In the Atotsugawa region, particularly along the profile AA', three-dimensional heterogeneity of resistivity may exist. We used the apparent resistivity and the phase of the TM mode in the process of modeling because the TM mode gives a good approximation for a three-dimensional resistivity structure (Ting and Hohmann, 1981). The inverse method used here was developed by Uchida and Ogawa(1993). The width of the 2-D model is taken to be about 1400km and the bottom depth is taken to be 1900km. The 2-D model is constructed using elements of horizontally about 70 and vertically 33. The horizontal size of each block is 0.8km near the Atotsugawa fault and becomes wider near the edge. The vertical size also

becomes thicker as a depth of a block increases. About 400 unknown parameters of the resistivity are assigned to these elements. The mesh in modeling used for the Atotsugawa region is shown in Fig. 4-12. An uniform earth of 1000 Ω m is chosen as an initial model for the inversion. We changed the background resistivity of the initial model and found that the resistivity of the initial model did not so affect the final model.

There are two steps for the correction of the static shift, as described in Chapter 3. In the first inversion, the surface block beneath each site are not included in the calculation of the smoothness. As a result, the static-shift factor which is a bias error of the apparent resistivity is estimated at each site. Along the profile AA', the factor is maximum (0.2) at Site 8 and minimum (-1.1) at Site 6. And the factor along BB' is ranging from 0.1 (at Site 11) to -0.4 (at Site 14). As the static shift along each profile still remains a little, it can be checked by comparing with AMT data. On the basis of the AMT sounding at Site 14, the apparent resistivity is 130 Ω m at about 10kHz. We applied the Bostick inversion (Bostick, 1977) to the data and estimated the resistivity to be 140 Ω m at about 50m in depth. Then, in the first inversion to estimate the static shift factors, we fixed the resistivity of the surface block beneath Site 14 as 140 Ω m and recalculated the static shift factor at sites along BB'. And we compared this with the calculated static shift factor under the condition that all resistivities of the model are treated as free parameters in the inversion. As a result, the static shift factors calculated were similar without regard to the fixed or the free condition for the surface resistivity at Site 14. It seems therefore that the average static shift along BB' is considered to be small. The good correlation of structures between the resistivity and the seismic P-wave velocity along BB', described in the later

chapter, also supported that the correction of the static shift proposed is effective. On the other hand, the averaged static shift factor along the profile AA' are not calculated because there are no information on the surface resistivity at observation sites along AA'. However, the VLF-MT sounding, which is one of the MT sounding and whose frequency is about 20kHz, were carried out near AA'. Nakayama (1995, pers. comm.) measured the surface resistivity near the Atotsugawa fault around Miyagawa, located about 10km east from Site 2. He found that the averaged apparent resistivity near the fault was about 300 Ω m. This value is very similar to that of the surface resistivity at Site 2, near the Atotsugawa fault, obtained by the result of the first inversion. So, we conclude that the averaged static shift is also small along the profile AA'. At least, the resistivity of the two-dimensional model along AA' may be higher than the determined value shown in Fig. 4-16, described later, because all sites are located on the alluvium which shows lower resistivity than the underlying basic rocks and makes a negative static-shift effect.

The inverse process is very stable and yields the most probable model with 10 iterations of the algorithm. First, the most probable model along the profile AA' is shown in Fig. 4-13. The numbers of iteration for the first and second inversions are both four. This model well explains the observed apparent resistivity and phase. The apparent resistivities and the phases calculated from the model in Fig. 4-13 are shown in Fig. 4-14 together with observed responses. We showed the sensitivity of the model in Fig. 4-15. Although the sensitivity indicates that the resolution is comparatively low beneath the Atotsugawa fault, the sensitivity is enough high to discuss the physical property of rocks in the following chapters.

The most remarkable and well-resolved feature in the model is probably the existence of the vertical boundary of resistivity near the Atotsugawa fault. The boundary cut the upper crust from the surface to a depth of 15km at least and discriminated the northern resistive zone (> about 3000Ω m) from the southern relatively conductive zone(< about 3000Ω m). The tendency, that the northern side of the fault is resistive and the southern side is conductive, is also expected from the observed data only. That is, the apparent resistivity becomes higher in lower frequencies at the northern sites of the Atotsugawa fault and becomes lower at the southern sites. The most suitable model along AA' shown in Fig. 4-13 is consistent with this feature.

An additional feature in the suitable model along the profile AA' is also found. There exists a resistive body beneath the northern area of a width of 7km from the Atotsugawa fault. Sites 6 and 8 ,showing the lowest phase along AA', are sensitive to this resistive body. These low phases are not explained well without existence of such a resistive body. The calculated response does not still satisfy the low phase at about 10Hz on Site 6. The resistive body, however, may have higher resistivity value. Otherwise, a small-scale and three-dimensional resistivity anomaly may underlie near Site 6 because the resistivity strike at Site 6 tends to a different direction as compared with Sites 5 and 8 (see Fig. 4-6). The resistivity beneath Sites 4 and 5 become comparatively low as compared to beneath Site 6. So, there also exists a vertical boundary of resistivity near the place at 7km north from the Atotsugawa fault, which is a smaller gap compared with the Atotsugawa fault.

Next, the final model of resistivity for the profile BB' is shown in Fig. 4-16. The numbers of iterations for the first and second inversions are 7 and 8, respectively. The fitness of the calculated apparent resistivities and phases to the observed ones is better than that of the model along AA'. The apparent resistivities and the phases calculated from the model shown in Fig. 4-16 are shown in Fig. 4-17 together with observed responses. We also shows the sensitivity of the model in Fig. 4-18. It is concluded that the resistivity of the model is well-resolved , especially in the southern area along the profile BB'.

In the most suitable model along the profile BB' , two features are obvious. One is that the resistive layer ($> 1000\,\Omega$ m) underlies widely beneath the area of the profile BB' at a depth of about 3km. Another feature is that there exists the conductive layer ($< 300\,\Omega$ m) below the depth of about 10km in the southern side of the Atotsugawa fault. The widely spreading resistive layer becomes more resistive especially beneath Sites 14 (on the Atotsugawa fault) and 18. This resistive layer is also expected from the observed feature that the apparent resistivity and the phase along BB' is very similar to those along the profile AA'. The deep conductive layer is also expected from the observed high phase value (≈ 60 degrees for ϕ_{xy}, and ≈ 75 degrees for ϕ_{yx}) at 0.1Hz

Fig. 4-1 The distribution of the epicenter around the Atotsugawa region. Lines indicate locations of active faults.

Fig. 4-2 Locations of sites(Circles) and the Atotsugawa fault(the edge is indicated by the triangles). Dashed lines indicate the surveying profiles in this study.

Fig. 4-3 (a) An example of the biased apparent resistivity. The apparent resistivity at the frequencies lower than 1Hz is strongly distorted. (b) the selectively stacked apparent resistivity

Fig. 4-4 Two apparent resistivities at Site 11 calculated with the remote reference method. Circle : the reference site is located in the Atotsugawa region. Cross: the reference site is located to about 200km far west from Site 11

Fig. 4-5 The distribution of the strike direction averaged in the whole frequencies at each site

Fig. 4-6 The stability of the strike in regard to the frequency
(a) for the profile AA', (b) for the profile BB'

Fig. 4-7 The induction arrows around the Atotsugawa region. Circles mean the location of the site. Bars tend to the " conductive" zone.

Fig. 4-8 (a)The observed apparent resistivity and (b)the impedance phase along the profile AA'

Fig.4-9 (a)The observed apparent resistivity and (b)the impedance phase

along the profile BB'

Fig. 4-10 The observed multiple coherency between the electric field and the magnetic field. Skewness is also shown in the figure.

Fig. 4-11 The apparent resistivity and the phase obtained by the AMT sounding at site 14, on the profile BB'

Fig. 4-12 The mesh in modeling used for the Atotsugawa region

Fig. 4-13 The two-dimensional most suitable resistivity model along the profile AA'. The locations of the site of our MT measurements are indicated by arrows and the location of the Atotsugawa fault is indicated by an solid red triangle. In addition, location of the Ushikubi fault is indicated an open red triangle.

Fig. 4-14 The apparent resistivities(a) and the phases(b) calculated from the model in Fig. 4-13(solid lines) together with the observed ones (circles)

Fig. 4-15 The sensitivity of the model in Fig. 4-13

Fig. 4-16 The two-dimensional suitable resistivity model along the profile BB'. The locations of the Yokoyama thrust type fault is indicated by an open blue triangle. Further details is shown in the caption of Fig. 4-13.

Fig. 4-17 The apparent resistivities(a) and the phases(b) calculated from the model in Fig. 4-16(solid lines) together with the observed ones

(circles)

Fig. 4-18 The sensitivity of the model in Fig. 4-16

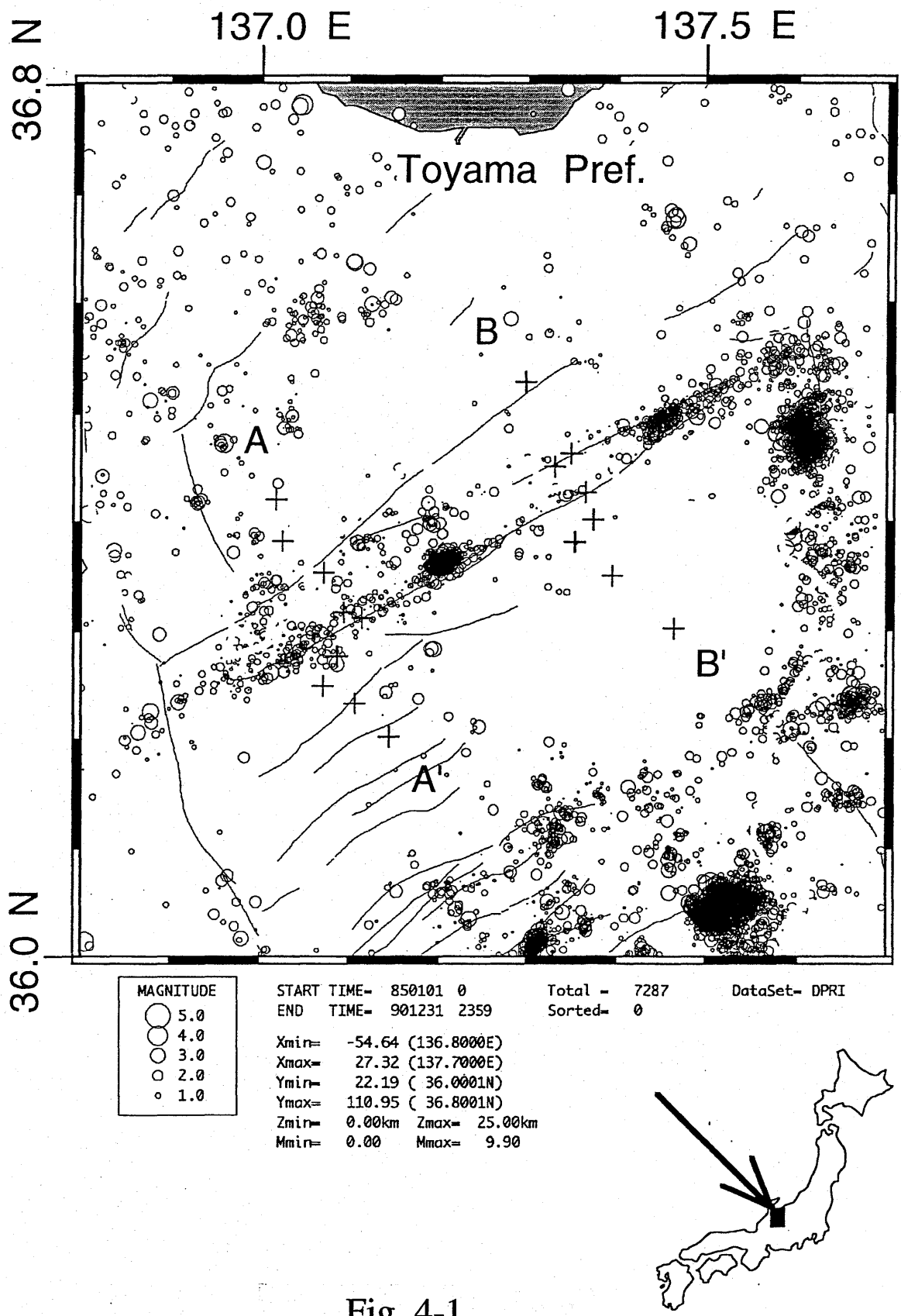
137.0 E
137.5 E
36.8 N
36.0 N
Toyama Pref.
A
A'
B
B'
MAGNITUDE
5.0
4.0
3.0
2.0
1.0
START TIME= 850101 0
END TIME= 901231 2359
Total = 7287
Sorted= 0
DataSet= DPRI
Xmin= -54.64 (136.8000E)
Xmax= 27.32 (137.7000E)
Ymin= 22.19 (36.0001N)
Ymax= 110.95 (36.8001N)
Zmin= 0.00km Zmax= 25.00km
Mmin= 0.00 Mmax= 9.90

Fig. 4-1

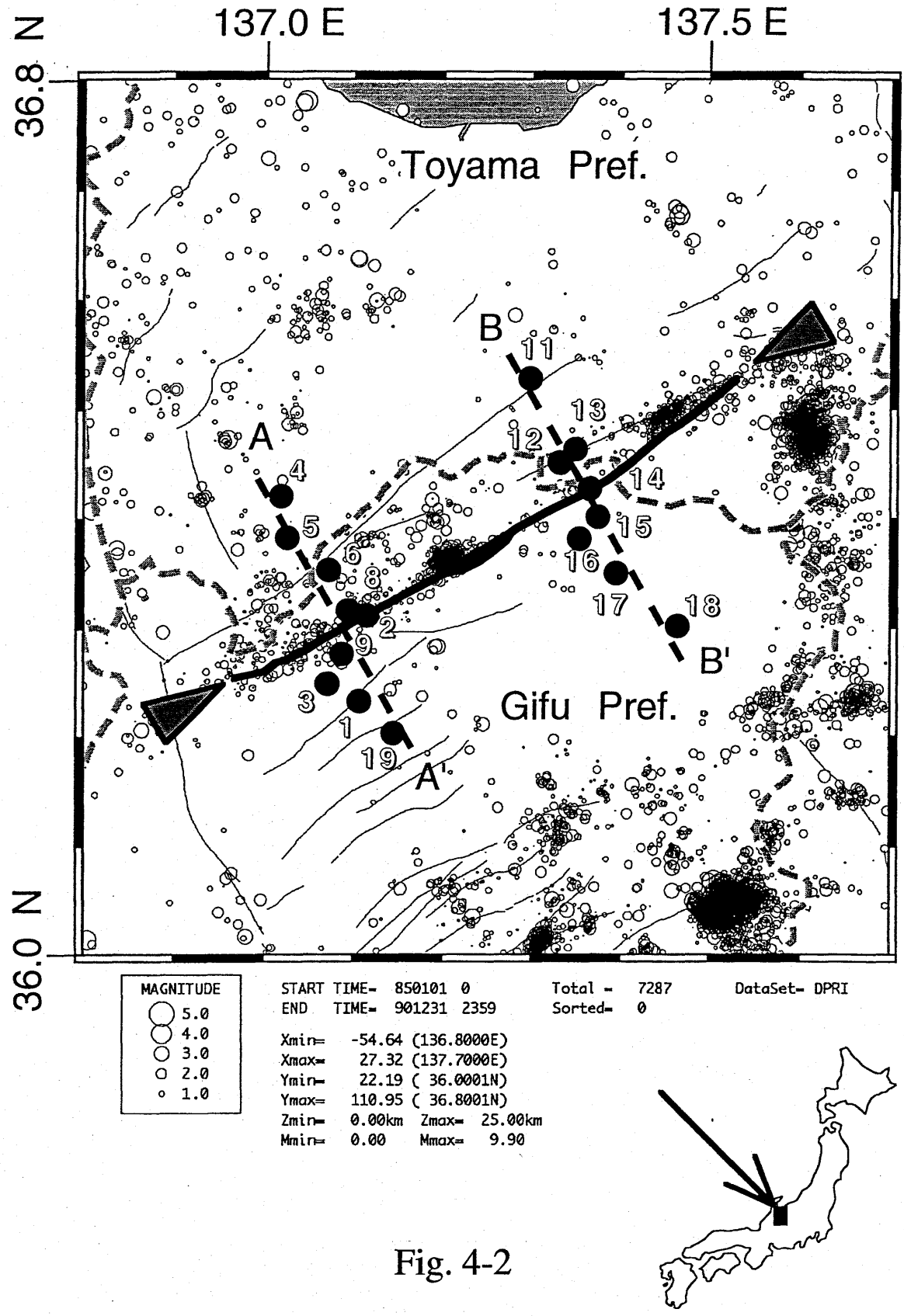
137.0 E
137.5 E
36.8 N
36.0 N
Toyama Pref.
Gifu Pref.
A
A'
B
B'
1
2
3
4
5
6
8
9
11
12
13
14
15
16
17
18
19
MAGNITUDE
5.0
4.0
3.0
2.0
1.0
START TIME= 850101 0
END TIME= 901231 2359
Total = 7287
Sorted= 0
DataSet= DPRI
Xmin= -54.64 (136.8000E)
Xmax= 27.32 (137.7000E)
Ymin= 22.19 (36.0001N)
Ymax= 110.95 (36.8001N)
Zmin= 0.00km Zmax= 25.00km
Mmin= 0.00 Mmax= 9.90

Fig. 4-2

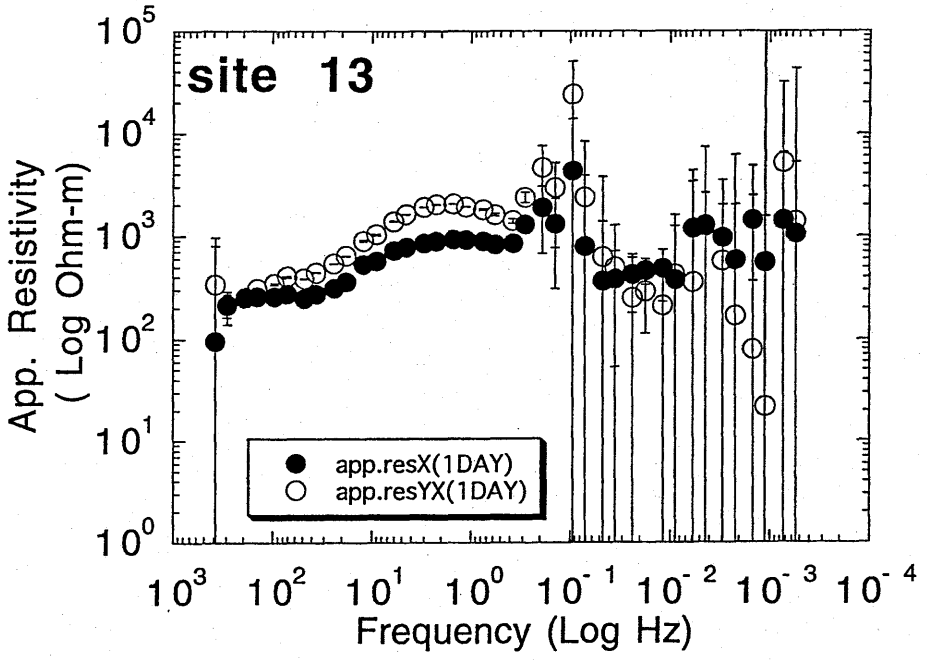
site 13
App. Resistivity
(Log Ohm-m)
10^5
10^4
10^3
10^2
10^1
10^0
app.resX(1DAY)
app.resYX(1DAY)
10^3 10^2 10^1 10^0 10^{-1} 10^{-2} 10^{-3} 10^{-4}
Frequency (Log Hz)

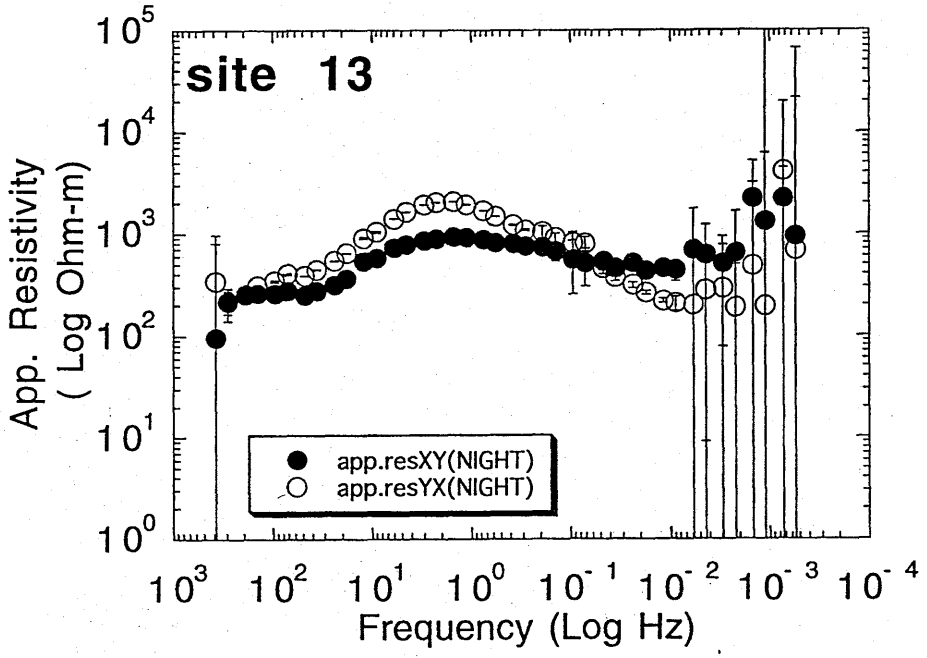
site 13
App. Resistivity
(Log Ohm-m)
10^5
10^4
10^3
10^2
10^1
10^0
app.resXY(NIGHT)
app.resYX(NIGHT)
10^3 10^2 10^1 10^0 10^{-1} 10^{-2} 10^{-3} 10^{-4}
Frequency (Log Hz)

Fig. 4-3

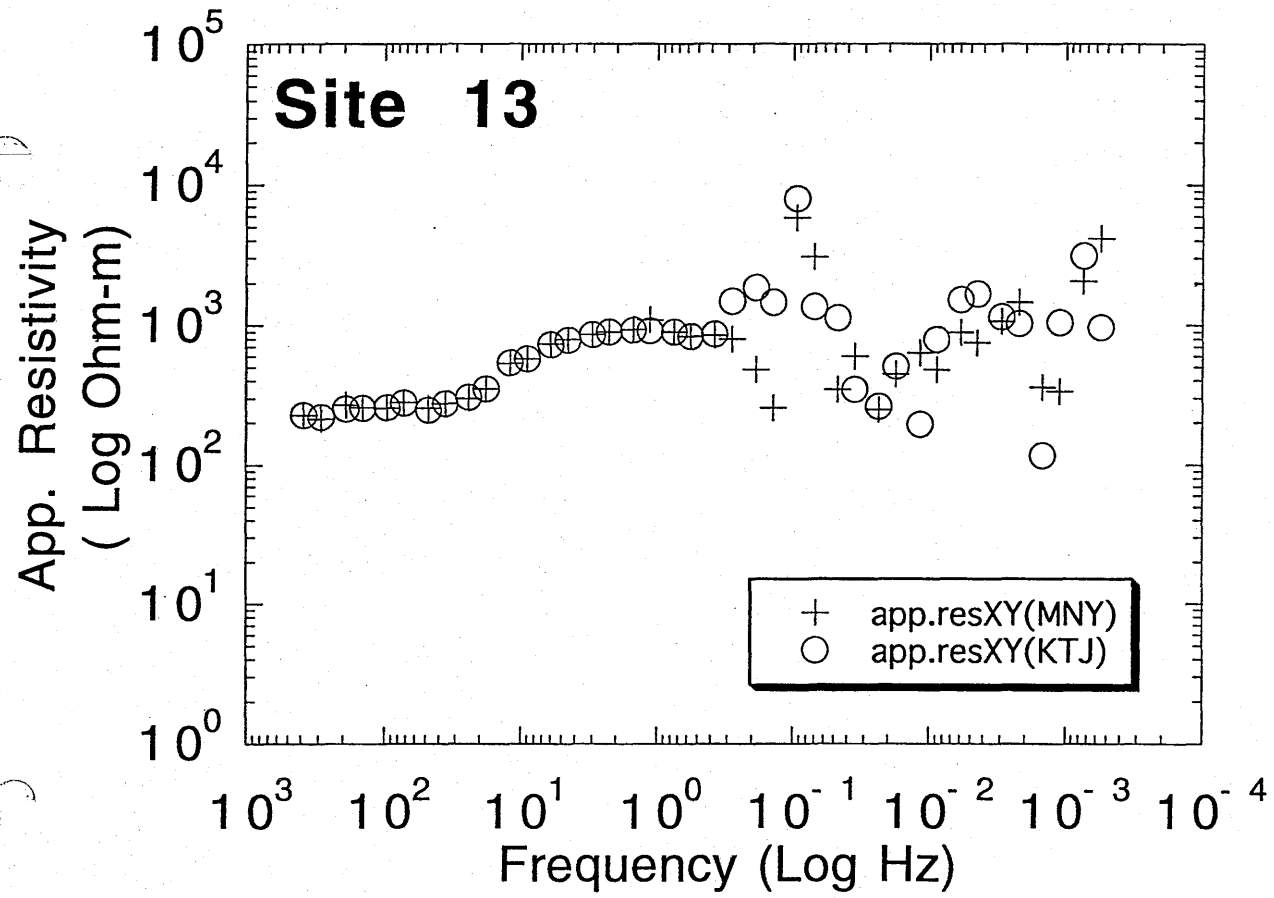
Site 13
App. Resistivity
(Log Ohm-m)
10^5
10^4
10^3
10^2
10^1
10^0
10^3 10^2 10^1 10^0 10^-1 10^-2 10^-3 10^-4
Frequency (Log Hz)
app.resXY(MNY)
app.resXY(KTJ)

Fig. 4-4

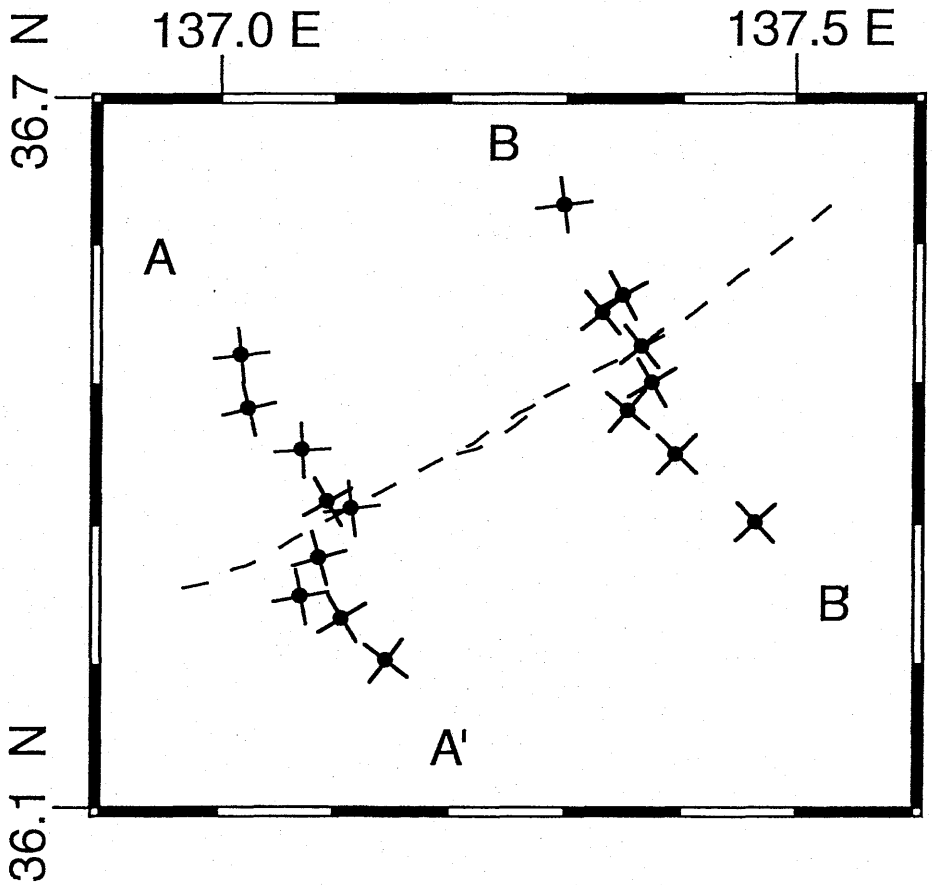

Fig. 4-5

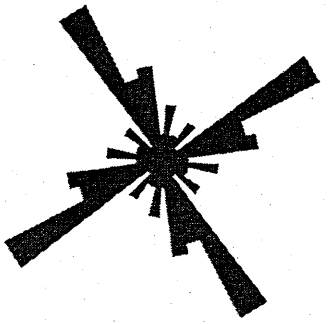

100 - 10 Hz

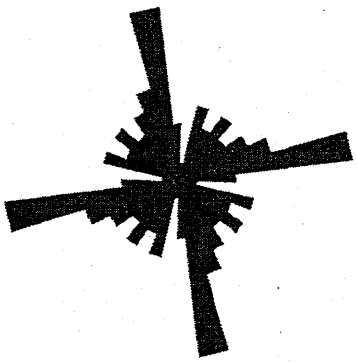

0.1 - 0.01 Hz

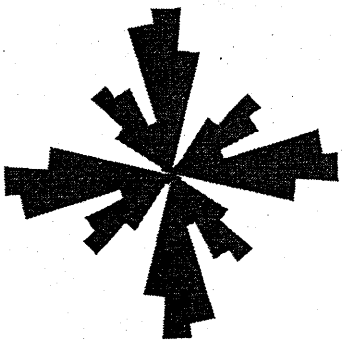

10 - 1 Hz

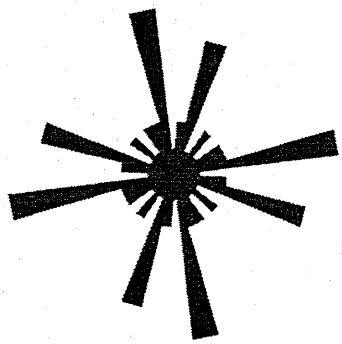

0.01 - 0.0005 Hz

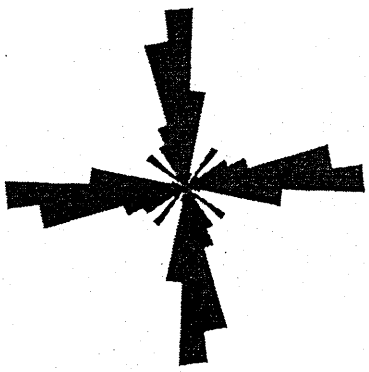

1 - 0.1 Hz

Profile AA'

Fig. 4-6(a)

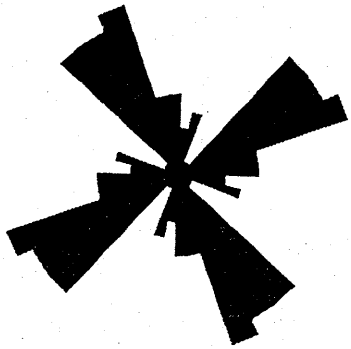

100 - 10 Hz

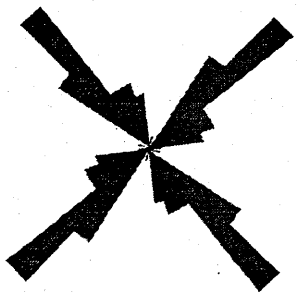

0.1 - 0.01 Hz

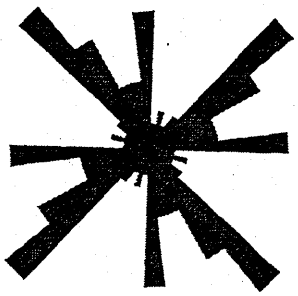

10 - 1 Hz

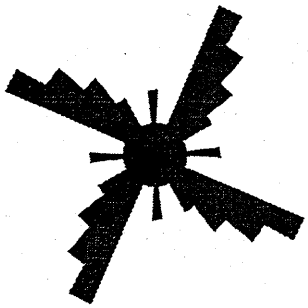

0.01 - 0.0005 Hz

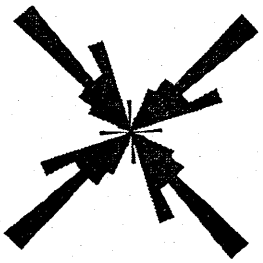

1 - 0.1 Hz

Profile BB'

Fig. 4-6(b)

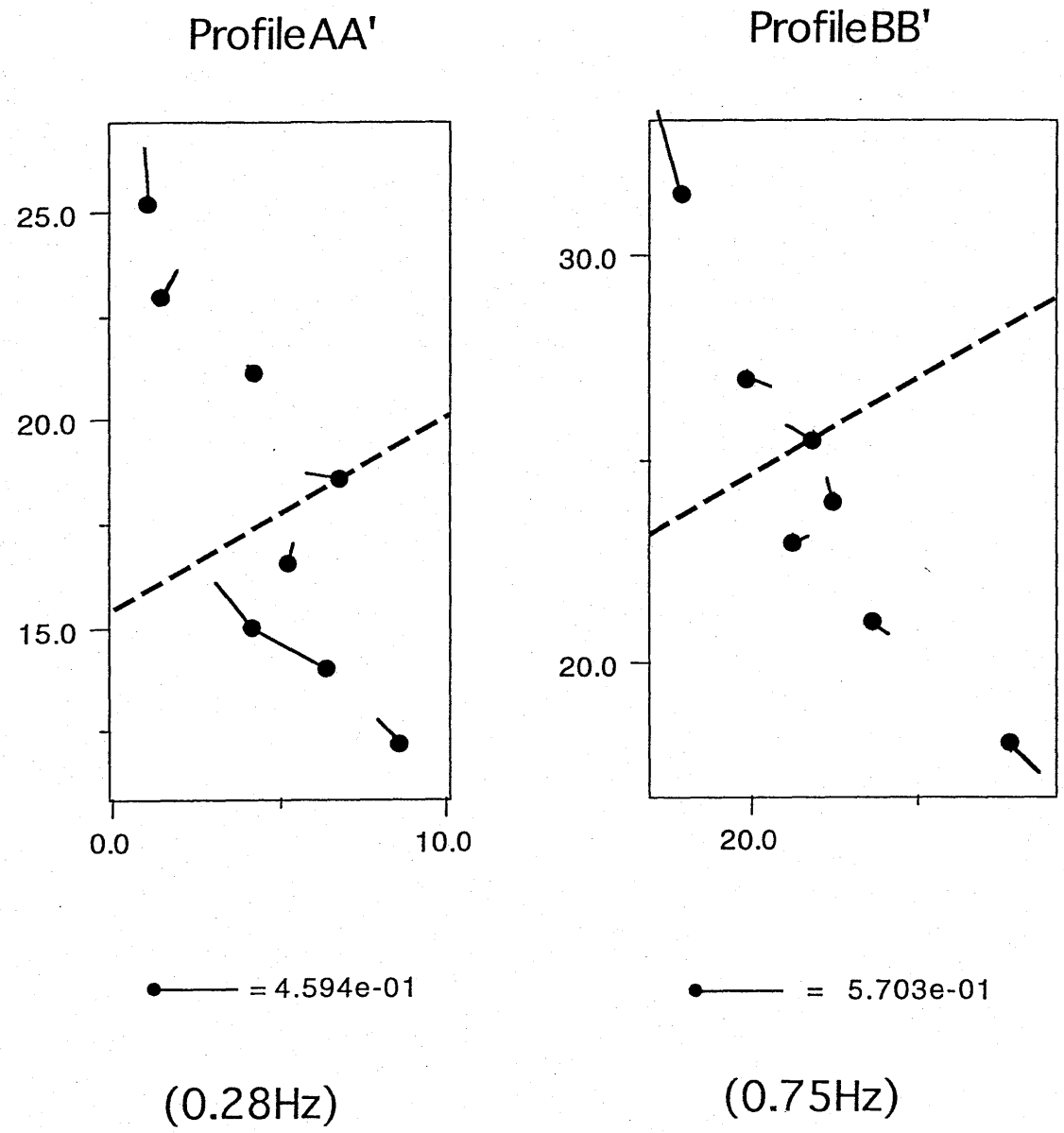
ProfileAA'
ProfileBB'
25.0
20.0
15.0
0.0
10.0
30.0
20.0
20.0
= 4.594e-01
= 5.703e-01
(0.28Hz)
(0.75Hz)

Fig. 4-7

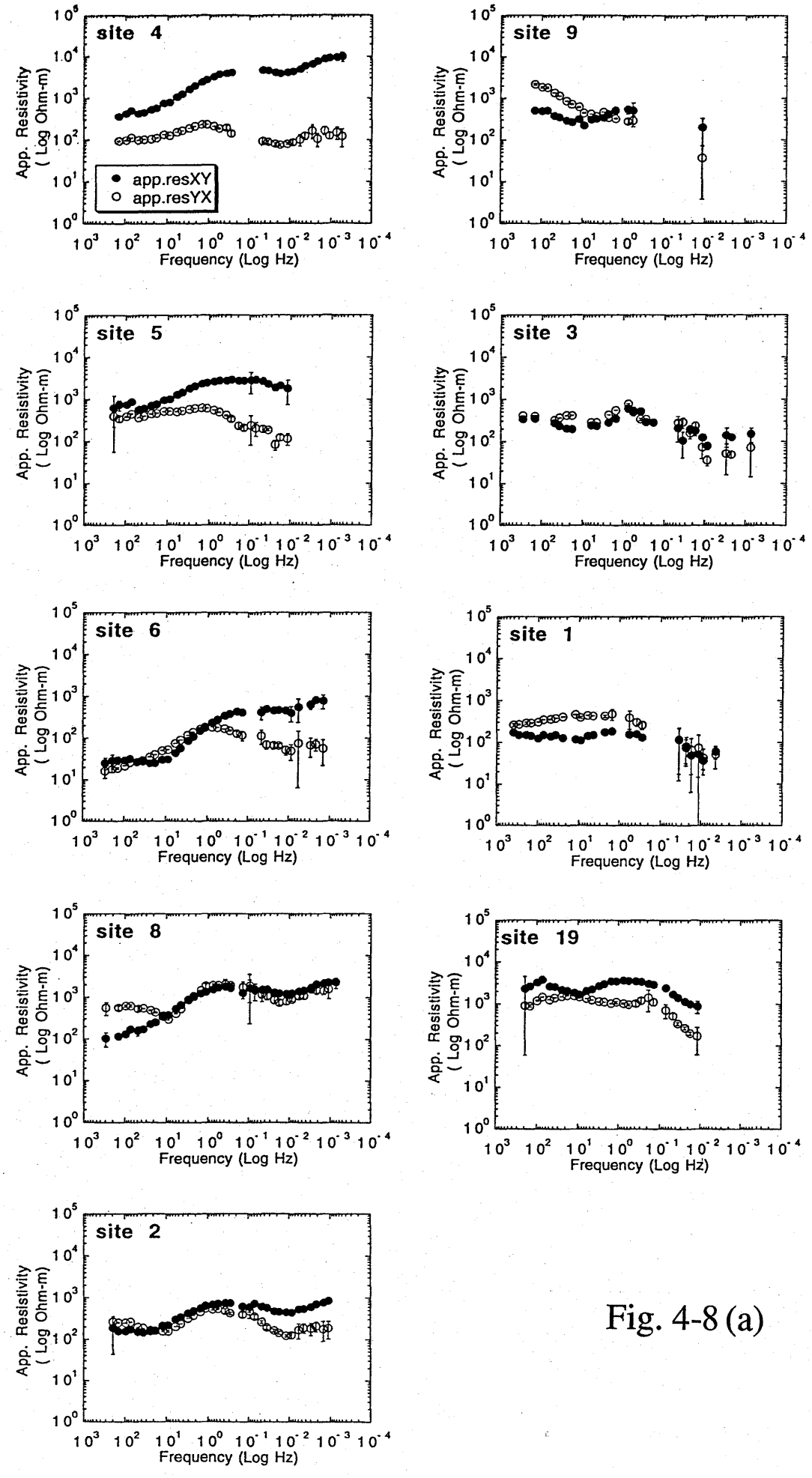
site 4
app.resXY
app.resYX
site 9
site 5
site 3
site 6
site 1
site 8
site 19
site 2
App. Resistivity (Log Ohm-m)
Frequency (Log Hz)

Fig. 4-8 (a)

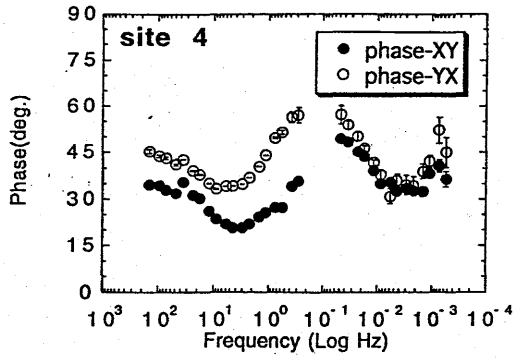
site 4
phase-XY
phase-YX
Phase(deg.)
Frequency (Log Hz)

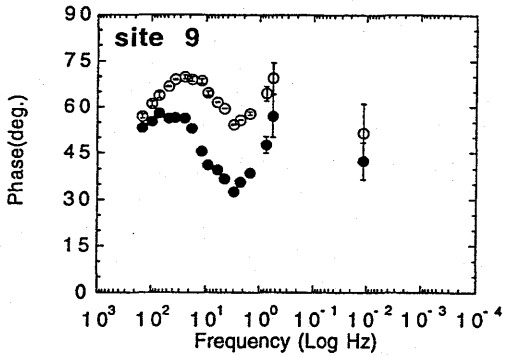
site 9
Phase(deg.)
Frequency (Log Hz)

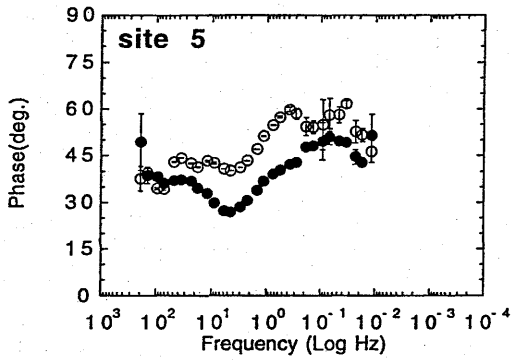
site 5
Phase(deg.)
Frequency (Log Hz)

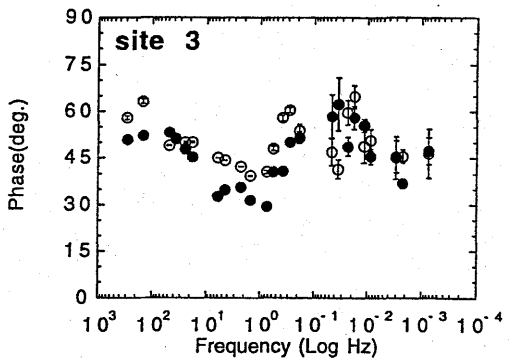
site 3
Phase(deg.)
Frequency (Log Hz)

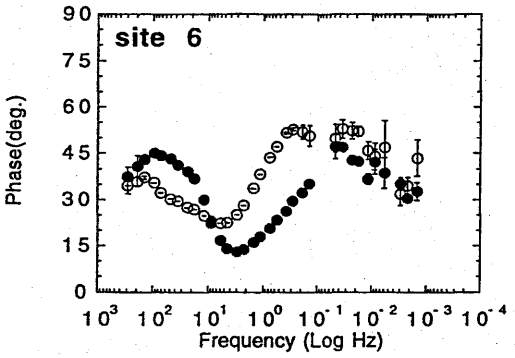
site 6
Phase(deg.)
Frequency (Log Hz)

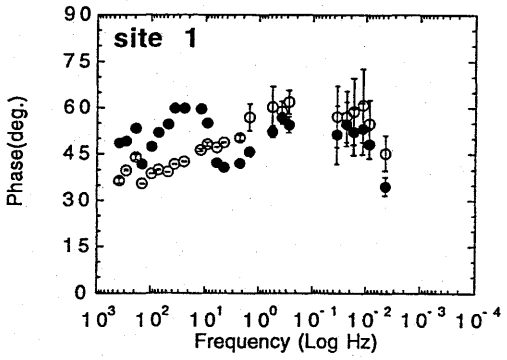
site 1
Phase(deg.)
Frequency (Log Hz)

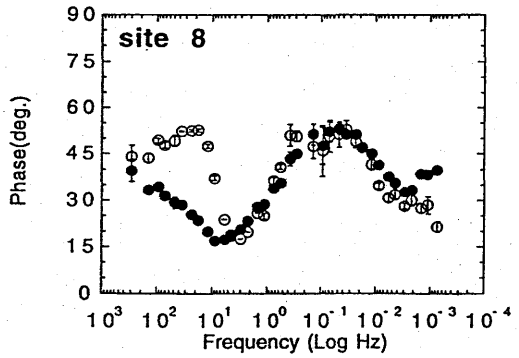
site 8
Phase(deg.)
Frequency (Log Hz)

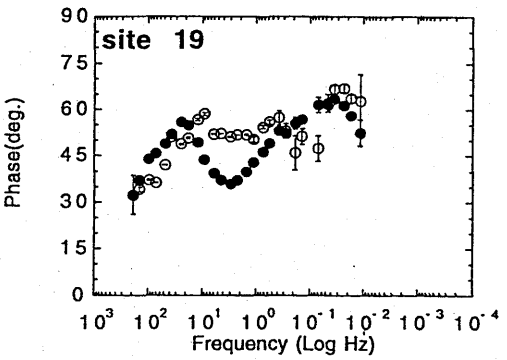
site 19
Phase(deg.)
Frequency (Log Hz)

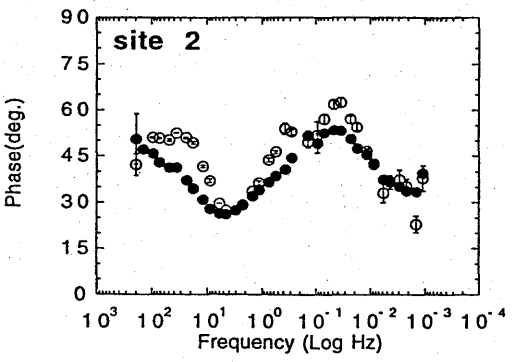
site 2
Phase(deg.)
Frequency (Log Hz)

Fig. 4-8(b)

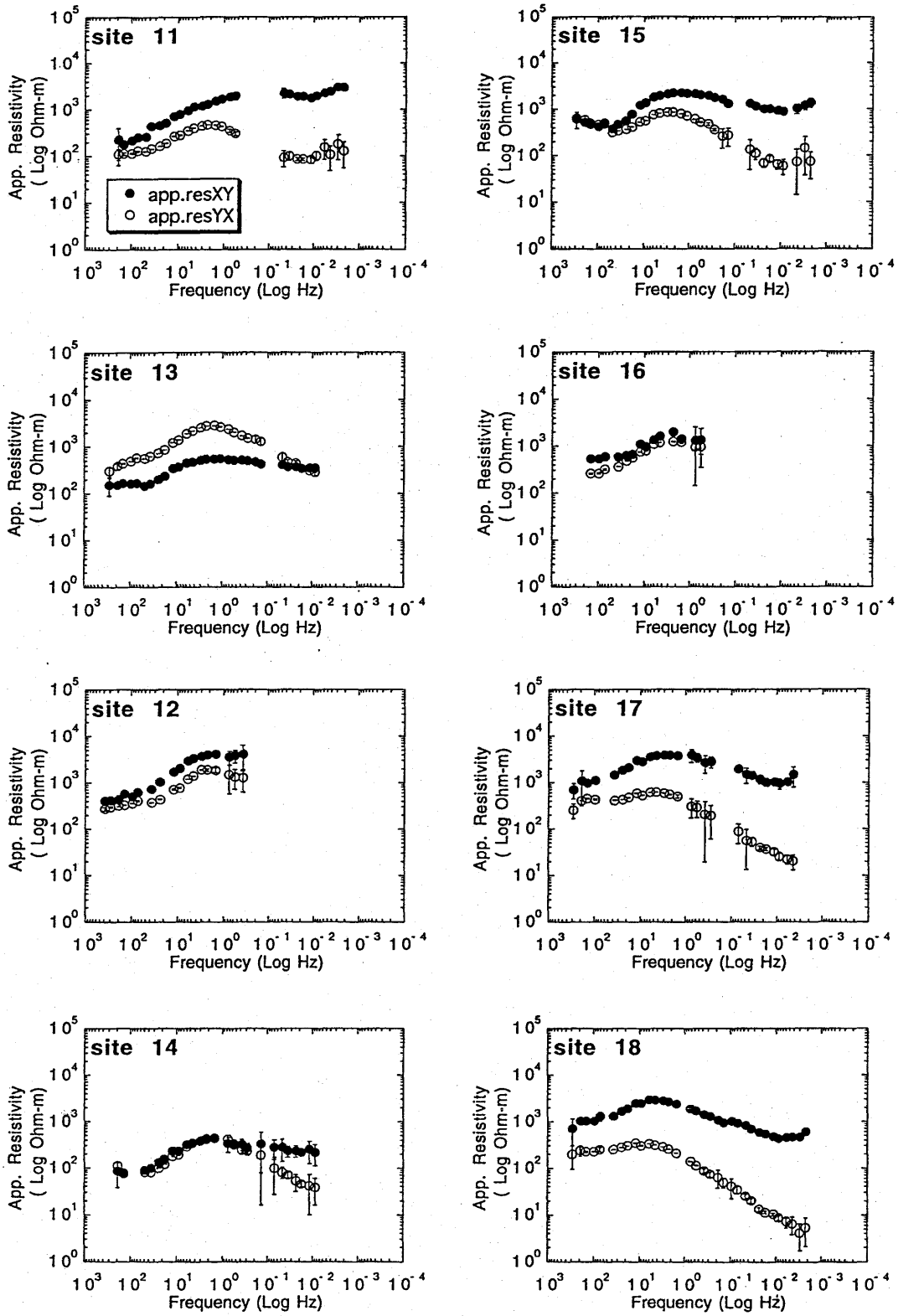
site 11
app.resXY
app.resYX
site 15
site 13
site 16
site 12
site 17
site 14
site 18
App. Resistivity (Log Ohm-m)
Frequency (Log Hz)

Fig.4-9(a)

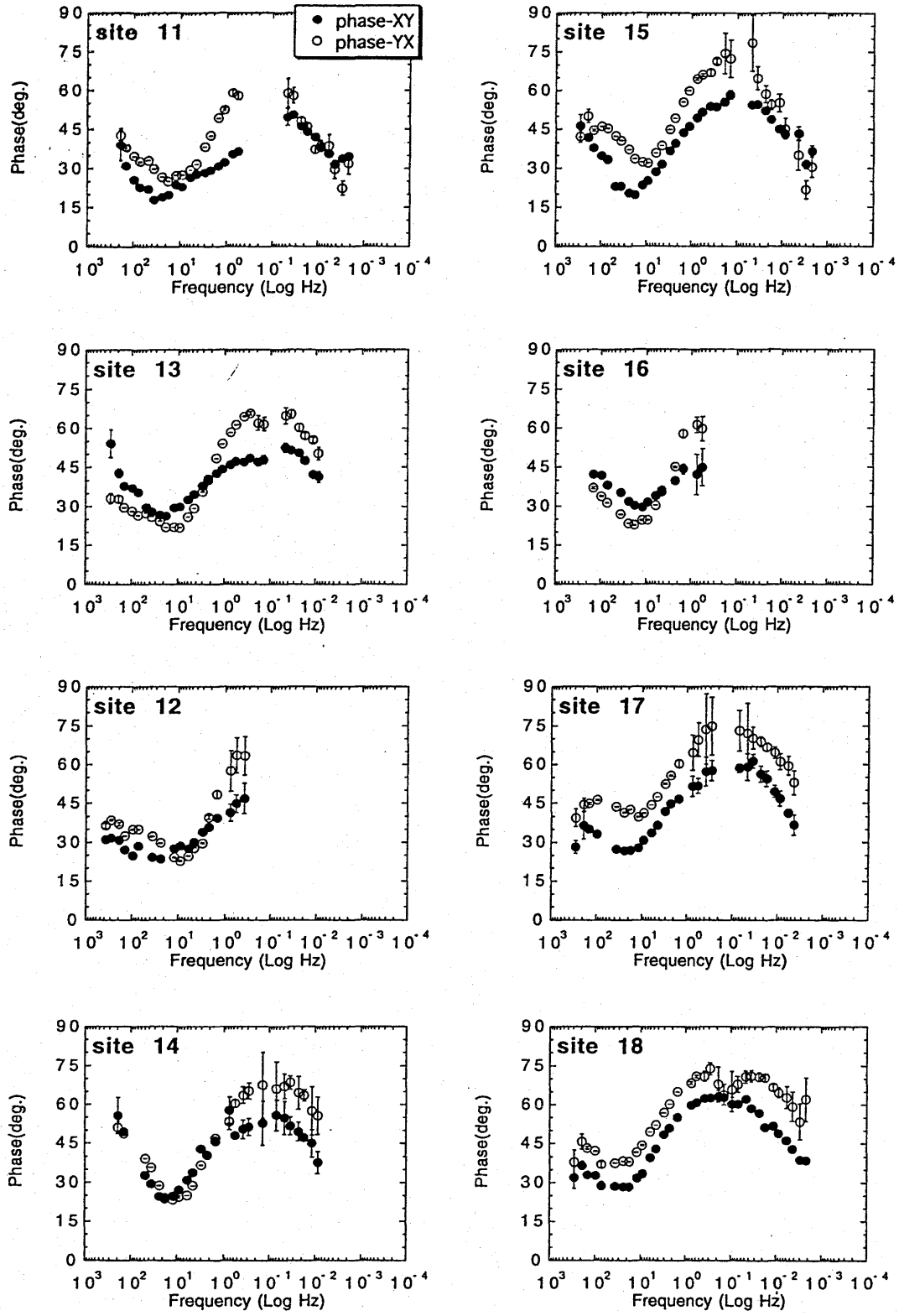
site 11
phase-XY
phase-YX
site 15
site 13
site 16
site 12
site 17
site 14
site 18
Phase(deg.)
Frequency (Log Hz)

Fig.4-9(b)

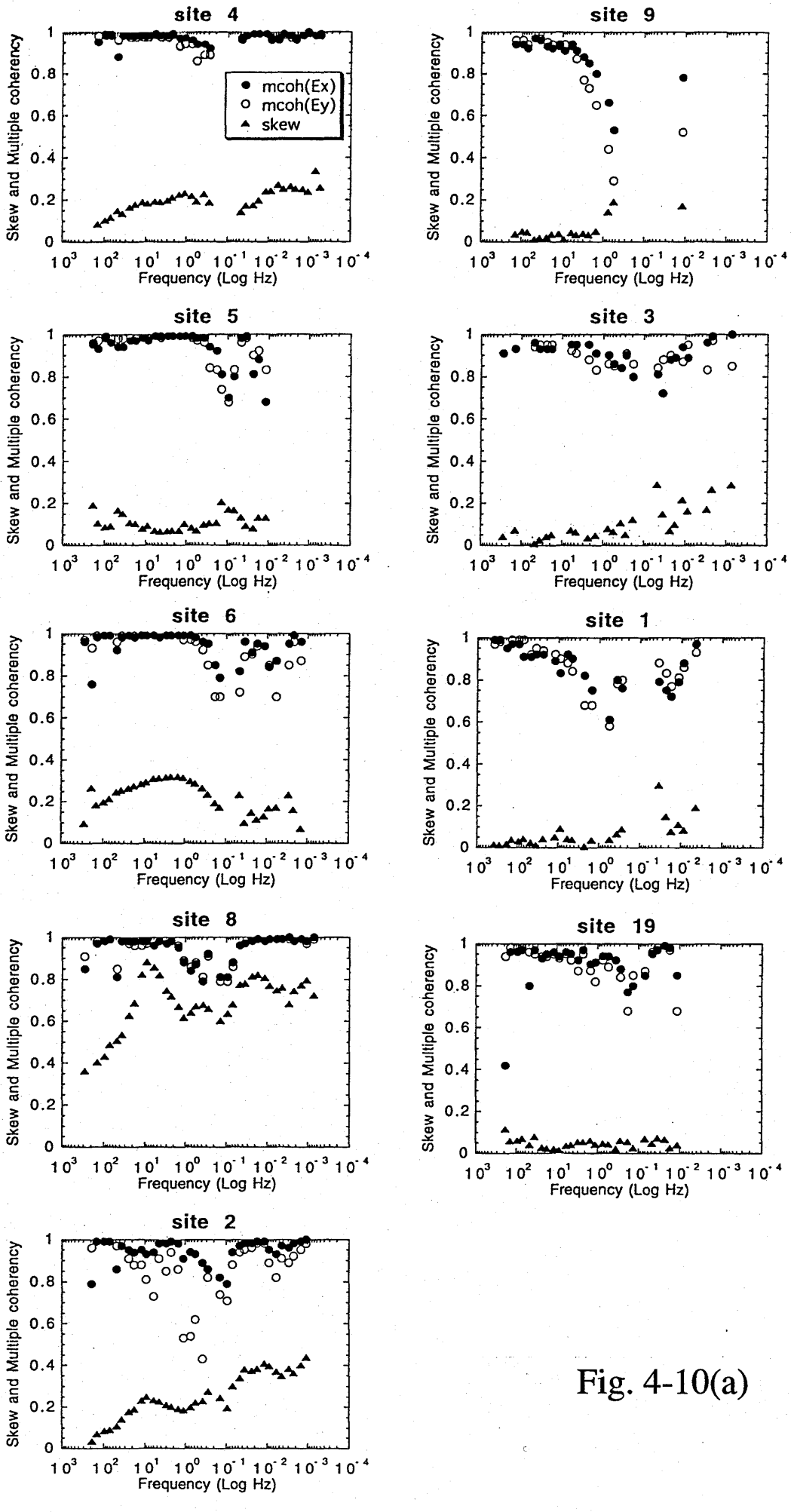
site 4
site 9
site 5
site 3
site 6
site 1
site 8
site 19
site 2
mcoh(Ex)
mcoh(Ey)
skew
Skew and Multiple coherency
Frequency (Log Hz)

Fig. 4-10(a)

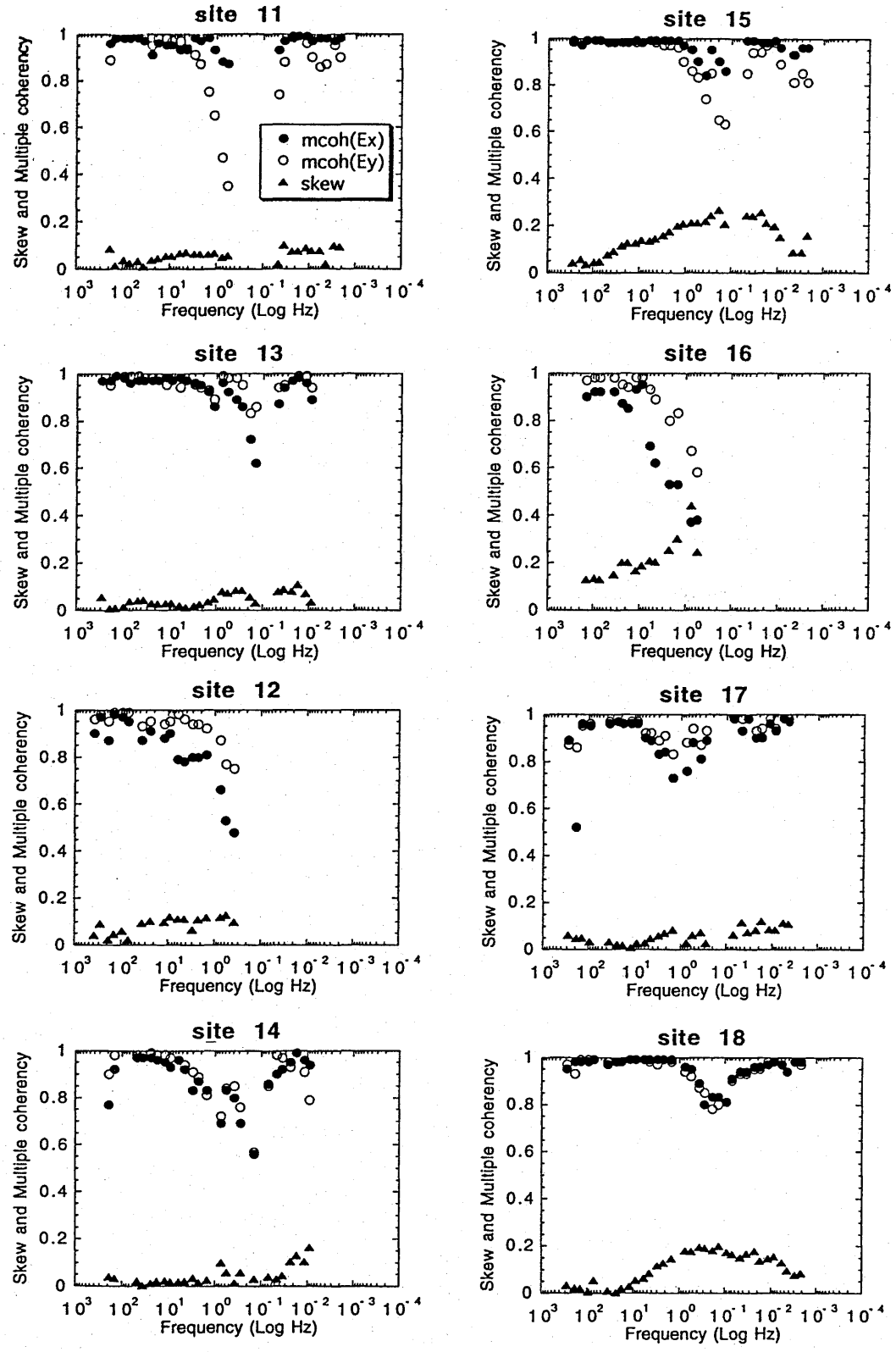
site 11
site 15
site 13
site 16
site 12
site 17
site 14
site 18
Skew and Multiple coherency
Frequency (Log Hz)
mcoh(Ex)
mcoh(Ey)
skew

Fig. 4-10(b)

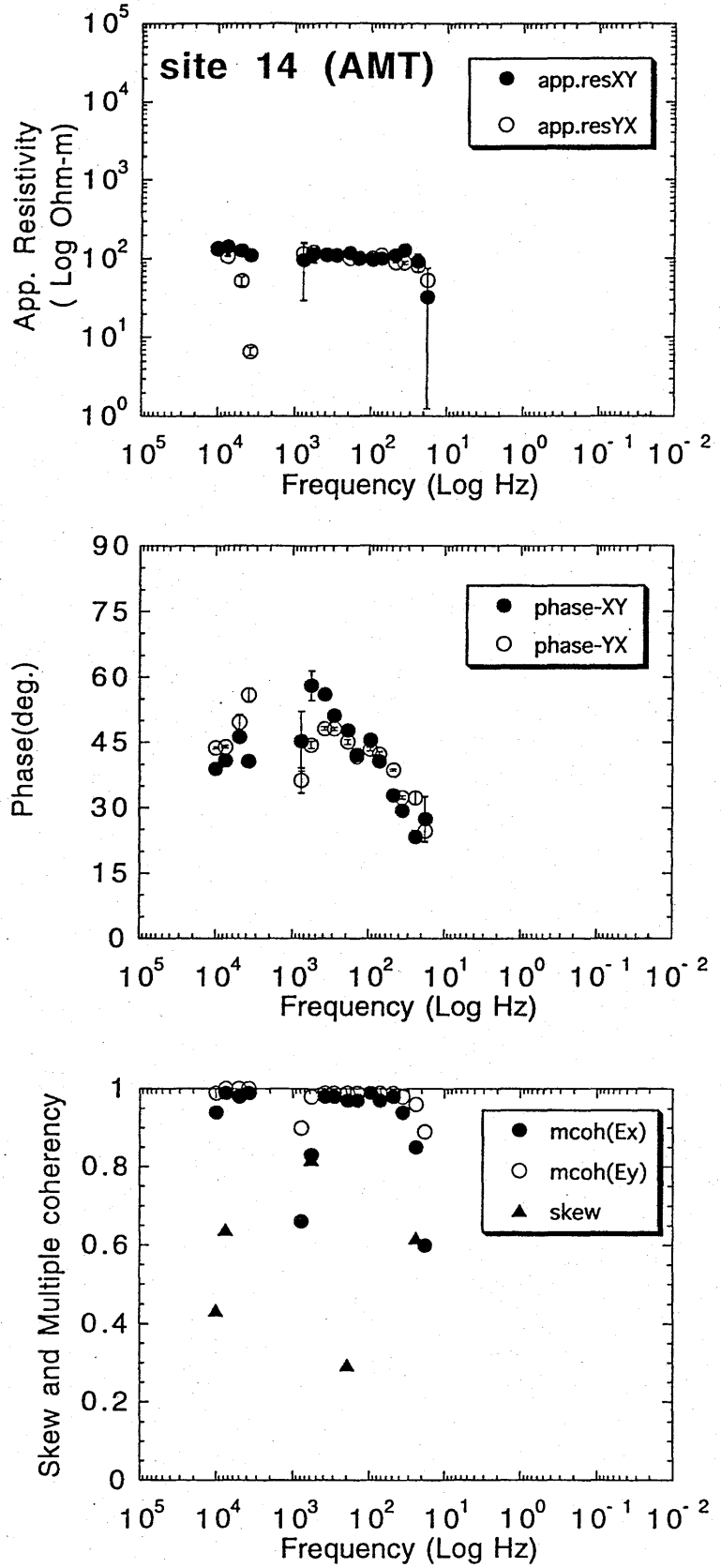
site 14 (AMT)
app.resXY
app.resYX
App. Resistivity (Log Ohm-m)
Frequency (Log Hz)
phase-XY
phase-YX
Phase(deg.)
Frequency (Log Hz)
mcoh(Ex)
mcoh(Ey)
skew
Skew and Multiple coherency
Frequency (Log Hz)

Fig. 4-11

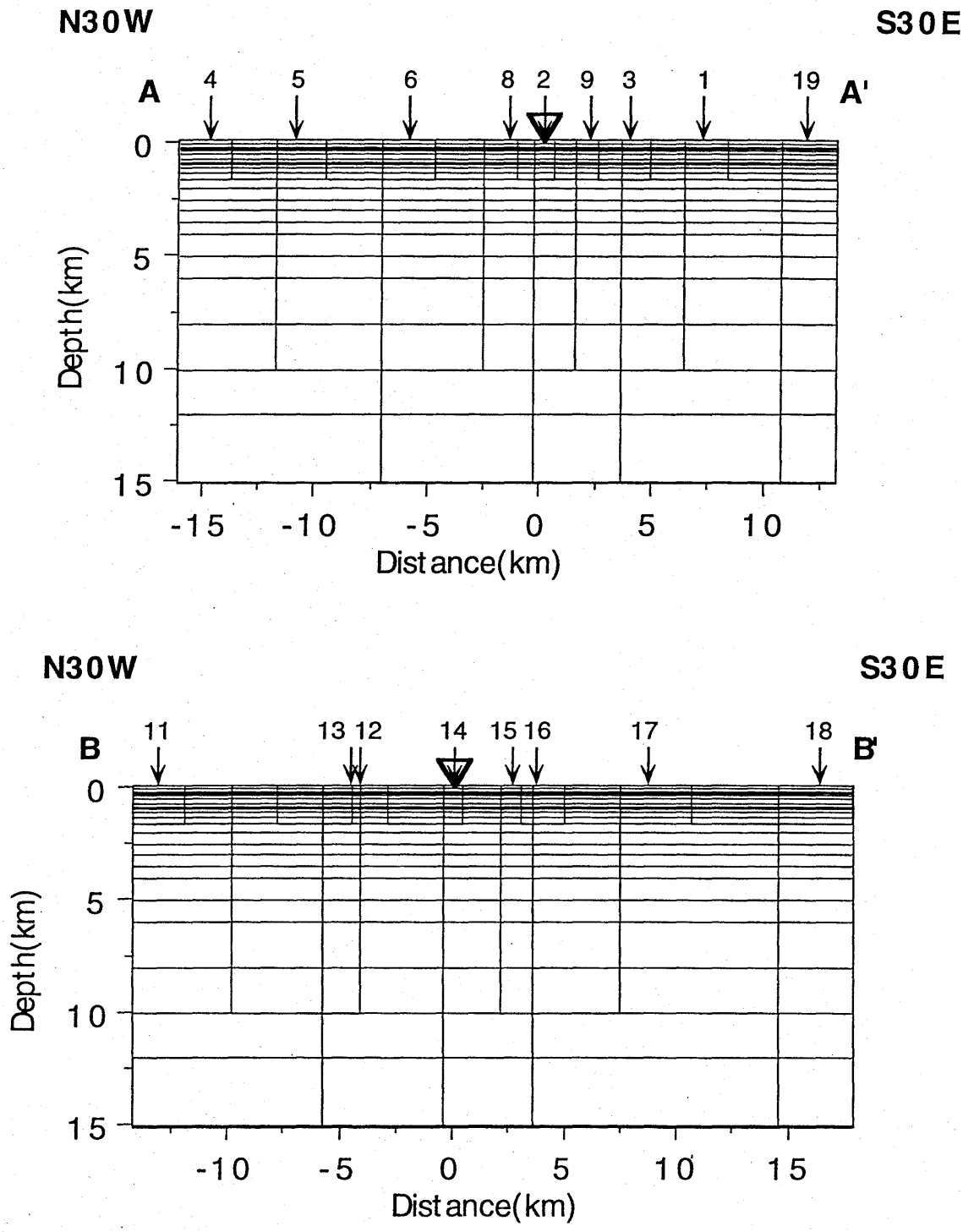
N30W
S30E
A
A'
4
5
6
8
2
9
3
1
19
0
5
10
15
Depth(km)
-15
-10
-5
0
5
10
Distance(km)
N30W
S30E
B
B'
11
13
12
14
15
16
17
18
0
5
10
15
Depth(km)
-10
-5
0
5
10
15
Distance(km)

Fig. 4-12

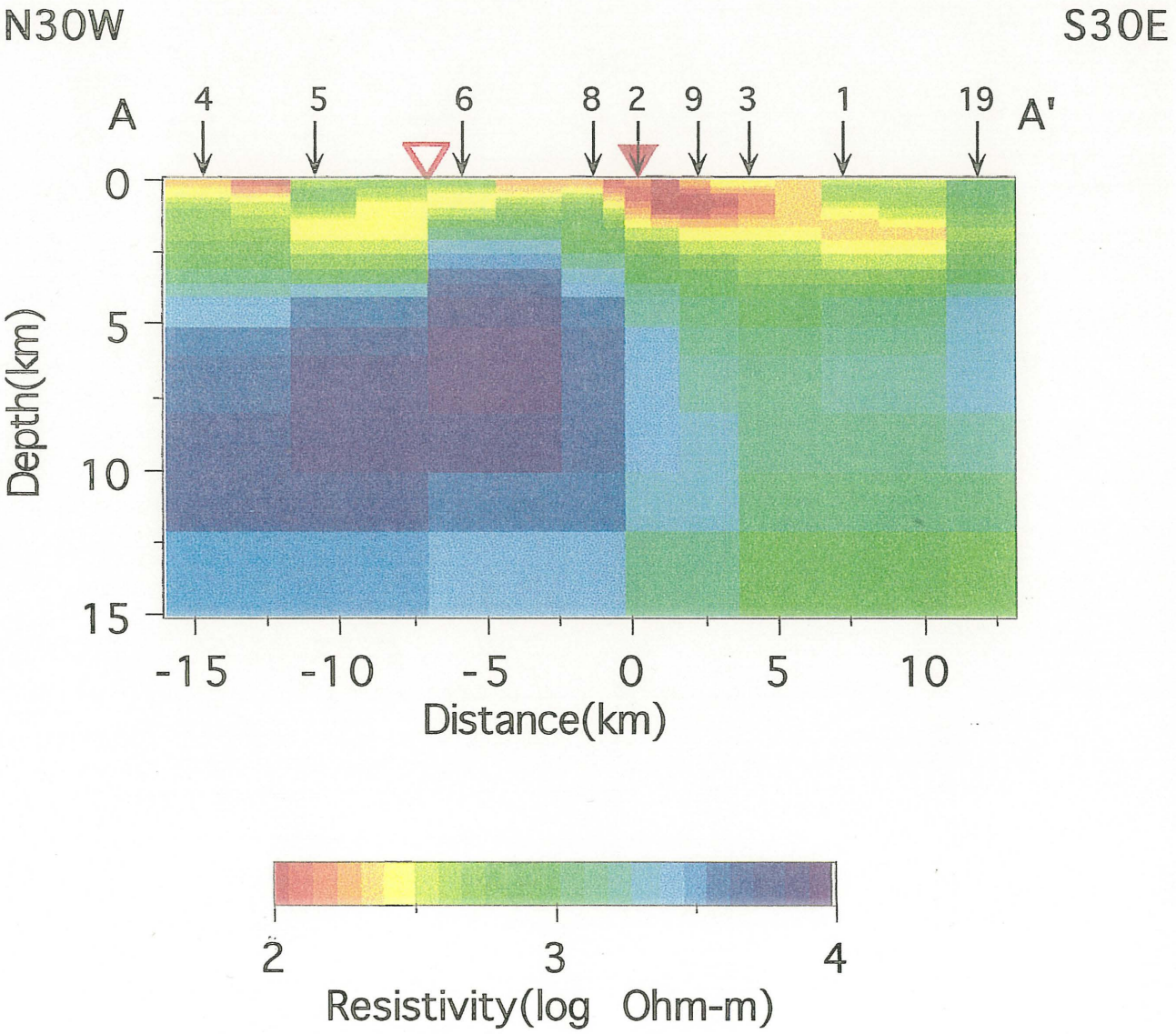
N30W
S30E
A
A'
4
5
6
8
2
9
3
1
19
0
5
10
15
Depth(km)
-15
-10
-5
0
5
10
Distance(km)
2
3
4
Resistivity(log Ohm-m)

Fig. 4- 13

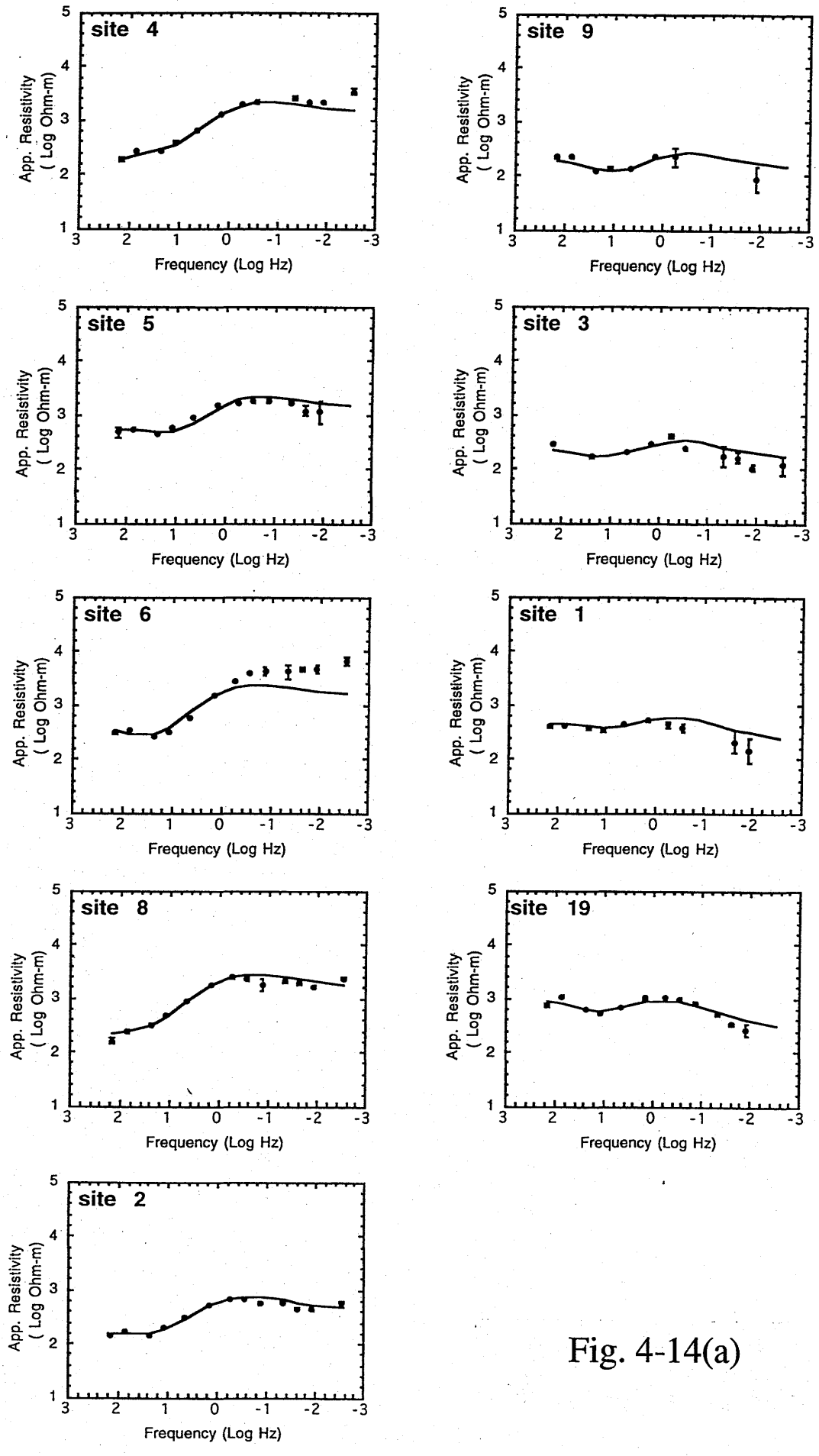
site 4
site 9
site 5
site 3
site 6
site 1
site 8
site 19
site 2
App. Resistivity (Log Ohm-m)
Frequency (Log Hz)
5
4
3
2
1
3 2 1 0 -1 -2 -3

Fig. 4-14(a)

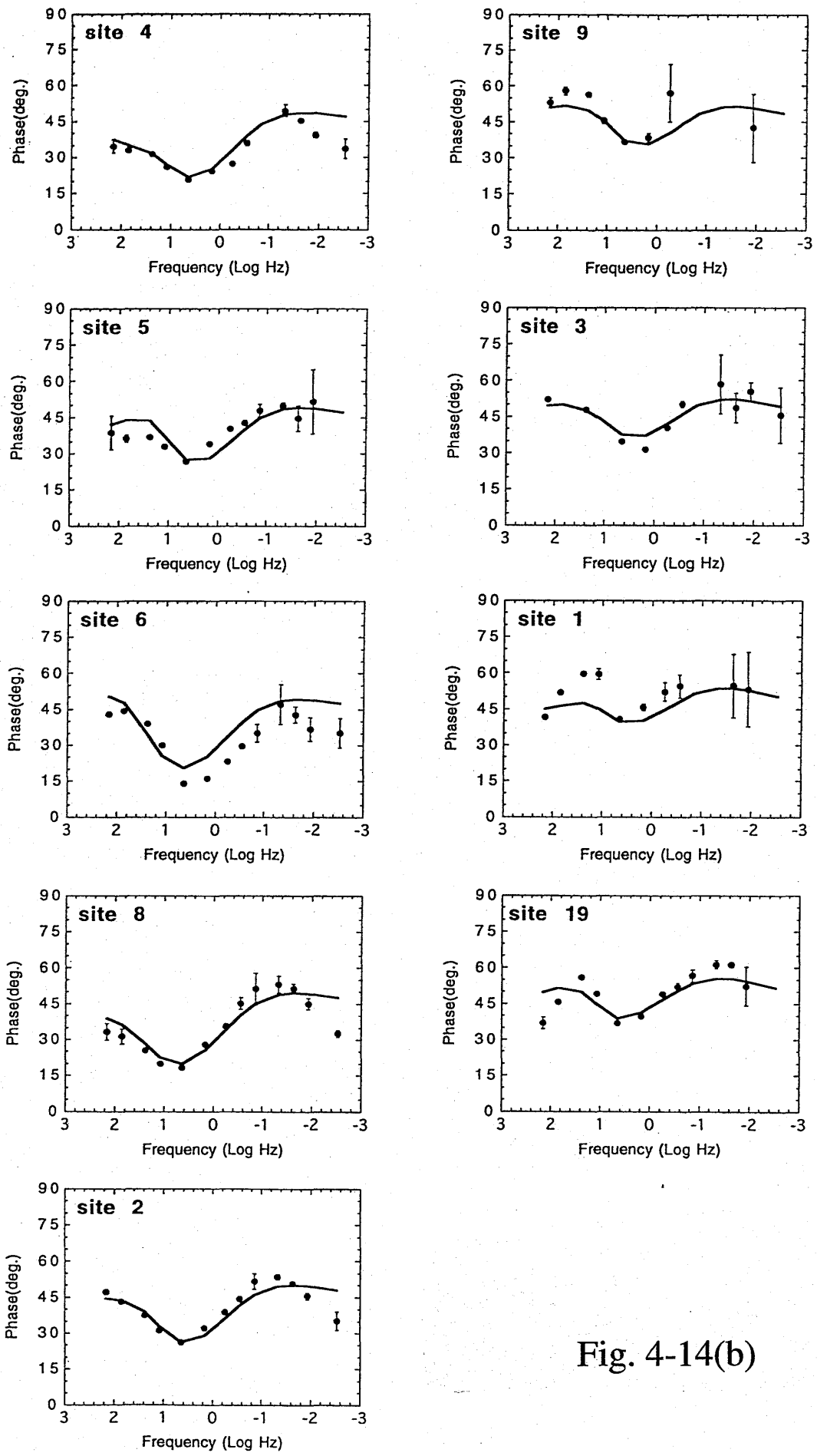
site 4
site 9
site 5
site 3
site 6
site 1
site 8
site 19
site 2
Phase(deg.)
Frequency (Log Hz)

Fig. 4-14(b)

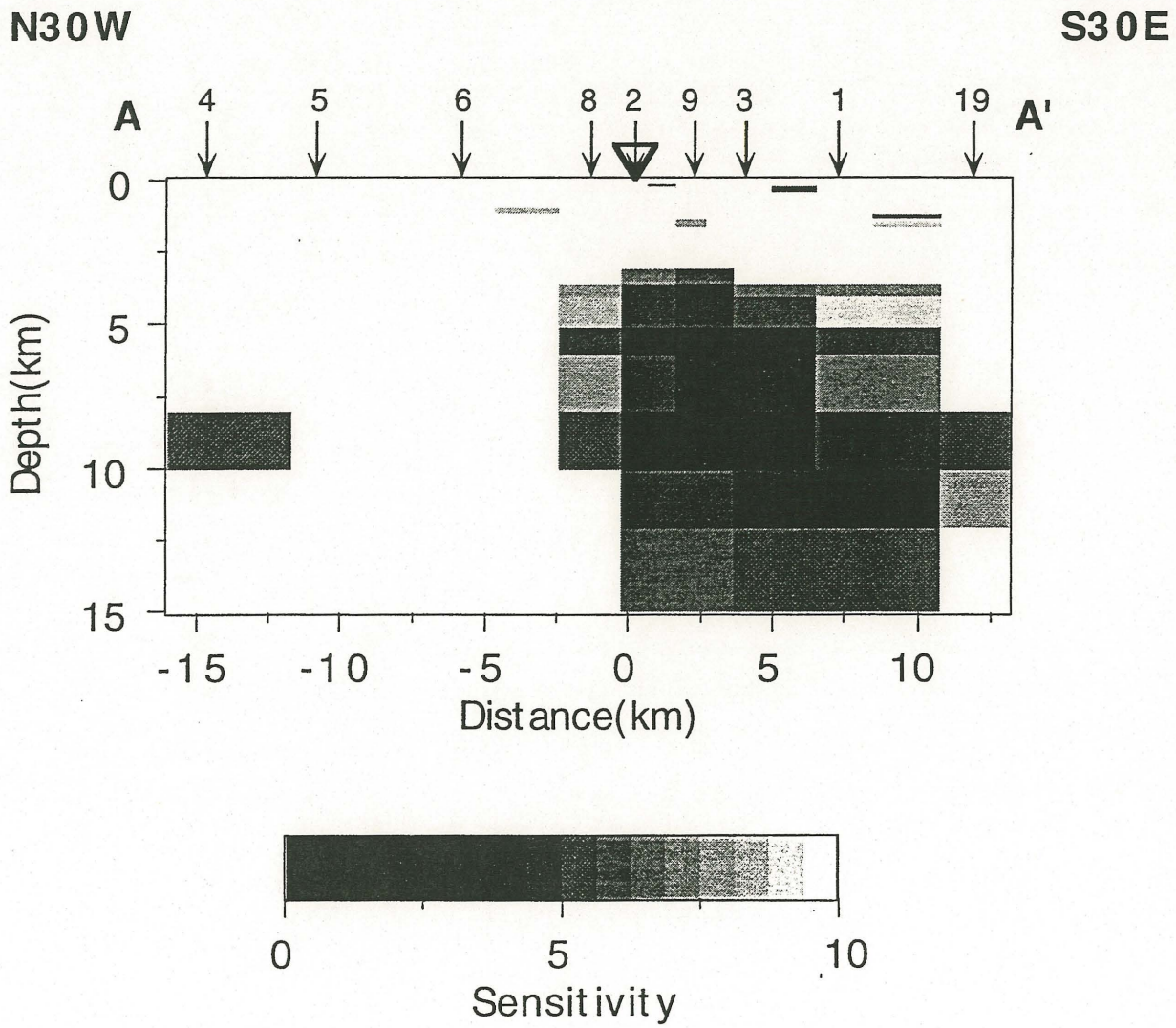
N30W
S30E
A
A'
4
5
6
8
2
9
3
1
19
0
5
10
15
Depth(km)
-15
-10
-5
0
5
10
Distance(km)
0
5
10
Sensitivity

Fig. 4-15

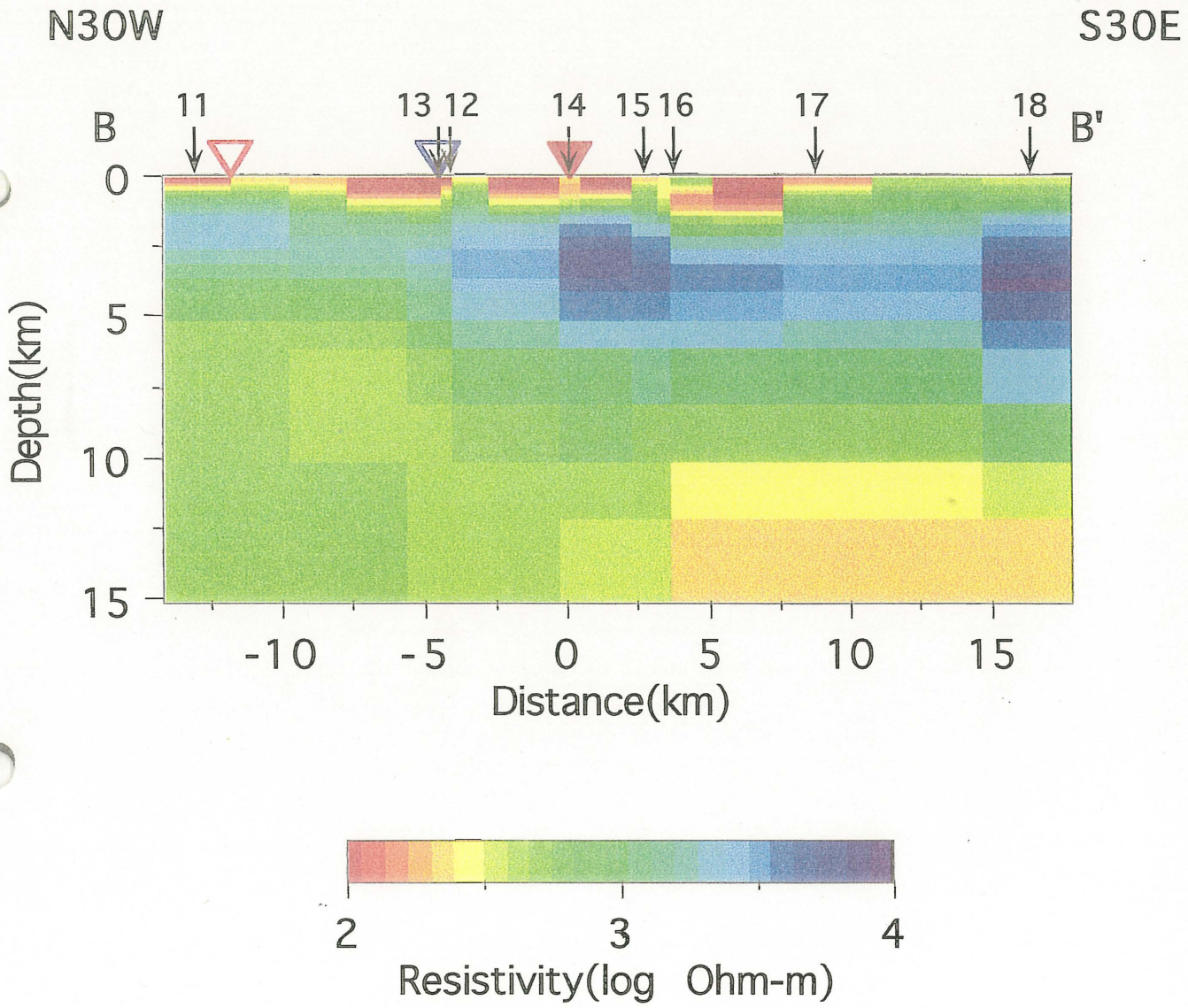
N30W
S30E
B
B'
11
13
12
14
15
16
17
18
0
5
10
15
Depth(km)
-10
-5
0
5
10
15
Distance(km)
2
3
4
Resistivity(log Ohm-m)

Fig. 4-16

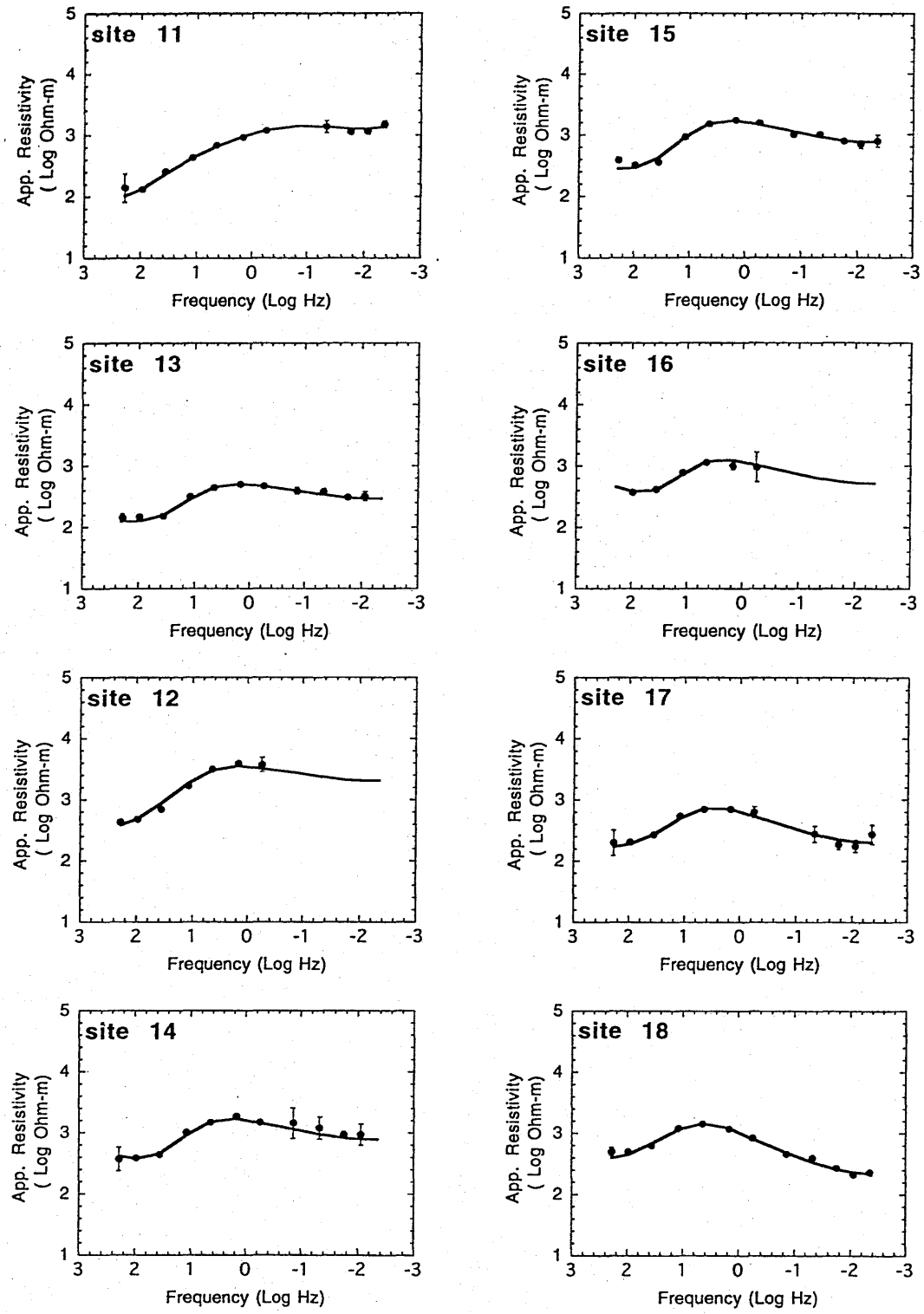
site 11
site 15
site 13
site 16
site 12
site 17
site 14
site 18
App. Resistivity (Log Ohm-m)
Frequency (Log Hz)
5
4
3
2
1
3
2
1
0
-1
-2
-3

Fig. 4-17(a)

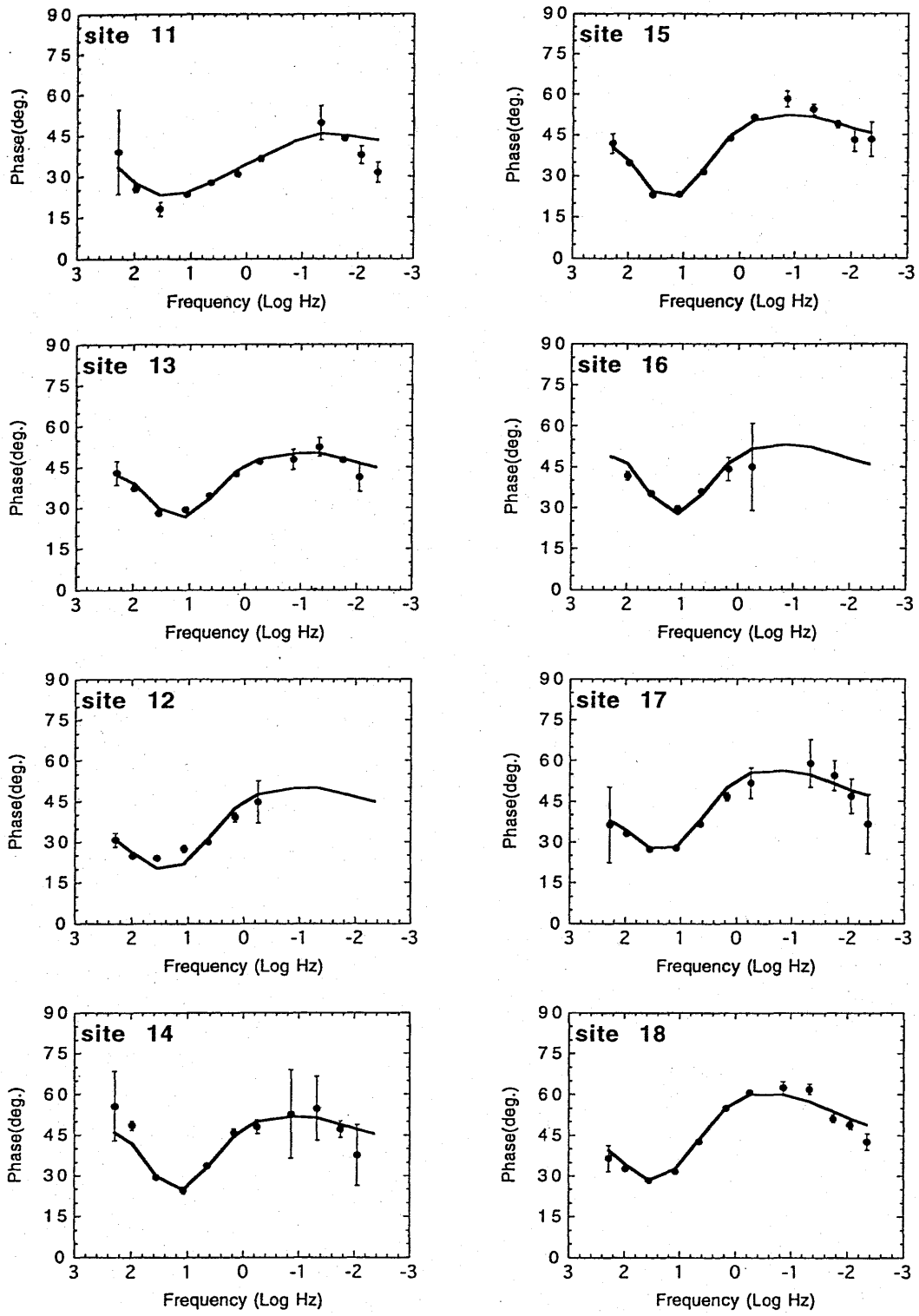
site 11
site 15
site 13
site 16
site 12
site 17
site 14
site 18
Phase(deg.)
Frequency (Log Hz)
90
75
60
45
30
15
0
3
2
1
0
-1
-2
-3

Fig. 4-17(b)

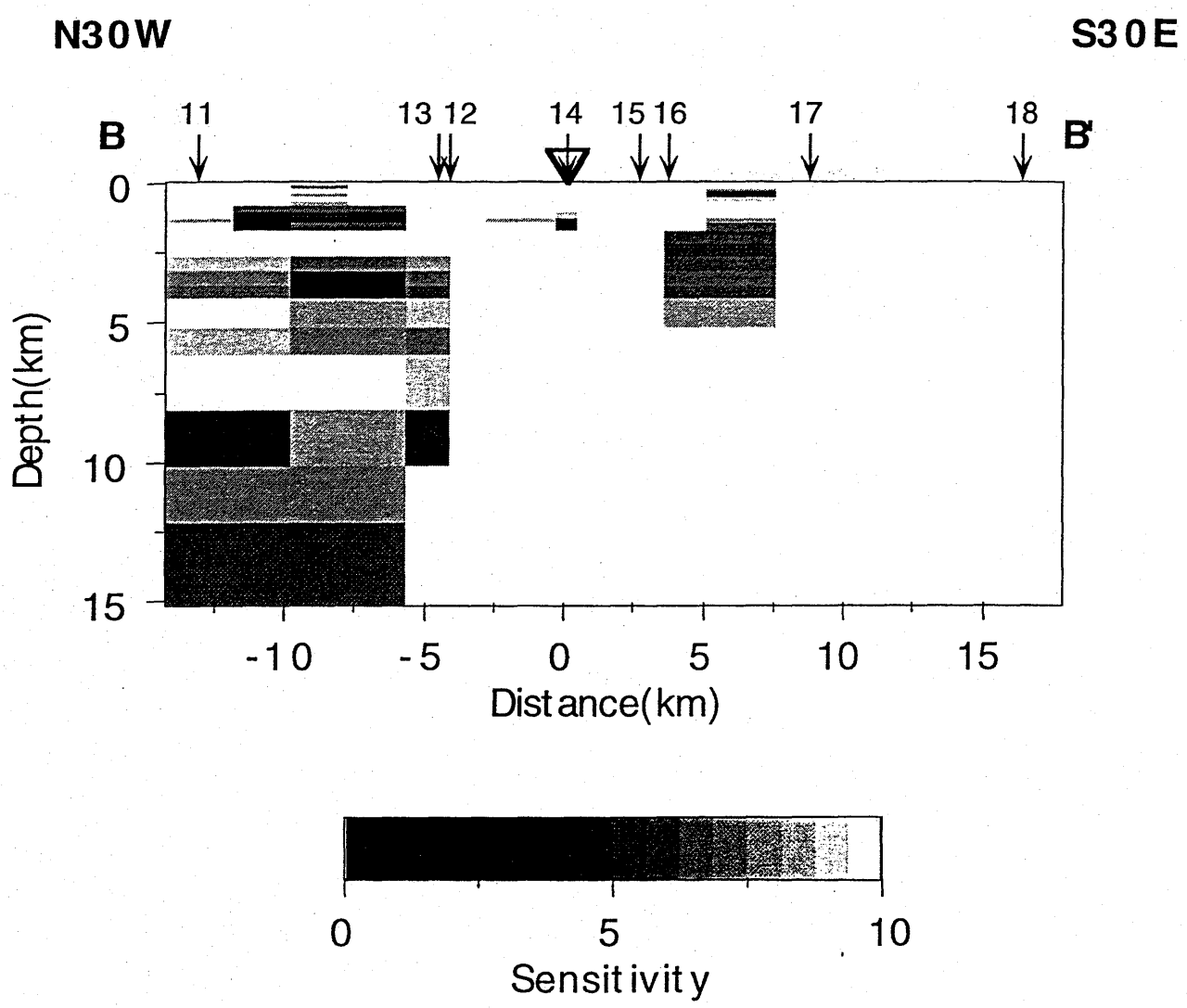
N30W
S30E
B
B'
11
13
12
14
15
16
17
18
0
5
10
15
Depth(km)
-10
-5
0
5
10
15
Distance(km)
0
5
10
Sensitivity

Fig. 4-18

5. Observation and modeling in the Ebino region

5. 1. The Ebino earthquake swarm

The purpose of the MT survey in the Ebino region is to investigate the resistivity structure around the hypocentral area of the Ebino earthquake swarm and to clarify how fluid has something to do with the mechanism of the occurrence of the swarms from the view point of the resistive structure of the earth's crust.

The Ebino earthquake swarm occurred during the period from 1968 - 1969 in Ebino, inside the Kakuto caldera, in the southern Kyushu district, Japan (Minakami et al. 1969, 1970). The Kakuto caldera is located at the northeastern foot of the Kirishima volcanoes. The magnitude of the largest earthquake was M6.1. Locations of epicenters are shown in Fig.5-1. Minakami et al. (1970) reported that hypocenters of the Ebino earthquake swarm distributed at depths from 3 to 9 km and with a width of 5 - 10 km. In the Kakuto caldera, several earthquake swarms have observed several times during the past one hundred years (Miyazaki et al., 1976) and the 1968-1969 Ebino earthquake swarm was the largest one. However, the recent seismicity inside the Kakuto caldera is rather low (Kagiyama, 1992). Minakami et al. (1970) found that the volcanic activities of the Kirishima volcanoes occasionally followed the earthquake swarms in the Kakuto caldera. They, therefore, inferred that the 1968-1969 Ebino earthquake swarm related to the magma supply system of Kirishima volcanoes. However, they did not detect a particular evidence of the movement of magma at that time.

In this paper, we mention to the significance of fluid possibly related to the occurrence of the 1968-1969 Ebino earthquake swarm. The reason is

derived from the fact that Watanabe(1970) observed a relation between the frequency of the seismic P wave of the Ebino earthquake swam and the location of its hypocenters. He pointed out that the earthquakes around the center of the focal area generated the seismic P wave with the lower frequency than those near the periphery of the focal area. This feature became gradually clear with time. The attenuation of the seismic wave increases with crack density if cracks are saturated by fluid (O'Connell and Budiansky, 1977). In addition, Miyazaki et al.(1969) carried out the leveling survey on the hypocentral area of the Ebino earthquake swarm before and after the swarm. In their observation, the crustal deformation associated with the Ebino earthquake swarm was found. It showed the ridge in the central zone of the surveyed area beneath which the earthquake swarm occurred. Since the mechanism of the Ebino earthquake swarm is mostly strike-slip type (Minakami et al, 1969; Watanabe 1970) , other causes such as expelled fluid from the deep interior of the earth is necessary to consider the result of the leveling survey. Therefore, we tentatively conclude that fluid would be related with the Ebino earthquake swarm.

5. 2. Observation in the Ebino region

Research group for Crustal Resistivity Structure in Japan (referred to as RGCRS) carried out the magnetotelluric(MT) soundings and the geomagnetic depth soundings(GDS) at 26 sites around the Kakuto caldera in 1994 (Sasai, 1995). The location of the sites is shown in Fig. 5-2. RGCRS used the V5 MT observation systems. The detail configuration of the V5 system is described in Chapter 3. RGCRS observed natural fluctuation of the magnetic and electric fields through about three days at each site. Using these data, we calculate the impedance tensor, the apparent resistivity, the impedance phase

and other electromagnetic responses in the broad band of the almost continuous frequencies between 384Hz to 0.00055Hz. These response functions are calculated according to the remote reference processing(Gamble et al., 1979). The reference site was set up in a distance of several kilometers far from the analyzed site.

5. 3. Strike direction and induction arrow

It is necessary at first to determine the direction of the regional strike around the studied area. We again apply the method of Chakridi et al.(1992) to the estimation of the direction of the strike at each site. This method is successful to avoid the effect of the surficial galvanic distortion (Groom and Bailey, 1989). In addition, we also tried another method of Jones and Groom (1993, eqs.10 and 11) which was similar to the Chakridi's method but was more robust to a one dimensional resistivity structure.

After all, we calculated the regional strike using both the Chakridi's method and the Jones and Groom's method, and determined the strike so as the least standard deviation for the observed frequencies is obtained. The estimated directions of the regional strike are shown in Fig.5-3 with a rose diagram. We can recognize that the regional strike points to approximately N-S or E-W directions. The induction arrows at all site are also calculated. It is found that induction arrows tend to south at the period of about 10 seconds as shown in Fig.5-4. Judging from the distribution of the strike and the induction arrow, we conclude that the resistivity structure under the studied area is approximately two-dimensional with the strike of the E-W direction. This is supported from the fact that the observed skewness values are lower than 0.3 at all site.

5. 4. The apparent resistivity and the phase

The apparent resistivities and the impedance phases roughly show similar tendencies at all sites, respectively. The apparent resistivity, the phase, the multiple coherency and the skewness at each site are shown in Fig. 5-5 to Fig. 5-9. It is recognized that the apparent resistivity values have a minimum commonly around several Hz and gradually increase as the frequency decreases beyond 1Hz.

Additionally, the apparent resistivities and the phases obtained in the epicentral area of the Ebino earthquake swarm have different features from those in the surrounding regions of the epicentral area. The typical curves of the apparent resistivity in and around the epicentral area is show in Fig. 5-10. At all sites, in general, the apparent resistivity increases as the frequency decreases beyond 1Hz as mentioned above. However, above the hypocentral area, increasing of the apparent resistivity is very steep and the apparent resistivity value at a frequency around 0.1Hz is almost the same or rather higher than the apparent resistivity at a frequency around 300Hz(see Fig. 5-10., Sites 1 and 10). On the other hand, in the surrounding regions of the epicentral area, the apparent resistivity at about 0.1Hz is lower than that at about 300Hz(see Fig. 5-10, Sites 7 and 15). These features are important to consider the resistivity structure around the studied area. We will discuss this point later.

5. 5. Modeling for the Ebino profiles

Models of the two-dimensional resistivity structure beneath the studied area are constructed. The direction of the strike is assumed to be E-W as mentioned in the previous section. We took four analyzing profiles in the studied area as shown in Fig.5-11. The two-dimensional least square inversion with the smoothness constraint coded by Uchida and Ogawa(1993) is applied to the data of each profile to construct the most suitable resistivity model. The inversion is carried out using the observed apparent resistivities and phases of both TE and TM mode. The initial model for the inversion is given with a uniform resistivity of 1000 ohm-m. The inversion was executed very stably and four or five iterations for each profile were needed to reach a sufficient convergence.

The most suitable model of the two-dimensional resistivity structure along each profile well explained the observed electromagnetic responses. First, we show the most suitable resistivity model along the profile AA' in Fig. 5-12, which goes just across the area of the epicenters of the Ebino earthquake swarm. The outline of the hypocentral area demonstrated in Fig. 5-12, and Fig. 5-14 shown later, is based on Minakami et al.(1970). In our model, we set the conductive layer at a depth of about 0.5 - 1 km. The conductive layer is responsible to the low apparent resistivity at several Hz. We also recognize that the hypocentral area of the Ebino earthquake swarm is more resistive than the surrounding area. The fitting of the calculated responses to the observed data is indicated in Fig. 5-13. The calculated responses well explain the steep increase of the apparent resistivity at the frequency of about 1Hz observed above the hypocentral area.

Secondly, we show the resistivity model along the analyzing profile of

BB'. The resistivity model along the profiles BB' is similar to that along the profile AA'. The most probable model for BB' is shown in Fig. 5-14. The calculated responses from the model show a suitable fitness with the observed ones (see Fig. 5-15). We can find that the conductive layers beneath 1 km depth also exist along the profiles BB'. In addition, the resistive zone corresponding with the hypocentral area of the Ebino earthquake swarm becomes thinner than that recognized in the profile AA'.

At last, We show the resistivity model along the analyzing profile of CC' and DD' in Figs. 5-16 and 5-18, respectively , which are located at the northern foot of Mt. Karakuni-dake, one of the Kirishima volcanoes. The calculated responses are also shown in Figs. 5-17 and 5-19 together with the observed one. These resistivity models along these profiles have a high degree of a similar fitness to that along the profile AA'. The models for the profiles CC' and DD' also show the conductive layer at a depth of about 1 km. Additionally, we can recognize the existence of a conductive zone near the Kirishima volcanoes at a depth deeper than about 6 km. Similar conductive zone is also shown beneath the profile DD', which is deeper but more conductive than that below CC'. However, the resistive zone corresponding with the hypocentral area of the Ebino earthquake swarm is not recognized along these profiles. The lack of the resistive zone along the profiles CC' and DD' is inferred from Fig. 5-20, in which the spatial distribution of the resistivity at the depth of 6 km is indicated with a bird-eye's picture.

Fig. 5-1 The distribution of the hypocenters of the Ebino earthquake swarm after Minakami et al.(1970)

Fig. 5-2 The location of the sites(circles). The triangle indicates the location of Mt. Karakuni-dake, one of Kirishima volcanoes. The hatched area means the epicentral area of the Ebino earthquake swarm.

Fig. 5-3 The directions of the regional strike estimated from all observation sites with the rose diagrams.

Fig. 5-4 Induction arrows at the period of about 10 seconds

Fig.5-5 (a) Observed apparent resistivities, (b) phases and (c) skewness and multiple coherency between the electric field and the magnetic field.

Fig. 5-6 (a) Observed apparent resistivities, (b) phases and (c) skewness and multiple coherency between the electric field and the magnetic field.

Fig. 5-7 (a) Observed apparent resistivities, (b) phases and (c) skewness and multiple coherency between the electric field and the magnetic field.

Fig. 5-8 (a) Observed apparent resistivities, (b) phases and (c) skewness and multiple coherency between the electric field and the magnetic field.

Fig. 5-9 (a) Observed apparent resistivities, (b) phases and (c) skewness and multiple coherency between the electric field and the magnetic field.

Fig.5-10 The typical curves of apparent resistivity at representative sites obtained in the epicentral area of the Ebino earthquake swarm

Fig. 5-11 The locations of the surveying profiles. The profile(dashed lines) and observation sites used for the analysis of that profile are connected with thin lines. Opens circle indicate the sites never used in modeling.

Fig. 5-12 The two-dimensional most suitable resistivity model along the profile AA'. The area where the hypocenters of the Ebino earthquake swarm distributed (Minakami et al., 1970) is indicated dashed circle. The locations of observation sites are indicated by arrows.

Fig. 5-13 (a)The calculated apparent resistivities and observed ones along the profile AA'
(b)The calculated phases and observed ones along the profile AA'

Fig. 5-14 The two-dimensional most suitable resistivity model along the profile BB'. The area where the hypocenters of the Ebino

earthquake swarm distributed is indicated by a dashed circle. The locations of observation sites are indicated by arrows with number with indicates site number.

Fig. 5-15 (a)The calculated apparent resistivities and observed ones along the profile BB'
(b)The calculated phases and observed ones along the profile BB'

Fig. 5-16 The two-dimensional most suitable resistivity model along the profile CC'. The locations of observation sites are indicated by arrows.

Fig. 5-17 (a)The calculated apparent resistivities and observed ones along the profile CC'
(b)The calculated phases and observed ones along the profile CC'

Fig. 5-18 The two-dimensional most suitable resistivity model along the profile DD'. The locations of observation sites are indicated by arrows.

Fig. 5-19 (a)The calculated apparent resistivities and observed ones along the profile DD'
(b)The calculated phases and observed ones along the profile DD'

Fig. 5-20 The Bird eye's image of the resistivity structure beneath the Ebino area. Color bar is the same as in Fig. 5-12. Blue circles means the location of the sites. The area where the hypocenters of the Ebino earthquake swarm distributed is indicated by a dashed circle.

Ebino Earthquake Swarm
(1968~69, max. M6.1)

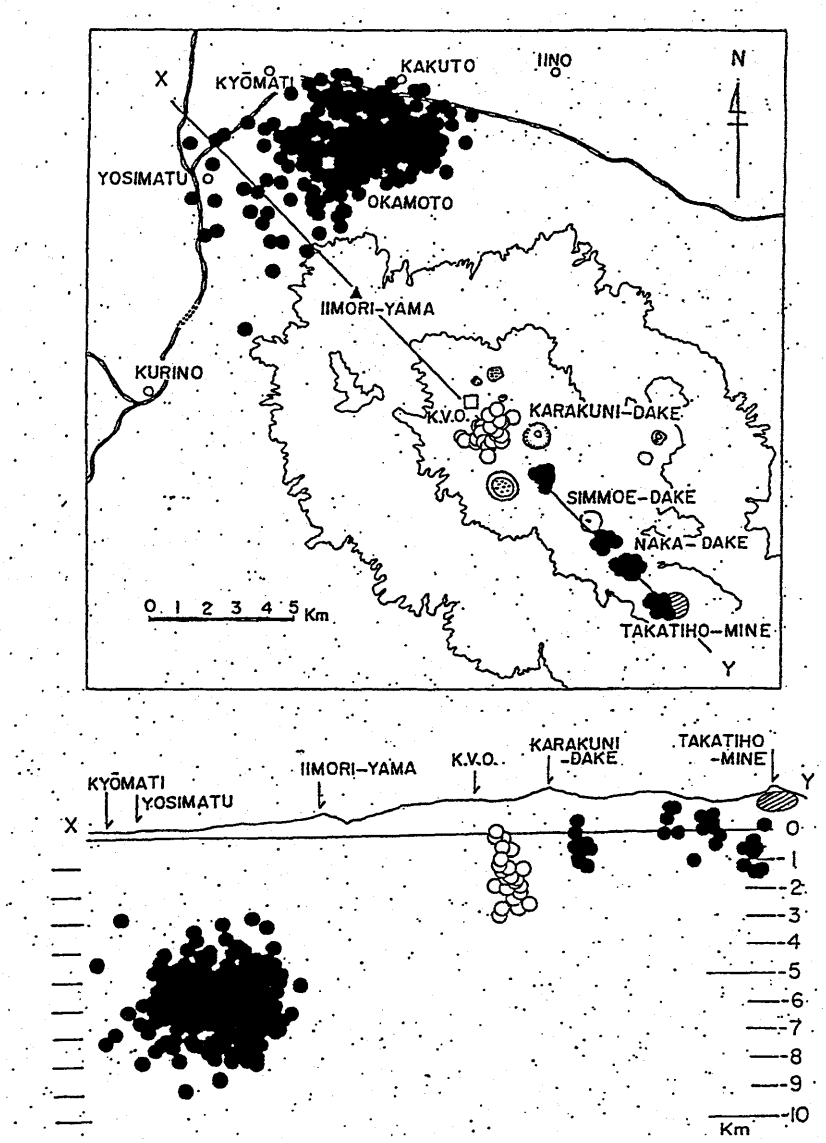

Fig. 5-1

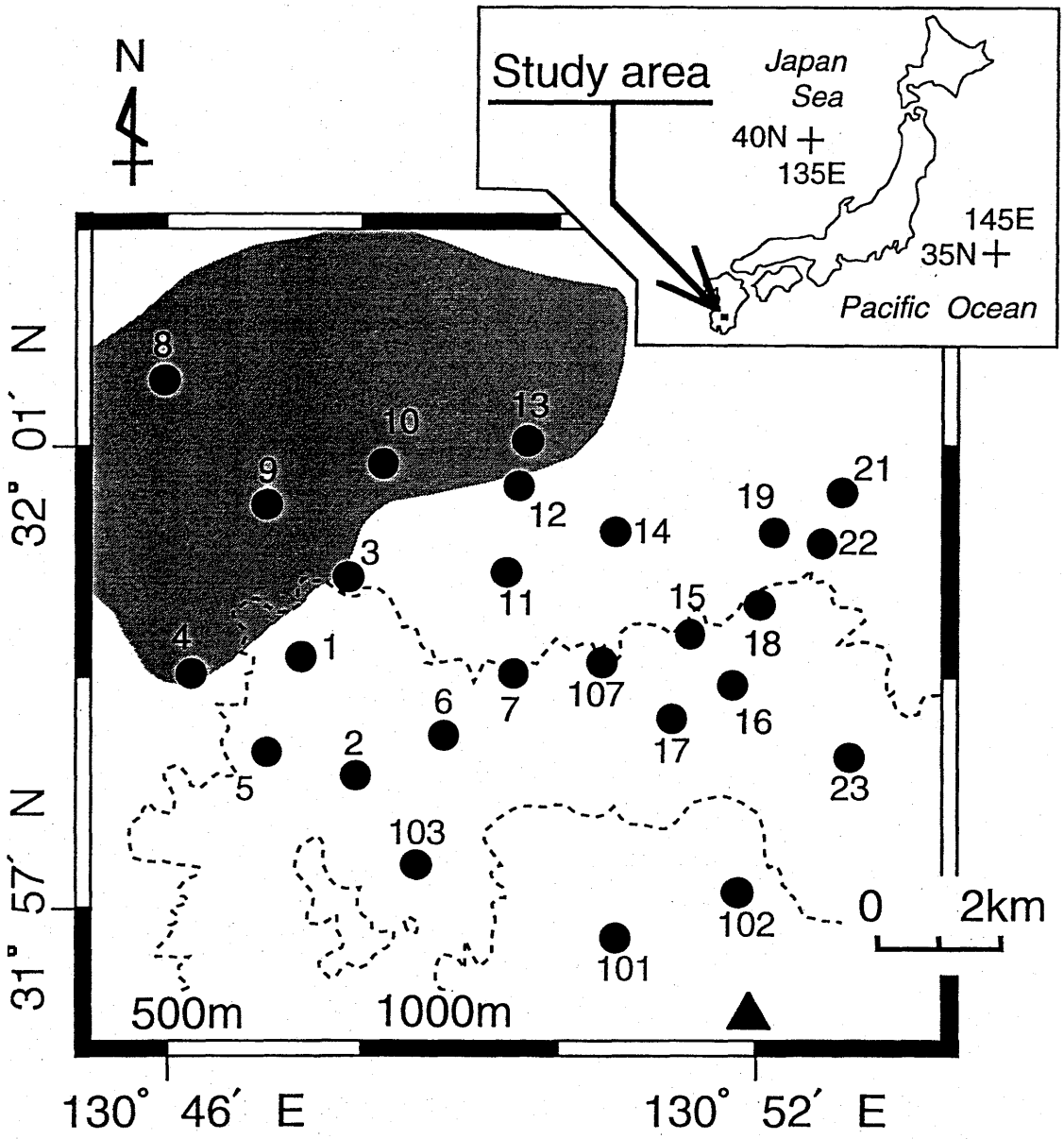
N
Study area
Japan
Sea
40N
135E
145E
35N
Pacific Ocean
32° 01′ N
31° 57′ N
130° 46′ E
130° 52′ E
500m
1000m
0
2km
1
2
3
4
5
6
7
8
9
10
11
12
13
14
15
16
17
18
19
21
22
23
101
102
103
107

Fig. 5-2

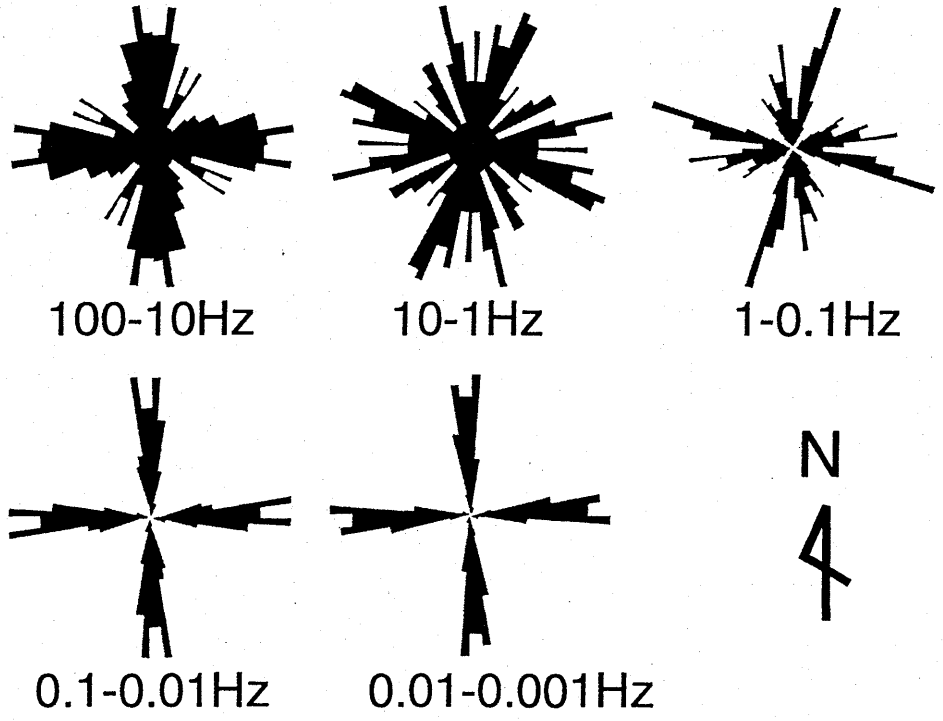

Fig. 5-3

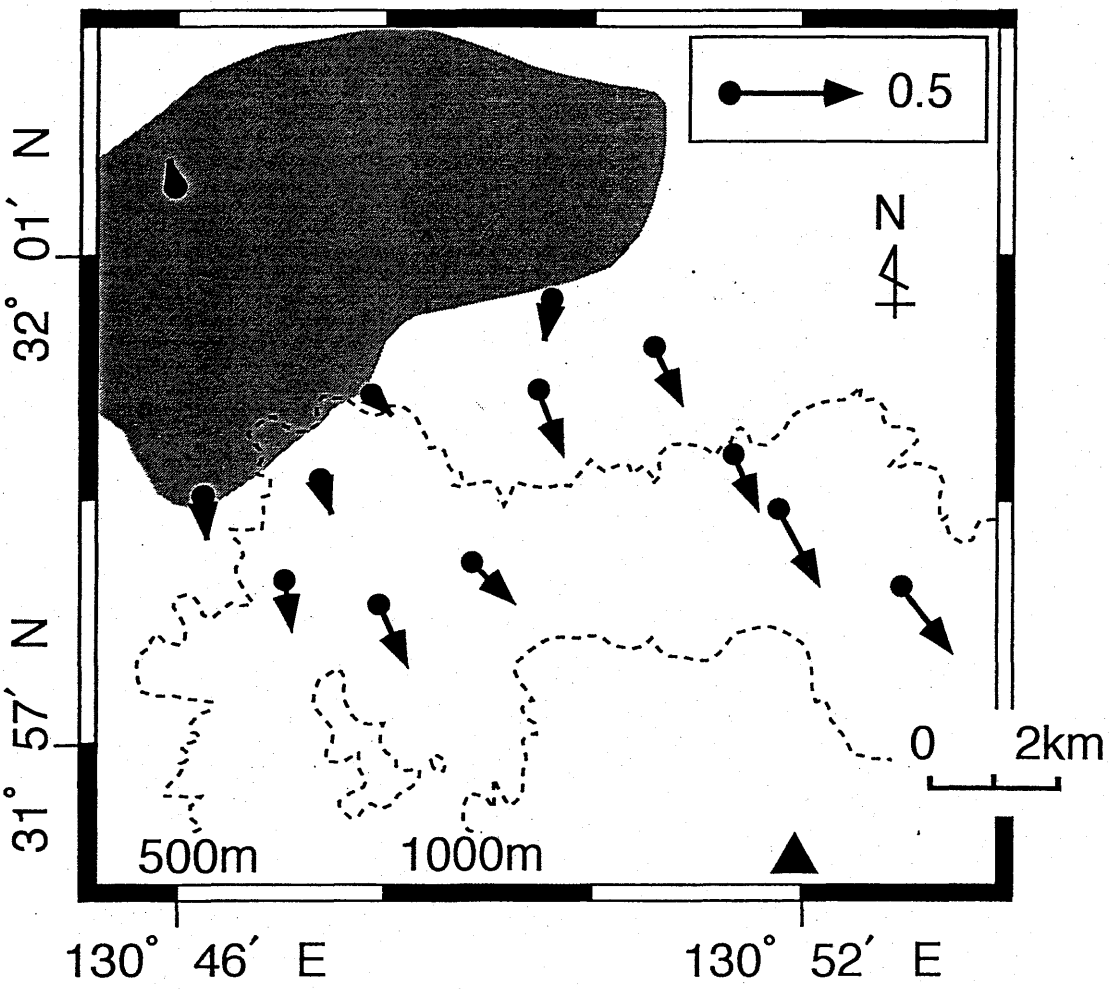

Fig. 5-4

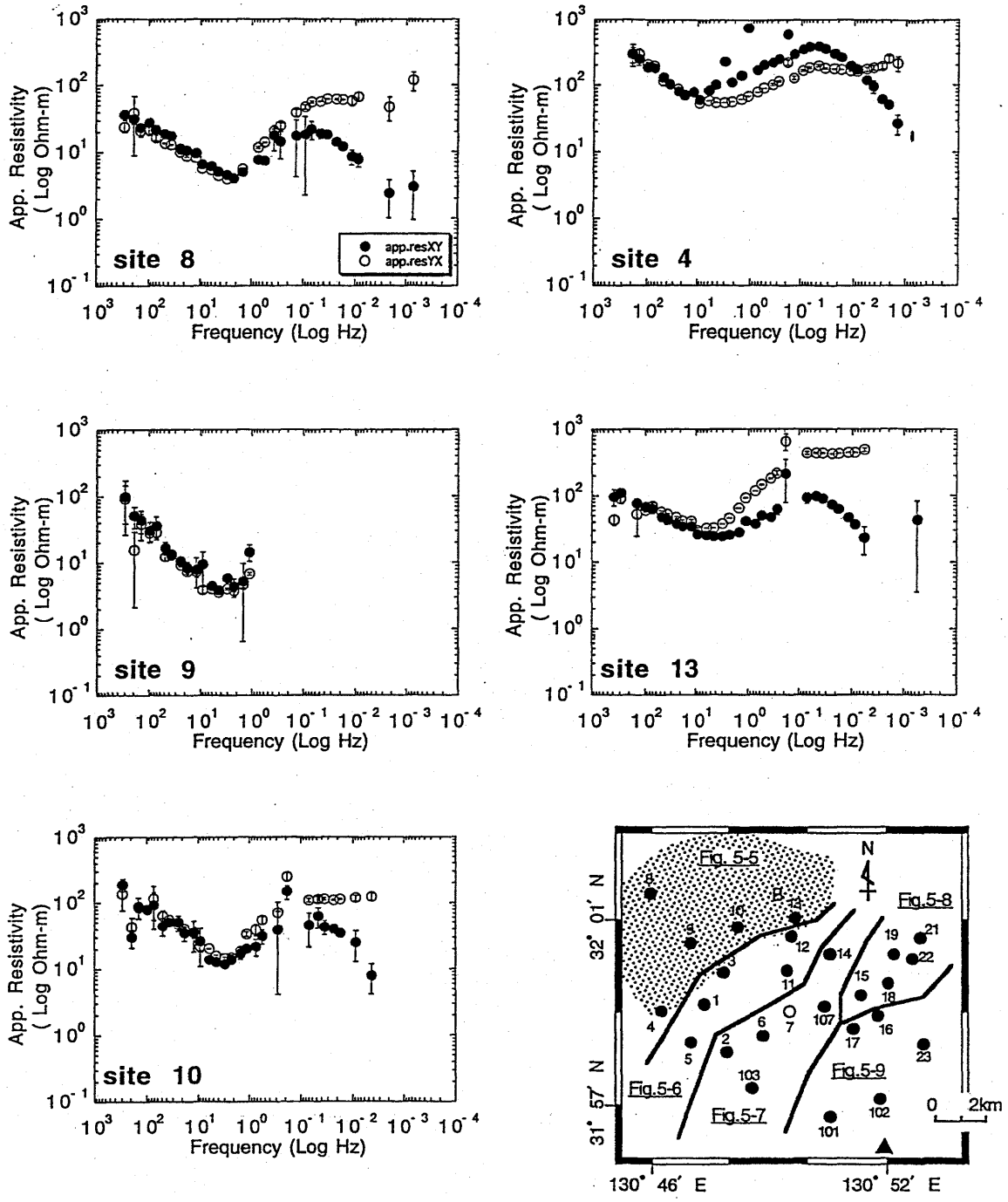
App. Resistivity (Log Ohm-m)
Frequency (Log Hz)
site 8
app.resXY
app.resYX
site 4
site 9
site 13
site 10
Fig. 5-5
Fig.5-8
Fig.5-6
Fig.5-7
Fig.5-9
N
32° 01′ N
31° 57′ N
130° 46′ E
130° 52′ E
0 2km

Fig.5-5(a)

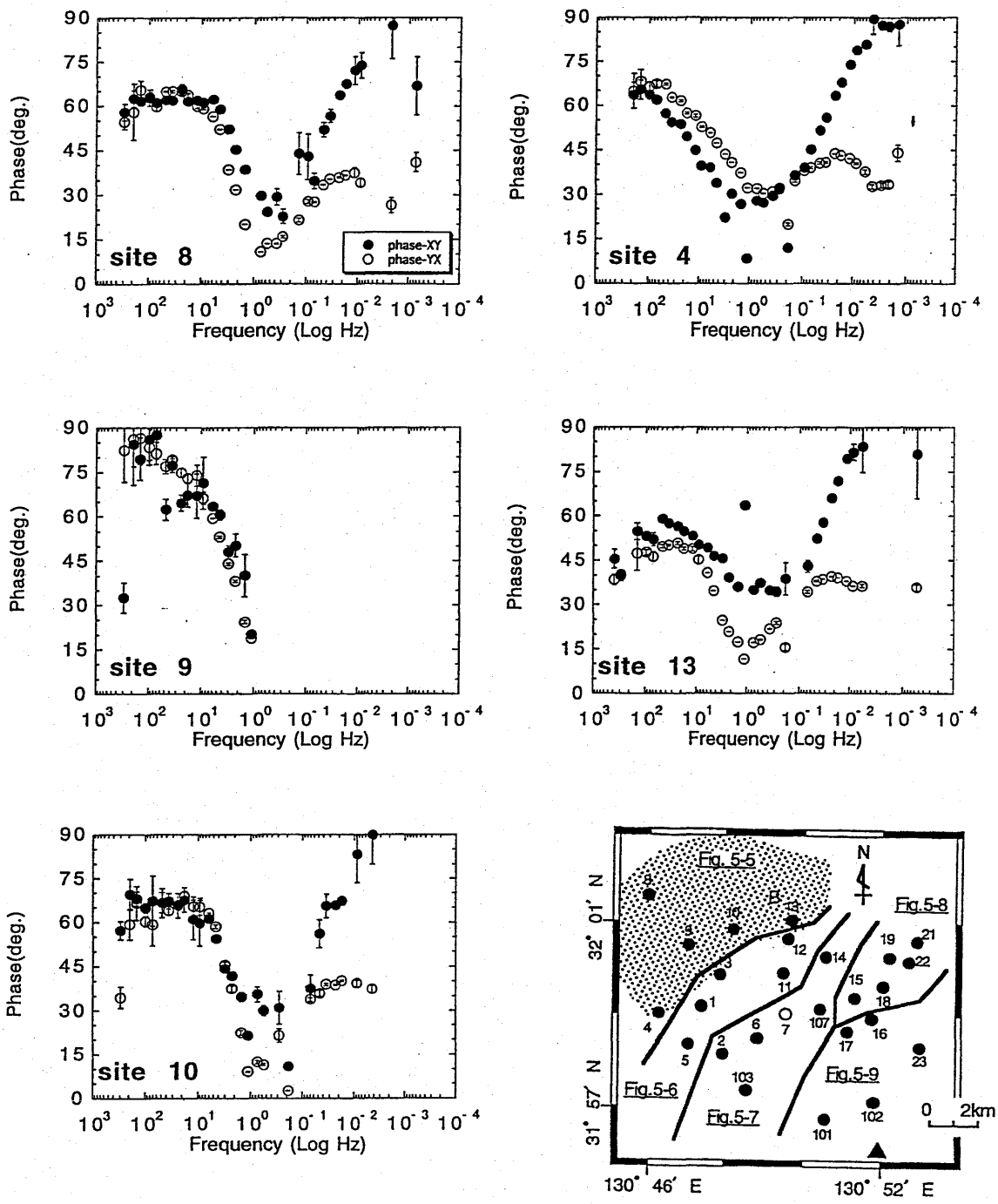
site 8
phase-XY
phase-YX
site 4
site 9
site 13
site 10
Phase(deg.)
Frequency (Log Hz)
Fig.5-5
Fig.5-6
Fig.5-7
Fig.5-8
Fig.5-9
N
32° 01′ N
31° 57′ N
130° 46′ E
130° 52′ E
0 2km

Fig.5-5(b)

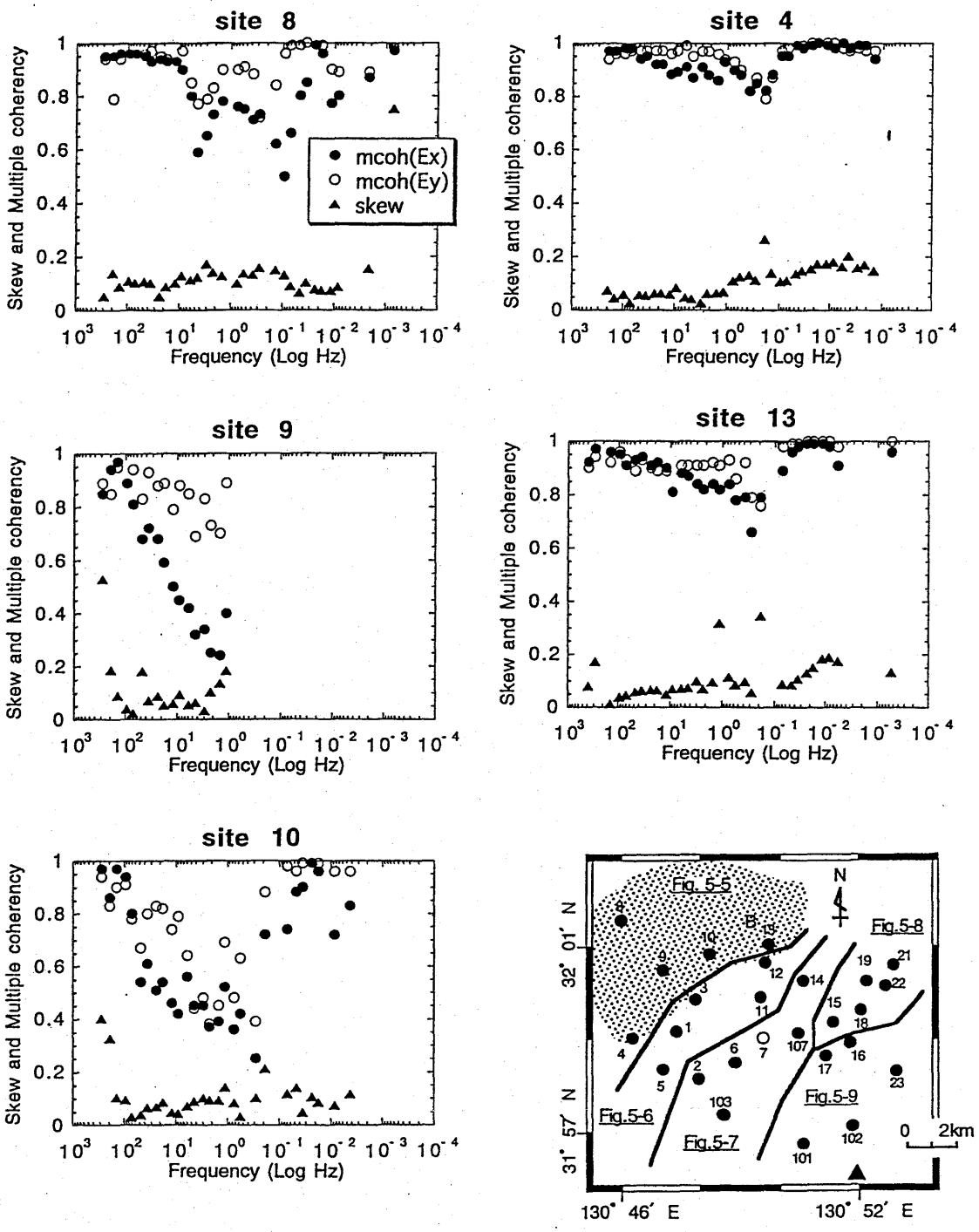
site 8
site 4
site 9
site 13
site 10
Skew and Multiple coherency
Frequency (Log Hz)
mcoh(Ex)
mcoh(Ey)
skew
Fig.5-5
Fig.5-6
Fig.5-7
Fig.5-8
Fig.5-9
N
32° 01′ N
31° 57′ N
130° 46′ E
130° 52′ E
0 2km

Fig.5-5(c)

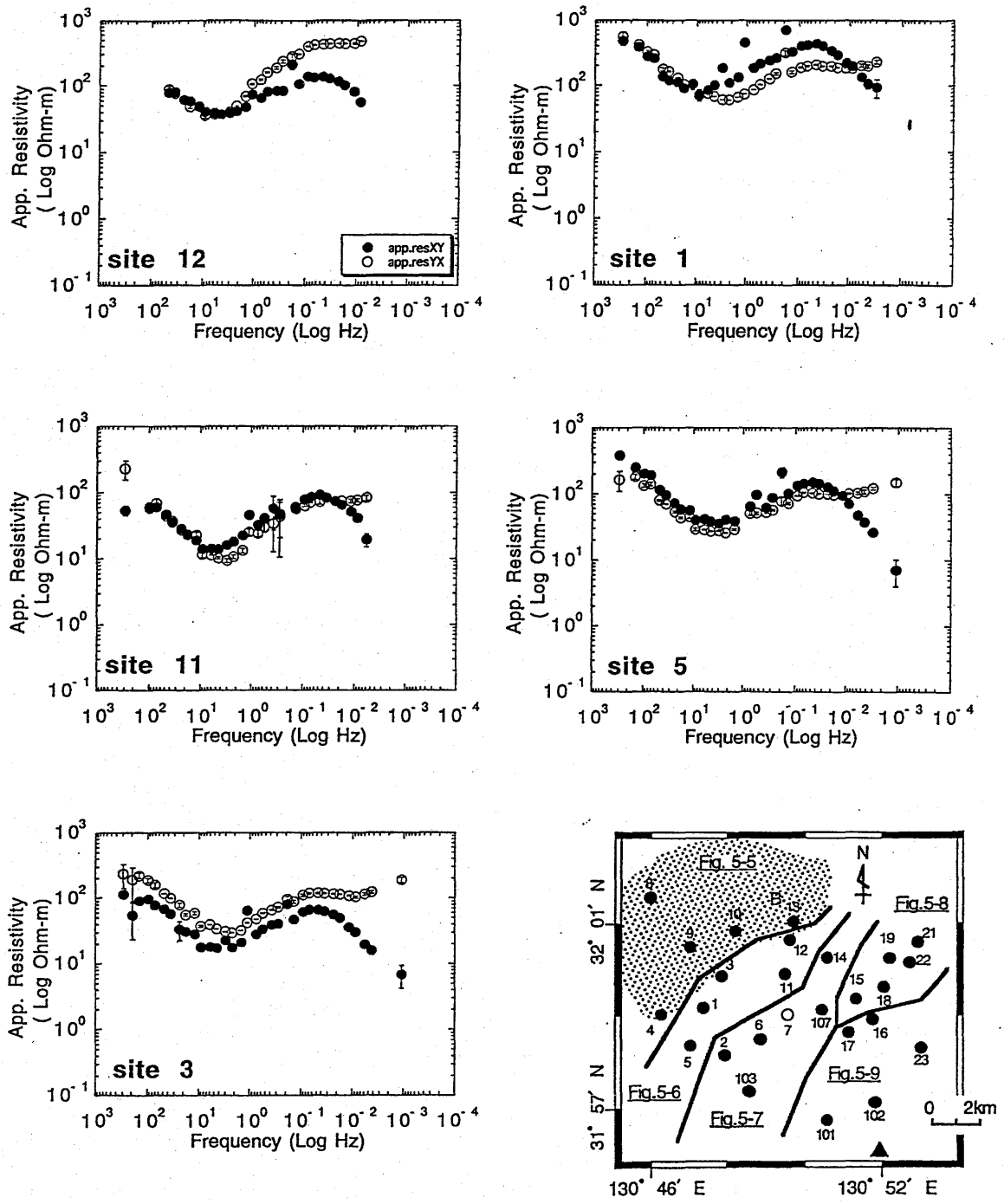
App. Resistivity (Log Ohm-m)
Frequency (Log Hz)
site 12
app.resXY
app.resYX
site 1
site 11
site 5
site 3
Fig. 5-5
Fig.5-6
Fig.5-7
Fig.5-8
Fig.5-9
N
32° 01′ N
31° 57′ N
130° 46′ E
130° 52′ E
0 2km

Fig. 5-6(a)

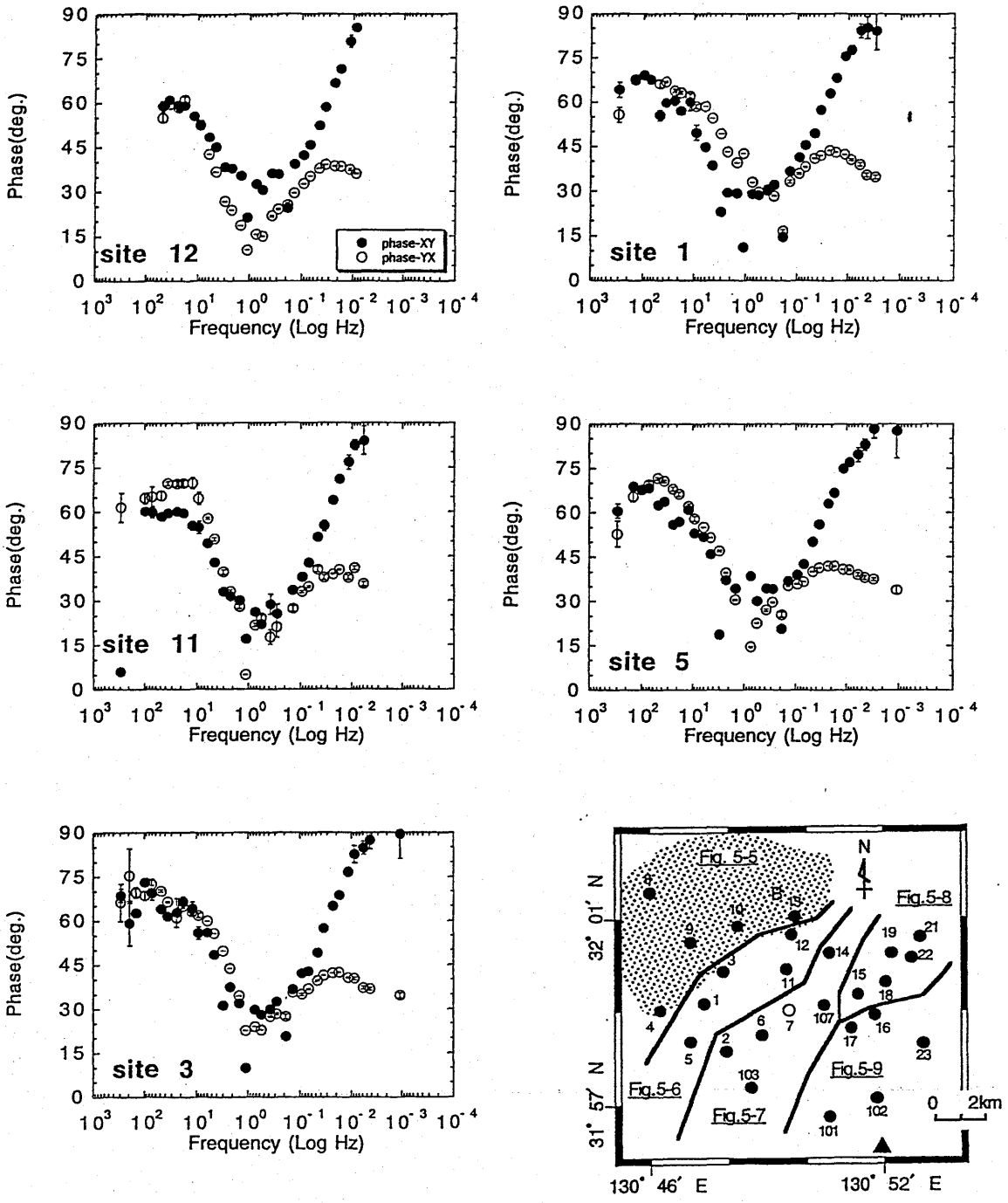
Phase(deg.)
Frequency (Log Hz)
site 12
phase-XY
phase-YX
site 1
site 11
site 5
site 3
Fig.5-5
Fig.5-6
Fig.5-7
Fig.5-8
Fig.5-9
N
0 2km
32° 01′ N
31° 57′ N
130° 46′ E
130° 52′ E

Fig.5-6(b)

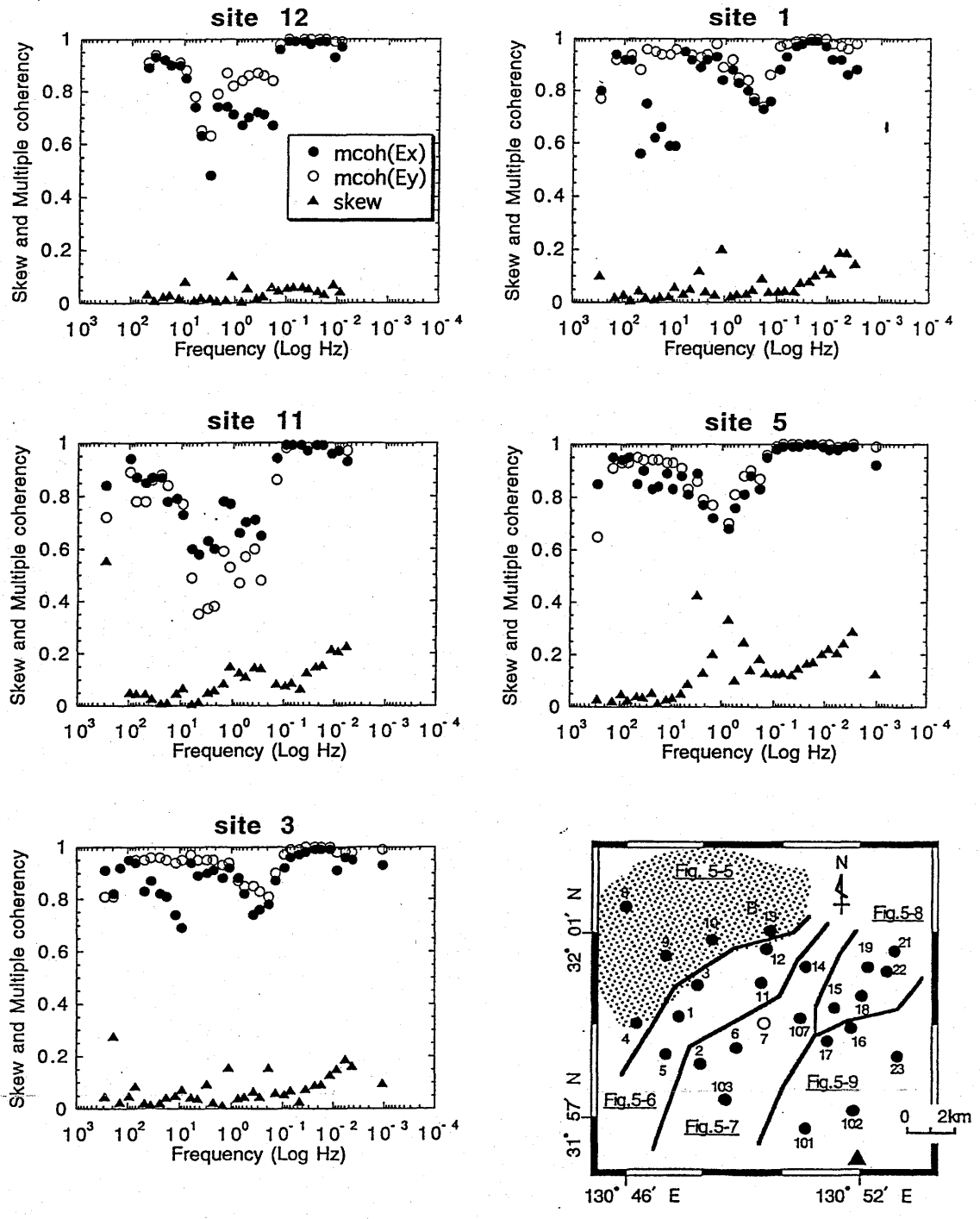
site 12
site 1
site 11
site 5
site 3
Skew and Multiple coherency
Frequency (Log Hz)
mcoh(Ex)
mcoh(Ey)
skew
Fig.5-5
Fig.5-6
Fig.5-7
Fig.5-8
Fig.5-9
N
0 2km
32° 01′ N
31° 57′ N
130° 46′ E
130° 52′ E

Fig.5-6(c)

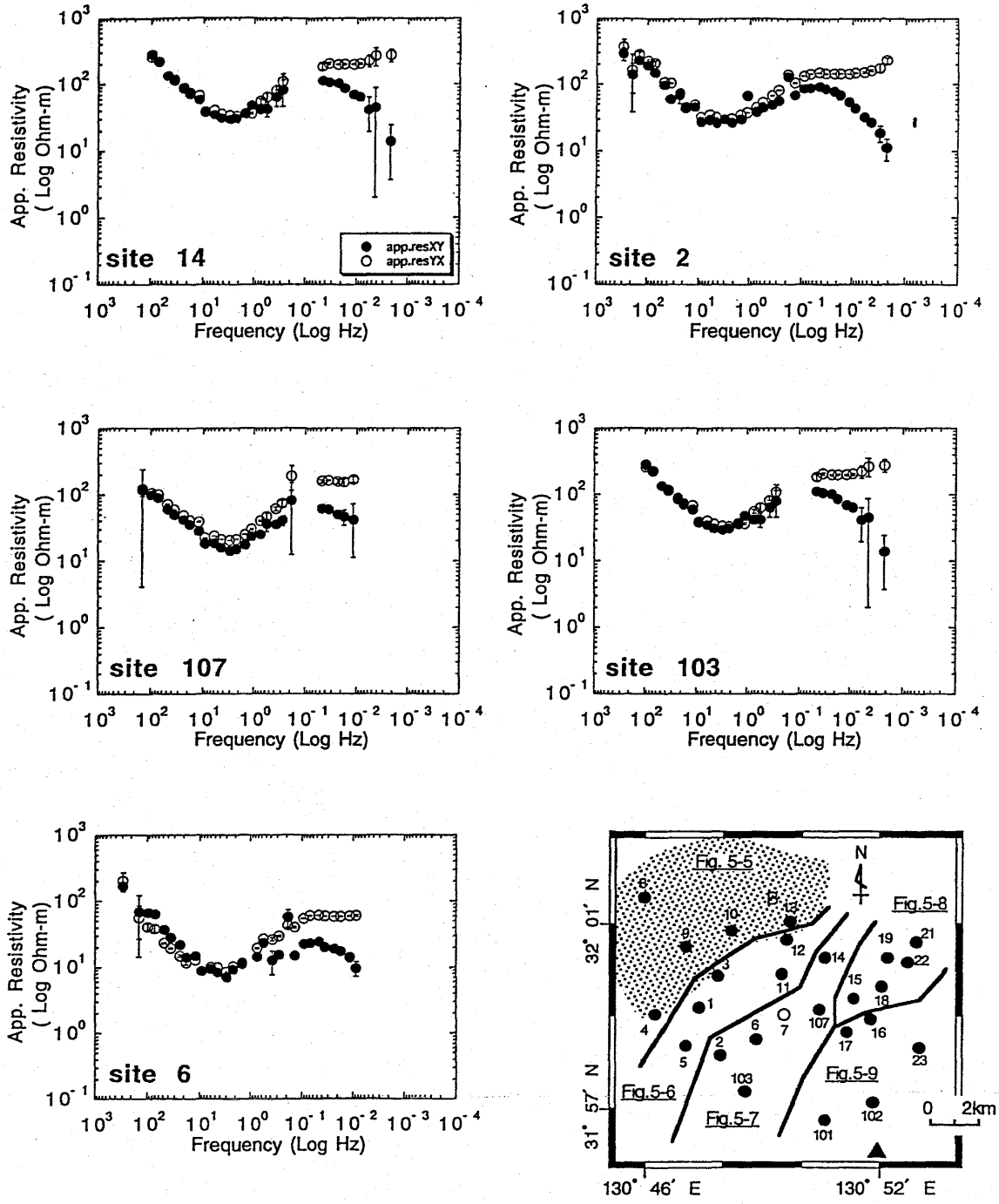
App. Resistivity (Log Ohm-m)
Frequency (Log Hz)
site 14
app.resXY
app.resYX
site 2
site 107
site 103
site 6
Fig.5-5
Fig.5-6
Fig.5-7
Fig.5-8
Fig.5-9
N
32° 01′ N
31° 57′ N
130° 46′ E
130° 52′ E
0 2km

Fig. 5-7(a)

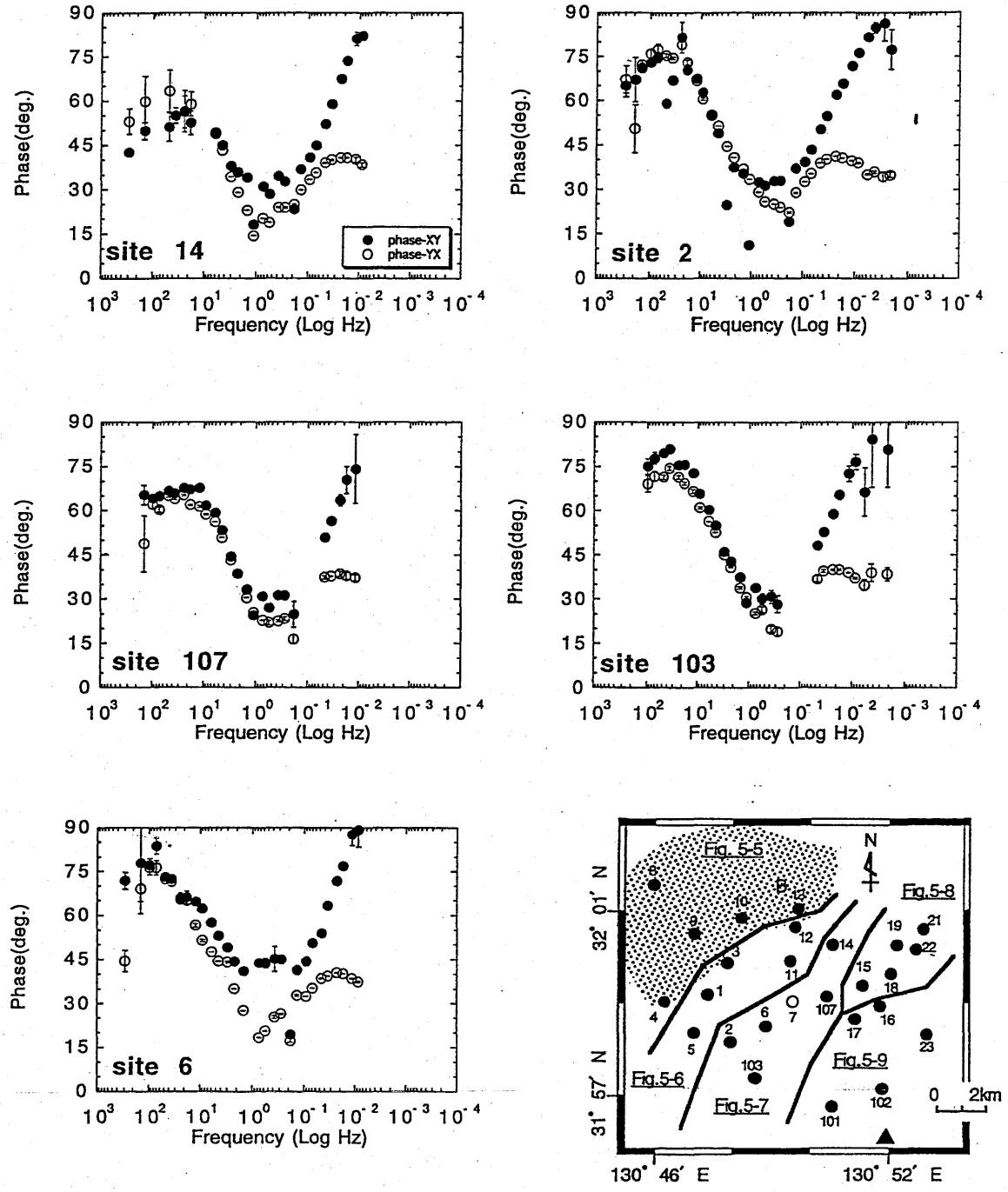
Phase(deg.)
Frequency (Log Hz)
site 14
phase-XY
phase-YX
site 2
site 107
site 103
site 6
Fig.5-5
Fig.5-6
Fig.5-7
Fig.5-8
Fig.5-9
N
0 2km
32° 01′ N
31° 57′ N
130° 46′ E
130° 52′ E

Fig.5-7(b)

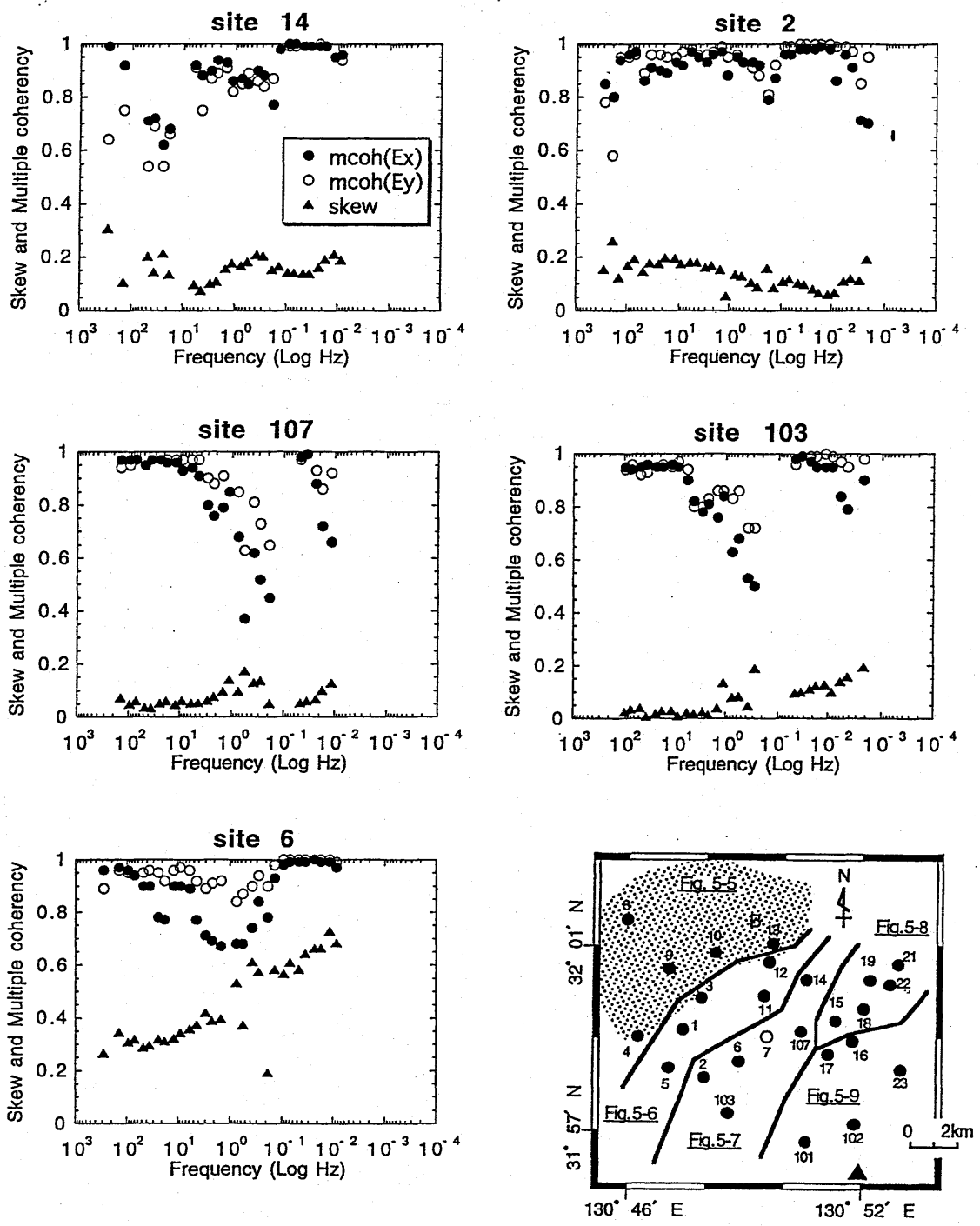
site 14
site 2
site 107
site 103
site 6
Skew and Multiple coherency
Frequency (Log Hz)
mcoh(Ex)
mcoh(Ey)
skew
Fig. 5-5
Fig.5-6
Fig.5-7
Fig.5-8
Fig.5-9
N
0 2km
32° 01′ N
31° 57′ N
130° 46′ E
130° 52′ E

Fig.5-7(c)

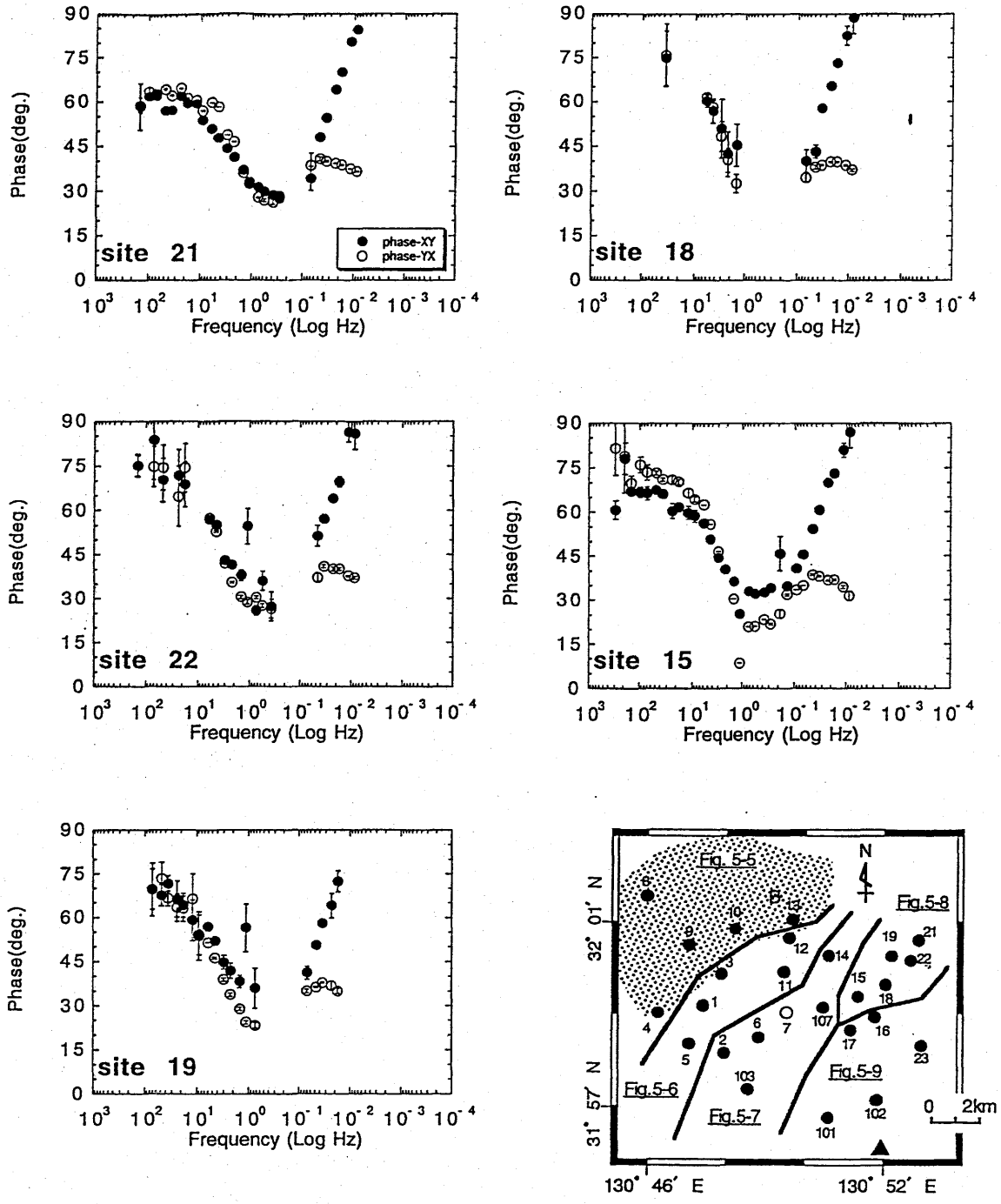
Phase(deg.)
Frequency (Log Hz)
site 21
phase-XY
phase-YX
site 18
site 22
site 15
site 19
Fig. 5-5
Fig.5-8
Fig.5-6
Fig.5-7
Fig.5-9
N
0 2km
32° 01′ N
31° 57′ N
130° 46′ E
130° 52′ E

Fig. 5-8(a)

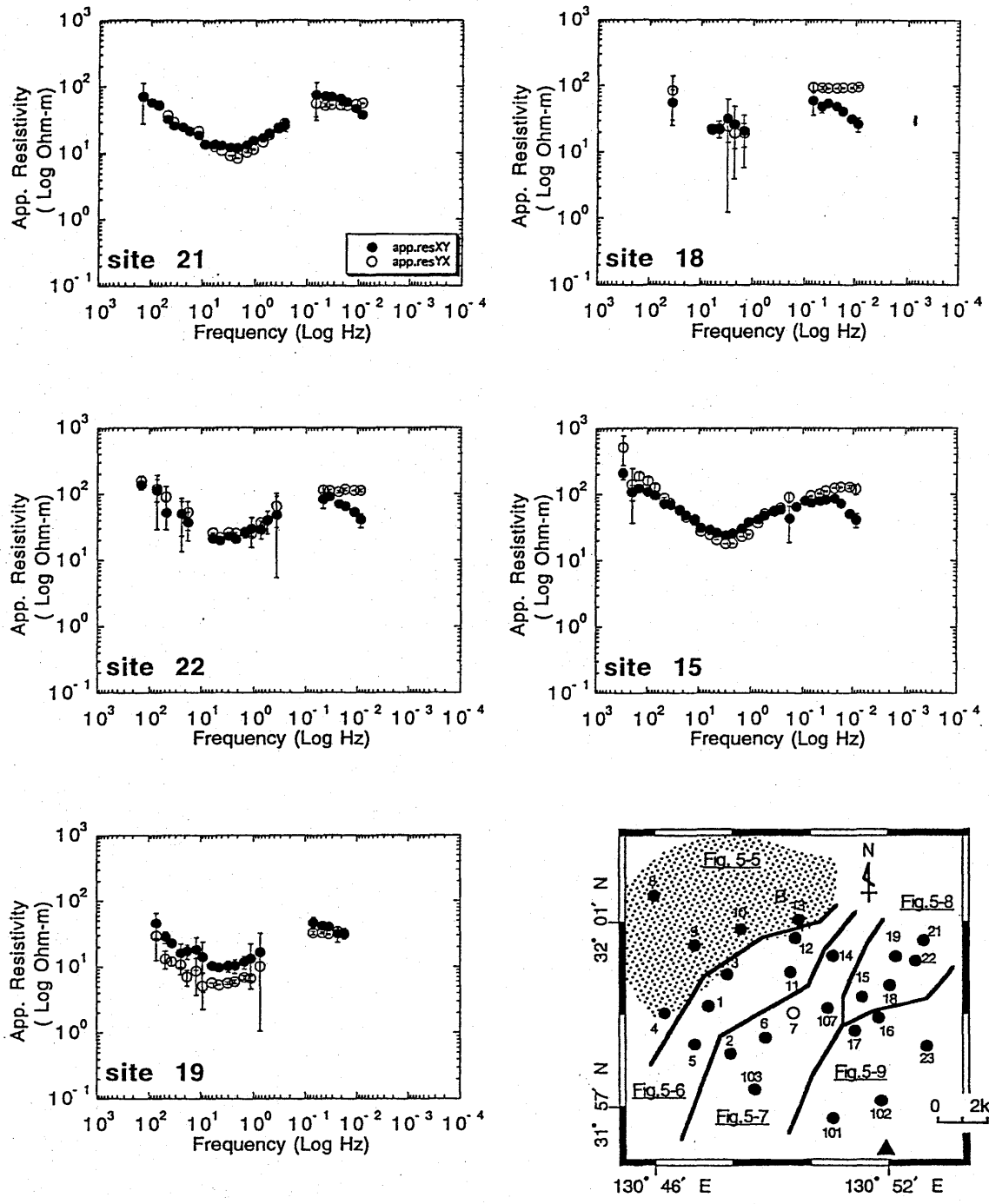
App. Resistivity (Log Ohm-m)
Frequency (Log Hz)
site 21
app.resXY
app.resYX
site 18
site 22
site 15
site 19
Fig.5-5
Fig.5-6
Fig.5-7
Fig.5-8
Fig.5-9
N
32° 01′ N
31° 57′ N
130° 46′ E
130° 52′ E
0 2km

Fig.5-8(b)

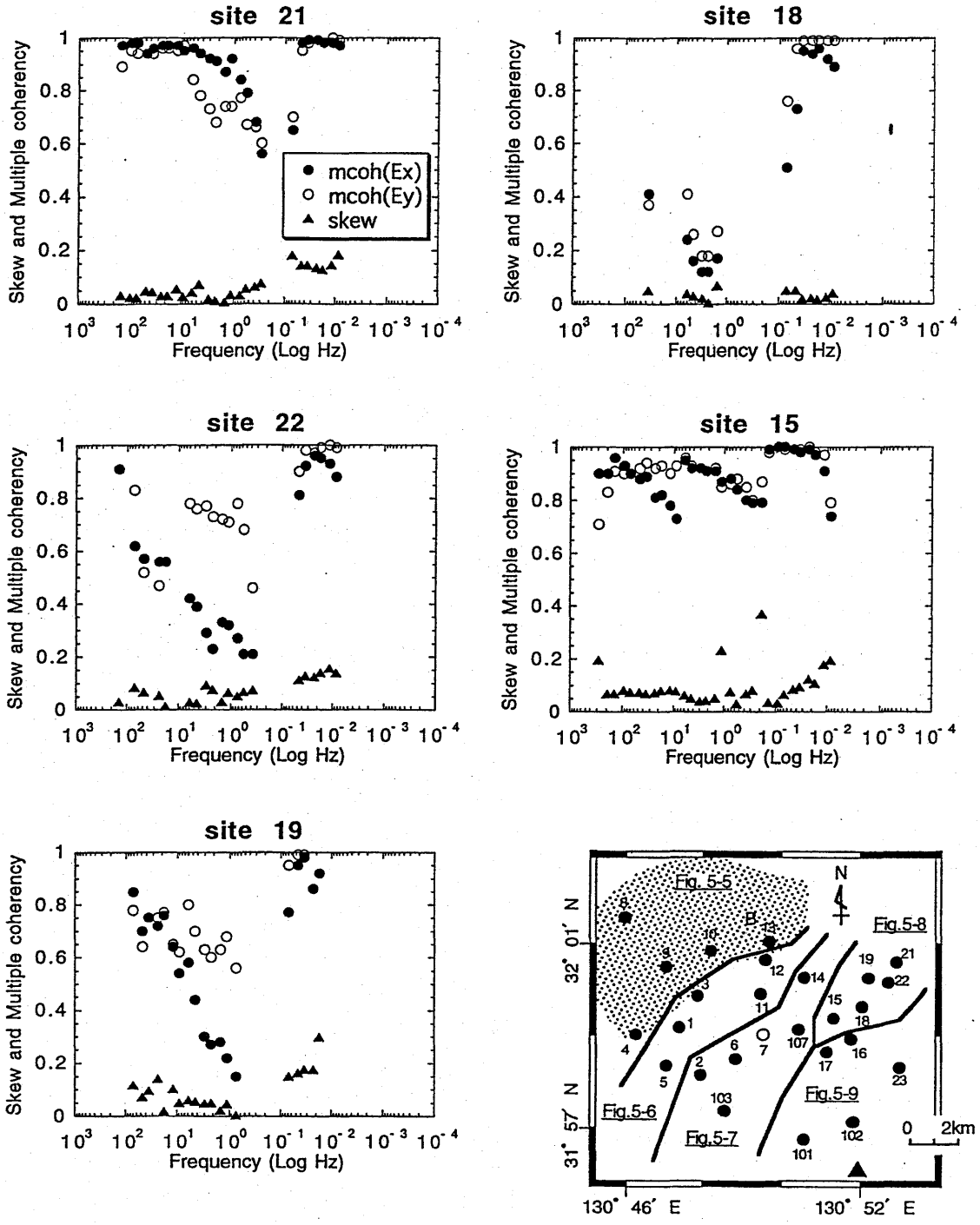
site 21
site 18
site 22
site 15
site 19
Skew and Multiple coherency
Frequency (Log Hz)
mcoh(Ex)
mcoh(Ey)
skew
Fig. 5-5
Fig.5-6
Fig.5-7
Fig.5-8
Fig.5-9
N
0 2km
130° 46′ E
130° 52′ E
32° 01′ N
31° 57′ N

Fig.5-8(c)

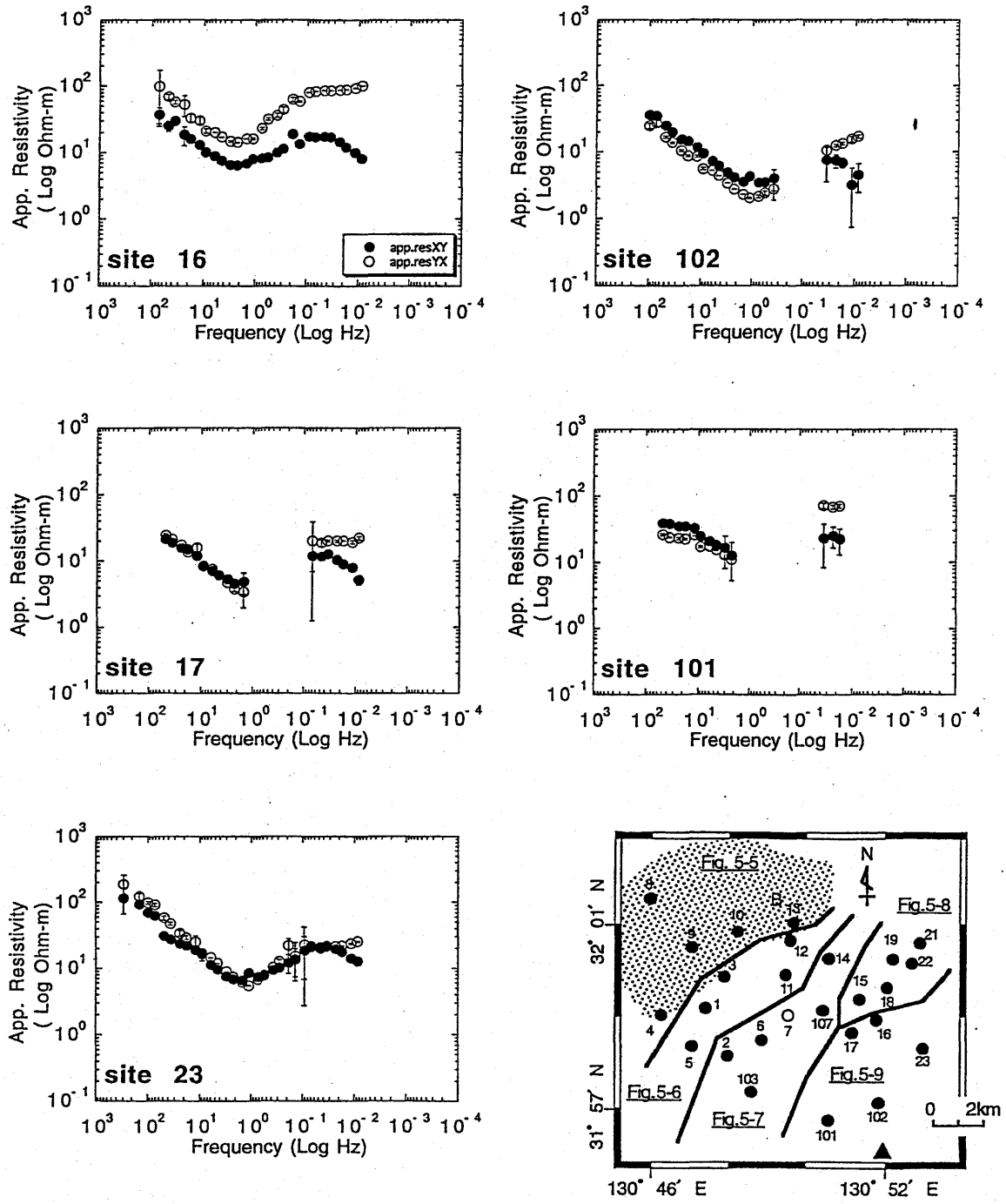
App. Resistivity (Log Ohm-m)
Frequency (Log Hz)
site 16
app.resXY
app.resYX
site 102
site 17
site 101
site 23
Fig. 5-5
Fig.5-6
Fig.5-7
Fig.5-8
Fig.5-9
N
32° 01′ N
31° 57′ N
130° 46′ E
130° 52′ E
0 2km

Fig. 5-9(a)

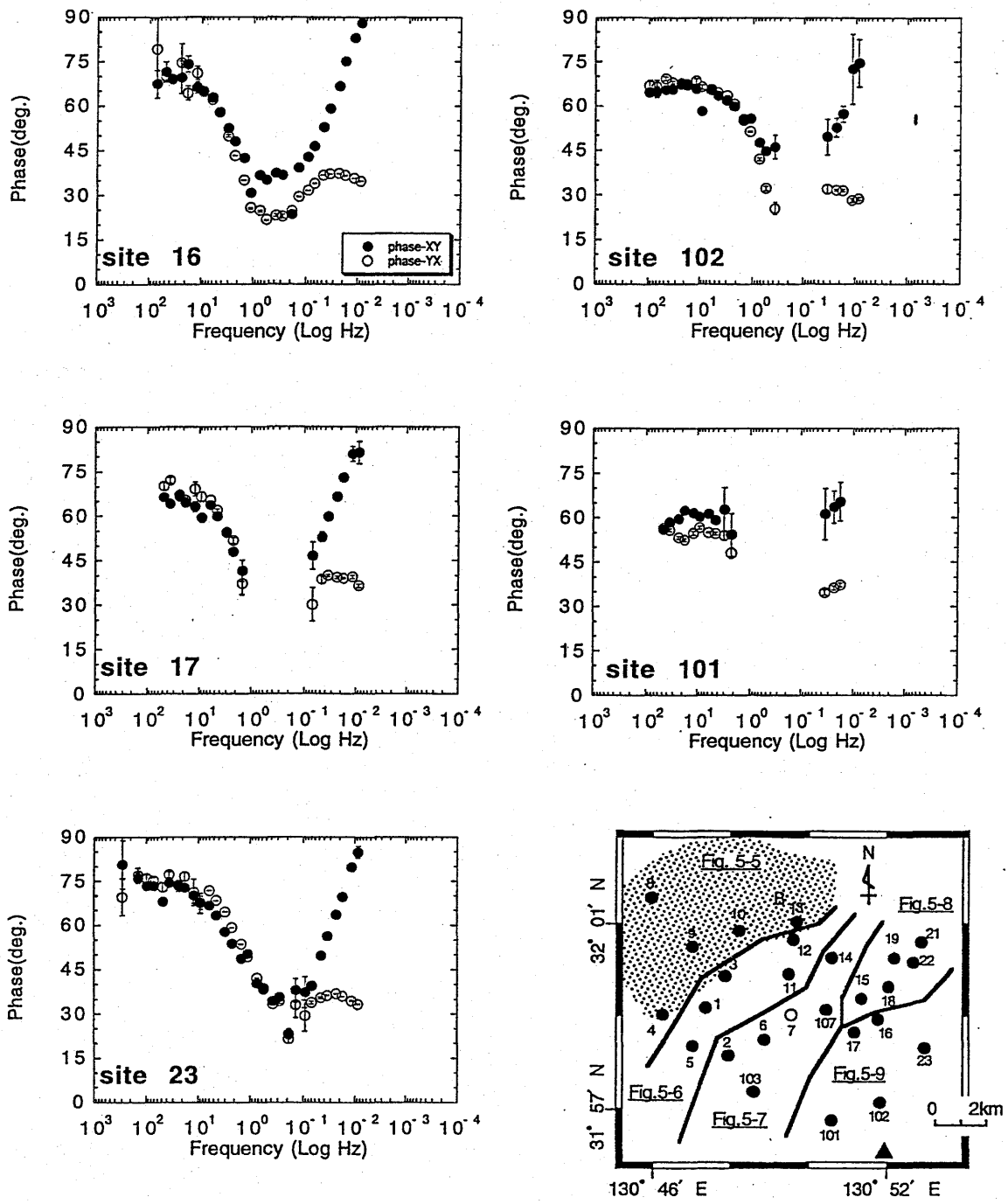
site 16
phase-XY
phase-YX
site 102
site 17
site 101
site 23
Phase(deg.)
Frequency (Log Hz)
Fig.5-5
Fig.5-6
Fig.5-7
Fig.5-8
Fig.5-9
N
32° 01′ N
31° 57′ N
130° 46′ E
130° 52′ E
0 2km

Fig.5-9(b)

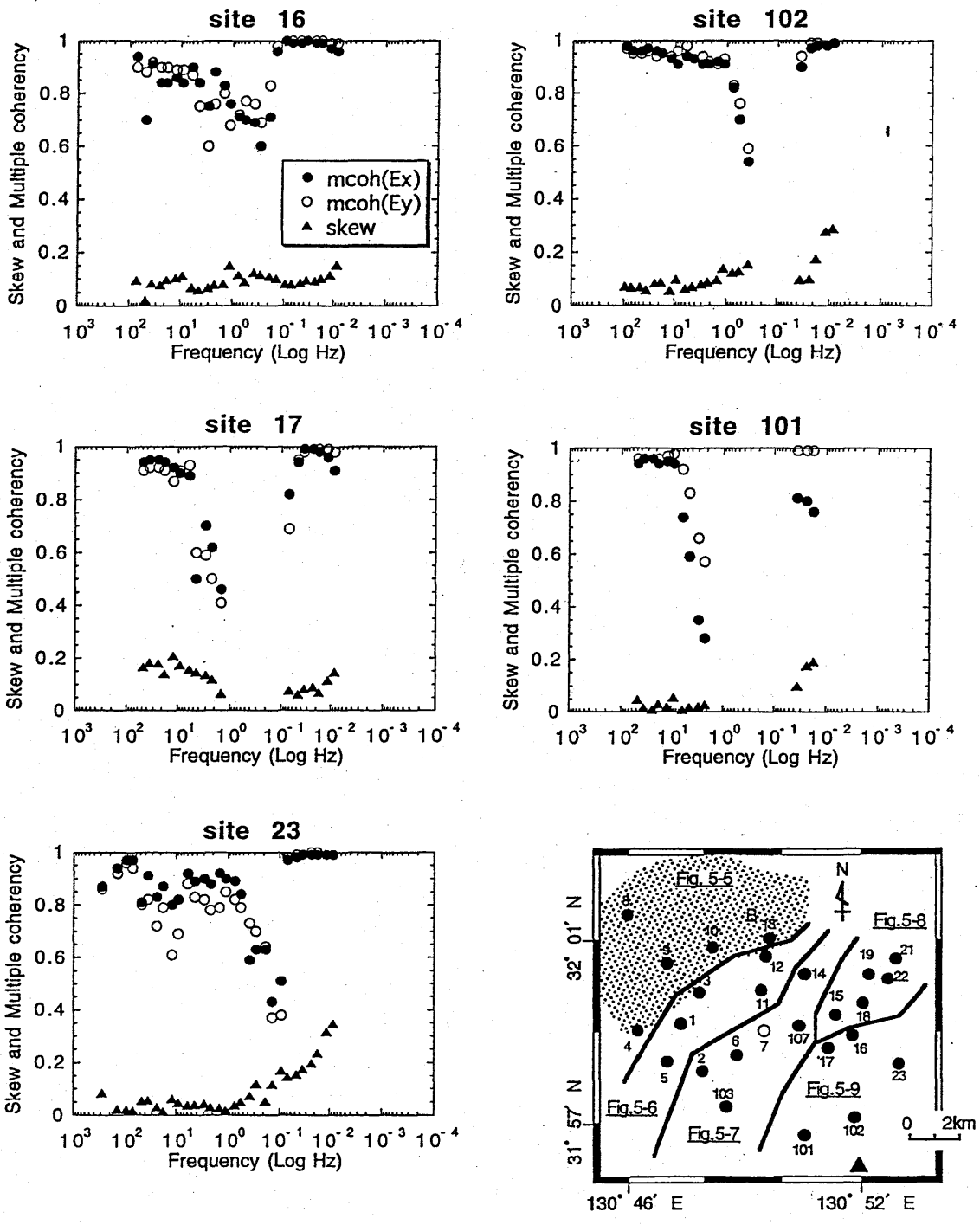
site 16
site 102
site 17
site 101
site 23
Skew and Multiple coherency
Frequency (Log Hz)
mcoh(Ex)
mcoh(Ey)
skew
Fig.5-5
Fig.5-6
Fig.5-7
Fig.5-8
Fig.5-9
N
32° 01′ N
31° 57′ N
130° 46′ E
130° 52′ E
0 2km

Fig.5-9(c)

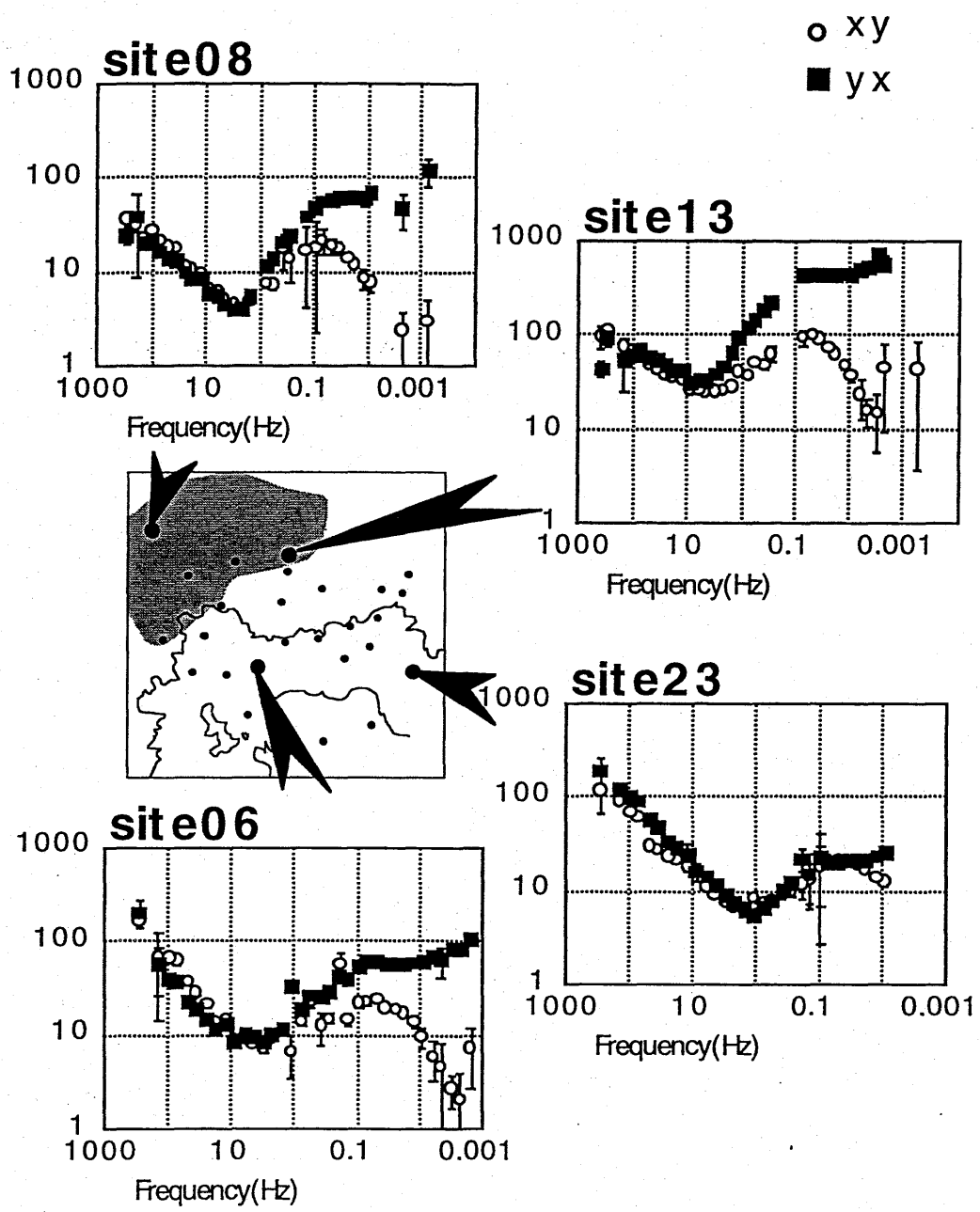
Apparent Resistivity(Ohm-m)
o xy
■ yx
site08
1000
100
10
1
1000 10 0.1 0.001
Frequency(Hz)
site13
1000
100
10
1
1000 10 0.1 0.001
Frequency(Hz)
site23
1000
100
10
1
1000 10 0.1 0.001
Frequency(Hz)
site06
1000
100
10
1
1000 10 0.1 0.001
Frequency(Hz)

Fig.5-10

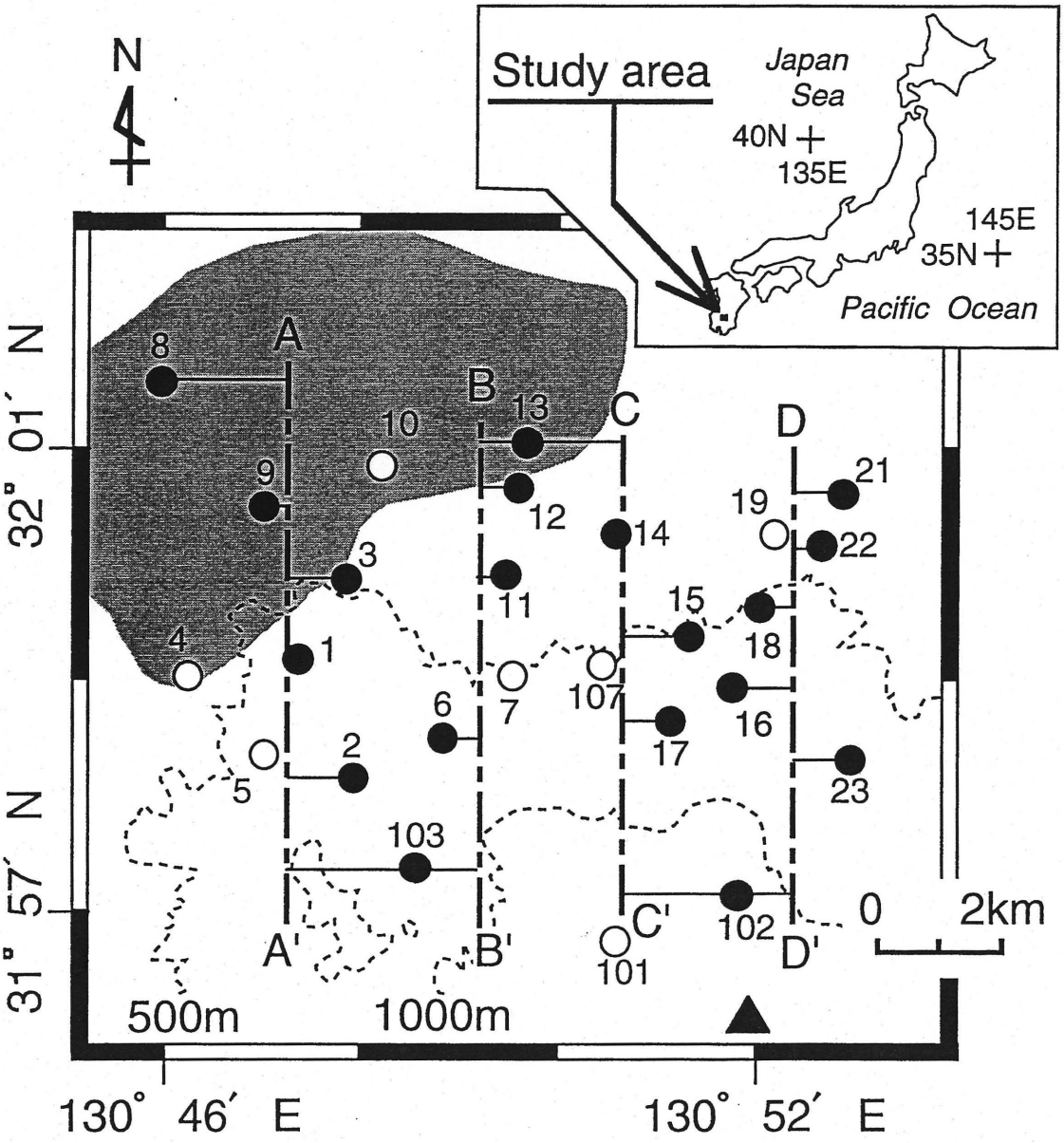
N
Study area
Japan
Sea
40N
135E
145E
35N
Pacific Ocean
32° 01′ N
31° 57′ N
130° 46′ E
130° 52′ E
500m
1000m
0
2km
A
B
C
D
A'
B'
C'
D'
1
2
3
4
5
6
7
8
9
10
11
12
13
14
15
16
17
18
19
21
22
23
101
102
103
107

Fig. 5-11

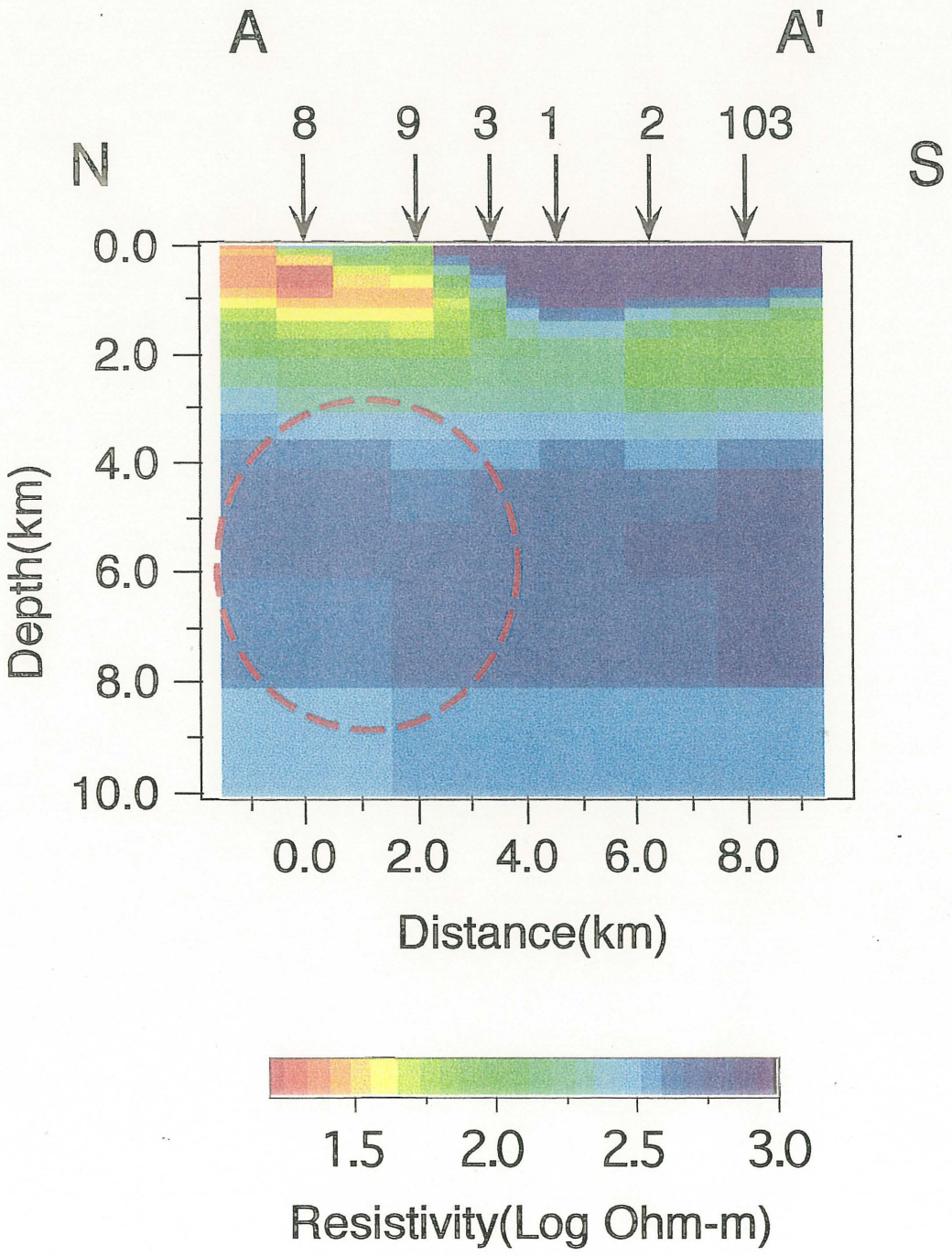
A
A'
N
S
8
9
3
1
2
103
0.0
2.0
4.0
6.0
8.0
10.0
Depth(km)
0.0
2.0
4.0
6.0
8.0
Distance(km)
1.5
2.0
2.5
3.0
Resistivity(Log Ohm-m)

Fig. 5-12

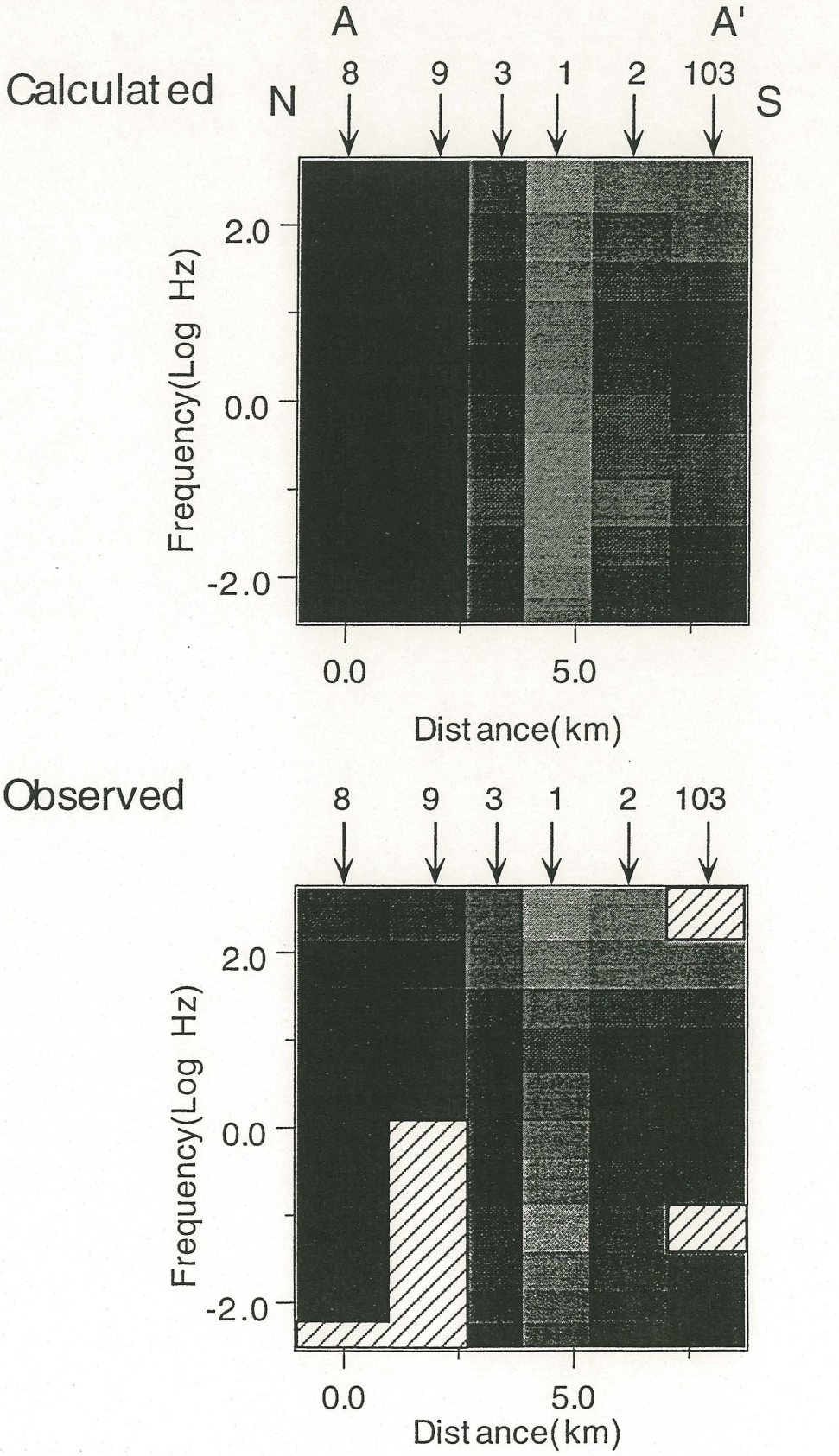
A
A'
Calculated
N
8
9
3
1
2
103
S
2.0
0.0
-2.0
Frequency(Log Hz)
0.0
5.0
Distance(km)
Observed
8
9
3
1
2
103
2.0
0.0
-2.0
Frequency(Log Hz)
0.0
5.0
Distance(km)
1.0
2.0
3.0
4.0
Apparent Resistivity (Log Ohm-m)

Fig. 5-13(a)

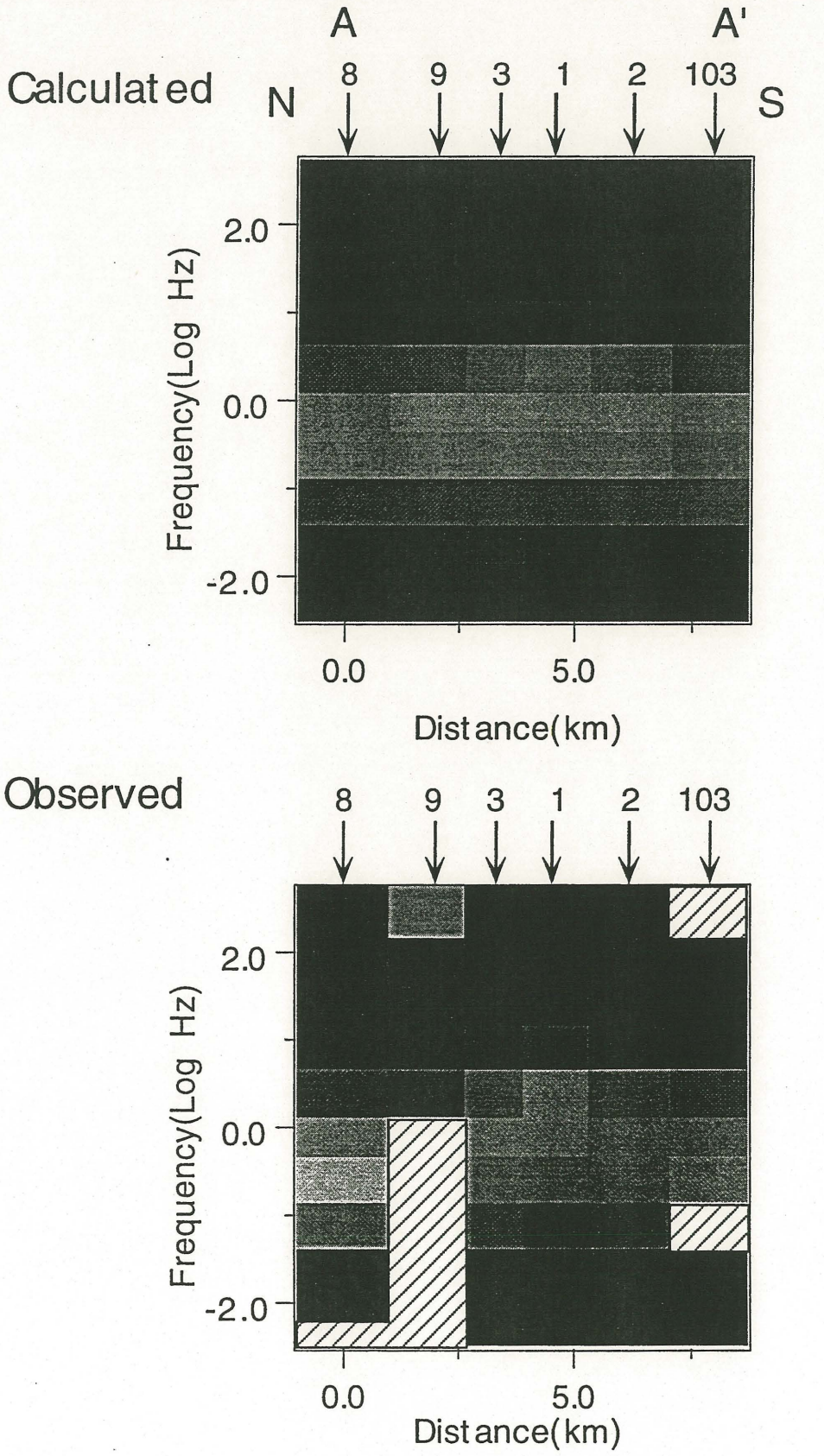
Calculated
A
A'
N
S
8
9
3
1
2
103
2.0
0.0
-2.0
Frequency(Log Hz)
0.0
5.0
Distance(km)
Observed
8
9
3
1
2
103
2.0
0.0
-2.0
Frequency(Log Hz)
0.0
5.0
Distance(km)
15.0
30.0
45.0
60.0
75.0
Phase(deg.)

Fig. 5-13(b)

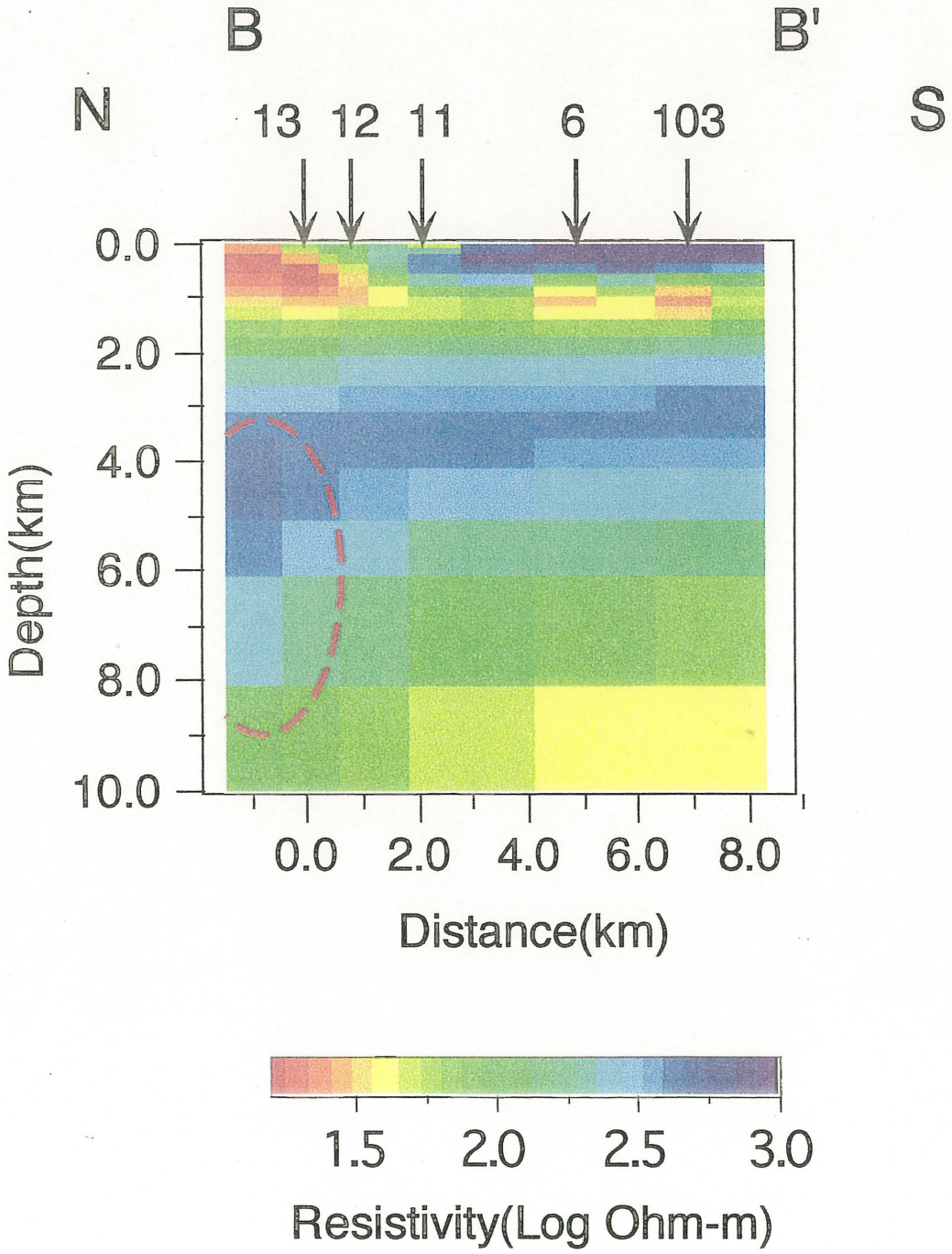
B
B'
N
S
13
12
11
6
103
0.0
2.0
4.0
6.0
8.0
10.0
Depth(km)
0.0
2.0
4.0
6.0
8.0
Distance(km)
1.5
2.0
2.5
3.0
Resistivity(Log Ohm-m)

Fig. 5-14

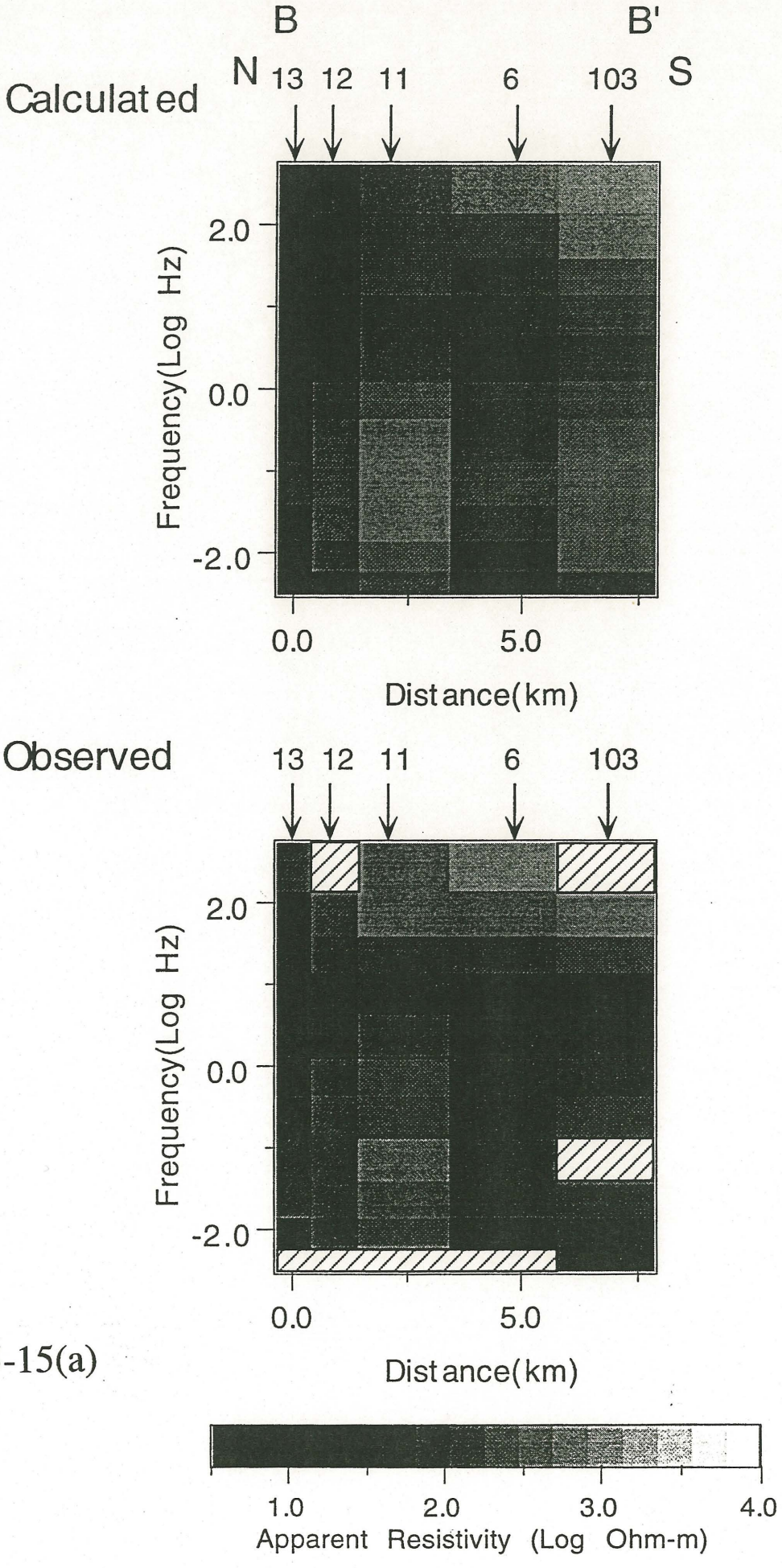
B
B'
N
S
Calculated
13
12
11
6
103
2.0
0.0
-2.0
Frequency(Log Hz)
0.0
5.0
Distance(km)
Observed
13
12
11
6
103
2.0
0.0
-2.0
Frequency(Log Hz)
0.0
5.0
Distance(km)
1.0
2.0
3.0
4.0
Apparent Resistivity (Log Ohm-m)

Fig. 5-15(a)

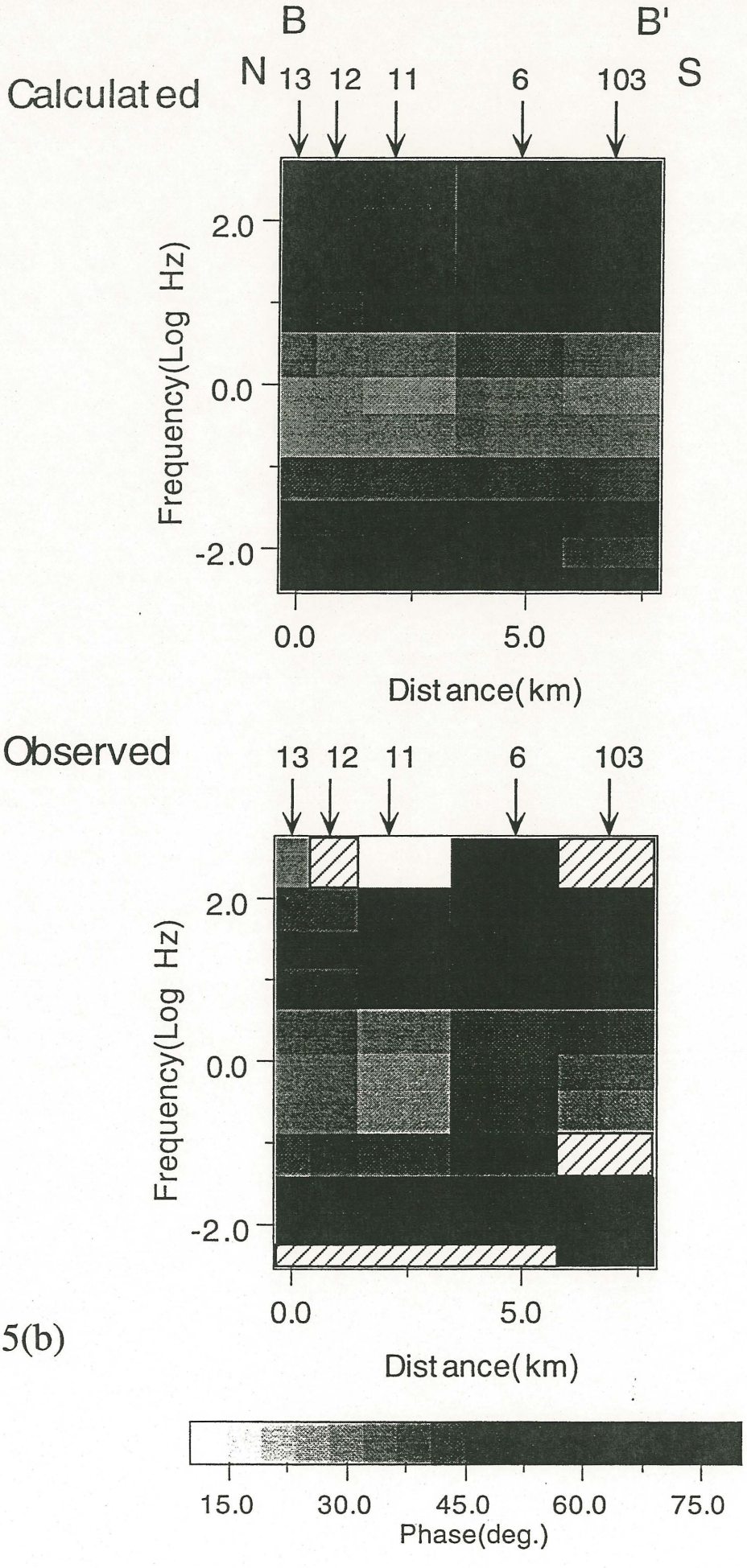
B
B'
Calculated
N
13
12
11
6
103
S
2.0
0.0
-2.0
Frequency(Log Hz)
0.0
5.0
Distance(km)
Observed
13
12
11
6
103
2.0
0.0
-2.0
Frequency(Log Hz)
0.0
5.0
Distance(km)
15.0
30.0
45.0
60.0
75.0
Phase(deg.)

Fig. 5-15(b)

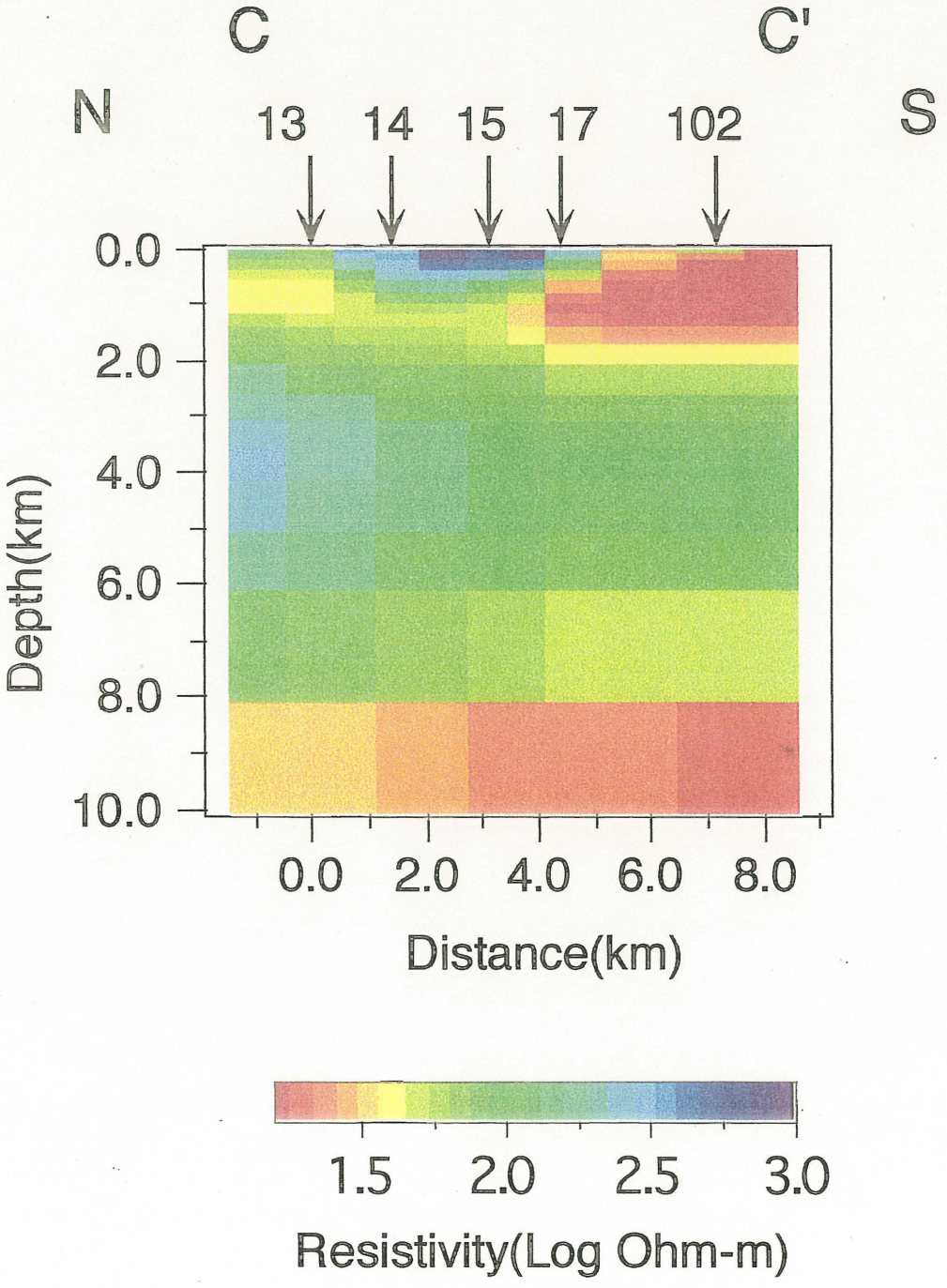
C
C'
N
S
13
14
15
17
102
0.0
2.0
4.0
6.0
8.0
10.0
Depth(km)
0.0
2.0
4.0
6.0
8.0
Distance(km)
1.5
2.0
2.5
3.0
Resistivity(Log Ohm-m)

Fig. 5-16

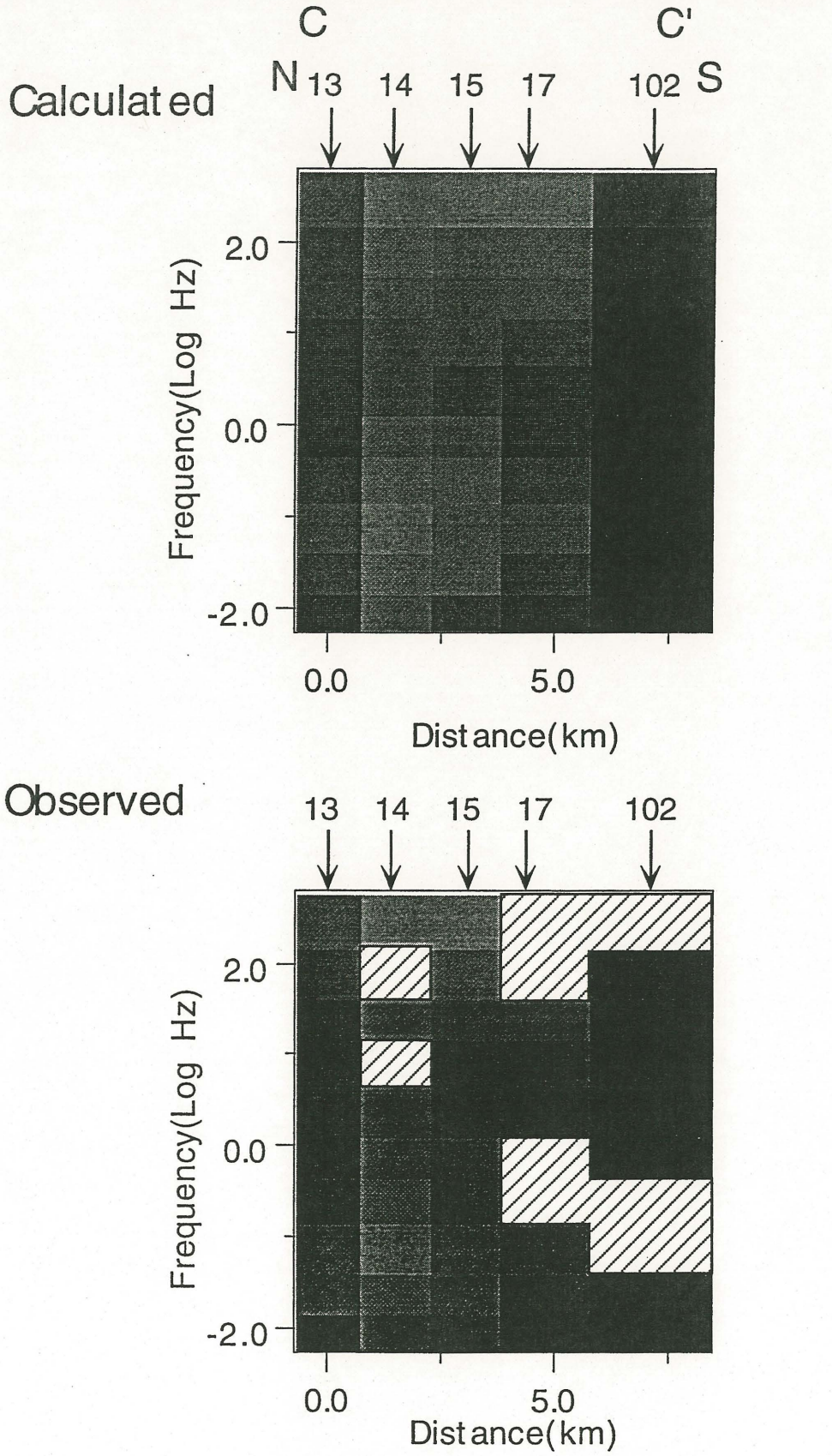
C
C'
N
13
14
15
17
102
S
Calculated
2.0
0.0
-2.0
Frequency(Log Hz)
0.0
5.0
Distance(km)
Observed
13
14
15
17
102
2.0
0.0
-2.0
Frequency(Log Hz)
0.0
5.0
Distance(km)
1.0
2.0
3.0
4.0
Apparent Resistivity (Log Ohm-m)

Fig. 5-17(a)

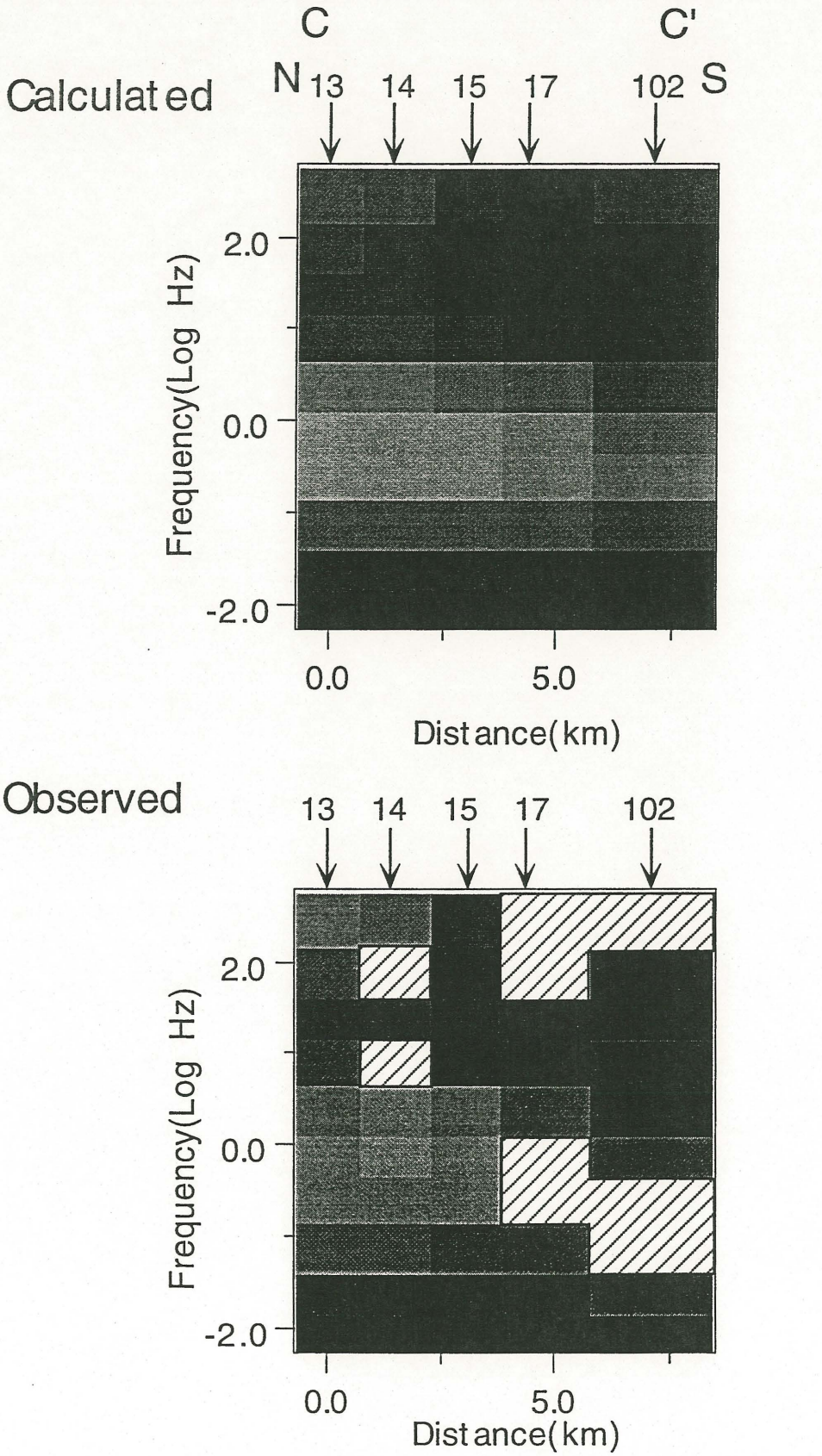
C
C'
Calculated
N
13
14
15
17
102
S
2.0
0.0
-2.0
Frequency(Log Hz)
0.0
5.0
Distance(km)
Observed
13
14
15
17
102
2.0
0.0
-2.0
Frequency(Log Hz)
0.0
5.0
Distance(km)

Fig. 5-17(b)

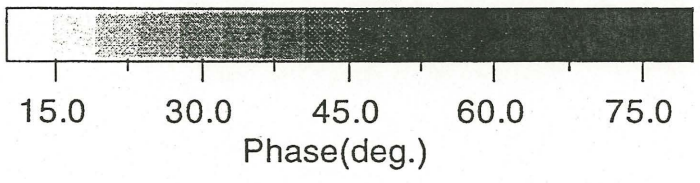
15.0
30.0
45.0
60.0
75.0
Phase(deg.)

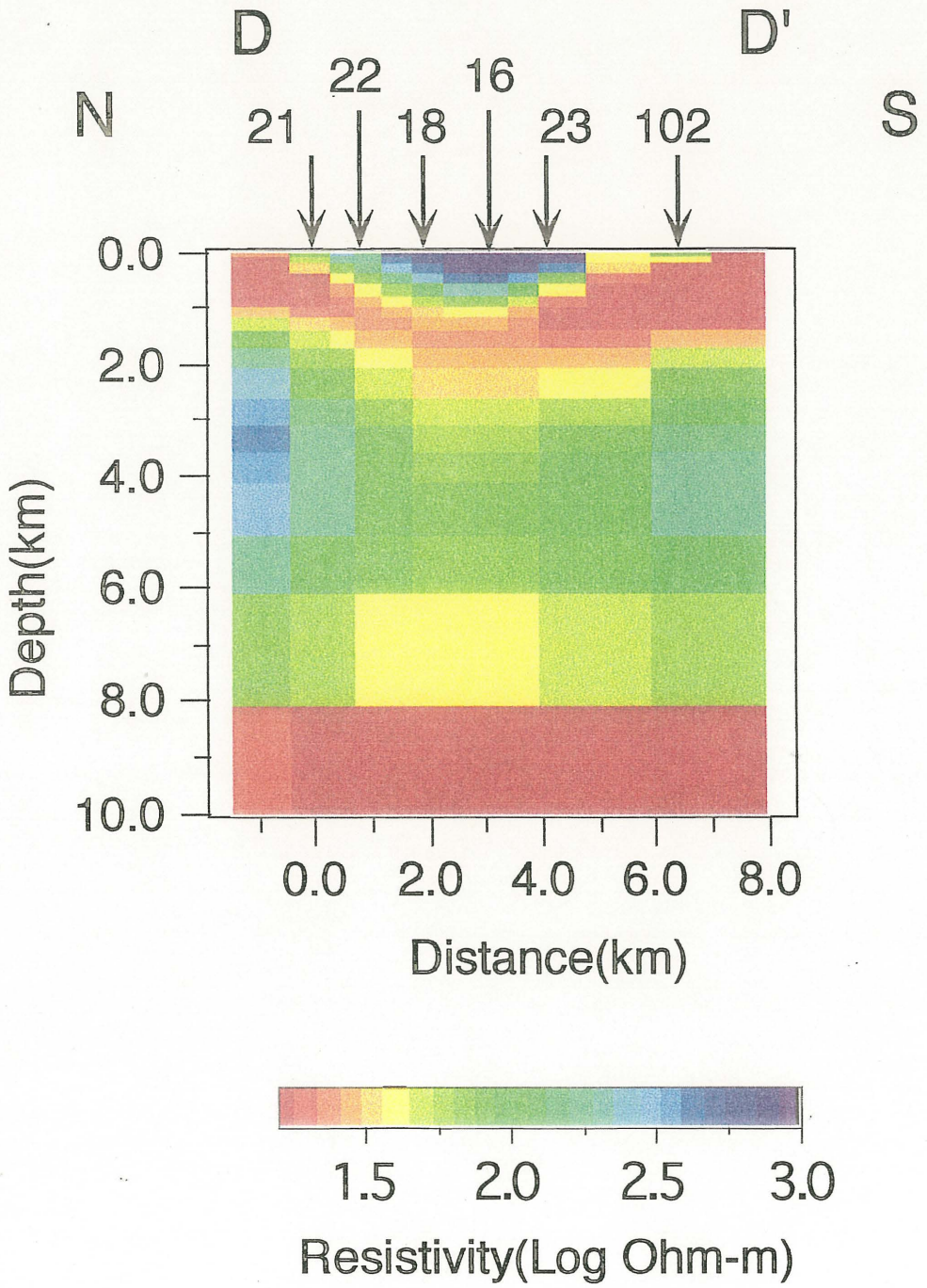
D
D'
N
S
21
22
18
16
23
102
0.0
2.0
4.0
6.0
8.0
10.0
Depth(km)
0.0
2.0
4.0
6.0
8.0
Distance(km)
1.5
2.0
2.5
3.0
Resistivity(Log Ohm-m)

Fig. 5-18

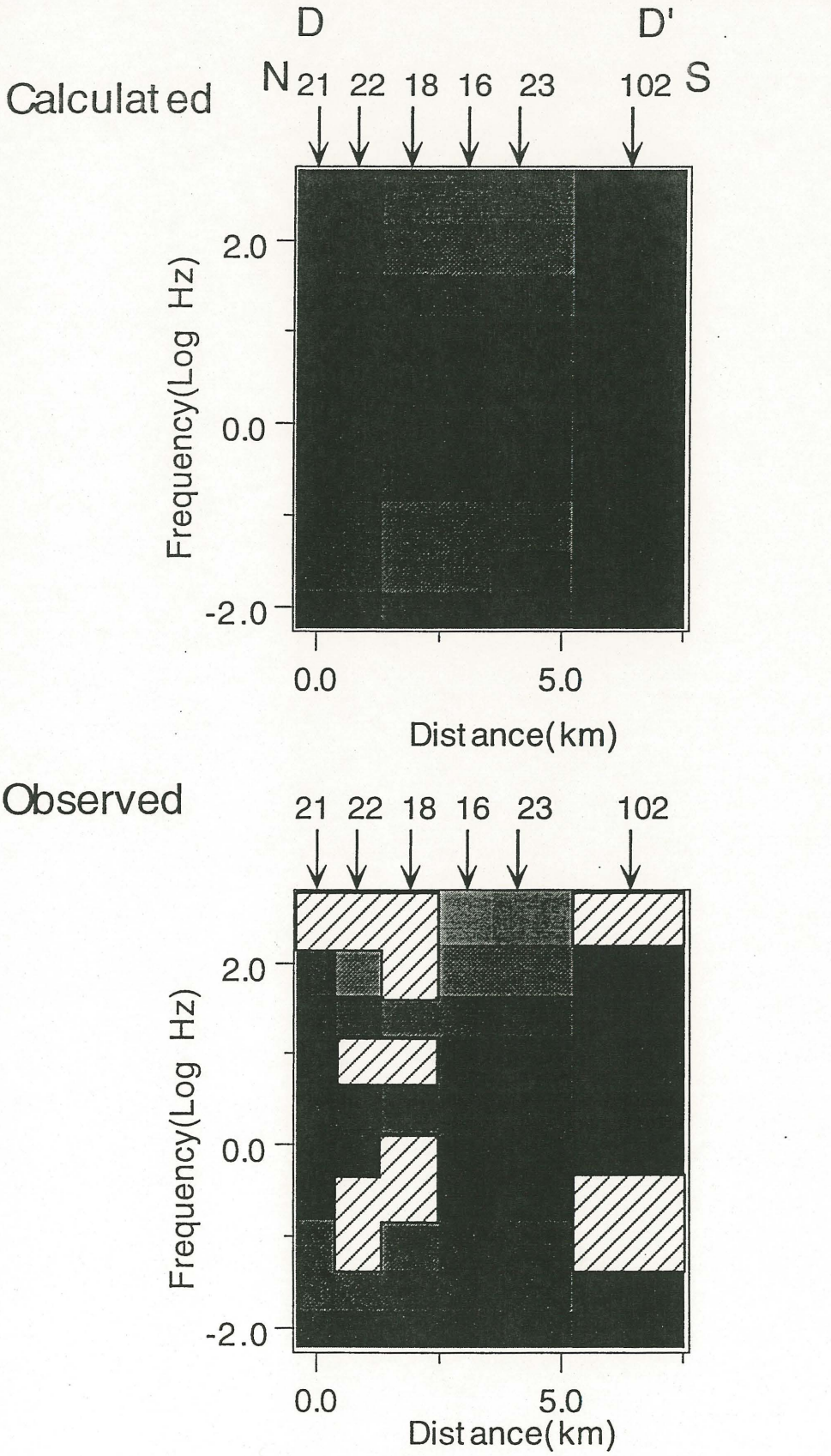
D
D'
Calculated
N 21 22 18 16 23 102 S
2.0
0.0
-2.0
Frequency(Log Hz)
0.0
5.0
Distance(km)
Observed
21 22 18 16 23 102
2.0
0.0
-2.0
Frequency(Log Hz)
0.0
5.0
Distance(km)
1.0
2.0
3.0
4.0
Apparent Resistivity (Log Ohm-m)

Fig. 5-19(a)

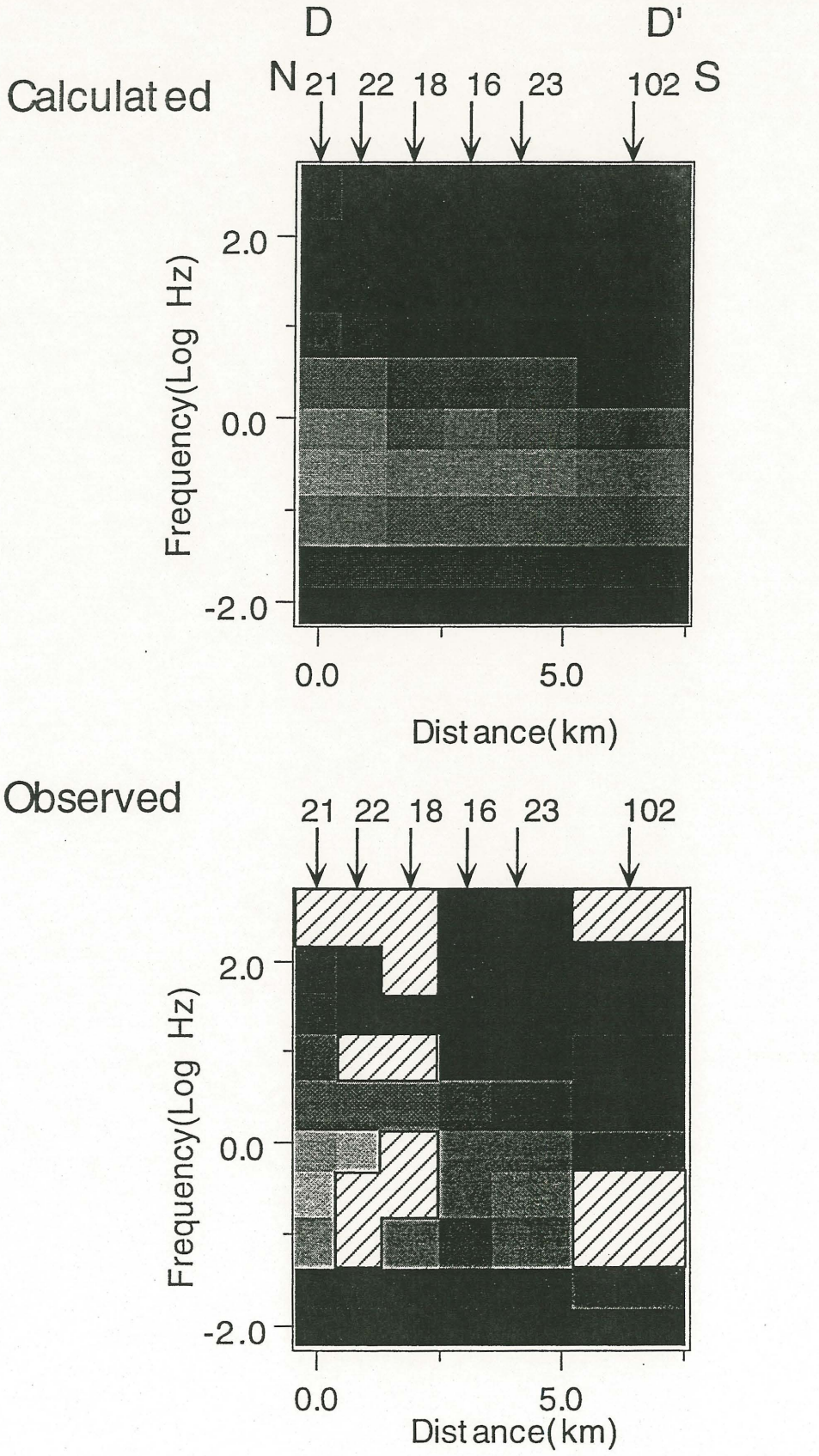
D
D'
Calculated
N 21 22 18 16 23 102 S
2.0
0.0
-2.0
Frequency(Log Hz)
0.0
5.0
Distance(km)
Observed
21 22 18 16 23 102
2.0
0.0
-2.0
Frequency(Log Hz)
0.0
5.0
Distance(km)
15.0
30.0
45.0
60.0
75.0
Phase(deg.)

Fig. 5-19(b)

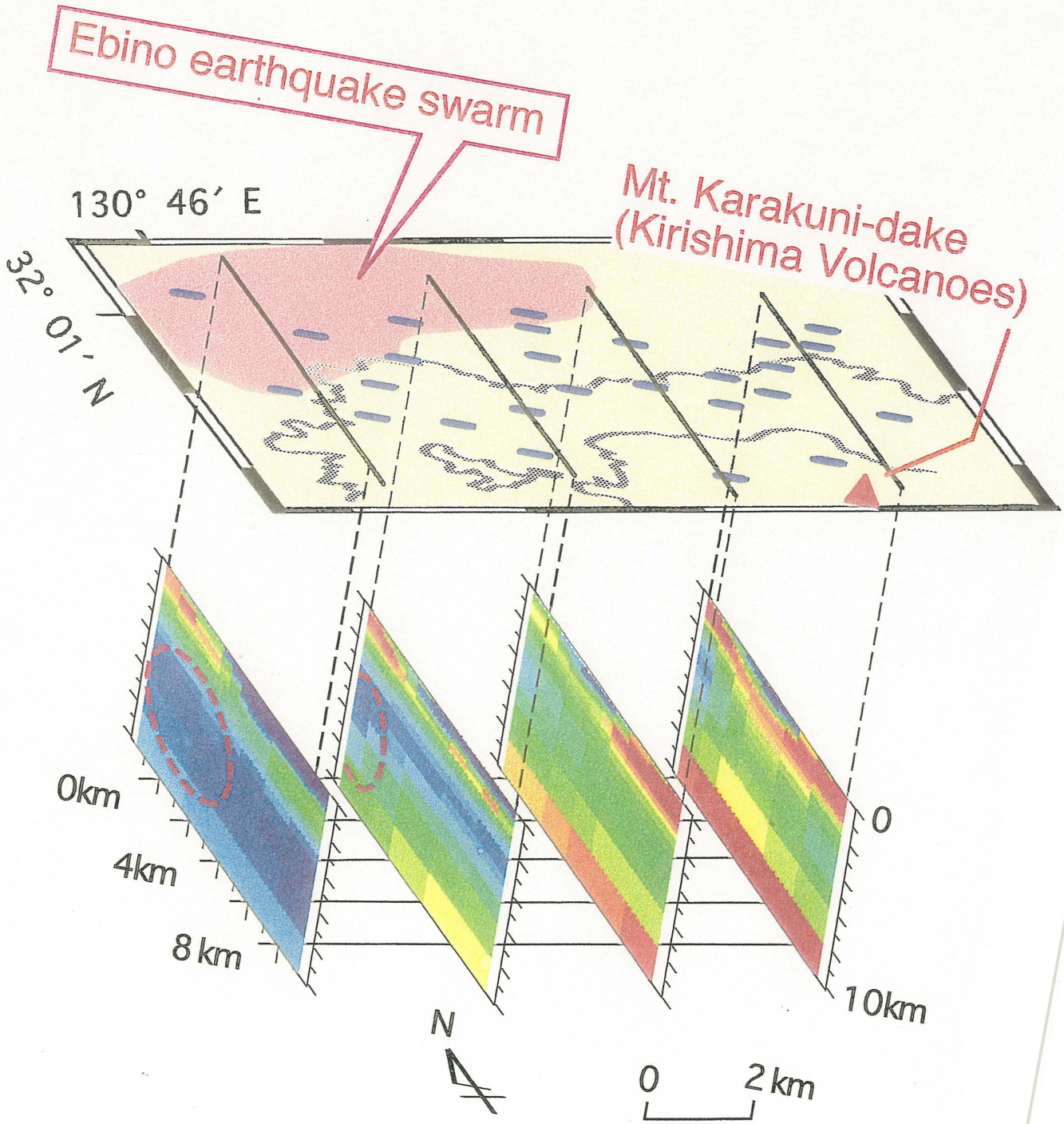
Ebino earthquake swarm
Mt. Karakuni-dake
(Kirishima Volcanoes)
130° 46′ E
32° 01′ N
0km
4km
8 km
0
10km
N
0
2 km

Fig. 5-20

6. Discussion

6. 1. Interpretation of the resistivity structure along the Atotsugawa profiles

We compare the two resistivity models of the profile AA' and BB' with other geophysical and geological studies around the Atotsugawa region. And then, we consider the relationship between the resistivity structure and the seismic activity around this whole region.

An obvious similarity can be seen between the structures of resistivity and seismic P wave velocity. Shimada (1996, pers. comm.) estimates the three-dimensional structure of the P wave velocity around the Atotsugawa fault. The seismic velocity structure calculated by Shimada(1996) is basically similar to one by Hirahara et al.(1986), though Shimada's structure is more resolved horizontally. The seismic velocity structure along the profiles AA' and BB' together with MT sites are shown in Figs. 6-1 and 6-2, respectively. Comparing the seismic velocity structure shown in Fig. 6-2 with the resistivity structure shown in Fig. 4-16, it is easy to find out a good correlation between the two structures. In particular, the good correlation is clearly recognized along the profile BB'. Along BB', the resistive layer underlying at a depth of 3km just corresponds to the high velocity zone at a depth of 3 - 5km. In addition, the low resistive (conductive) zone beneath 10km in depth of the southern side of the Atotsugawa fault also corresponds to the low velocity zone at the same depth. This good correspondence verifies that the both structures of the resistivity and seismic velocity are well resolved along the profile BB'. In particular, we conclude that the correction method for the static shift presented in this paper is so useful that the static shift is effectively removed.

Both the structures of the seismic P wave velocity and the resistivity along the profile AA' are also very similar with each other. The seismic velocity structure along AA' is shown in Fig. 6-1 together with MT sites. The high velocity zone is found in the northern area of the Atotsugawa fault at a depth of 5km, which roughly corresponds to the resistive body beneath the northern area of the fault. This high velocity anomaly was also seen in the model of Hirahara et al.(1986). However, the similarity between the resistivity and the seismic velocity becomes vague below 9km in depth. It may be due to the fact that the number of the seismic ray path used in analysis for the deeper zone below 9km is a few near the profile AA' because the location of the seismic observation site used is not suitable for the tomography. So, the velocity structure deeper than 9km have poor resolutions.

The density model for the gravimetric interpretation across the Atotsugawa fault also roughly corresponds with the resistivity structure. Okubo et al.(1988) estimated the density model based on both the gravity anomaly and the seismological explosion data. The density model near the BB' profile is shown in Fig. 6-3. In this model, the thickness of the basement rock layer whose density is assumed to be 2.67g/cm^3 is about 10km in the south of the Atotsugawa fault and become thin gradually in the northern side of the Atotsugawa fault. Okubo et al.(1988) reported that this variation was necessary to explain the steep gravity change near the Atotsugawa fault. Although the depth is different from the resistivity model , the shape of the bottom of 2.67g/cm^3 layer is very similar to the resistive layer in the resistivity model along the profile BB' , and at the same time, similar to high velocity layer revealed by the seismic tomography. Thus, the existence of the broad resistive layer beneath the whole area of the profile BB' is undoubted.

We infer what kind of rocks is able to compose the resistive and high velocity zone found in the both profile of AA' and BB'. Let us first look at the distribution of the gravity anomaly in the Atotsugawa region. Fig. 6-4 shows the relative gravity anomaly with the wave length shorter than 30km obtained by Furuse and Kono(1988) together with the surveying profiles in this investigation. They pointed out that this gravity anomaly is well consistent with the geology in the Atotsugawa region. They found that the high gravity anomaly approximately corresponds to the area where the Funatsu granitic rocks and Hida metamorphic rocks are exposed. They concluded that the Funatsu granitic rocks and the Hida metamorphic rocks have a high density value. They also found that the low gravity anomalies correspond to the Nohi rhyolites and concluded that this low anomaly is explained by the relatively low density materials with thickness of several kilometers. In Fig. 6-4, we found that another low gravity anomaly near the profile BB' was surrounded by the high gravity anomaly described above. Since the low gravity anomaly roughly coincides with the Tedori group composed of the Cretaceous sedimentary rocks, and the Oamamiya group composed of pylocrastic materials, we think that the low gravity anomaly near BB' will be also explained by a low density material near the surface such as the Nohi rhyolite, and that a high density layer widely underlies beneath BB'.

As discussed above, the high resistive zone corresponding to the high velocity zone underlies the whole area along the profile BB' and the northern area along AA' at a depth of 5km. These areas show the relatively high gravity anomaly (Fig.6-4). We conclude that the resistive layer beneath the whole of BB' and the northern part of AA' possibly consist of rocks with a high seismic velocity and a relatively high density. In the geological map

shown in Fig. 6-5, the Funatsu granitic rocks and the Hida metamorphic rocks distribute mainly in a broad area along BB' and in the northern area of the Atotsugawa fault near AA'. This geological feature supports the suggestion that the resistive layer is possibly composed of the granitic rocks and / or the metamorphic rocks. On the other hand, the southern side of the Atotsugawa fault near AA', where the relatively high gravity anomaly is also found and the Funatsu granite distribute, shows lower resistivity than the northern side. It may be caused that the rocks beneath the southern area of the Atotsugawa fault along AA' include much water than the northern area because there exist many faults with low seismicity in the southern area(see Fig. 4-1).

The surface layer, in which granitic rocks are exposed, has a lower resistivity than that of the underlying resistive layer beneath the profiles AA' and BB' at about 5km in depth. The difference in the resistivity is possibly explained by the effect of pressure. On the basis of laboratory measurements, Brace et al.(1965) reported that the resistivity of the granitic rock increases by one order when the pressure increases up to 3kbar. If the density of the upper crust is assumed to be 2.67g/cm^3 based on Okubo et al.(1988), the hydrostatic pressure at 5km is about 1.3kbar and then, the resistivity becomes about several times higher than the surficial value. This is consistent to the resistivity model proposed along the both profiles if the granitic rock compose this underlying resistive layer.

Next, let us consider some factors probably causing the conductive layer beneath the profile BB'. One of the most important candidates is a thermal effect. Mikumo et al.(1988) concluded that the cutoff depth of the occurrence of micro-earthquakes is strongly related to the thermal structure beneath the Atotsugawa region. In this region, the heat flow data were summarized in Uyeda and Horai(1964) and Li et al.(1989) . According to their

investigations, heat flow at Kamioka, near Site 16 in the profile BB', is 1.80HFU and the thermal gradient is 2.77℃/100m. If we extrapolate it to the earth's interior, the temperature at the corresponding depth for the conductive layer beneath Site 16 (10km) amounts to about 300℃. It is consistent with the temperature of the cutoff depth of earthquakes(Sibson, 1984) and in fact, the cutoff depth of the seismic activity is also about 10km (Mikumo et al, 1988). However, the conductive layer found beneath the southern side of the profile BB' can not be fully explained only by the effect of the temperature since the temperature is too low. Olhoeft (1981) described that the resistivity of the granite changes about 20% as the temperature varies from the room temperature to 300℃. On the other hand, the resistivity value estimated fro the resistivity model is 10,000Ω m at a depth of 5km and decreases to about 300Ω m at 10km. Thus, the thermal structure controls the cutoff depth of earthquakes and may relate to the resistivity, though other factor would cause the conductive layer beneath BB'.

We mention the significance of fluid in the lower crust as one of the factors responsible for the conductive layer beneath the profile BB'. Research Group for Crustal Resistivity Structure has carried out the MT surveys in various regions in Japan and presented the large-scale resistivity structures beneath Japan Arc (e.g. Utada, 1987; Ogawa et al., 1986). In the central Japan, Utada(1987) studied the two-dimensional resistivity structure of the crust and the upper mantle and found that the conductive layer with a resistivity of 10Ω m exists in the lower crust. He concluded that the conductive layer in the lower crust can not be explained by only thermal origins and pointed out the significance of water content in the lower crust. The laboratory experiments support the possibility of the existence of the free water in the crust. Kariya and Shankland(1983) showed that the resistivity of rocks in a dry state has in general a very high value at the thermal condition

for the lower crust. Other experiments show that free water remarkably reduces the resistivity of rocks (e.g. Olhoeft, 1981; Shankland and Ander, 1983). Of course, other mechanisms for good conduction may relate to such conductive layer. One of the candidates is conductive mineral such as magnetite or graphite (e.g. Stesky and Brace, 1973; Duba et al., 1988). However, the seismic reflection survey also support the existence of fluid in central Japan. According to Ito et al.(1993), the reflective layers of the seismic wave at depths of 15 - 20 km exist beneath a part of the Atotsugawa region and the eastern part of the Hida mountain range. The conductive minerals do not make a reflector while free water easily make a strong reflective layer. Thus, these investigations strongly suggest that the existence of free water which is a major factor causing the conductive zone at depths of the lower crust, although other factor might be responsible for this conductive layer.

Utada(1987) also found that a conductive layer exists at the top of the subducting slab. According to his study, the southern edge of the lower crustal conductor coincides with the location where the slab-top conductor reaches to a depth of 60km. This fact agrees with the petrologic studies of the Island arc (Takahashi, 1978; Tatsumi et al,. 1983). Tatsumi et al.(1983) suppose a water rich state in the mantle wedge where water is continuously supplied from the squeezed sediments on the subducting slab and the dehydrated oceanic crust. Utada's resistivity model across Japan island supports the petrological model. Hirahara et al. (1986) identified the three-dimensional distribution of the seismic velocity beneath central Japan. A low velocity zone at depths ranging from 50 to 150 km found by them also supports the petrological model. These investigation suggests that free water in the lower crust may be supplied from the subducting slab.

As described in Chapter 1, the active fault is often accompanied by a distinguished low resistivity zone. However, the resistivity structures along the profile AA' and BB' do not indicate such low resistivity zones along the Atotsugawa fault. Ohshiman et al.(1987) investigated the magnetic anomalies along the Atotsugawa fault , finding that this anomaly can be explained by a dyke of which the susceptibility is larger than that of the surrounding rocks and intrudes along the fault plane. The similar model for the magnetic anomaly along the Atotsugawa fault was proposed by Murakami et al.(1984). They suggested that highly magnetized materials are possibly intruded or concentrated along the fault plane. The width of the anomaly is about 50m, which is small comparing with the block size in the resistivity models near the Atotsugawa fault. Considering the results of the magnetic survey, we suggest that the fracture zone along the Atotsugawa fault is so narrow as the width is several tens of meters, and / or that the fault may be filled with the mafic intrusion along the fault.

6. 2. Comparison of the resistivity structure with seismic activities around the Atotsugawa fault

We compare the resistivity model along the two profiles in the Atotsugawa region with the seismic activity around the Atotsugawa fault. The projections of hypocenters of micro-earthquakes to the resistivity models (Figs. 6-6 and 6-7) indicates that there exist many micro-earthquakes near the vertical boundary of the resistivity. The hypocenters are determined based on the data by the Kamitakara observatory belonging to Research Center for Earthquake Prediction, Disaster Prevention Research Institute, Kyoto Univ. The projection along AA' in Fig. 6-6 shows that the seismic activity is high on the side of the resistive body in the northern area of the Atotsugawa fault.

These earthquakes have occurred along the Atotsugawa and Ushikubi faults. Considering the precision of the determination of hypocenters and the resolution of the resistivity model, this resistive body beneath AA' may be sandwiched between the two strike-slip active faults (the Atotsugawa and the Ushikubi faults) and the micro-earthquakes may not occur inside the resistive body but its the edge. In contrast to the profile AA', the projection along BB' in Fig. 6-7 shows that the seismic activity is very low in the resistive layer at about 5km in depth. Thus, these similarities with the resistivity structure and the low seismic activity along the Atotsugawa fault suggest that the seismic activity is comparatively high only along the vertical resistivity boundaries while the seismic activity is low in the resistive layer.

Although many possible causes of the non-uniform seismic activity along the Atotsugawa fault are considered, what is the major factor controlling the seismicity ? We have pointed out a significance of fluid on the basis of the comparison of the resistivity structure to the seismic activity.

Hirahara et al.(1986) showed that the horizontal scale of the low velocity zone is about 100km. Comparing this horizontal scale, the areas along AA' and BB' are very close each other. If the low velocity zone is due to the existence of fluid originated from the subducting slab, it is suggested that the content of free water supplied in the lower crust should be common beneath AA' and BB'. The lower crust beneath the Atotsugawa region, therefore, should show similarly low resistivities.

However, the resistivities of the lower crust beneath the profiles AA' and BB' are different. The resistivity at a depth of 10km beneath AA' is about 3 times larger than that of the conductive layer beneath BB'. The difference in the resistivity of the lower crust can be explained by the distribution of the

resistive layer at a depth of about 5km. Along the profile BB', the resistive layer widely overlies the conductive layer at 5km in depth. By the way, free water in the lower crust will upwell toward the surface because of its own buoyancy. In that case, the fluid does not remain and not produce a conductive zone in the lower crust. The resistive layer at 5km in depth may capture free water in the underlying lower crust and keep it conductive. In the contrast to the profile BB', the resistive layer at a depth of 5km along AA' is recognized only in the northern side of the Atotsugawa fault. This means that free water beneath AA' easily diffuses to the surface because of the lack of the resistive layer ,and the resistivity of the lower crust becomes high as compared with beneath BB'.

The seismicity is largely affected by the existence of fluid. As described in Chapter 1, fluid basically is reducible the frictional strength of a fault, resulting in easy slip of a fault (Sibson, 1984). The existence of fluid would explain the heterogeneity of the seismic activity along the Atotsugawa fault if such fluid is compressed with a high pressure.

In addition, some studies argue that the near-surface fluid flows along the Atotsugawa fault. Ohshiman et al. (1987) carried out the electrical self-potential measurements across the Atotsugawa fault. The survey profile is located about 10km northeast from the profile AA'. They found remarkable anomalies of the self-potential(SP) along the Atotsugawa fault. This study implies that a water flow or a fluid circulation exists in the fracture zone of the fault near the surface. Satake and Hayashi (1984) investigated the content of CO_2 gas near the Atotsugawa and Ushikubi faults. According to their study, the high concentration of CO_2 is recognized around these faults. They concluded that the source of CO_2 gas is subjected to near the surface. Because of high solubility of CO_2 gas to water, we suggest that the source is

related to the fluid flow near the surface along the fault. These studies showed that a part of the Atotsugawa fault is a path of fluid, although it is limited in the shallow depth.

Combining the resistivity structure and the seismic activity together with experimental facts, we think that fluid in the crust is a possible and an important factor causing the difference of the seismicity along the Atotsugawa fault . That is , it is considered that the high seismic activity along the Atotsugawa fault near the profile AA' may be caused mainly by the upwelling fluid from the lower crust along the fault. Such upwelling fluid near the profile AA' also can cause the relatively "resistive" lower crust compared to beneath BB'. In addition, it is inferred that the low seismic activity along the Atotsugawa fault near BB' is due to the underlying resistive layer which probably prevents fluid from upwelling in the lower crust. This supposition can also explain high conductivity in the lower crust beneath BB' with the fluid-rich state. Of course, the seismicity along the Atotsugawa fault may be controlled by more microscopic structure which can not be imaged in the resistivity structure obtained in this study. And we cannot completely deny the possibility that other factors such as temperature and physical properties of rocks also bind the seismic activity along the fault. However, fluid has the most important role for the seismicity around the Atotsugawa fault because it can explain both the seismic activity and the resistivity structure around there.

The difference in the resistivity structure between the profiles AA' and BB' may be attributed to the heterogeneous activity of the Atotsugawa fault. It is possible to consider that high active fault movements in a high-seismicity part of the Atotsugawa fault have destroyed the resistive cap rock as a result. On the other hand, low fault activity in a low-seismicity part may keep the

resistive layer which is able to capture water. However, in this hypothesis, the upwelling fluid from the lower crust is necessary to explain the difference in the resistivity of the lower crust beneath two profiles. Such pressurized fluid relates to the occurrence of earthquakes and fault activity either. Therefore, we pointed out the significance of the fluid to explain the seismicity along Atotsugawa fault as we have suggested.

Mikumo et al. (1988) claimed that the 1858 Hida earthquake, which is a large earthquakes and whose magnitude is inferred as 7.0, might occur by a displacement of the central part of the Atotsugawa fault. This is derived from the distribution of the seismicity and of the damaged houses during the 1858 Hida earthquake along the Atotsugawa fault. Their suggestion is consistent with our hypothesis proposed in this thesis that pressurized fluid is deeply related to the occurrence of earthquakes in the fault. As described above, there exists the resistive layer in the central part of the Atotsugawa fault, which may prevents the fluid from upwelling because of very low permeability. However, if such trapped fluid exists and the pore pressure exceed the such limit that the resistive layer can not capture fluid below, the highly pressurized fluid may intrude into the resistive layer. Then it reduces the effective stress rapidly and may enable to generate a large earthquake.

6. 3. Interpretation of the resistivity structure along the Ebino profiles

We interpret the resistivity structure of the Ebino region and consider the relationship between the resistivity structure and the occurrence of the Ebino earthquake swarm

At the first time, we discuss the existence of fluid or partial melting in the hypocentral area of the Ebino earthquake swarm. It has been revealed that the resistivity of the hypocentral area of the Ebino earthquake swarm is larger than those of the surrounding areas. This means that a large volume of fluid has not probably existed in the hypocentral area even if the Ebino earthquake swarm is induced by fluid, intruded from the earth's interior. The seismic velocity structure in this area also does not support the existence of a large mass of fluid or partial melting. Yamamoto et al.(1994) studied the seismic velocity structure around the Kirishima volcanoes using the three dimensional tomography method and reported that the seismic P wave velocity in the hypocentral area is almost same as those of the surrounding areas. The resistivity structure and the seismic velocity structure around the studied area possibly imply that differences of the porosity of rocks in this area are small. Even if rocks involve small quantity of fluid in pore, we concluded that pores are not effectively connected with each other in the hypocentral area because it is expected that the conductivity becomes very high if pores are connected. Also, it is suggested that the partial melting does not exist in the hypocentral area.

Next, we consider the relationship between fluid and the Ebino earthquake swarm. Although fluid is considered as a candidates of the cause of the Ebino earthquake swarm, why does the hypocentral area show highly

resistive , the absence of fluid and the low connectivity of pores? One possible explanation is that the fluid might not be related to the occurrence of the Ebino earthquake swarm. Ito et al.(1993) pointed out that the cutoff depth of the earthquakes around the Kirishima volcanoes decreases towards the center of the Shinmoedake crater located in the central of Kirishima volcanoes. The result suggests that earthquakes in the Ebino and Kirishima regions are not controlled by fluid but the thermal structure. If the temperature is a major cause for the occurrence of earthquakes, it is suggested that the resistive zone corresponding the hypocentral zone of the Ebino earthquake swarm has lower temperature as compared with the surrounding area at the same depth and may be under the brittle condition. However, the crustal deformation at the surface of the hypocentral area of the Ebino earthquake swarm can not be explained if only the thermal structure governs the occurrence of the earthquake swarm (Miyazaki et al., 1969). Other mechanism generating the uplift on the surface is required in this case.

As other possible cause to explain the relationship between resistive layer and the hypocentral zone, let us consider again a role of a small amount of the highly pressurized fluid for earthquake occurrences. It is pointed out that the earthquake swarm has been generated in the area where the crack density in rocks is low. In such areas, the vertical flow of fluid would be trapped when the fluid upwelled from deep layers. Nakamura et al.(1996) studied the Inagawa earthquake swarm which have occurred in Kinki district of west Japan since 1995. They found that the layer of high seismicity indicates seismically low anisotropy, while the low seismicity layer just beneath the high seismicity layer is characterized by the relatively high anisotropy. Nakamura et al.(1996) concluded that the fluid, which probably upwells thorough the layer of high crack density, might be trapped by the layer of low crack density, and the trapped fluid would increase the pore pressure. As

described in Chapter 1, the high pore pressure reduces the frictional strength and rocks yield to be broken. The measured high pore pressure in the borehole supports his suggestion (Cho et al., 1996, pers. comm.). They measured the stress field at 1km depth and Nakamura (1996, pers. comm.) estimated that the pore pressure reach over about 150% of the hydrostatic pressure. In the case of the Ebino earthquake swarm, there remains a possibility that a small amount of the upwelling fluid might be trapped in the area of a low porosity and a low connectivity, and might cause the earthquake swarm. Such fluid can also explain the crustal deformation associated with the Ebino earthquake swarm (Miyazaki et al., 1969).

The conductive layer extending beneath the surveyed area at a depth of about 0.5 - 1 km was also found by the MT surveys on the Kirishima volcanoes (Utada et al., 1994). Utada et al.(1994) found that there exists a conductive layer at a depth of a few hundred meters. On the basis of the geological and the logging data in the Kakuto caldera, Aramaki(1968) found that the shallow layer consists of thick lava flows, and that hydrothermally altered tuff and andesitic lava with clay minerals underlie at depths from 370 to 430m. The logging data by NEDO(1994) also show the much aquifer exists and the resistivity of rocks decrease at the depth of 650-700m. Referring to these investigation, we suggest that the existence of the conductive layer widely spreading around the Kirishima volcanoes possibly reflects the shallow hydrothermal activity.

On the other hand, Utada et al.(1994) also found that a deep conductor exists at about 10 km in depth below the surface of the surveying area and tends to be shallower beneath the Kirishima volcanoes. The conductor beneath Mt. Karakuni-dake corresponds with the conductive zone beneath the surveyed area in this study at a depth deeper than 6 km. These conductive

zones also correspond with the seismic low velocity zone(Yamamoto et al., 1994) and with the seismic attenuation zone(Oikawa et al., 1994) beneath Mt. Karakuni-dake. It is, therefore, suggested that the deep conductor at a depth of about 6 km may be related to the magma supply system.

There remains so many problems to be solved in the relationship between fluid and the earthquake swarm. We, however, conclude that a large amount of fluid does not probably exist in the hypocentral area even if such fluid might relate to the Ebino earthquake swarm, or such fluid was not related to the occurrence of the Ebino earthquake swarm. In this study, we treated the resistivity structure as the two-dimensional. This treatment provides insufficient resolution to confirm the accurate boundary of the resistive block because the resistivity structure beneath the area studied seems to be weakly three-dimensional. A three-dimensional resistivity model around this surveying area should be constructed in the near future to make the relationship more clear between the resistivity structure around the hypocentral area and the Ebino earthquake swarm.

6. 4. Comparisons with the previous studies on the relationship between the resistivity structure and the seismicity distribution

One of the important features obtained in this thesis is that large intraplate earthquakes such as the 1858 Hida earthquake and the 1968 Ebino earthquake swarm is possibly related to the resistive layer in the upper crust, although the correlation between the 1858 Hida earthquake and the resistive layer is speculative. A similar correlation between the resistive layer and the large earthquake have been found roughly in the previous studies. As mentioned in Chapter 1, the 1989 Loma Prieta earthquake occurred in a high resistivity region near the San Andreas fault (Eberhart-Phillips et al.,1990). The hypocentral region of the 1993 Latur earthquake is also seen in the high resistive layer overlying the low resistivity zone. Similar results were reported by the seismic velocity structure: the high velocity corresponds to the region where the large earthquake occurred. For example, Zhao and Kanamori(1995) investigated the three-dimensional velocity structure around the hypocentral region of the 1994 Northridge earthquake. They concluded that the hypocenter of the main shock is involved in the high velocity zone. Thus, it is strongly plausible that the resistive layer in the seismogenic zone is related to the occurrence of large earthquakes. The reason has been still unknown here, but it is suggested that rocks comprised in such a resistive layer have a large strength to the stress or is capable to capture the high pressured fluid beneath the layer itself because of the lower porosity than the surrounding area.

Some results of the previous studies on the relationship between the resistivity and the seismicity do not seem to be consistent with the result in this study that the resistive layer is related to the occurrence of a large

earthquake. As described in Chapter 1, the seismically active zone shows low resistivity in many regions in Japan (Ogawa, 1994; Kanda, 1996; Ichiki, 1997 ; Yamaguchi, 1997, pers. comm.). However, most of these earthquakes are very small with its magnitude smaller than 3 approximately. This is different from the fact that the high resistivity is seen in the seismogenic zone described previous sections. The difference between the low and high resistive zone in the seismogenic region may be explained by the existence of fluid. Beneath the Hidaka main thrust, the seismically active zone shows the low resistivity and the low seismic velocity (Ogawa, 1994). It may be caused by the free water trapped in the seismically active zone beneath the Hidaka main thrust. Other seismically active zones with the low resistivity may be caused by the existence of the fluid. As described in Chapter 1, such fluid can decrease both the resistivity and possibly the frictional strength. However, the resistive layer in the seismogenic zone may comprise the rocks with low porosity and involves low content of fluid usually. This layer is able to trap the upwelling pressurized fluid beneath it and eventually may cause a large earthquake. In this case, the high resistive layer in the seismogenic zone will overlie the low resistive layer. In fact, such paired resistivity structure near a seismogenic zone in the upper crust is recognized. One is the Atotsugawa region in this investigation. Along the profile BB', the resistive layer overlies the conductive layer (Fig. 4-16). The resistivity increases to a depth of about 5km and decreases below 5km in depth. Wada et al.(1995) determined the hypocenters of recent micro-earthquakes near BB' with a higher accuracy than that of the previous analysis. They concluded that no micro-earthquakes are there in the central part of the Atotsugawa fault at the depth ranging from the surface to a depth of about 5km. That is, the seismic activity along the central part of the Atotsugawa fault is limited to the conductive layer rather than the overlying resistive layer. A similar paired resistivity structure is recognized in India as described before. Gupta et al.

(1996) found the resistive layer corresponds to the hypocentral area of a large earthquake (the 1993 Latur earthquake) and the underlying conductive zone beneath the resistive one. The existence of the paired resistivity layer may support the explanation of various relationships between the resistivity and the seismicity with the existence of fluid.

On the other hand, the lack of the resistive "capture" layer on the conductive layer may allow fluid to ascend and successive seismic activity in the upper crust. The previous studies on the relationships between the earthquake occurrences and the resistivity structure were mainly carried out the micro-earthquake zone in the contrast to our surveyed area. As described in Chapter 1, these studies showed the correlation between the conductive zone and the micro-earthquake zone in the upper crust. It is concluded that this correlation is related to the occurrence of the fluid (e.g. Kanda et al,. 1996, Ichiki et al., 1996). We also conclude that the existence of fluid in the lower crust and the resistive layer in the upper crust governs not only the occurrence of the large earthquakes, but also of the micro-earthquakes in the upper crust to some extent.

Some other case was recognized that the low resistivity zone in the upper crust shows the seismicity of the micro-earthquakes is low and no historically large earthquakes were found there. One is the Shikoku district (Shiozaki , 1993) and the other is the Kii peninsular(Fujita, 1994). However, the low velocity anomaly have not been observed in these regions. Moreover, those low resistivity zones exists near the surface (shallower than several kilometers) and beneath the metamorphic rocks and accretionary rocks (Kimura et al., 1991). Such metamorphic rocks are possibly abundant to the conductive minerals such as graphite or serpentines. Duba and Shankland (1982) and Duba et al.(1988) conducted the laboratory measurements and

concluded that films of solid carbon on grain boundaries such as graphite make a remarkably conductive zone. Field measurements(e.g. Stanley, 1988; 1989) also show the large low resistivity zone possibly due to the existence of graphite. These seismological and geological views, and the laboratory and the field measurements suggest that the low resistivity layer beneath the Shikoku district and Kii peninsular would not be related to fluid but conductive minerals in the metamorphosed rocks. This anomalous conductive and seismically active zone will be found in the accretionary prism.

Fig. 6-1 The seismic P wave velocity structure along the profile AA' in the Atotsugawa region by Shimada(1997, pers. comm.). The locations of the site of our MT measurements are also indicated by arrows and the location of the Atotsugawa fault is indicated by an triangle.

Fig. 6-2 The seismic P wave velocity structure along the profile BB' in the Atotsugawa region by Shimada(1997, pers. comm.). See Fig. 6-1 in detail.

Fig. 6-3 (Upper)
The density model across the Atotsugawa fault by Okubo et al. (1988) . The unit of the density in this figure is g / cm^3.

Fig. 6-4 (Lower)
The gravity anomaly with the wave length shorter than 30km after Furuse and Kono(1988). Lines indicate the MT profile in this investigation. The unit of the gravity anomaly in this figure is mgal.

Fig. 6-5 The simplified geological map around the Atotsugawa region (after Hirokawa et al., 1978). 1: Quaternary sediments, 2: Tertiary sedimentary rocks, 3 : Mesozoic/ Paleozoic sedimentary rocks , 4: Volcanic rocks and 5 : Granitic / Metamorphic rocks. A solid line indicates the location of the Atotsugawa fault.

Fig. 6-6 The distribution of the hypocenters of micro-earthquakes beneath the profile AA' projected to the resistivity model shown in Fig. 4-

Fig. 6-7 The distribution of the hypocenters of the micro-earthquakes beneath the profile BB' projected to the resistivity model shown in Fig. 4-16

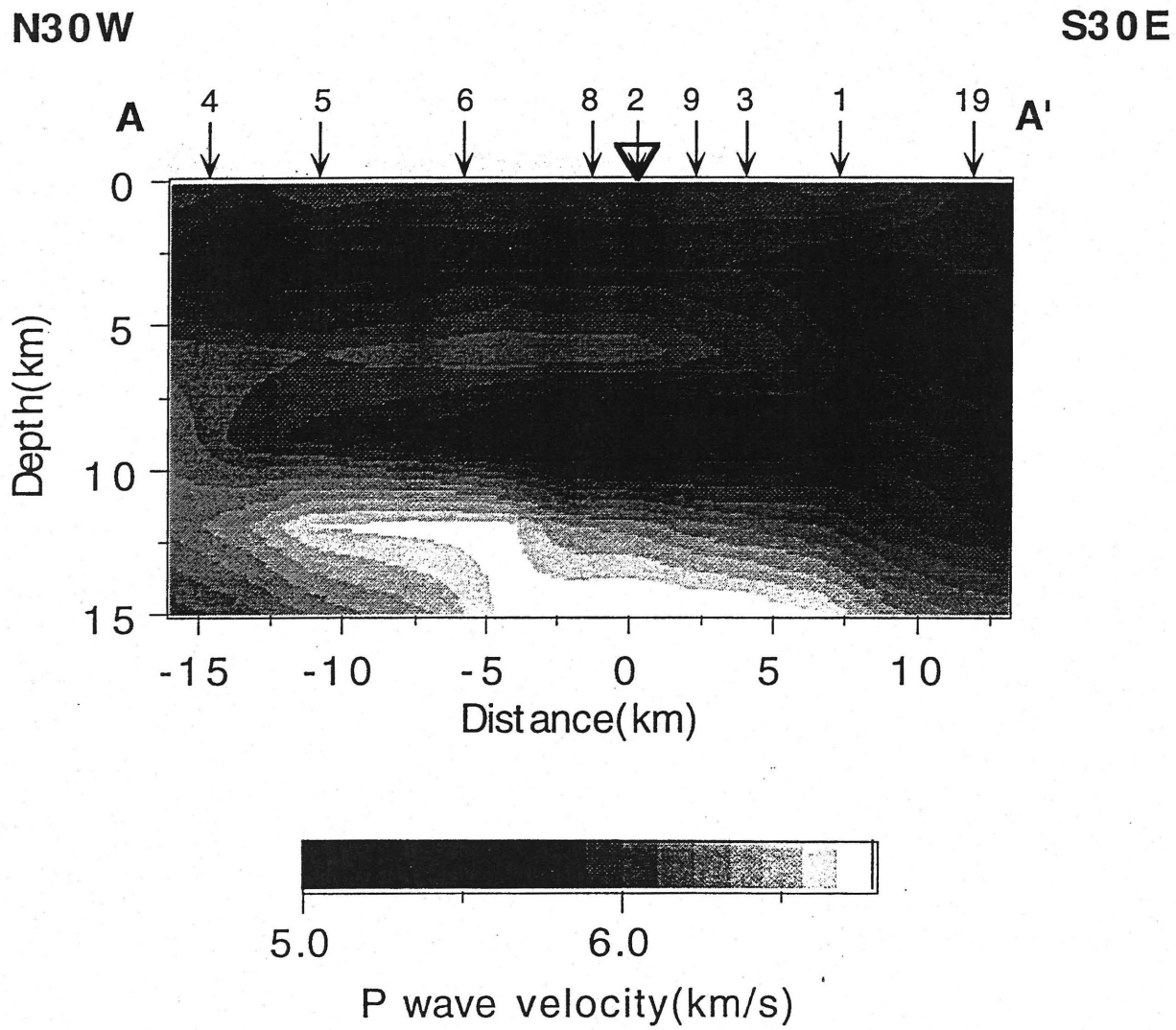
N30W
S30E
A
A'
4
5
6
8
2
9
3
1
19
0
5
10
15
Depth(km)
-15
-10
-5
0
5
10
Distance(km)
5.0
6.0
P wave velocity(km/s)

Fig. 6-1

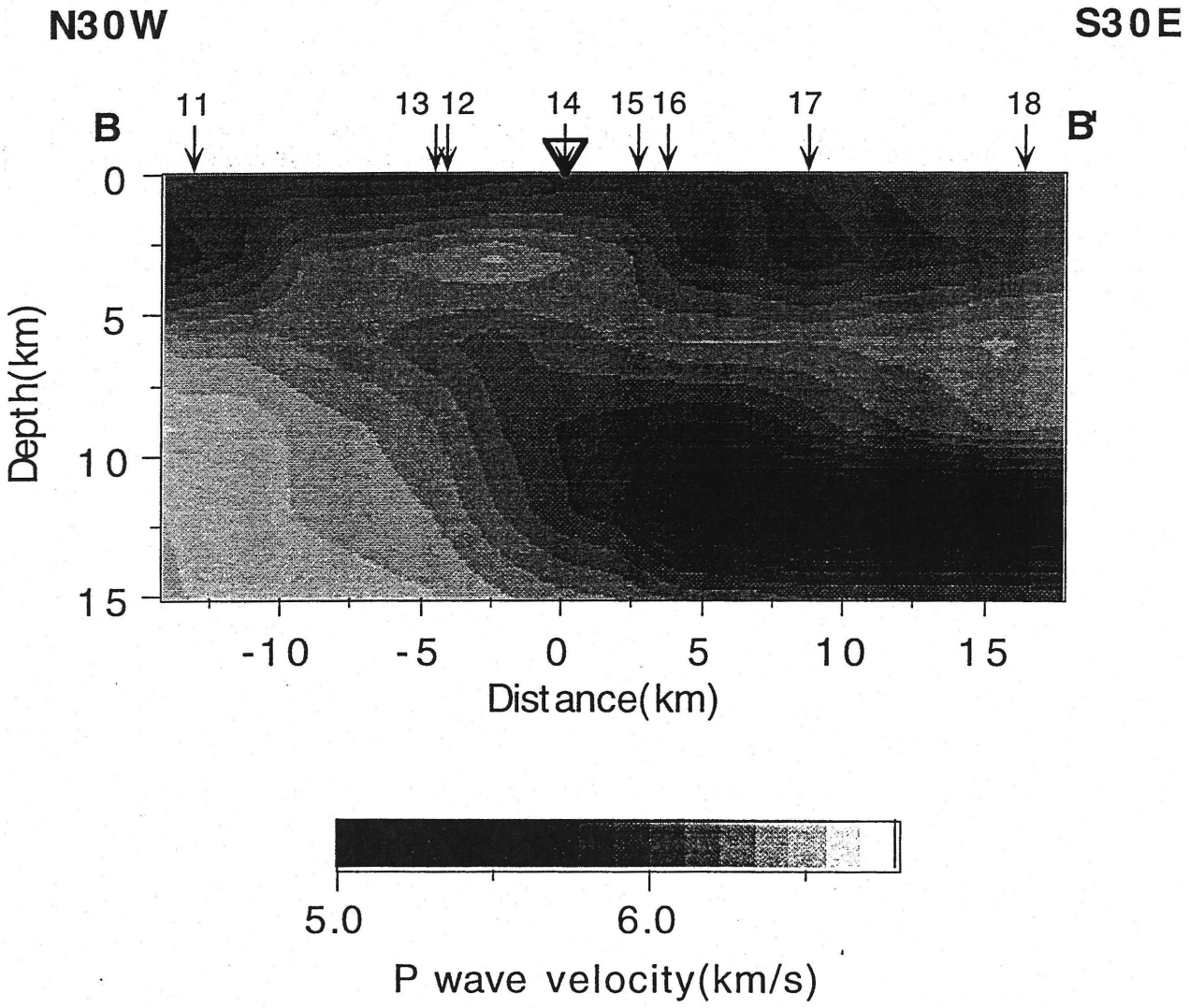
N30W
S30E
B
B'
11
13
12
14
15
16
17
18
0
5
10
15
Depth(km)
-10
-5
0
5
10
15
Distance(km)
5.0
6.0
P wave velocity(km/s)

Fig. 6-2

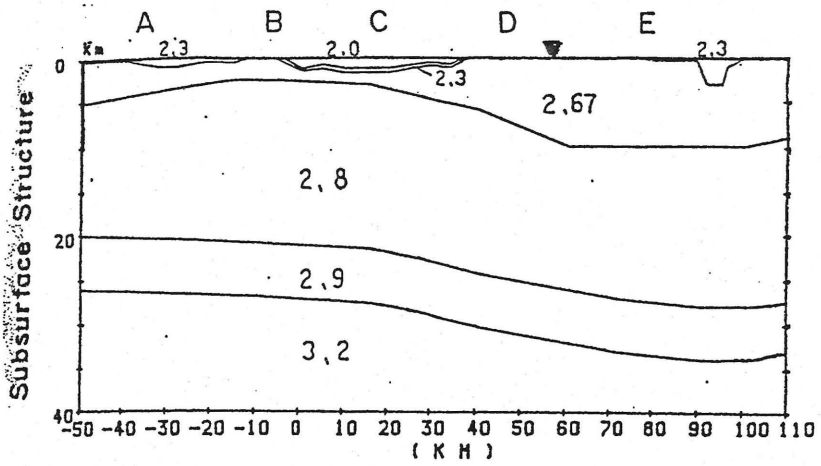
A
B
C
D
E
Km
2.3
2.0
2.3
2.3
2.67
2.8
2.9
3.2
0
20
40
Subsurface Structure
-50 -40 -30 -20 -10 0 10 20 30 40 50 60 70 80 90 100 110
(K M)

Fig. 6-3

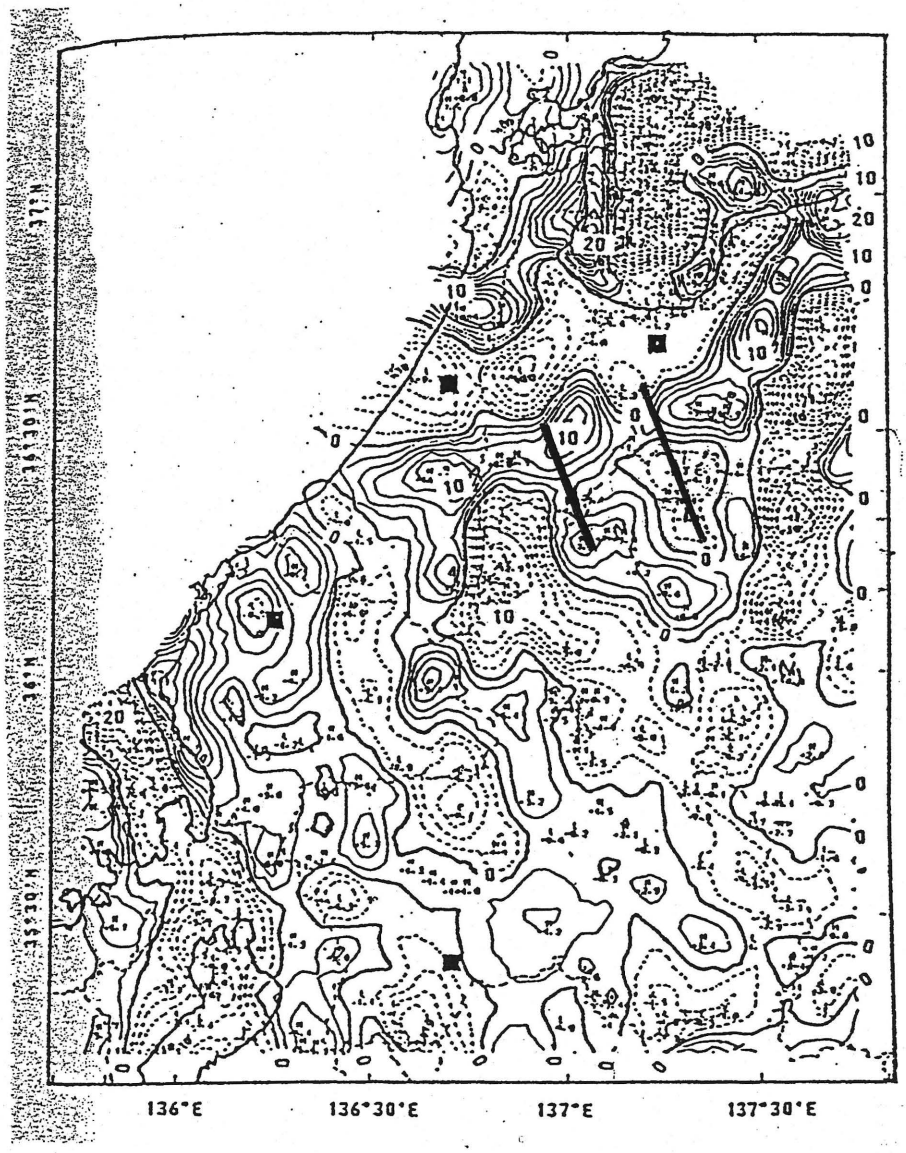
136°E
136°30'E
137°E
137°30'E

Fig. 6-4

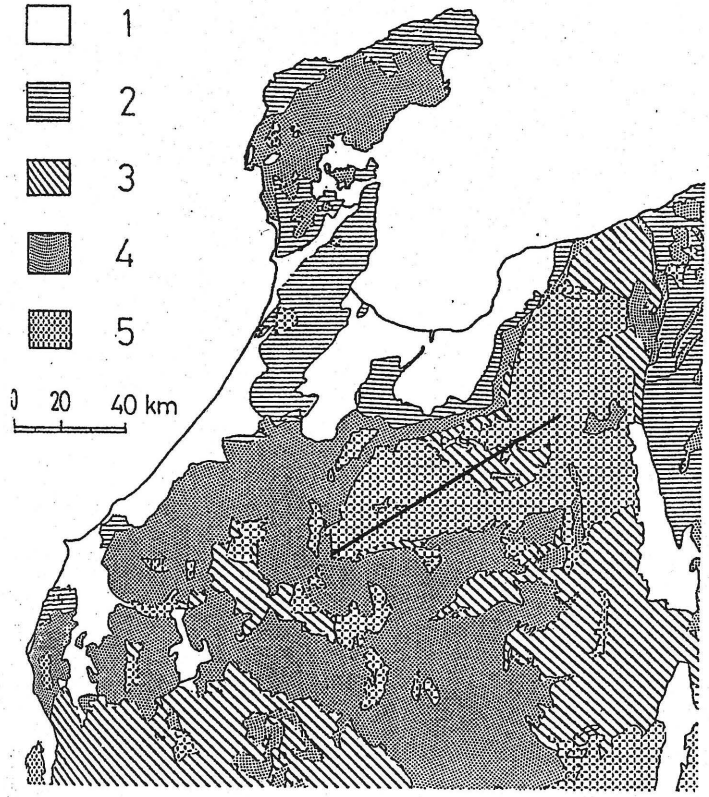

Fig. 6-5

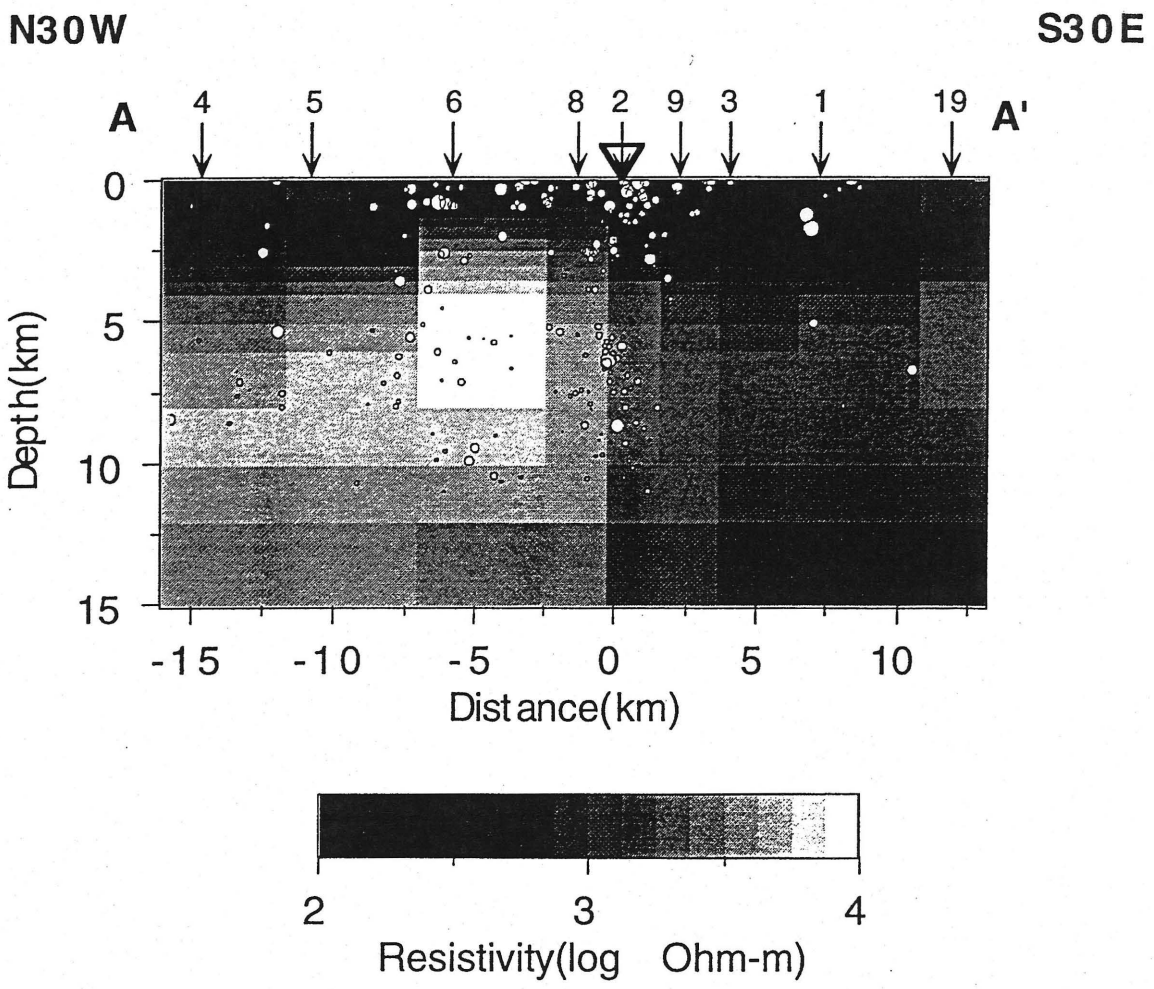
N30W
S30E
A
A'
4
5
6
8
2
9
3
1
19
0
5
10
15
Depth(km)
-15
-10
-5
0
5
10
Distance(km)
2
3
4
Resistivity(log Ohm-m)

Fig. 6-6

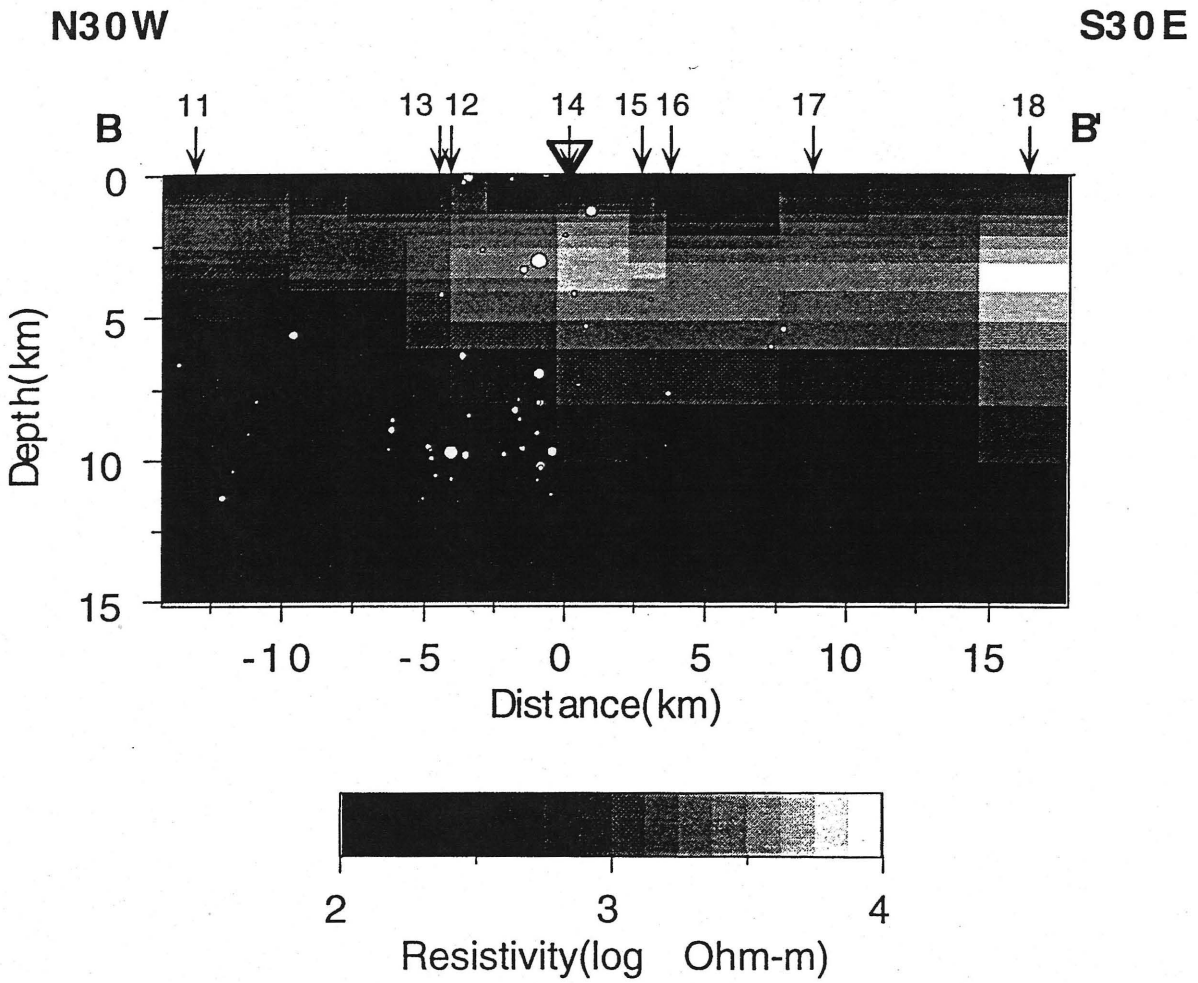
N30W
S30E
B
B'
11
13 12
14
15 16
17
18
0
5
10
15
Depth(km)
-10
-5
0
5
10
15
Distance(km)
2
3
4
Resistivity(log Ohm-m)

Fig. 6-7

7. Conclusion

We carried out the magnetotelluric soundings around the two different seismogenic zones. The meaningful relationships between the resistivity structure and the seismic activity were identified in the two regions: One is in the Atotsugawa region including the active fault, and another is in the Ebino region including the hypocentral zone of the earthquake swarm. We summarize the concluding remarks as follows

Around the Atotsugawa fault, two profiles across the low and high seismicity portions of the fault are made. The distribution of the strike direction on the resistivity structure shows that the structure is roughly two-dimensional. We adopted the inversion method for modeling the two-dimensional resistivity structure. The two resistivity models along the two profiles show different features. Comparing with the seismic activity, we summarize these features as follows.

(1) The resistive layer widely underlies beneath the region showing low seismicity of the Atotsugawa fault.

(2) A similar resistive zone is found only in the northern side of the fault across the high seismicity section.

(3) The moderately conductive layer underlies broadly in the Atotsugawa region. In particular, the resistivity below a depth of about 10km is low beneath the low seismicity section of the Atotsugawa fault.

Thus, there are several differences between the resistivity structure across the low and high seismicity part of the Atotsugawa fault. In order to explain both the features of the resistivity structure and the heterogeneity of the seismicity in the Atotsugawa region, we pointed out the significance of a role

of fluid. Fluid is possible to be attributed the conductive layer in the lower crust beneath the Atotsugawa region. It is suggested that the spatial variation of the resistivity in the lower crust in the Atotsugawa region, as described in above(3) , reflects the content of fluid in the lower crust. Considering the correspondence that the lower crust beneath the seismically active and non-active segment of the fault shows relatively low and high resistivities respectively, we propose that the high-seismicity section of the Atotsugawa fault may be related to the upwelling of fluid from the lower crust, and the low-seismicity section may be related to the captured fluid in the lower crust.

Around the Ebino region, we conducted dense MT soundings. The strike directions indicate that the resistivity structure is approximately two-dimensional. After the modeling of the resistivity structure using the inverse method, following relation between the resistivity structure and the seismic activity is recognized.

(4) The resistive zone is recognized in the hypocentral area of the Ebino earthquake swarm. In the same depth of the surrounding areas, such resistive zone is not found

This means that a large volume of fluid has not probably existed in the hypocentral area even if the Ebino earthquake swarm is induced by fluid, intruded from the earth's interior. However, we propose a hypothesis to explain the relationship between resistive layer and the hypocentral zone that a high resistivity zone in the seismogenic region may trap a small amount of fluid, which will increase the pore pressure and reduce the effective stress. In the Atotsugawa region, a correlation between a high resistive zone and a occurrence of a large earthquake, named the 1858 Hida earthquakes, may be

also found. It is suggested that a resistive zone and captured fluid may be deeply concerned with the occurrence of a large intraplate earthquake.

Some problems are still remained unsolvable: why is the conductive zone not recognized around the hypocentral zone of the Ebino earthquake swarm if fluid might be related to the occurrence of the large earthquakes as discussed in Chapter 6? The problem seems to be like a puzzle. In addition, although the significant role of fluid in the occurrence of earthquakes along the Atotsugawa fault is strongly suggested, it is not get confirmed whether fluid is a major cause to generate earthquakes along the fault. The measurement of the stress field together with the pore pressure will solve these problems. If we get more knowledge of the pore pressure and the contributions of fluid to earthquakes, the resistivity structure obtained by the EM survey will provide us more information on the source of fluid including its location and extent, existence of the cap-rock structure and the significance of fluid to the regional seismicity.

Aramaki , S. , Geology of the Kakuto basin, southern Kyushu, and the earthquake swarm from February, 1968 (in Japanese with English abstract) , Bull. Earthq. Res. Inst. , 46 , 1325-1343 , 1968

Archie, G. E. , The electrical resistivity log as an aid in detrmining some resorvoir characteristics , Trans. Am. Inst. Min. Metall. Eng. , 146 , 54-67 , 1942

Behrens, K., S. Goldflam, P. Heikkinen, H. Hirschleber, G. Lindqvist and C. E. Lund , Reflection seismic measurements across the Granulite Belt of the POLAR profile in the northern Baltic shield, northern Finland , Tectonophysics , 162 , 101-111 , 1989

Blanpied, M. L., D. A. Lockner and J. D. Byerlee , An earthquake mechanism based on rapid sealing of faults , Nature , 358 , 574-576 , 1992

Bostick, F. X. , A simple almost exact method of MT analysis , Workshop on electrical methods in geothermal exploration, U. S. Geol. Surv., Contract No. 14080001-8-359 , 1977

Brace, W. F., A. S.Orange and T. R. Madden , The effect of pressure on the electrical resistivity of water-saturated crystalline rocks , J. Geophys. Res. , 70 , 5669-5678 , 1965

Byerlee, J. , Friction, overpressure and fault normal compression , Geophys. Res. Let. , 17 , 2109-2112 , 1990

Cagniard, L. , Basic thory of the magnetotelluric method , Geophysics , 28 , 605-635 , 1953

Chakridi, R., M. Chouteau and M. Mareschal , A simple technique for analysing and partly removing galvanic distortion from the magnetotelluric immpedance tensor : application to Abitibi and Kapuskasing data (Canada) , Geophys. J. Int. , 108 , 917-929 , 1992

d'Erceville, I. and G. Kunetz , Some observations regarding naturally occuring electromagnetic fields in applied geophysics , Geophysics , 27 , 666-676 , 1962

deGroot-Hedlin, C. , Removal of static shift in two dimensions by regularized inversion , Geophysics , 56 , 2102-2106 , 1991

deGroot-Hedlin, C. , Inversion for regional 2-D resistivity structure in the presence of galvanic scatterers , Geophys. J. Int. , 122 , 877-888 , 1995

Duba, A. G., E. Huenges, G. Nover and G. Will , Impedane of bleck shale form Munsterland 1 borehole: an anomalously good conductor? , Geophys. J. , 94 , 413-419 , 1988

Eberhart-Phillips, D., V. F. Labson, W. D. Stanley, A. J. Michael and B. D. Rodriguez, Preliminary velocity and resistivity models of the Loma Prieta Earthquake region, Geophys. Res. Lett., 17, 1235-1238, 1990

Electromagnetic Research Group for the Active Fault , Low electrical resistivity along an active fault, the Yamasaki fault , J. Geomag. Geoelect. , 34 , 103-127 , 1982

Electromagnetic Research Group for the Active Fault , Electrical resistivity structure of the Tanna and the Ukihashi faults , Bull. Earthq. Res. Inst. , 58 , 265-286 , 1983

Fujita, K. , The study of the electrical resistivity structure bendath the Kii-peninsula using the electromagnetic method , Doctral thesis, Kobe university , 127pp , 1994

Furuse, N. and Y. Kono , The densitiy distribution from the surface to the depth of 30km in the western part of central Japan inferred from the gravity anomalies , Chikyu Monthly , 11 , 75-83 , 1989

Gammble, T. D., W. M. Goubau and J. Clarke , Magnetotellurics with a remote magnetic reference , Geophysics , 44 , 53-68 , 1979

Gayer, R. G. , The effect of a dipping contact on the behavior of the electromagnetic field , Geophysics , 37 , 337-350 , 1972

Gough, D. I. , Seismic reflectors, conductivity, water and stress in the cntinental crust , Nature , 323 , 143-144 , 1986

Green, A. G., B. Milkereit, L. Mayrand, C. Spence, R. Kurtz and R. M. Clowes , Lithoprobe seismic reflection profiling across Vancouver Island : results from reprocessing , Geophys. J. R. astr. Soc , 89 , 85-90 , 1987

Groom, R. W. and R. C. Bailey , Decomposition of magnetotelluric impedance tensors in the presence of local three-dimensional galvanic distortions , J. Geophys. Res. , 94 , 1913-1925 , 1989

Haak, V. and V. R. S. Hutton , Electrical resistivity in continental lower crust , In: J. B. Dawson, D. A. Carswell, J. Hall and K. H. Wedepohl (Editors), The Nature of the Lower Continental Crust. Geol. Soc. London, Spec. Publ. , 24 , 35-49 , 1986

Handa,S and N. Sumitomo , The geoelectric structure of the Yamsaki and the Hanaori faults, southwest Japan , J. Geomag. Geoelect. , 37 , 93-106 , 1985

Hirahara, K., A. Ikami, M. Ishida and T. Mikumo , Three-dimensional P-wave structure beneath cenral Japan: low velocity bodies in the wedge portion of the upper mantle above high-velocity subducting plates , Tectonophysics , 163 , 63-73 , 1989

Ichiki, M., M. Mishina, T. Goto, N. Oshiman, N. Sumitomo and H. Utada , ELF- and ULF-MT investigations for seismically active region in northern Miyagi prefecture, northeastern Japan , J. Geomag. Geoelectr. , 1997

Ito, K. , Cutoff depth of seismicity and large eartuquakes near active volcanoes in Japan , Tectonophysics , 217 , 11-21 , 1993

Ito, K., I. Kawasaki, M. Hurumoto, H. Isobe and T. Nagai , Seismic survey in northern Chubu district, Japan. Toyama-Kamitakara line , Ann. Disas. Prev. Res. Inst., Kyoto Univ. , 36 , 325-328 , 1993

Jiracek, G. R. , Near-surface and topographic distortions in electromagnetic induction , Survey in Geophysics , 11 , 163-203 , 1990

Jiracek, G. R., E. P. Gustafson and P. S. Mitchell , Magnetotelluric results opposing magma origin of crustal conductors in the Rio Grande rift , Tectonophysics , 94 , 299-326 , 1983

Jiracek, G. R., W. L. Rodi and L. L. Vanyan , Implications of magnetotelluric modeling for the dddp crustal environment in the Rio Grande rift , Phys. Earth Planet. Inter. , 45 , 179-192 , 1987

Jones, A. G. , MT and reflection : an essential combination , Geophys. J. R. astr. Soc , 89 , 7-18 , 1987

Jones, A. G. , Static shift of magnetotelluric data and its removal in a sedimentary basin environment , Geophysics , 53 , 967-978 , 1988

Jones, A. G. , Electrical conductivity of the continental lower crust , In : D.M. Fountain, R. Arculus and R. W. Kay (Editor), Continental lower crust, Elsevier , 81-143 , 1992

Jones,A. G., R. D.Kurtz, D. E.Boerner, J. A.Craven,G. W.McNeice, D.I. Gough, J. M.DeLaurier and R. G.Ellis , Electromagnetic constraints on strike-slip fault geometry- the Fraser river fault system , Geology , 20 , 561-564 , 1992

Jones, A. G. and R. W. Groom , Strike-angle determination from the magnetotelluric impedance tensor in the presence of noise and local distortion : rotate at your peril! , Geophys. J. Int. , 113 , 524-534 , 1993

Kagiyama , T. , Geophysical background of Kirishima volcanoes , Rep. Geol. Surv. Japan , 279 , 89-92 , 1992

Kanda, W., H. Utada, M.Mishina and N. Sumitomo , A deep transient EM experiment in the northern part of Miyagi prefecture, northeastern Japan , J. Geomag. Geoelectr. , 48 , 1265-1280 , 1996

Kariya, K. A. and T. J. Shankland , Electrical conductivity of dry lower crustal rocks , Geophysics , 48 , 52-61 , 1983

Kaufman, A. A. and G. V. Keller , The magnetorelluric sounding method , Elseivier Science Publ. , 1981

Korja, T., S. E. Hjelt, P. Kaikkonen, K. Koivukoski, T. M. Rasmussen and R. G. Roberts , The geoelectric model of the POLAR profile, northern Finland , Tectonophysics , 162 , 113-133 , 1989

Kurtz, R. D., J. M. DeLaurier and J. C. Gupta , A magnetotelluric sounding across Vancouver Island detects the subducting Juan de Fuca plate , Nature , 321 , 596-599 , 1986

Kurtz, R. D. and J. C. Gupta , Shallow and deep crustal conductivity studies in the Miramichi earthquake zone, New Brunswick , Can. J. Earth. Sci , 29 , 1549-1564 , 1992

Li, X., Y. Furukawa, T. Nagao, S. Uyeda and H. Suzuki , Heat flow in cenral Japan and its relations to geological and geophysical features , Bull. Earthq. Res. Inst. , 64 , 1-36 , 1989

Matsuda, T. , Strike-slip faulting along the Atotsugawa fault (in Japanese with English abstract) , Bull. Earthq. Res. Inst. , 44 , 1179-1212 , 1966

Mikumo, T., H. Wada and M. Koizumi , Seismotectonics of the Hida region, central Honshu, Japan , Tectonophysics , 147 , 95-119 , 1988

Minakami ,T., M. Hagiwara , M. Yamaguchi , E. Koyama and K. Hirai , The Ebino earthquake swarm and the seismic activity in the Kirishima volcanoes, in 1968-1969, Part 4. - Shift of seismic activity from the Kakuto caldera to Shinmoe-dake, Naka-dake and Takatiho-mine , Bull. Earthq. Res. Inst. , 48 , 205-233 , 1970

Minakami ,T., S. Utibori , M. Yamaguchi , N. Gyoda , T. Utsunomiya , M. Hagiwara and K. Hirai , The Ebino earthquake swarm and the seismic activity in the Kirishima volcanoes, in 1968-1969, Part 1. - Hypocentral distribution of the 1968 Ebino earthquakes inside the Kakuto caldera , Bull. Earthq. Res. Inst. , 47 , 721-743 , 1969

Mituhata, Y. and Y. Ogawa , Central-induction trasient electromagnetic

survey and static shift correction of MT data in Sengan-Sumikawa geothermal field , Butsuri-Tansa , 47 , 11-23 , 1994

Miyazaki , T., M. Yamagichi , F. Masutani and H. Terao , The earthquake swarms in the northern area of the Kirishima volcanoes, 1975-1976(in Japanese with English abstract) , Bull. Earthq. Res. Inst. , 51 , 115-149 , 1976

Miyazaki, T., S. Hiraga and T. Minakami , The Ebino earthquake swarm and the seismic activity in the Kirisima volcanoes, in 1968-1969, part 3. Crustal Deformation inside the Kakuto caldera relating to the 1968 Ebino earthquakes , Bull. Earthq. Res. Inst. , 47 , 769-781 , 1969

Murakami, H., I. Yamada and U. Kobayashi , Geomagnetic total force anomalies asociated with active fault -Observation of the geomagnetic total force aroud Atotsugawa fault and Atera fault - , Zisin 2nd ser. , 37 , 397-405 , 1984

Nakamura , M., M. Ando , K. Kusunose and T. Sato , Depth-dependent crustal anisotropy at mid western Honshu, Japan , Geophys. Res. Lett. , in press , 1996

O'Connell , R. J., and B. Budiansky , Viscoelastic properties of fluid-saturated cracked solids , J. Geophys. Res. , 82 , 5719-5735 , 1977

Ogaw, Y. and Y. Mitsuhata , Separation of magnetorelluric (MT) data of strong three-dimensionality into regional induction and locar telluric distortion - Application to MT data across southern Kitakami mountains , Bull. Geol. Surv. Japan , 45 , 703-713 , 1994

Ogawa, Y. , Deep crustal resistivity structure revealed by wideband magnetotellurics - Tohoku and Hokkaido region - , Doctoral thesis, University of Tokyo , 1992

Ogawa,Y., M. Uyeshima, Y. Honkura, H. Utada and S. Koyama , Audio-frequency Magnetotelluric imaging of an active strike slip fault , J. Geomag. Geoelect. , 48 , 403-408 , 1994

Ogawa, Y., T. Yukutake and H. Utada , Two dimensional modeling of resisitivy structure beneath the Tohoku district , northern Honshu of Japan, by a finite element method , J. Geomag. Geoelectr. , 38 , 45-79 , 1986

Ogawa, Y. and T.Uchida , A two-dimensional magnetotelluric inversion assuming Gaussian static shift , Geophys. J. Int., 1996 (in press)

Ogawa, Y. and T. Uchida , Resistivity structure beneath the southern part of Onikobe caldera, in Northeastern Japan, as inferred from the magnetotelluric survey , Butsuri-Tansa , 40 , 22-41 , 1987

Ogawa ,Y., Y. Nishida and M. Makino, A collision boundary imaged by magnetotellurics, Hidaka Mountains, cenral Hokkaido, Japan, J. Geophys. Res., 99, 22373-22388, 1994

Ohshiman, N., Y. Honkura, K. Kuge and H. Sakai , Electric and magnetic anomalies at the Atotsugawa fault and their implications fo fault activity , J. Geomag. Geoelectr. , 39 , 143-158 , 1987

Oikawa , J., K. Yamamoto and Y. Ida , High attenuation region of seismic waves beneath Kirishima volcanoes(in Japanese with English abstract) , Bull. Earthq. Res. Inst. , 69 , 291-307 , 1994

Okada, M. and Y. Kymaki , Geological Study of the Terrace at Miyagawa and the displacemetn along the Atotsugawa fault. , Chikyu Monthly , 5 , 411-416 , 1983

Okubo, Y., H. Tsu and K. Ogawa , Estimation of Curie point temperature and geothermal structure of island arcs of Japan , Tectonophysics , 159 , 279-290 , 1989

Okubo, Y., N. Furuse and Y. Kono , Bouguer anomalies and crustal structure models aroud the Atotsugawa fault, central Japan , Zisin 2nd ser. , 41 , 97-102 , 1988

Olhoeft, G. R. , Electrical properties of granite with implications for the lower cr;ust , J. Geophys. Res. , 86 , 931-936 , 1981

Pascoe, L. J. and F. W. Jones , Boundary conditions and calculation of surface values for the general two-dimensional electromagnetic induction problem , Geophys. J. R. astr. Soc , 27 , 179-193 , 1972

Pous,J., J. Ledo, A. Marcuello and M. Daignieres , Electrical resistivity model of the drust and upper mantle from a magnetotelluric survey through the central Pyrenees , Geophys. J. Int. , 121 , 750-762 , 1995

Raleigh, C. B., J. H. Healy and J. D. Bredehoeft , An experiment in earthquake control at Rangely, Colorado , Science , 191 , 1230-1237 , 1976

Reddy, I.K., D. Rankin and R. J. Phillips , Three-dimensional modelling in magnetotelluric and magnetic variational sounding , Geophys. J. R. astr. Soc. , 51 , 313-325 , 1977

Reddy, I. K. and D. Rankin , Magnetotelluric response of a two-dimensional sloping contact by the finite element method , Pure and applied Physics , 105 , 847-857 , 1973

Research Group for Active Faults, 1991) , Acrive faults in Japan : Sheet maps and inventories , Univ. Tokyo Press , 363pp , 1980

Research Group for Crustal Resistivity Structure , Preliminary report on a study of resisitivity structure beneath the norther Honsyu of Japan , J. Geomag. Geoelectr. , 35 , 589-608 , 1983

Research Group for Excavation of the Atotsugawa fault , Trenching excavation across the Atotsugawa fault , Chikyu Monthly , 5 , 335-340 , 1983

Rice, J. R. , Fault stress states, pore pressure distributions, and the wakness of the San Andreas Fault , In Fault Mechanics and Transport Properties of Rocks, edited by B. Evans and T. -F. Wong, Academic, San Diego, Calif. , 475-503 , 1992

Rodi, W. L. , A technique for improving the accuracy of finite element solutions for magnetotelluric data , Geophys. J. R. astr. Soc. , 44 , 483-

506 , 1976

Sasai, Y. , A mechanizm of the generation of the Matsushiro earthquake swarm - the natural and large hydrofracturing by the upwelling fluid(In Japanese) , Proc. 1944 Conductivity Anomaly Symp. , 181-195 , 1994

Sasai , Y., H. Utada and N. Sumitomo , Geoelectric and geomagnetic surveys in southern Kyushu(in Japanese) , Proc. 1995 Conductivity Anomaly Symp. , 1-3 , 1995

Satake, H., M. Ohashi and Y. Hayashi , Discharge of H2 from the Atotsugawa and Ushikubi faults, Japan, and its relation to earthquakes , Pageoph , 122 , 185-193 , 1984

Schmucker, U. , Anomalies of geomagnetic variations in the southern United States , Bull. Scripps Inst. Oceanogr., Univ. Calif. Press, Berkeley and Los Angeles , 13 , 165pp , 1970

Shankland, T. J. and M. E. Ander , Electrical conductivity, temperatures, and fluids in the lower crust , J. Geophys. Res. , 88 , 9475-9484 , 1983

Shiozaki, I. , The study on the electrical resistivity structure beneath Shikoku and Chugoku district, Japan , Doctoral thesis, Kobe university , 1993

Sibson, R. H. , Roughness at the base of the seismogenic zone : contributing factors , J. Geophys. Res. , 89 , 5791-5799 , 1984

Sibson, R. H. , F. Robert and H. Poulsen , High-angle reverse faults, fluid pressure cycling, and mesothermal gold-quartz deposits , Geology , 16 , 551-555 , 1988

Simpson, D. W., W. S. Leith and C. H. Scholz , Two types of reservoir induced seismicity , Bull. Seismol. Soc. Am. , 78 , 2025-2040 , 1988

Sternberg, B. K.,J. C. Washburne and L. Pellerin , Correction for the static shift in magnetotellurics using transient electromagnetic soundings , Geophysics , 53 , 1459-1468 , 1988

Stesky, R. M. and W. F. Brace , Electrical conductivity of serpentinized rocks to 6 kilobars , J. Geophys. Res. , 41 , 529-547 , 1978

Swift, C. M. , A magnetotelluric investigation of an electrical conductivity anomaly in the southwestern United States , Ph.D. Thesis, M. I. T. , 211 , 1967

Takagi, A., A. Hasegawa and N. Umino, Seismic activity in the northeastern Japan Arc. J. Phys. Earth, 25, S95-S104, 1977

Takahashi, E. , Petrologic model of the crust and upper mantle of the Japanese island arcs , Bull. Volcano. , 41 , 529-547 , 1978

Takakura, S. , Correction for the static effect in CSAMT using horizontal magnetic fields , Butsuri-Tansa , 46 , 7-14 , 1993

Tanaka, K. , Spreading and growth of the hypocentral area of earthquake swarms(in Japanese) , Chikyu monthly , 132 , 331-335 , 1990

Tatsumi, Y., M. Sakuyama, M. Fukuyama and I. Kushiro , Generation of arc basalt magmas and thermal structure of the mantle wedge in subduction zones , J. Geophys. Res. , 88 , 5815-5825 , 1983

Ting, S. C. and G. W. Hohmann , Integral equation modeling of three-dimensional magnetotelluric response , Geophysics , 46 , 192-197 , 1981

Toge,. M. and A. Okada , Activity of the Atotsugawa fault from the view of the topographic displacement , Chikyu Monthly , 5 , 359-366 ,

Torres-Verdin, C. and F.X.Bostick , Principles of spatial surface electirc field filtering in magnetotellurics: Electromagnetic array profilings(EMAP) , Geophysics , 57 , 603-622 , 1992

Uchida, T. , Smooth 2-D inversion for magnetotelluric data based on statistical criterion ABIC , J. Geomag. Geoelectr. , 45 , 841-858 , 1993

Uchida, T. and Y. Ogawa , Development of FORTRAN code for two-dimensional magnetotelluric inversion with smoothness constraint , Open-File Report, Geol. Surv. Japan , 205 , 115pp , 1993

Utada, H. , A direct inversion method for two-dimensional modeling in the geomagnetic induction problem , Doctoral thesis, University of Tokyo ,

409 , 1987

Utada , H., T. Kagiyama and EM Research Group for Kirishima Volcano , Deep resistivity structure of Kirishima volcano (I) (in Japanese with English abstract) , Bull. Earthq. Res. Inst. , 69 , 241-255 , 1994

Uyeda, S. and K. Horai , Terrestiral heat flow in Japan , J. Geophys. Res. , 69 , 2121-2141 , 1964

Vozoff, K. , The magnetorelluric method in exploration of sedimentary basins , Geophysics , 37 , 98-141 , 1972

Wada, H., K. Ito, M. Ando and K. Wada , Observation of the earthquakes in the Mozumi tunnel at the Kamioka mine, central Honshu, Japan , Ann. Disas. Prev. Res. Inst., Kyoto Univ. , 39B-1 , 241-250 , 1996

Wada, H. and K. Ito , Seismic activity in the vicinity of the Atotsugawa fault, central Japan , Ann. Disas. Prev. Res. Inst., Kyoto Univ. , 38B-1 , 235-250 , 1995

Waff, H. , Theoretical considerations of electrical conductivity in a partially molten mantle with implications ofr geothermometry , J. Geophys. Res. , 79 , 4003-4010 , 1974

Watanabe , K. , Some investigations about Ebino earthquake swarm (in Japanese with English abstract) , Zisin 2nd ser. , 23 , 32-40 , 1970

Weaver, J. T. , B. V. LeQuang, and G. Fischer , A comparison of analytic and numerical results ofr a two-dimensional control model in electromagnetic induction -1. B-polarization calculations , Geophys. J. R. astr. Soc , 82 , 263-277 , 1985

Weaver, J. T. , B. V. LeQuang, and G. Fischer , A comparison of analytic and numerical results ofr a two-dimensional control model in electromagnetic induction -2. E-polarization calculations , Geophys. J. R. astr. Soc , 87 , 917-948 , 1986

Wight, D. E. and F. X. Bostick , Cascade decimation - a technique for real time estimation of power spectra , Proceedings IEEE international

conference on acoustic speech and processing , 626-629 , 1980

Yamamoto , K. and Y. Ida , Three-dimensional P-wave velocity structure of Kirishima volcanoes using regional seismic events (in Japanese with English abstract) , Bull. Earthq. Res. Inst. , 69 , 267-289 , 1994

Yamazawa, K. , The great earthquake of Hida-Tsunogawa on February 2, Ansei 5 , ZISIN I , 1 , 125-128 , 1929

Yukutake, T. , A review of studies on the electrical resisitivty structure of the crust in Japan , Earthq. Predict. Res. , 3 , 345364 , 1985

The Resistivity Structure around the Hypocentral Area of the Ebino Earthquake Swarm in Kyushu district, Japan

Tadanori GOTO, Naoto OSHIMAN and Norihiko SUMITOMO

Research Center for Earthquake Prediction, Disaster Prevention Research Institute, Kyoto University, Gokasho, Uji City, Kyoto Prefecture 611, Japan

(Received November 1, 1996; Revised ; Accepted)

We carried out wide band and dense MT soundings on the hypocentral area of the Ebino earthquake swarm which occurred in 1968 in southern Kyushu. The purpose of this study is to examine the relationship between the resistivity structure and the earthquake swarm. Before determining the resistivity structure beneath the studied region, we calculated the regional strike and the induction arrow. We constructed a two-dimensional model of the resistivity structure beneath the surveyed area using the inversion technique. The most suitable model shows that the hypocentral area is relatively resistive more than the surrounding area. We conclude that a large mass of fluid does not exist in the hypocentral area.

1. Introduction

Recently, much interest have been focused on that the upwelling of the fluid from a deep interior of the Earth's crust is one of the causes of the earthquake swarm. It has been argued as seismogenic models that fluid makes an important role in the occurrence of earthquakes(RICE, 1992 ; BYERLEE, 1990, BLANPIED *et al.*, 1992). For example, SIBSON *et al.* (1988) suggested that the overpressured fluid below the seismogenic zone are periodically expelled upward through the fault zone during process of an earthquake rupture. On the other hand, some observations seems likely to accept their models for explaining of the occurrence of earthquake swarms. The time variation of the geomagnetic total force occurred before the Matsushiro earthquake swarm in central Japan is considered to be caused by the upwelling of large mass of fluid from the lower crust (SASAI, 1994). TANAKA (1990) studied the spreading of the hypocentral area of the several earthquake swarms in Japan and suggested that there exists a relation between earthquake swarms and fluid. If fluid exists in the hypocentral area, then the resistivity should be low there. However, the detailed structure of resistivity around the hypocentral area of the earthquake swarm have not been made clear and such fluid have not been identified except for the Matsushiro earthquake swarm. The purpose of the present study is to investigate the resistivity structure around the hypocentral area of the Ebino earthquake swarm and to consider whether fluid has existed in the hypocentral area.

The Ebino earthquake swarm was occurred in the time from 1968 - 1969 in Ebino, under the Kakuto caldera, in southern Kyushu district in Japan (MINAKAMI *et al.* 1969, 1970). The Kakuto caldera is situated at the northeastern foot of the Kirishima volcanoes. The magnitude of the largest earthquake was M6.1. Locations of epicenters are indicated in Fig. 1. MINAKAMI *et al.* (1970) reported that the hypocenters of the Ebino earthquake swarm were distributed in the depth from 3 to 9 km and in the width of 5 - 10 km. In the Kakuto caldera, several earthquake swarms have observed several times during the past one hundred years (MIYAZAKI *et al.*, 1976) and the 1968-1969 Ebino earthquake swarm was the largest one. However, the recent seismicity under the Kakuto caldera is low (KAGIYAMA, 1992). MINAKAMI *et al.*(1970) found that the volcanic activities of the Kirishima volcanoes occasionally followed the earthquake swarms in the Kakuto caldera. They therefore inferred that the 1968-1969 Ebino earthquake swarm related to the magma supplying system of Kirishima volcanoes. However, they did not detect a particular evidence of the movement of magma at that time.

In this paper, we consider that the occurrence of the 1968-1969 Ebino earthquake swarm was probably induced by fluid. WATANABE(1970) recognized that there is a relation between the frequency of the seismic P wave of the Ebino earthquake swam and the location of its hypocenters. He pointed out that the earthquakes around the center of the focal area generated the seismic P wave with the lower frequency than those

near the periphery of the focal area. This feature came gradually clear with time. The attenuation of the seismic wave increases with crack density if cracks are saturated by fluid (O'CONNELL and BUDIANSKY, 1977). Therefore, we considered that fluid would be related with the Ebino earthquake swarm.

2. Data acquisition and analyses

Research group for Crustal Resistivity Structure in Japan (referred to as RGCRS) carried out the magnetotelluric(MT) soundings and the geomagnetic depth soundings(GDS) at 26 sites around the Kakuto caldera in 1994 (SASAI, 1995). The location of the sites is shown in Fig. 1. RGCRS used the MT measuring system manufactured by Phoenix Geophysics Ltd. Magnetic sensors of this system were induction coils. Electrodes were Pb-$PbCl_2$ type and were usually separated about 50m for the measurement of the electric fields. RGCRS observed natural fluctuation of the magnetic and the electric fields for about three days at each site. After that, we calculated the impedance tensor, the apparent resistivity, the impedance phase and other electromagnetic responses in the broad band of the almost continuous frequencies between 384Hz to 0.00055Hz. These response functions are calculated according to the remote reference processing(GAMBLE *et al.*, 1979). The reference site was set up in the distance of several kilometers far from the analyzed site.

It is necessary at first to determine the direction of the regional strike around the studied area. We applied the method of CHAKRIDI *et al.*(1992) to the estimation of the direction of the strike at each site. This method is successful to avoid the effect of the surficial galvanic distortion (GROOM and BAILEY, 1989). However, it was not able to obtain stable directions against every frequency at some sites. This may be because the Chakridi's method is not effective to the one dimensional structure of the resistivity. In such the cases, we also tried another method of JONES and GROOM (1993, eq.10 and 11) which is similar to the Chakridi's method but is more robust to a one dimensional resistivity structure.

After all, we calculated the regional strike using both the Chakridi's method and the Jones and Groom's method, and determined the strike so as the least standard deviation for the observed frequencies is obtained. The estimated directions of the regional strike are shown in Fig. 2 with the rose diagrams. We can recognize that the regional strike points to approximately N-S or E-W directions. The induction arrows at all site are also calculated. It is found that induction arrows tend to point to south at the period of about 10 seconds as shown in Fig. 3. Judging from the distribution of the strike and the induction arrow, we concluded that the resistivity structure under the studied area is approximately two-dimensional with the strike of the E-W direction. This is supported from the fact that the observed skewness values are lower than 0.3 at all site.

The apparent resistivities and the impedance phases roughly show similar tendencies at all sites, respectively. The typical curves of apparent resistivity at representative sites are shown in Fig. 4. It is recognized that apparent resistivity values have a minimum commonly around several Hz and gradually increase as the frequency decreases beyond 1Hz.

Additionally, the apparent resistivities and the phases obtained in the epicentral area of the Ebino earthquake swarm have different features from those in the surrounding region of the epicentral area. At all sites, in general, the apparent resistivity increases as the frequency decrease beyond 1Hz as above mentioned. However, above the hypocentral area, increasing of the apparent resistivity is very steep and the apparent resistivity value at the frequency around 0.1Hz is almost the same or rather higher than the apparent resistivity at the frequency around 300Hz(see Fig. 4., Site 1 and Site 10). On the other hand, in the surrounding region of the epicentral area, the apparent resistivity at about 0.1Hz are lower than that at about 300Hz(see Fig. 4, Site 7 and Site 15). These features are important to consider the resistivity structure around the studied area. We will discuss this point later.

3. Modeling

Models of the two-dimensional resistivity structure beneath the studied area are constructed. The direction of the strike is assumed to be E-W as mentioned in the previous section. We took four analyzing profiles in the studied area as shown in Fig. 1. We used site 1 - 6 for the analysis along the profile AA', site 6 - 10 for the profile BB', site 10 - 14 for the profile CC' and site 15 - 20 for the profile DD', respectively. The two-dimensional least square inversion with the smoothness constraint coded by UCHIDA and OGAWA(1993) is applied to the data of each profile to construct the most suitable resistivity model. The inversion is carried out using the observed apparent resistivities and phases of both TE and TM mode. The initial model for the inversion is given with a uniform resistivity of 1000 ohm-m. The inversion was executed very stably and four or five iterations for each profile were needed to reach a sufficient convergence.

The most suitable model of the two-dimensional resistivity structure along each profile well explained the observed electromagnetic responses. First, we show the most suitable resistivity model along the profile AA' in Fig. 5, which goes just across the area of the epicenters of the Ebino earthquake swarm. The outline of the hypocentral area drawn in Fig. 5 is based on MINAKAMI *et al.*(1970). In our model, we set the conductive layer at the depth of about 0.5 - 1 km. The conductive layer is responsible to the low apparent resistivity at several Hz. We also recognize that the hypocentral area of the Ebino earthquake swarm is more resistive than the surrounding area. The fitting of the calculated responses to the observed data is indicated in Fig. 6. The calculated responses

well explain the steeply increase of the apparent resistivity at the frequency of about 1Hz observed above the hypocentral area.

Secondly, We show the resistivity model along the analyzing profile of DD' in Fig. 7 , which is located at the northern foot of Mt. Karakuni-dake, one of the Kirishima volcanoes. This resistivity model along the profile DD' has degree of a similar fitness to that along the profile AA'. The model for the profile DD' also shows the conductive layer at the depth of about 1 km. Additionally, we can recognize the existence of a conductive zone near the Kirishima volcanoes at the depth deeper than about 6 km.

The resistivity model along the profiles BB' and CC' is similar to that along the profile AA'. We can find that the conductive layers beneath 1 km depth also exist along the profiles BB' and CC'. However, the resistive zone corresponding with the hypocentral area of the Ebino earthquake swarm is not recognized along these profiles. The lack of the resistive zone along the profiles BB' and CC' is inferred from Fig. 8, in which the spatial distribution of the resistivity at the depth of 6 km is indicated with contour lines. The resistivity values are obtained from the most suitable resistivity model along each analyzing profile. When the observation sites (Site 6 and 10) are belonged to the two different analyzing profiles, the averaged values of the resistivity of each model are adopted.

4. Discussion and Conclusion

At the first time, we discuss about the existence of fluid or partial melting in the hypocentral area of the Ebino earthquake swarm. It was revealed that the resistivity of the hypocentral area of the Ebino earthquake swarm is larger than that of the surrounding areas. This suggests that a large volume of fluid has probably not existed in the hypocentral area even if the Ebino earthquake swarm would be induced by fluid, and that partial melting has not occurred. The seismic velocity structure in this area also does not support the existence of the large mass of fluid and partial melting. YAMAMOTO *et al.*(1994) studied the seismic velocity structure around the Kirishima volcanoes using the three dimensional tomography method and reported that the seismic P wave velocity in the hypocentral area is approximately equivalent to those of the surrounding area. The resistivity structure and the seismic velocity structure around the studied area possibly imply that differences of the porosity of rocks in the surveyed area are little, and that even if rocks involve small quantity of fluid in pore, pores are not connected with each other in the hypocentral area because the conductivity become very high if pores are connected. Also, it is suggested that the partial melting does not exist in the hypocentral area.

Next, we consider the relationship between fluid and the Ebino earthquake swarm. So far as our analysis, the absence of fluid and the low connectivity of pores around the hypocentral are sure. If the upwelling of the fluid followed the Ebino earthquake

swarm, any fluid should be left because we are not able to find any evidence which demonstrate overflows of fluid from underground or eruptions of a lot of vapor on the earth surface. And such remained fluid should result in keeping the low resistivity around the hypocentral area. This is not not harmony with the our result obtained. Judging from this result, we may consider that the fluid might be not related to the occurrence of the Ebino earthquake swarm.

On the other hand, it is pointed out that the earthquake swarm has been generated in the rocks with the low density of cracks, where the vertical flow of fluid would be trapped if the fluid is upwelled below. NAKAMURA *et al.*(1996) studied the Inagawa earthquake swarm which have occurred in Kinki district of west Japan since 1995. They found that the layer of high seismicity indicates the low seismic anisotropy, while the low seismicity layer beneath this high seismicity layer indicates the relatively high anisotropy. NAKAMURA *et al.*(1996) concluded that the fluid, which upwells from the layer of high crack density, might be trapped by the layer of low crack density, and the trapped fluid would increase the pore pressure. Such the high pore pressure forces cracks to slip(NUR and BYERLEE, 1971). In the case of the Ebino earthquake swarm, there remains a possibility that a small amount of the upwelling fluid might be trapped in the area of a low porosity and a low connectivity, and might caused the earthquake swarm.

The conductive layer spreading beneath the surveyed area at the depth of about 0.5 - 1 km and the conductive zone beneath the Kirishima volcanoes deeper than 6 km depth are also observed by the MT surveys on the Kirishima volcanoes (UTADA *et al.*, 1994). UTADA *et al.*(1994) found that there exists a conductive layer at the depth of a few hundred meters. On the basis of the geological and the logging data in the Kakuto caldera, ARAMAKI(1968) found that the shallow layer consists of thick lava flows, and that hydrothermaly altered tuff and andesitic lava with clay minerals underlie at the depth about 370-430m. Referring to his investigation, we suggest that the existence of the conductive layer widely spreading around the Kirishima volcanoes possibly reflects the shallow hydrothermal activity. On the other hand, UTADA *et al.*(1994) also found that a deep conductor exists at about 10 km depth below the surface of the surveyed area and tends to shallower beneath the Kirishima volcanoes. The conductor beneath Mt. Karakuni-dake corresponds with that conductor above mentioned and also corresponds with the seismic low velocity zone(YAMAMOTO *et al.*, 1994) , where is equivalent to the seismic attenuation zone(OIKAWA *et al.*, 1994) beneath Mt. Karakuni-dake. We, therefore, suggest that the deep conductor at the depth of about 6 km may be related to the magma supply system.

There remains so many problems to be made clear in the relationship between fluid and the earthquake swarm. We, however, conclude that a large mass of fluid has not probably existed in the hypocentral area even if such fluid might relate to the Ebino

earthquake swarm, or such fluid was not related to the occurrence of the Ebino earthquake swarm. In this study, we treated the resistivity structure as the two-dimensional. This treatment provides insufficient resolution to confirm accurate boundary of the resistive block because the resistivity structure beneath the studied seems to be weakly three-dimensional. We will construct the three-dimensional resistivity model around this studied area in a near future to make the relationship more clear between the resistivity structure around the hypocentral area and the Ebino earthquake swarm.

The MT and GDS data analyzed in this paper were acquired by Research Group for Crustal Resistivity Structure in Japan (RGCRS). We greatly thanks RGCRS, especially Dr. S. Takakura, Dr. I. Shiozaki, Dr. Y. Tanaka, Dr. M. Uyeshima, Dr. Y. Sasai and Dr. H. Utada. We thanks Phoenix Geophysics Ltd. for maintaining the instruments in the field. The authors express a deep sense of gratitude to Dr. T. Uchida and Dr. Y. Ogawa in Geological Survey of Japan for providing their inversion code for MT data. We also thanks Dr. T. Kagiyama in Earthquake Research Institute, University of Tokyo for his helpful advise.

REFERENCES

ARAMAKI, S., Geology of the Kakuto basin, southern Kyushu, and the earthquake swarm from February, 1968., *Bull. Earthq. Res. Inst.* , **46**, 1325–1343, 1968 (in Japanese with English abstract).

BLANPIED, M. L., D. A. LOCKNER and J. D. BYERLEE, An earthquake mechanism based on rapid sealing of faults, *Nature*, **358**, 574–576, 1992.

BYERLEE, J., Friction, overpressure and fault normal compression, *Geophys. Res. Lett.*, **17**, 2109–2112, 1990.

CHAKRIDI, R., M. CHOUTEAU and M. MARESCHAL, A simple technique for analyzing and partly removing galvanic distortion from the magnetotelluric impedance tensor: application to Abitibi and Kapuskasing data (Canada), *Geophys. J. Int.*, **108**, 917–929, 1992.

GAMBLE, T. D., W. M. GOUBAU and J. CLARKE, Magnetotellurics with a remote magnetic reference, *Geophys.*,**44**, 53–68, 1979.

GROOM, R. W. and R. C. BAILEY, Decomposition of magnetotelluric impedance tensor in the presence of local three-dimensional galvanic distortion, *J. Geophys. Res.*, **94**, 1913–1925, 1989.

JONES, A. G. and R. W.GROOM, Strike-angle determination from the magnetotelluric impedance tensor in the presence of noise and local distortion: rotate at your peril!, *Geophys. J. Int.*, **113**, 524–534,1993.

KAGIYAMA, T., Geophysical background of Kirishima volcanoes, *Rep. Geol. Surv. Japan*, **279**, 89–92, 1992.

MINAKAMI,T., M. HAGIWARA, M. YAMAGUCHI, E. KOYAMA and K. HIRAI, The Ebino earthquake swarm and the seismic activity in the Kirishima volcanoes, in 1968-1969, Part 4. - Shift of seismic activity from the Kakuto caldera to Simmoe-dake, Naka-dake and Takatiho-mine., *Bull. Earthq. Res. Inst.*, **48**, 205–233, 1970.

MINAKAMI,T., S. UTIBORI, M. YAMAGUCHI, N. GYODA, T. UTSUNOMIYA, M. HAGIWARA and K. HIRAI, The Ebino earthquake swarm and the seismic activity in the Kirishima volcanoes, in 1968-1969, Part 1. - Hypocentral distribution of the 1968 Ebino earthquakes inside the Kakuto caldera, *Bull. Earthq. Res. Inst.*, **47**, 721–743, 1969.

MIYAZAKI, T., M. YAMAGICHI, F. MASUTANI and H. TERAO, The earthquake swarms in the northern area of the Kirishima volcanoes, 1975-1976, *Bull. Earthq. Res. Inst.*, **51**, 115–149, 1976 (in Japanese with English abstract).

NAKAMURA, M., M. ANDO, K. KUSUNOSE and T. SATO, Depth-dependent crustal anisotropy at mid western Honshu, Japan, *Geophys. Res. Lett.*, in press, 1996.

NUR, A. and J. D. BYERLEE, An exact effective stress law for elastic deformation of rock with fluids, *J. Geophys. Res.*, **76**, 6414–6419, 1971

O'CONNELL, R. J., and B. BUDIANSKY, Viscoelastic properties of fluid-saturated cracked solids, *J. Geophys. Res.*, **82**, 5719–5735, 1977.

OIKAWA, J., K. YAMAMOTO and Y. IDA, High attenuation region of seismic waves beneath Kirishima volcanoes, *Bull. Earthq. Res. Inst.*, **69**, 291–307, 1994 (in Japanese with English abstract).

RICE, J. R., Fault stress states, pore pressure distributions, and the weakness of the San Andreas Fault, in *Fault Mechanics and Transport Properties of Rocks*, edited by B. Evans and T. -F. Wong, 475–503, Academic, San Diego, Calif., 1992.

SASAI, Y., A mechanism of the generation of the Matsushiro earthquake swarm - the natural and large fracturing by upwelling fluid†, *Proc. 1994 Conductivity Anomaly Symp.*, 181–195, 1994 (in Japanese).

SASAI, Y., H. UTADA and N. SUMITOMO, Geoelectric and geomagnetic surveys in southern Kyushu†, *Proc. 1995 Conductivity Anomaly Symp.*, 1–3, 1995 (in Japanese).

SIBSON, R. H., F. ROBERT and K. H. POULSEN, High-angle reverse faults, fluid-pressure cycling, and mesothermal gold-quartz deposits, *Geology*, **16**, 551-555, 1988.

TANAKA , K., Spreading and growth of the hypocentral area of earthquake swarms†, Chikyu monthly, **132**, 331–335 ,1990 (in Japanese).

UCHIDA, T. and Y. OGAWA, Development of FORTRAN code for two-dimensional magnetotelluric inversion with smoothness constraint, *Open-File Report, Geological Survey of Japan*, No. 205, pp115, 1993.

UTADA, H., T. KAGIYAMA and EM RESEARCH GROUP FOR KIRISHIMA VOLCANO, Deep resistivity structure of Kirishima volcano (I), *Bull. Earthq. Res. Inst.*, **69**, 241–255, 1994 (in Japanese with English abstract).

WATANABE, K., Some investigations about Ebino earthquake swarm, Zisin 2nd ser., **23**, 32–40, 1970 (in Japanese with English abstract).

YAMAMOTO, K. and Y. IDA, Three-dimensional P-wave velocity structure of Kirishima volcanoes using regional seismic events, *Bull. Earthq. Res. Inst.*, **69**, 267–289, 1994 (in Japanese with English abstract).

†: These titles are translated by the author T.G.

Fig. 1. Locations of the study area and magnetotelluric stations(circles). Four profiles are discussed in this paper (AA', BB', CC' and DD'; dashed-dot lines). Circles with number mean locations of the sites used for the modeling of the two-dimensional resistivity structure. The epicentral area of the Ebino earthquake swarm (Minakami et al., 1970) is indicated by the hatched area. The location of Mt. Karakuni-dake, one of the Kirishima volcanoes, is also shown (triangle).

Fig. 2. Histograms of the strike, combined for all the sites, for respective frequency bands.

Fig. 3. Directions of the Induction arrow at the period of 10.7 seconds(real part). The GDS stations are located at the base of arrows. The epicentral area is also indicated as the hatched area.

Fig. 4. Curves of the apparent resistivity at the representative sites with the 68 per cent random error. Rectangulars and circles are obtained from the N-S and E-W component of the electric field, respectively.

Fig. 5. The most suitable 2-D model of the resistivity structure along profile AA'. Resistivity are expressed as logarithmic values. Locations of MT sites are indicated arrows with the site number. The outline of the hypocentral area of the Ebino earthquake swarm (after Minakami et al., 1970) is also indicated (the broken curve).

Fig. 6. Observed TE/TM data (rectangles and circles, respectively) along profile AA' and calculated TE/TM responses (solid and broken lines, respectively) from the model in Fig.5.

Fig. 7. The most suitable model of the resistivity along profile DD'.

Fig. 8. The spatial distribution of the resistivity at the depth of 6 km. Circles, the triangle and the hatched area is same as those in Fig.1.

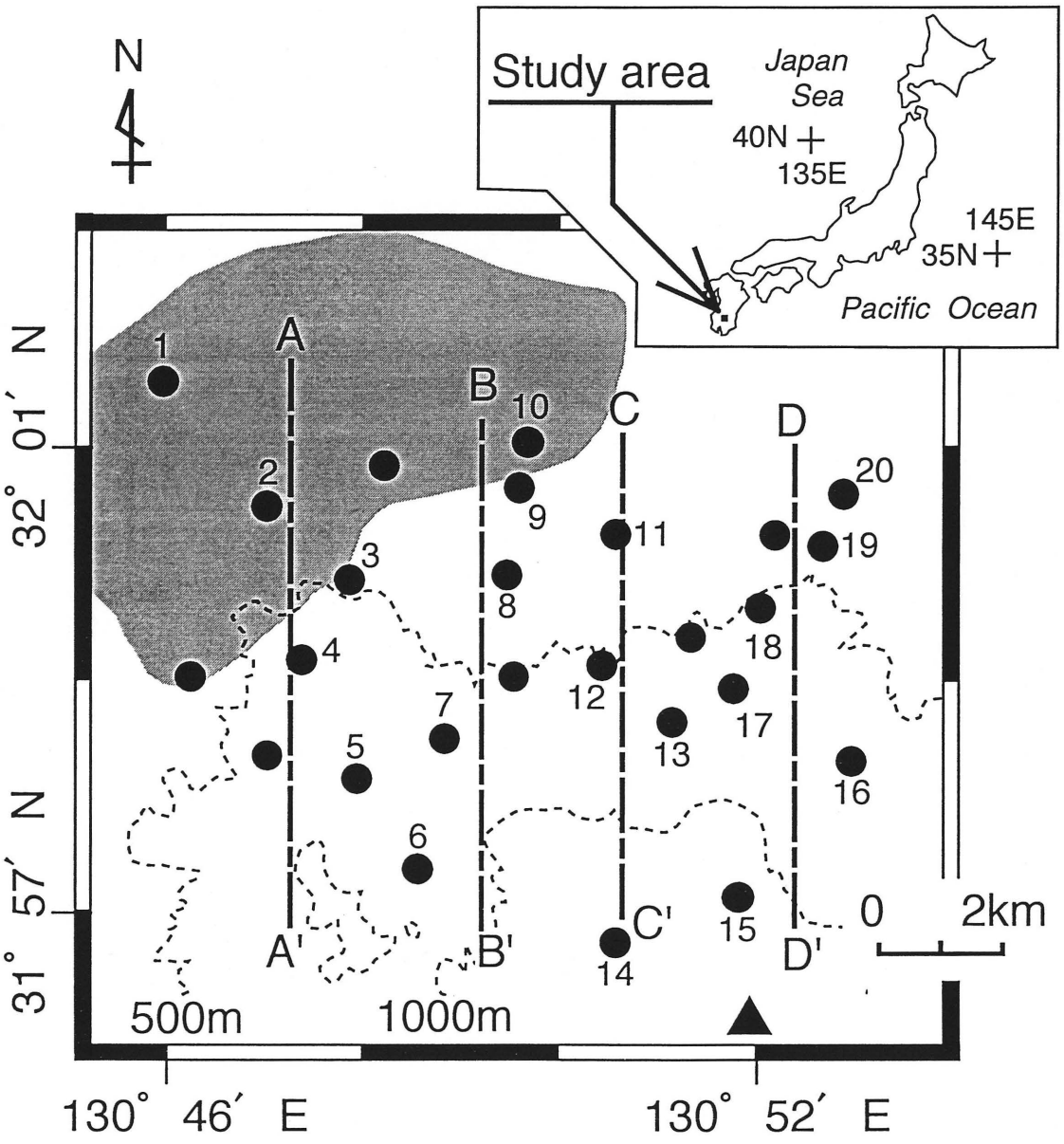
N
Study area
Japan
Sea
40N
135E
145E
35N
Pacific Ocean
32° 01′ N
31° 57′ N
130° 46′ E
130° 52′ E
A
B
C
D
A'
B'
C'
D'
1
2
3
4
5
6
7
8
9
10
11
12
13
14
15
16
17
18
19
20
500m
1000m
0
2km

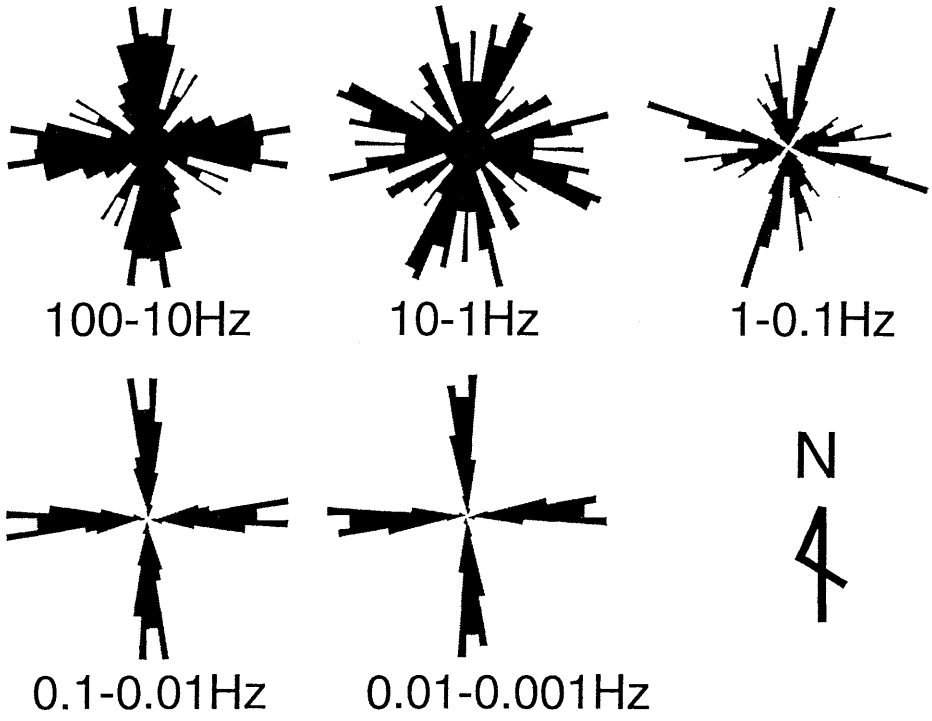
100-10Hz
10-1Hz
1-0.1Hz
0.1-0.01Hz
0.01-0.001Hz
N

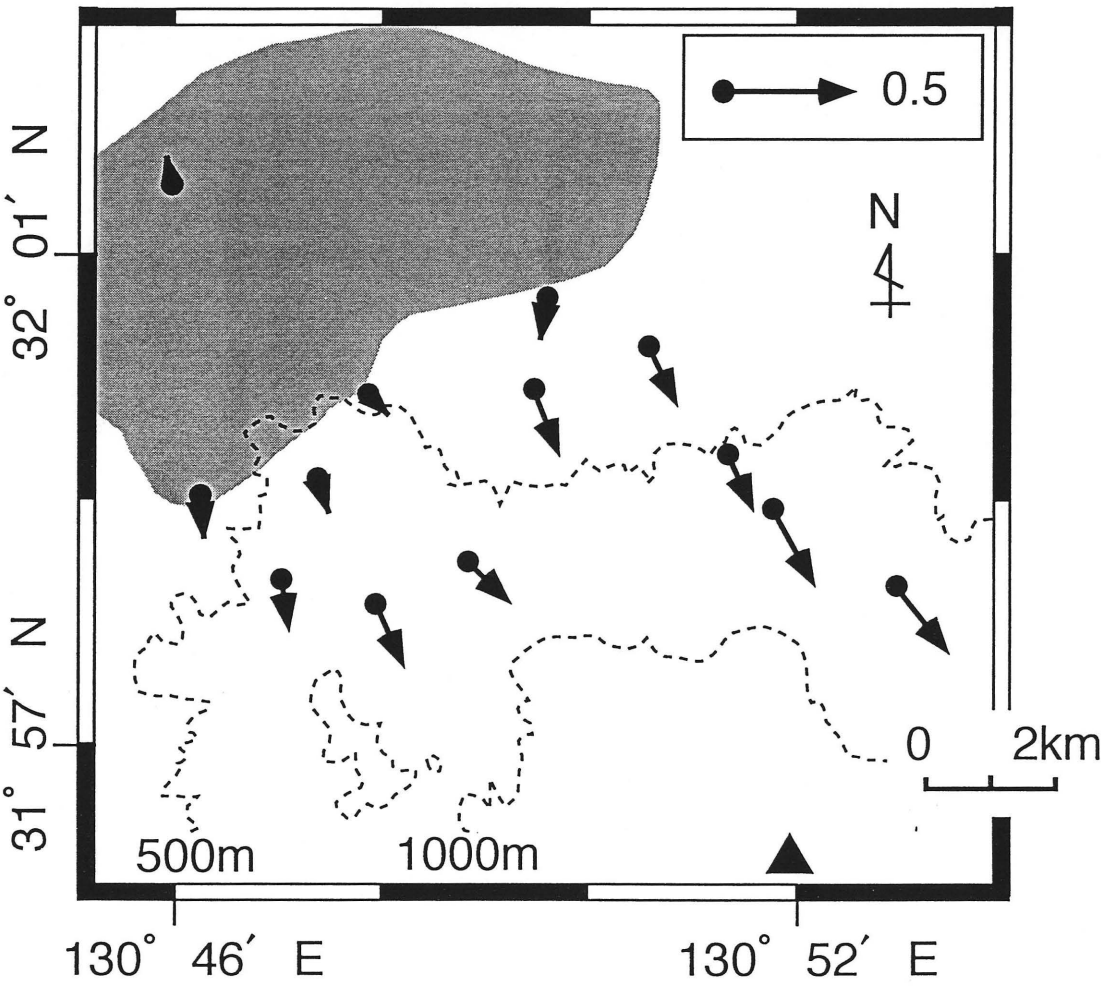
0.5
N
32° 01′ N
31° 57′ N
0
2km
500m
1000m
130° 46′ E
130° 52′ E

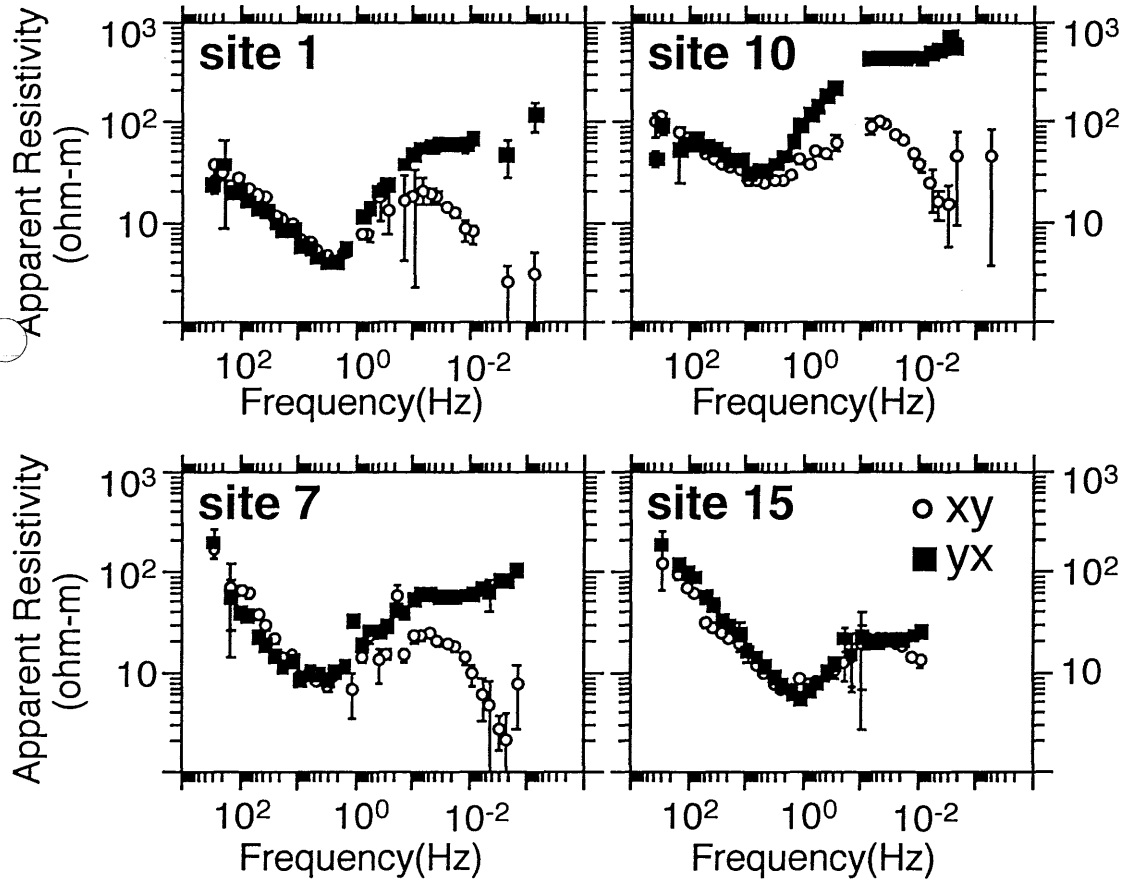
site 1
site 10
site 7
site 15
xy
yx
Apparent Resistivity (ohm-m)
Frequency(Hz)
10^3
10^2
10
10^2
10^0
10^{-2}

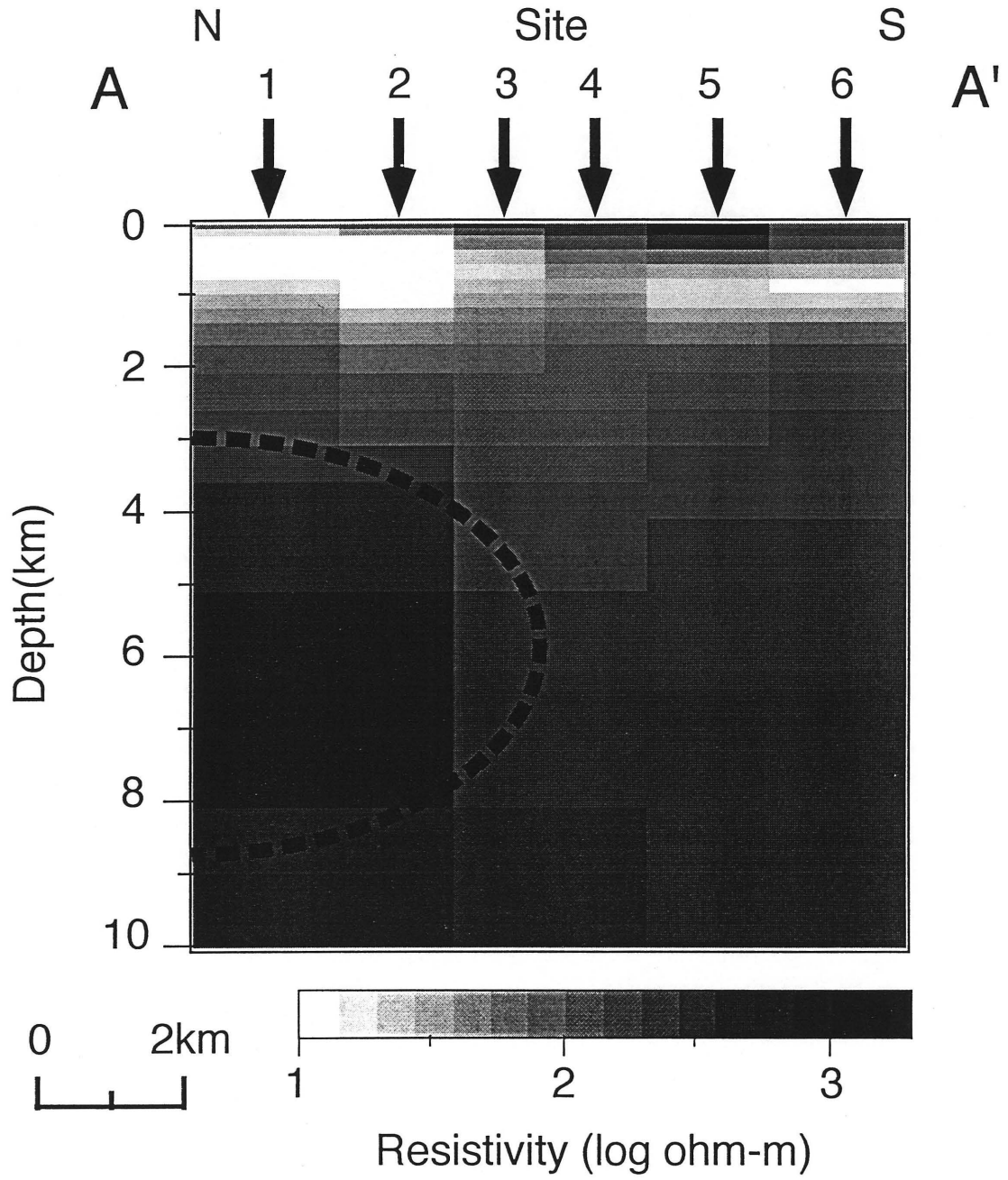
N
Site
S
A
1
2
3
4
5
6
A'
0
2
4
6
8
10
Depth(km)
0
2km
1
2
3
Resistivity (log ohm-m)

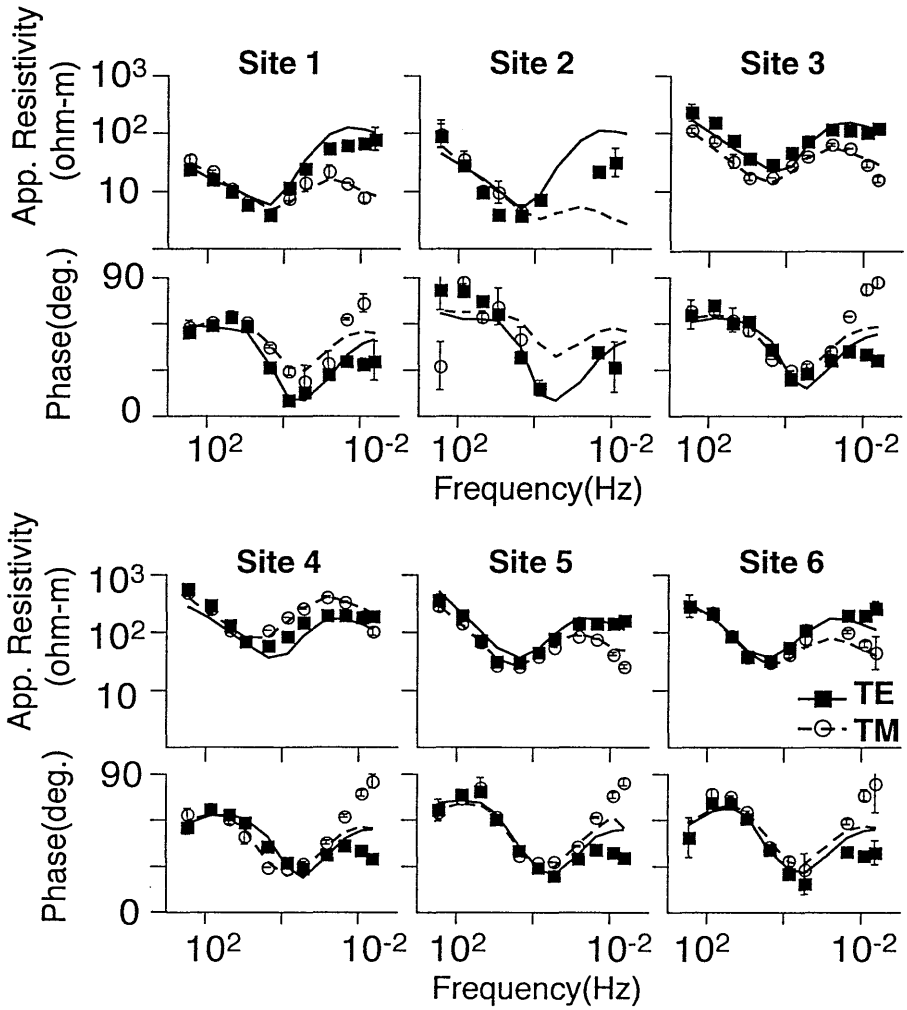
Site 1
Site 2
Site 3
Site 4
Site 5
Site 6
App. Resistivity (ohm-m)
10^3
10^2
10
Phase(deg.)
90
0
10^2
10^{-2}
Frequency(Hz)
TE
TM

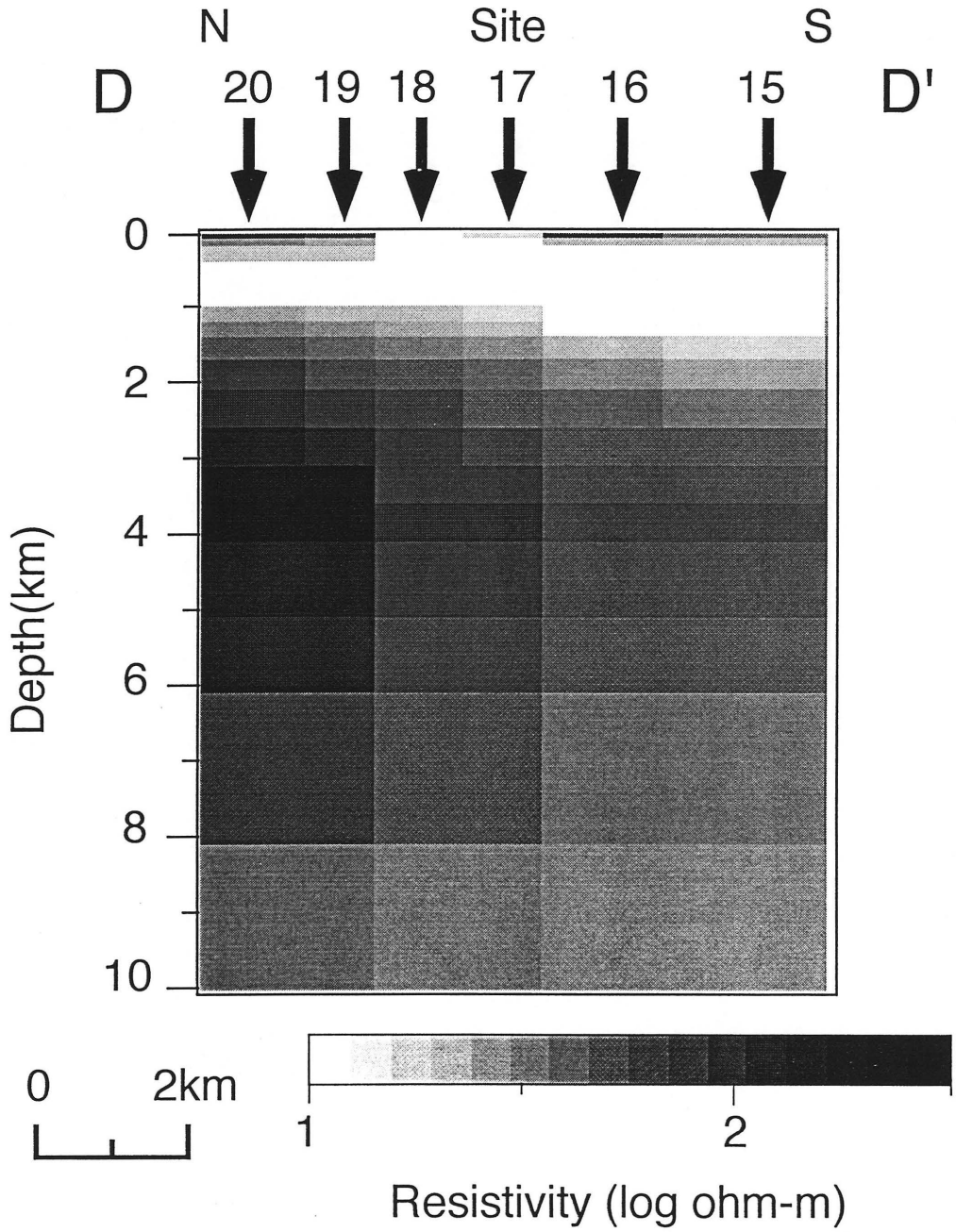
N
Site
S
D
20
19
18
17
16
15
D'
0
2
4
6
8
10
Depth(km)
0
2km
1
2
Resistivity (log ohm-m)

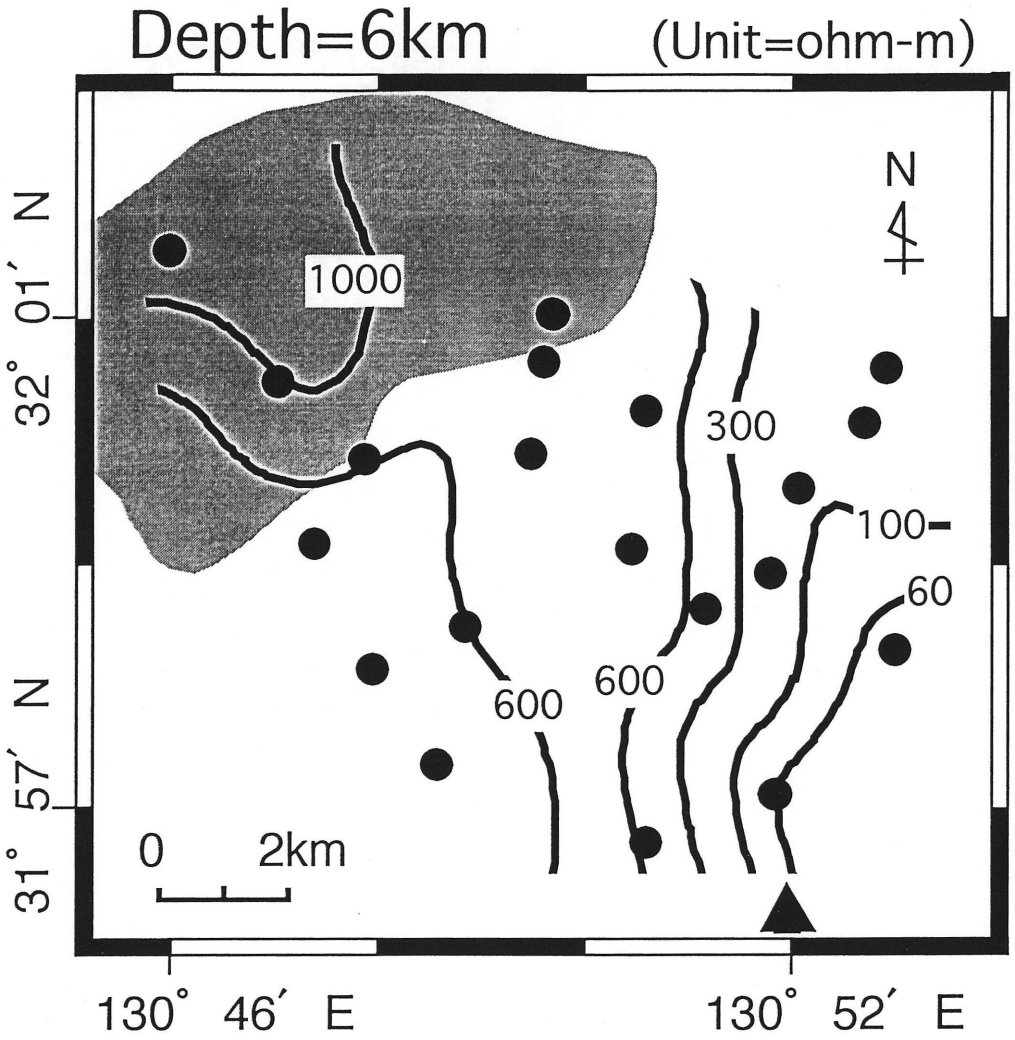
Depth=6km
(Unit=ohm-m)
N
1000
300
100
60
600
600
0
2km
32° 01′ N
31° 57′ N
130° 46′ E
130° 52′ E

The resistivity structure across the Atotsugawa fault, central Japan

Tadanori Goto, Naoto Oshiman
and Norihiko Sumitomo

Research Center for Earthquake Prediction, Disaster Prevention Research Institute, Kyoto University, Gokasho, Uji City, Kyoto Prefecture 611, Japan

Abstract

We studied the electrical resistivity structure around the Atotsugawa fault, located in central Japan, in order to constrain the major cause of inland earthquake occurrences. A lot of micro-earthquakes have actively occurred along this fault, although the central part shows low seismicity. After correcting the static shift and the local galvanic distortion, the two-dimensional models of the resistivity were constructed across both the low-seismicity part of the fault and the high-seismicity one using the inverse method. A clear structure difference between those resistivity models is found. A resistive layer at 3-7 km in depth is widely spread along the low-seismicity part, and a conductive layer also underlies broadly beneath 10 km in depth. On the other hand, such resistive and conductive layers are not found beneath the high-seismicity part, although the resistive zone at 3-12km in depth exists only on the northern side of the fault. To explain these features of the resistivity structure and the heterogeneity of the seismicity in the Atotsugawa region, we consider that the existence of fluid is probably concerned with the occurrence of earthquakes. Beneath the central part of the Atotsugawa fault, upwelling fluid from deep zones of the earth's crust may be trapped beneath the resistive layer, causing the conductive lower crust and the low-seismicity along the fault. On the other hand, beneath the western part of the Atotsugawa fault, fluid may upwell from deep zones of the earth's crust through the fault, and may attributable to the high-seismicity and the relatively resistive lower crust.

1.Introduction

The Atotsugawa fault, which runs and extends longer than 60km in central Japan(Fig. 1), is one of the most active faults in Japan (Research Group for Active Faults, 1991). The Atotsugawa fault is the strike-slip fault with a right lateral displacement(Matsuda, 1966; Togo et al., 1983; Okada et al., 1983). According to the geological studies, the average rate of displacements is estimated as being more than 1m / 10^3years. The strike of the fault trace is approximately N60E. The fault plane stands vertically ($90^\circ \pm 10^\circ$) near the

surface. The Atotsugawa fault began to move toward the latest Tertiary (Matsuda, 1966).

The topographical offset of 3km is found along the fault, which may be regarded as seismic displacements accumulated by repeated large earthquakes since late Tertiary. Mikumo et al.(1988) suggested that large earthquakes have occurred in Quaternary period about 1000 times, and the interval of successive large earthquakes would be about 1000-2000 years. The trenching survey across the Atotsugawa fault (Research Group for Excavation of the Atotsugawa fault, 1983) supported their suggestion of the recurrence interval of large earthquakes. The latest large earthquake of M=7.0 in the Atotsugawa region occurred in 1858, named the Ansei Hida earthquake (Yamazawa, 1929; Mikumo et al., 1988).

The seismicity along the Atotsugawa fault is very clearly recognized. The distribution of the epicenter around the Atotsugawa region is shown in Fig. 1. In Fig. 1, the two lineament of the epicenters coincide with the Atotsugawa fault, and Ushikubi fault. On the other hand, the seismicity in the adjacent zone, particluarly southern side, of these falut is remarkably low. Additionally, the spatial heterogeneity of the seismic activity along the Atotsugawa fault is also clearly recognized (Mikumo et al, 1988, Wada et al, 1996). In the central part of the Atotsugawa fault, the seismicity is rather low as compared with the eastern and the western part of the fault. Mikumo et al.(1988) suggested that the high seismicity at the eastern and the western of the fault may be due to the postseimic stress concentration after the 1858 Hida earthquake.

The resistivity structure of the crust may produce important information in association with the occurrence of the earthquakes because the resistivity is sensitive the state of water or temperature, or both, that have crucial effects on controlling the mechanical property on rocks. In addition, recently, much interest have been focused on the upwelling of the fluid from a deep interior of the Earth's crust as one of the causes of the occurrence of the earthquakes. It has been argued as one of seismogenic models that fluid makes an important role in the occurrence of earthquakes (Sibson et al.,1988 ; Rice, 1992 ; Byerlee, 1990, Blanpied et al., 1992). The basic concept is the reduction of the frictional strength of the fault by the highly pressurized fluid.

If fluid is concerned with a seismogenic zone along faults or a hypocentral zone of an earthquake swarm, then the resistivity should be low there. Therefore, the resistivity structure produces important information about the occurrence of the earthquakes, especially the relationship between the seismogenic zone and the fluid. However, the knowledge of deep resistivity structures of the fault is a very few. So, in this paper, we studied the resistivity structure around the Atotsugawa fault, one of the most active fault in Japan, where the high seismic activity is recognized. We selected two profiles of the MT soundings to cross sections of the fault where the seismicity is different from each other. In this paper, we construct the two-dimensional resistivity models along these profiles. After that, we interpret the resistivity structures and discuss the relationship between those structures and the seismicity, respectively. Finally, we propose a probably significant factor to consider the occurrence of the earthquakes.

In this area, several geophysical surveys were conducted and showed the discontinuity

of the properties of rocks around the Atotsugawa fault. Okubo et al. (1988) constructed the density model based on the gravity data. They found that the minor changes of the gravity anomaly observed and concluded that this is duc to small difference of the density around the fault. Okubo et al.(1989) estimated the distribution of the Currie point depth around Japan. It is reconginzed that the Currie point depth gradually change around the Atotsugawa fault. Additionaly, Hirahara et al. (1986) revealed the three-dimensional seismic velocity structure in central Japan. They showed that the seismic velocity changed at the western part of the Atotsugawa fault. These geophysical studies help us to interpret our resistivity structure inferred from MT soundings.

2. Observation

We observed natural fluctuations of the electric and the magnetic fields around the Atotsugawa region. Observations were carried out in June and August in 1994, and August in 1995. Total number of sites is 19. Locations of sites were shown in Fig. 1. We arranged these sites along the two survey lines in Fig. 1. The survey line AA' runs across the seismogenic zone of the Atotsugawa fault through Kawai village, Gifu prefecture. The survey line BB' runs across the aseismic zone of the Atotsugawa fault through Kamioka city, Gifu prefecture. We used two V5 MT systems and recorded two components of the electric field and three components of the magnetic field at each site during about three days. The total number of stacked cross power is about 20000 around 1Hz and about 100 around 0.01Hz. The V5 systems worked with the synchronized clocks and were separately set up at least 20km apart, acquiring time series data at the same time. The simultaneous time series data at two sites were used in the remote reference processing each other.

We carried out the AMT (audio-magnetotelluric) sounding at site 14 to investigate the shallow resistivity structure near the Atotsugawa fault. V5 MT system was also used for the AMT soundings. The covered frequencies for the AMT soundings ranges from 10kHz to about 1Hz. The system installs a high sampling A/D converter (500kHz) and three induction coils were replaced with shorter ones, which is more sensitive for the frequency band in the AMT sounding. The observed magnetic and electric fields were processed with the technique of the Cascade decimation (Wight and Bostick, 1980) on every site. Then, calculated cross powers and MT parameters were stored. Time series data of the AMT sounding are not stored, so the remote reference processing was not carried out in the AMT soundings.

For the procedure of the modeling, we have to reject poor quality impedances. In the following procedure, we used impedances of a small error, which is represented by percentage error of the apparent resistivity less then 100% and a error of the phase less than 30 degrees. We checked the data quality using the multiple coherency. The majority of multiple coherency was greater than 0.8, and impedances with a high quality were selected at the frequency between 400Hz and about 0.01Hz.

3. Strike direction and induction arrow

The strike directions were calculated with the method of Chakridi et al.(1992). The distribution of the strike direction was averaged in the whole frequencies at each site , and was shown in Fig. 2. The strike tends to NNW-SSE or ENE-WSW approximately. The average strike at 1- 0.01Hz along AA' and BB' were N10W and N45W, respectively. The stability of the strike in regard to the frequency was shown in Fig. 3 with the rose diagrams. The strike was not stable at the frequency range of 10 - 1Hz. This means that the 3-dimensional inhomogeneity exists at shallow depths. However, the strike was stable at the frequency ranging from 1 - 0.01Hz. The sounding depth at the frequency of 1Hz is greater than 10km considering the skin depth and the averaged apparent resistivity at that frequency. We infer that the strike of NNW-SSE or ENE-WSW is the regional strike of resistivity structure of the crust.

The induction arrows were also calculated around the Atotsugawa region. The distributions at some representative frequencies were shown in Fig. 4. The average directions along each profile were also shown. Generally, the induction arrows around the Atotsugawa region tends to NNW-SSE.

The skewness was small around the target area, especially along the profile BB'. The skewness along the BB' was lower than 0.3. Then, we consider that the resistivity structure beneath the profile BB' is approximately 2-dimensional. The skewness along the profile AA' was lower than 0.4 except for site 8, which was larger than along the BB'. It is inferred from the skewness that the 3-dimensional inhomogeneity of the resistivity exists beneath the profile AA'. However, the distribution of the strike showed a stable direction at the frequency of 1 - 0.01Hz, especially at site 8. It is judged that the 3-D imhomogeneity may exist near the surface or a shallow depth, and that the resistivity structure along the AA' is also regionally 2-dimensional. Considering the coincidence of the strikes, the induction arrows and the geological strike, the regional strike of the resistivity structure is regarded being N30W along the both profiles.

4. Apparent resistivity and phase

The observed apparent resistivity and the impedance phase along the profile AA' and BB' were shown in Fig. 5 and Fig. 6. Note again that the impedance phase is called "phase " simply. In these figures, N30W was taken as the X axis of the coordinate and N60W as the Y axis. Both apparent resistivities ρ xy and ρ yx, had not the same value but showed splitting at the highest frequency. This splitting of the apparent resistivity curve implies the existence of the static-shift effect.

The apparent resistivity and the phase changed sharply near the Atotsugawa fault. At the northern sites of the fault (site 4, 5, 6, 8, and 2), the increasing of the apparent resistivity is clearly recognized in both ρ xy and ρ yx with decreasing of the frequency.

On the other hand, the apparent resistivity decreases as the frequency increases at the southern sites of the fault (site 9, 3, 1, and 19). Since the averaged strike directions at site 6, 2, 9, 1 and 3 are similar with each other, the rotation of the impedance does not affect this sharp change of the apparent resistivity. The phase values also show the different feature between the northern and southern area of the Atotsugawa fault. The phases of the both axis (ϕ xy and ϕ yx) at the northern sites of the fault show low phase values (< 45 degrees) at the frequency higher than 1Hz. The phases at the southern sites show high values (> 45 degrees) at the corresponding frequency. These sharp changes of both the apparent resistivity and the phase near the Atotsugawa fault implies that the resistivity of the underlying layer beneath the surface is high in the northern area of the Atotsugawa fault and low in the southern area. In other word, the Atotsugawa fault would be one of the resistivity boundary.

On the contrary of the profile AA', the apparent resistivities and the phases along the BB ' are very similar with each other. The apparent resistivities at all sites along BB' increase around the frequencies of 10Hz and decrease around 0.1Hz. Similarly, the phase at all sites along BB' decrease around 10Hz and increase around 0.1Hz. These feature indicates that the underlying resistivity layer widely may spread beneath the profile BB'. Additionally, it is noteworthy that a very high value of the phase ($\approx$ 60 degrees for ϕ xy, and $\approx$ 75 degrees for ϕ yx) around the frequency of 0.1Hz is found at the southern site of the Atotsugawa fault (site 15, 17 and 18).

The apparent resistivity obtained by the AMT sounding at site 14 is about 130 Ω m at the frequency of 10kHz, which is similar value at the highest frequency of the MT sounding. These responses are used for the static-shift correction in the following process of modeling.

5. Modeling and its results

We constructed the 2-dimensional(2-D) resistivity models beneath the profile AA' and BB'. In the Atotsugawa region, particularly along the profile AA', 3-dimensional heterogeneity of resistivity may exists. We used the apparent resistivity and the phase of the TM mode in the process of modeling because the TM mode gives a good approximation for a 3-dimensional resistivity structure (Ting and Hohmann, 1981). The inverse method used here was developed by Uchida and Ogawa(1993). The width of the 2-D model is taken to be about 1400km and the bottom depth is taken to be 1900km. The 2-D model was constructed using elements of horizontally about 70 and vertically 33. The horizontal size of each block was 0.8km near the Atotsugawa fault and became wider near the edge. The vertical size also became thicker as a depth of a block increases. About 400 unknown parameters of the resistivity were assigned these elements. A uniform earth of 1000 Ω m is selected as an initial model for the inversion. We changed the background resistivity of the initial model and found that the resistivity of the initial model did not so affect the final model.

There were two steps for the correction of the static shift. In the first inversion, the surface block beneath each site were not included in the calculation of the smoothness. As a result, the static-shift factor which is a bias error of the apparent resistivity were estimated at each site. Along the profile AA', the factor is maximum (0.2) at site 8 and minimum (-1.1) at site 6. And the factor along BB' is ranging from 0.1 (at site 11) to -0.4 (at site 14). As the static shift along each profile still remains a little, it can be checked by comparing with AMT data. On the basis of the AMT sounding at site 14, the apparent resistivity was 130 Ω m at about 10kHz. We applied the Bostick inversion (Bostick, 1977) to this data and estimated the resistivity to be 140 Ω m at about 50m in depth. Then, in the first inversion to estimate the static shift factors, we fixed the resistivity of the surface block beneath site 14 as 140 Ω m and recalculated the static shift factor at sites along BB'. And we compared this with the calculated static shift factor under the condition in which all resistivities of the model are treated as free parameters in the inversion. As a result, the static shift factors calculated were similar without regard to the fixed or the free condition about the surface resistivity at site 14. It seems therefore that the average static shift along BB' is considered to be small. The good correlation of structures between the resistivity and the seismic P-wave velocity along BB', described later, also supported that the correction of the static shift proposed was effective. On the other hand, the averaged static shift factor along the profile AA' were not calculated because there were no information of the surface resistivity at just observed sites along AA'. However, the VLF-MT sounding, which is one of the MT sounding and the frequency is about 20kHz, were carried out near AA'. Nakayama (1995, pers. comm.) measured the surface resistivity near the Atotsugawa fault around Miyagawa, located about 10km east from site 2. He found that the averaged apparent resistivity near the fault is about 300 Ω m. This value is very similar to that of the surface resistivity at site 2, near the Atotsugawa fault, obtained by the result of the first inversion. So, we conclude that the averaged static shift is also small along the profile AA'. At least, the resistivity of the two-dimensional model along AA' may be higher than the determined value in Fig. 10, descrived later, because all sites were located on the alluvium which shows lower resistivity than the underlying basic rocks and make a negative static-shift effect.

The inverse process is very stable and yields the most probable model with 10 iterations of the algorithm. First, the most probable model along the profile AA' is shown in Fig. 7. The number of iteration for the first and second inversion is both 4. This model well explained the observed apparent resistivity and the phase. The calculated apparent resistivities and the phases from the model in Fig. 7 are shown in Fig. 8 with observed responses. We showed the sensitivity of the model in Fig. 9. The sensitivity indicated that the resolution is low beneath the Atotsugawa fault, but the approximate confidence bounds of each resistivity value is about several times as greater as the value of the resistivity in that block.

The most remarkable and the well-resolved feature in the model is the existence of the probably vertical boundary of resistivity near the Atotsugawa fault. The boundary cut the upper crust from the surface to the depth of 15km at least and discriminated the northern

resistive zone (> about 3000 Ω m) from the southern relatively conductive zone(< about 3000 Ω m). The tendency of the northern resistive and the southern conductive is also expected from the observed data only. That is, the apparent resistivity become high in lower frequencies at the northern sites of the Atotsugawa fault and become low at the southern sites. The most suitable model along AA' is consistent with this feature.

An additional feature in the suitable model along the profile AA' is found. There exists a resistive body beneath the area between the Atotsugawa fault and around 7km north of it. Site 6 and 8 ,showing the lowest phase along AA', are sensitive to this resistive body. These low phases are not explained without such a resistive body. The calculated response did not still satisfy the low phase at about 10Hz on site 6. The resistive body, however, may have higher resistivity value. Otherwise, a small-scale and 3-dimensional resistivity anomaly may underlie near site 6 because the resistivity strike at site 6 tended to a different direction as compared with site 5 and 8. The resistivity beneath site 4 and 5 became comparatively low as compared to beneath site 6. That is there also exists a vertical boundary of resistivity near the 7km north of the Atotsugawa fault, which is a smaller gap compared with the Atotsugawa fault.

Next, the final model of resistivity for the profile BB' was shown in Fig. 10. The number of iterations for the first and second inversion is 7 and 8, respectively. The fitness of the calculated apparent resistivities and phases to the observed ones was better than those of the model along AA'. The calculated apparent resistivities and phases were shown in Fig. 11 with observed responses. We also showed the sensitivity of the model in Fig. 12. It is concluded that the resistivity of the model is well-resolved in the southern area along the profile BB' and the approximate confidence bounds of each resistivity value is about several times of the resistivity in that block.

In the most suitable model along the profile BB' , two features are obvious. One is that the resistive layer (> 1000 Ω m) underlies widely beneath the area of the profile BB' at the depth of about 3km. Another feature is that there exists the conductive layer (< 300 Ω m) below the depth of about 10km in the southern side of the Atotsugawa fault. The widely spreading resistive layer especially become more resistive beneath site 14 (on the Atotsugawa fault) and beneath site 18. This resistive layer is expected from the observed feature that the apparent resistivity and the phase along BB' is very similar to those along the profile AA'. The deep conductive layer is also expected from the observed high phase ($\approx$60 degrees for ϕ xy, and $\approx$75 degrees for ϕ yx) at 0.1Hz

6. Discussion

We compare the two resistivity models of the profile AA' and BB' with other geophysical and geological studies around the Atotsugawa region. And then, we consider the relationship between the resistivity structure and the seismic activity around this whole region.

An obvious similarity can be seen between the structures of resistivity and seismic P

wave velocity. Shimada (1996, pers. comm.) estimated the 3-dimensional structure of seismic P wave velocity around the Atotsugawa fault. The seismic velocity structure calculated by Shimada is basically similar to one by Hirahara et al.(1986), though Shimada 's structure is more resolved horizontally. The seismic velocity structure along the profile AA' and BB' together with MT sites were shown in Fig. 13 and Fig. 14. Comparing the seismic velocity structure(Fig. 13) with the resistivity structure (Fig. 10), it is easy to find out a good correlation between the two structures. Especially, the good correlation is clearly recognized along the profile BB'. This good correspondence verifies that the both structures of the resistivity and seismic velocity are well resolved along the profile BB'. Especially, we conclude that the method of correction for the static shift presented in this paper is so useful as the static shift is effectively removed. Both the structure of the seismic P wave velocity and the resistivity structure along the profile AA' are also very similar with each other. However, the similarity between the resistivity and the seismic velocity became vague below 9km in depth. It may be due to the reason that the number of the seismic ray path used to analysis for the deeper zone below 9km is a few near the profile AA' because the location of the seismic observatory used is not suitable for the tomography. So, the velocity structure deeper than 9km have poor resolutions.

We infer what kind of rocks are able to compose the resistive and high velocity zone found in the both profile of AA' and BB'. Let us first look at the distribution of the gravity anomaly in the Atotsugawa region. Furuse and Kono(1988) showed the relative gravity anomaly with the wave length shorter than 30km. They pointed out that this gravity anomaly is well consistent with the geology in the Atotsugawa region. They found that the high gravity anomaly approximately corresponds to the area where the Funatsu granitic rocks and Hida metamorphic rocks are exposed. They concluded that the Funatsu granitic rocks and the Hida metamorphic rocks have a high density value.

As discussed above, the high resistivity zone corresponding to the high velocity zone underlies the whole area along the profile BB' and the northern area along AA' at about 5km depth. These area shows the relatively high gravity anomaly. We conclude that the resistive layer beneath whole of BB' and the northern part of AA' possibly consists of rocks with a high seismic velocity and a relatively high density. In the geological map, the Funatsu granitic rocks and the Hida metamorphic rocks distribute maily in a broad area along BB' and in the northern area of the Atotsugawa fault near AA'. This geological feature supports the suggestion that the resistive layer is possibly composed of the granitic rocks and / or the metamorphic rocks. On the other hand, the southern side of the Atotsugawa fault near AA', where the relatively high gravity anomaly was also found and the Funatsu granite distribute, shows lower resistivity than the northern side. It may be caused that the rocks beneath southern area of the Atotsufawa fault along AA' includes much water than the northern area because there exist many fault with low activity distribute in the southren area.

Next, let us consider some factors probably causing the conductive layer beneath the profile BB'. One of the most important candidates is thermal effects. Mikumo et al.(1988) concluded that the cutoff depth of micro-earthquakes is strongly related to the thermal

structure beneath the Atotsugawa region. In this region, the heat flow data were summarized in Uyeda and Horai(1964) and Li et al.(1989) . According to their investigations, heat flow at Kamioka, near site 16 in the profile BB', is 1.80HFU and the thermal gradient is 2.77℃ /100m. If we extrapolate it to the earth's interior, the temperature at the corresponding depth for the conductive layer beneath site 16 (10km) amount to about 300℃ . It is consistent with the temperature of the cutoff depth of earthquakes(Sibson, 1984) and in fact, the cutoff depth of the seismic activity is also about 10km (Mikumo et al, 1988). However, the conductive layer found beneath the southern side of the profile BB' can not be fully explained by the effect of the temperature only since the temperature is too low. Olhoeft (1981) described that the resistivity of the granite changes about 20% as the temperature varies from the room temperature to 300℃. On the other hand, the resistivity value was 10000Ω m at 5km in depth and decreases to about 300Ω m at 10km in depth. Thus, the thermal structure controls the cutoff depth of earthquakes and may relate to the resistivity, though other factor would cause the conductive layer beneath BB'.

We mention the significance of fluid in the lower crust as one of the factors responsible for the conductive layer beneath the profile BB'. Research Group for Crustal Resistivity Structure has carried out the MT surveys in various regions of Japan and presented the large-scale resistivity structures beneath Japan Arc (Utada, 1987; Ogawa et al., 1986). In the central Japan, Utada(1987) studied the 2-dimensional resistivity structure of the crust and the upper mantle and found that the conductive layer with the resistivity of 10Ω m exists in the lower crust. He concluded that the conductive layer in the lower crust can not be explained by only thermal origins and pointed out the significance of water content in the lower crust. The laboratory experiments support the possibility of the existence of the free water in the crust. Kariya and Shankland(1983) showed that the resistivity of rocks in a dry state has in general a very high value at the thermal condition for the lower crust. Other experiments show that free water remarkably reduces the resistivity of rocks (e.g. Olheft, 1981; Shankland and Ander, 1983). Of course, other mechanisms for good conduction will relate to such conductive layer. One of the candidates is conductive mineral such as magnetite or graphite (e.g. Stesky and Brace, 1973; Duba et al., 1988). The seismic reflection survey also support the existence of fluid in central Japan. According to Ito et al.(1993), the reflective layers of the seismic wave at the depths of 15 - 20 km exist beneath a part of the Atotsugawa region and the eastern part of the Hida mountain range. The conductive minerals will not make a reflector while free water easily make a strong reflective layer. Thus, these investigations strongly suggest that the existence of free water which is a major factor causing the conductive zone at depths of the lower crust, although other factor will responsible for this conductive layer.

Utada(1987) also found a conductive layer exists at the top of the subducting slab. According to his study, the southern edge of the lower crustal conductor coincides with the location where the slab-top conductor reach to the depth of 60km. This fact agrees with the petrologic studies of the Island arc (Takahashi, 1978; Tatsumi et al,. 1983). Tatsumi et al. supposed a water rich state in the mantle wedge where water is continuously

supplied from the squeezed sediments on the subducting slab and the dehydrated oceanic crust. Utada's resistivity model across Japan island supports the petrological model. Hirahara et al. (1986) identified the 3-dimensional distribution of the seismic velocity beneath central Japan. A low velocity zone at the depths ranging from 50 to 150 km found by them also support the petrological model. These investigation suggests that free water in the lower crust may be supplied from the subducting slab.

Although the active fault is often accompanied with a distinguished low resistivity zone, the resistivity structures along the profile AA' and BB' do not indicate such low resistivity zones along the Atotsugawa fault. Ohshiman et al.(1987) investigated the magnetic anomalies along the Atotsugawa fault , finding that this anomaly can be explained by a dyke of which susceptibility is larger than that of the surrounding rocks and intrudes along the fault plane. The similar model for the magnetic anomaly along the Atotsugawa fault was proposed by Murakami et al.(1984). They suggested that highly magnetized materials are possibly intruded or concentrated along the fault plane. The width of the anomaly is about 50m, which is small comparing with the block size in the resistivity models near the Atotsugawa fault. Considering the results of the magnetic survey, we suggest that the fracture zone along the Atotsugawa fault is so narrow as the width is several tens of meters, and / or that the fault may be filled with the mafic intrusion along the fault.

We compare the resistivity model along the two profiles in the Atotsugawa region with the seismic activity around the Atotsugawa fault. The projections of hypocenters of micro-earthquakes to the resistivity models (Fig. 15 and Fig. 16) indicates that there exist many micro-earthquakes near the vertical boundary of the resistivity. The hypocenters are determined based on the data by the Kamitakara observatory which is subjected to Research Center for Earthquake Prediction, Disaster Prevention Research Institute, Kyoto Univ. The projection along AA' (Fig. 15) shows that the seismic activity is high on the side of the resistive body in the northern area of the Atotsugawa fault. These earthquakes have occurred along the Atotsugawa and Ushikubi fault. Considering the precision of the determination of hypocenters and the resolution of the resistivity model, this resistive body beneath AA' may be sandwiched by the two strike-slip active fault (the Atotsugawa and the Ushikubi fault) and the micro-earthquakes may not occur in the resistive body but at the edge of it. On the contrast to the profile AA', the projection along BB' (Fig. 16) shows that the seismic activity is very low in the resistive layer at about 5km in depth. Thus, these similarity with the resistivity structure and the low seismic activity along the Atotsugawa fault suggest that the seismic activity is comparatively high only along the vertical resistivity boundaries while the seismic activity is low in the resistive layer.

Hirahara et al.(1986) showed that the horizontal scale of the low velocity zone is about 100km. Comparing this horizontal scale, the area along AA' and BB' is very close each other. If the low velocity zone is due to the existence of fluid originated from the subducting slab, it is suggested that the content of free water supplied in the lower crust should be common beneath AA' and BB'. The lower crust beneath the Atotsugawa region, therefore, should show similarly low resistivities. However, the resistivities of the lower crust beneath the profile AA' and BB' are different. The resistivity at the depth of 10km

beneath AA' is about 3 times as large as that of the conductive layer beneath BB'. The difference of the resistivity of the lower crust can be explained by the distribution of the resistive layer at the depth of about 5km. Along the profile BB', the resistive layer widely overlies the conductive layer at 5km in depth. By the way, free water in the lower crust will upwell toward the surface because of its own buoyancy. In that case, the fluid does not remain and not produce a conductive zone in the lower crust. We infer that the resistive layer at 5km in depth may capture free water in the underlying lower crust and keep it conductive. On the contrary to the profile BB', the resistive layer at 5km depth along AA' is recognized only in the north of the Atotsugawa fault. This means that free water beneath AA' easily diffuse to the surface because of the lack of the resistive layer , and the resistivity of the lower crust become high as compared with beneath BB'.

Although many possible causes of the non-uniform seismic activity along the Atotsugawa fault are considered, what does the major factor control the seismicity ? We have pointed out the significance of fluid on the basis of the comparison of the resistivity structure to the seismic activity. Combining the resistivity structure and the seismic activity together with experimental facts, we think that fluid in the crust is a possible and an important factor causing the difference of the seismicity along the Atotsugawa fault . That is , it is considered that the high seismic activity along the Atotsugawa fault near the profile AA' may be caused mainly by the upwelling fluid from the lower crust along the fault. The upwelling fluid to the surface also can cause the relatively "resistive" lower crust compared to beneath BB'. In addition, it is inferred that the low seismic activity along the Atotsugawa fault near BB' is due to the underlying resistive layer which probably prevent fluid from upwelling in the lower crust. This supposition can also explain high conductivity in the lower crust beneath BB' with the fluid-rich statement. Of course, the seismicity along the Atotsugawa fault may be controlled by more microscopic structure which can not be imaged in the resistivity structure in this study. And it is undoubtful that other factors such as temperature and physical properties of rocks are also bound the seismic activity along the fault. However, fluid is the important cause for the seismicity around the Atotsugawa fault because it can explain both the seismic activity and the resistivity structure around there.

The difference of the resistivity structure between the profile AA' and BB' may be attributed to the heterogeneous activity of the Atotsugawa fault. It is possible to consider that a high active motion of the fault in a high-seismicity part of the Atotsugawa fault have destroyed the resistive cap rock as a result. On the other hand, a low activity of the fault in a low-seismicity part may keep the resistive layer which is able to capture the water. However, in this hypothesis, the upwelling fluid from the lower crust is necessary to explain the difference of the resistivity of the lower crust beneath two profiles. Such pressurrized fluid relates to the occurrence of earthquakes and fault activity either. Therefore, we pointed out the significance of the fluid to expalin the seismicity along Atotsugawa fault as we have suggested.

7. Conclusion

We carried out the magnetotelluric soundings around the Atotsugawa region including the active fault. Two profiles across the low and high seismicity section of the fault were set. The distribution of the strike direction on the resistivity structure shows that is is roughly two-dimensional. We adopted the inversion method for modeling the two-dimensional resistivity structure. The two resistivity model along the two profiles show different features. We summarize these features comparing with the seismic activity as follows.

(1) The resistive layer widely underlies in the region where is low seismicity of the Atotsugawa fault.

(2) A similar resistive zone is found only in the northern area across the high seismicity section of the Atotsugawa fault.

(3) The moderately conductive layer underlies broadly the Atotsugawa region. Especially, the resistivity is low beneath the low seismicity section of the Atotsugawa fault below the depth of about 10km

Thus, there is several differences between the resistivity structure across the low and high seismicity part of the Atotsugawa fault. In order to explain both the features of the resistivity structure and the heterogeneity of the seismicity in the Atotsugawa region, we proposed the significance of fluid. Fluid is possible to be attributed to the conductive layer in the lower crust beneath the Atotsugawa region. It is suggested that the spatial variation of the resistivity in the lower crust in the Atotsugawa region, described in above(3) , reflects the content of fluid in the lower crust. Considering the correspondence that the lower crust beneath the seismically active and non-active segment of the fault shows a relatively low and high resistivity respectively, we propose that the high-seismicity section of the Atotsugawa fault may be related to the upwelling of fluid from the lower crust, and the low-seismicity section may be related to the captured fluid in the lower crust.

Acknowledgments

We thank to K. Ito of Disaster Prevention Research Institute, Kyoto Univ. for the helpful discussion about the seismicity around the surveyed area. We also thank to S. Yamaguchi of Kobe Univ. and I. Shiozaki of Tottori Univ. for valuable comments. We thank to T. Uchida and Y. Ogawa of Geological Survey of Japan for providing their inversion code for MT data. We greatly thank to Y. Wada and H. Wada of Disaster Prevention Research Institute, Kyoto Univ. for their assists of the field work. We are grateful to S. Sakanaka, M. Ichiki, Y. Hori, H. Hori, K. Goto, T. Kasaya, K. Tanimoto, M. Amita and Y. Kobayashi for their assists of the field work.

References

Blanpied, M. L., D. A. Lockner and J. D. Byerlee , An earthquake mechanism based on rapid sealing of faults , Nature , 358 , 574-576 , 1992

Bostick, F. X. , A simple almost exact method of MT analysis , Workshop on electrical methods in geothermal exploration, U. S. Geol. Surv., Contract No. 14080001-8-359 , 1977

Byerlee, J. , Friction, overpressure and fault normal compression , Geophys. Res. Let. , 17 , 2109-2112 , 1990

Chakridi, R., M. Chouteau and M. Mareschal , A simple technique for analysing and partly removing galvanic distortion from the magnetotelluric immpedance tensor : application to Abitibi and Kapuskasing data (Canada) , Geophys. J. Int. , 108 , 917-929 , 1992

Duba, A. G., E. Huenges, G. Nover and G. Will , Impedane of bleck shale form Munsterland 1 borehole: an anomalously good conductor? , Geophys. J. , 94 , 413-419 , 1988

Furuse, N. and Y. Kono , The densitiy distribution from the surface to the depth of 30km in the western part of central Japan inferred from the gravity anomalies , Chikyu Monthly , 11 , 75-83 , 1989

Hirahara, K., A. Ikami, M. Ishida and T. Mikumo , Three-dimensional P-wave structure beneath cenral Japan: low velocity bodies in the wedge portion of the upper mantle above high-velocity subducting plates , Tectonophysics , 163 , 63-73 , 1989

Ito, K., I. Kawasaki, M. Hurumoto, H. Isobe and T. Nagai , Seismic survey in northern Chubu district, Japan. Toyama-Kamitakara line , Ann. Disas. Prev. Res. Inst., Kyoto Univ. , 36 , 325-328 , 1993

Kariya, K. A. and T. J. Shankland , Electrical conductivity of dry lower crustal rocks , Geophysics , 48 , 52-61 , 1983

Li, X., Y. Furukawa, T. Nagao, S. Uyeda and H. Suzuki , Heat flow in cenral Japan and its relations to geological and geophysical features , Bull. Earthq. Res. Inst. , 64 , 1-36 , 1989

Matsuda, T. , Strike-slip faulting along the Atotsugawa fault (in Japanese with English abstract) , Bull. Earthq. Res. Inst. , 44 , 1179-1212 , 1966

Mikumo, T., H. Wada and M. Koizumi , Seismotectonics of the Hida region, central Honshu, Japan , Tectonophysics , 147 , 95-119 , 1988

Murakami, H., I. Yamada and U. Kobayashi , Geomagnetic total force anomalies asociated with active fault -Observation of the geomagnetic total force aroud Atotsugawa fault and Atera fault - , Zisin 2nd ser. , 37 , 397-405 , 1984

Ogawa, Y., T. Yukutake and H. Utada , Two dimensional modeling of resisitivy structure beneath the Tohoku district , northern Honshu of Japan, by a finite element method , J. Geomag. Geoelectr. , 38 , 45-79 , 1986

Ohshiman, N., Y. Honkura, K. Kuge and H. Sakai , Electric and magnetic anomalies at the Atotsugawa fault and their implications fo fault activity , J. Geomag. Geoelectr.

, 39 , 143-158 , 1987
Okada, M. and Y. Kymaki , Geological Study of the Terrace at Miyagawa and the displacemetn along the Atotsugawa fault. , Chikyu Monthly , 5 , 411-416 , 1983
Okubo, Y., H. Tsu and K. Ogawa , Estimation of Curie point temperature and geothermal structure of island arcs of Japan , Tectonophysics , 159 , 279-290 , 1989
Okubo, Y., N. Furuse and Y. Kono , Bouguer anomalies and crustal structure models aroud the Atotsugawa fault, central Japan , Zisin 2nd ser. , 41 , 97-102 , 1988
Olhoeft, G. R. , Electrical properties of granite with implications for the lower cr;ust , J. Geophys. Res. , 86 , 931-936 , 1981
Research Group for Active Faults, Acrive faults in Japan : Sheet maps and inventories , Univ. Tokyo Press , 363pp , 1991
Research Group for Excavation of the Atotsugawa fault , Trenching excavation across the Atotsugawa fault , Chikyu Monthly , 5 , 335-340 , 1983
Rice, J. R. , Fault stress states, pore pressure distributions, and the wakness of the San Andreas Fault , In Fault Mechanics and Transport Properties of Rocks, edited by B. Evans and T. -F. Wong, Academic, San Diego, Calif. , 475-503 , 1992
Shankland, T. J. and M. E. Ander , Electrical conductivity, temperatures, and fluids in the lower crust , J. Geophys. Res. , 88 , 9475-9484 , 1983
Sibson, R. H. , Roughness at the base of the seismogenic zone : contributing factors , J. Geophys. Res. , 89 , 5791-5799 , 1984
Sibson, R. H. , F. Robert and H. Poulsen , High-angle reverse faults, fluid pressure cycling, and mesothermal gold-quartz deposits , Geology , 16 , 551-555 , 1988
Stesky, R. M. and W. F. Brace , Electrical conductivity of serpentinized rocks to 6 kilobars , J. Geophys. Res. , 41 , 529-547 , 1978
Takahashi, E. , Petrologic model of the crust and upper mantle of the Japanese island arcs , Bull. Volcano. , 41 , 529-547 , 1978
Tatsumi, Y., M. Sakuyama, M. Fukuyama and I. Kushiro , Generation of arc basalt magmas and thermal structure of the mantle wedge in subduction zones , J. Geophys. Res. , 88 , 5815-5825 , 1983
Ting, S. C. and G. W. Hohmann , Integral equation modeling of three-dimensional magnetotelluric response , Geophysics , 46 , 192-197 , 1981
Toge,. M. and A. Okada , Activity of the Atotsugawa fault from the view of the topographic displacement , Chikyu Monthly , 5 , 359-366 ,1983
Uchida, T. and Y. Ogawa , Development of FORTRAN code for two-dimensional magnetotelluric inversion with smoothness constraint , Open-File Report, Geol. Surv. Japan , 205 , 115pp , 1993
Utada, H. , A direct inversion method for two-dimensional modeling in the geomagnetic induction problem , Doctoral thesis, University of Tokyo , 409 , 1987
Uyeda, S. and K. Horai , Terrestiral heat flow in Japan , J. Geophys. Res. , 69 , 2121-2141 , 1964
Wada, H., K. Ito, M. Ando and K. Wada , Observation of the earthquakes in the Mozumi tunnel at the Kamioka mine, central Honshu, Japan , Ann. Disas. Prev. Res. Inst.,

Kyoto Univ. , 39B-1 , 241-250 , 1996

Wada, H. and K. Ito , Seismic activity in the vicinity of the Atotsugawa fault, central Japan , Ann. Disas. Prev. Res. Inst., Kyoto Univ. , 38B-1 , 235-250 , 1995

Wight, D. E. and F. X. Bostick , Cascade decimation - a technique for real time estimation of power spectra , Proceedings IEEE international conference on acoustic speech and processing , 626-629 , 1980

Yamazawa, K. , The great earthquake of Hida-Tsunogawa on February 2, Ansei 5 , ZISIN I , 1 , 125-128 , 1929

Figure Captions

Fig. 1 The distribution of the epicenter around the Atotsugawa region. Lines indicate the location of the active faults. Locations of sites(Circles) and the Atotsugawa fault(the edge is indicated by the triangles) are also shown. Dashed lines indicates the surveying profiles in this study.

Fig. 2 The distribution of the strike direction averaged in the whole frequencies at each site

Fig. 3 The stability of the strike in regard to the frequency
(a) : for the profile AA' (b): for the profile BB'

Fig. 4 The induction arrows around the Atotsugawa region. Circle means the location of the site. Bar tends to the " conductive" zone.

Fig. 5 (a)The observed apparent resistivity and (b)the impedance phase along the profile AA'

Fig.6 (a)The observed apparent resistivity and (b)the impedance phase along the profile BB'

Fig. 7 The two-dimensional most suitable resistivity model along the profile AA'. The locations of the site of our MT measurements are indicated by arrows and the location of the Atotsugawa fault is indicated by an solid red triangle. In addition, location of the Ushikubu fault is indicated a open red triangle.

Fig. 8 The calculated apparent resistivities(a) and the phases(b) from the modelin Fig. 8(solid lines) together with the observed ones(circles)

Fig. 9 The sensitivity of the model in Fig. 8

Fig. 10 The two-dimensional suitable resistivity model along the profile BB'. The locations of Yokoyama trust is indicated by an open blue triangle. Futher details is shown in the caption of Fig. 8.

Fig. 11 The calculated apparent resistivities(a) and the phases(b) from the modelin Fig. 11(solid lines) together with the observed ones(circles)

Fig. 12 The sensitivity of the model in Fig. 11

Fig. 13 The seismic P wave velocity structure along the profile AA' in the Atotsugwa

region by Shimada(1997, pers. comm.). The locations of the site of our MT measurements are also indicated by arrows and the location of the Atotsugawa fault is indicated by an triangle.

Fig. 14 The seismic P wave velocity structure along the profile BB' in the Atotsugwa region. See Fig. 14 in detail.

Fig. 15 The distribution of the hypocenters of the micro-earthquakes beneath the profile AA' projected to the resistivity model shown in Fig. 8

Fig. 16 The distribution of the hypocenters of the micro-earthquakes beneath the profile BB' projected to the resistivity model shown in Fig. 11

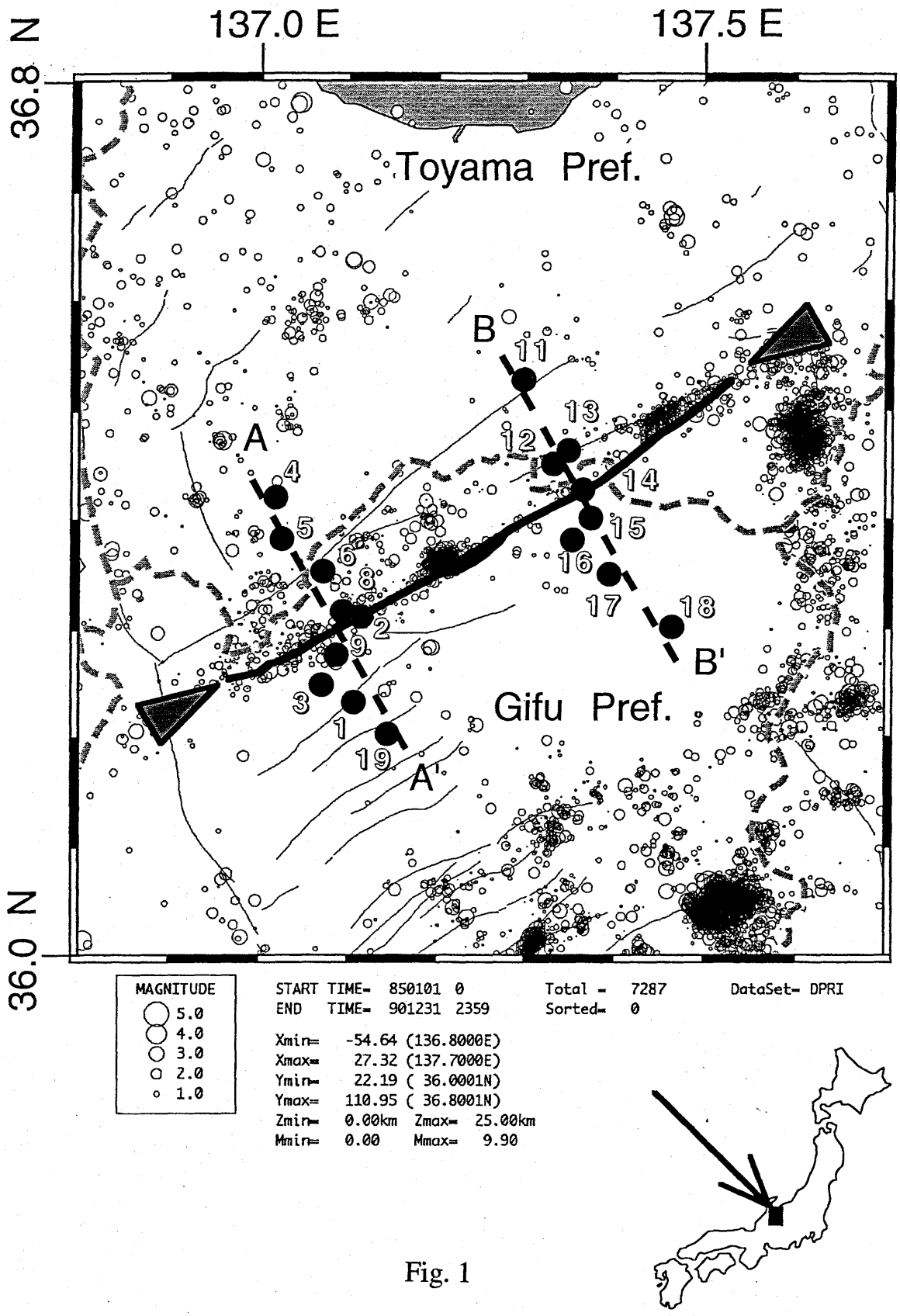
137.0 E
137.5 E
36.8 N
36.0 N
Toyama Pref.
Gifu Pref.
A
A'
B
B'
1
2
3
4
5
6
8
9
11
12
13
14
15
16
17
18
19
MAGNITUDE
5.0
4.0
3.0
2.0
1.0
START TIME= 850101 0
END TIME= 901231 2359
Total = 7287
Sorted= 0
DataSet= DPRI
Xmin= -54.64 (136.8000E)
Xmax= 27.32 (137.7000E)
Ymin= 22.19 (36.0001N)
Ymax= 110.95 (36.8001N)
Zmin= 0.00km Zmax= 25.00km
Mmin= 0.00 Mmax= 9.90

Fig. 1

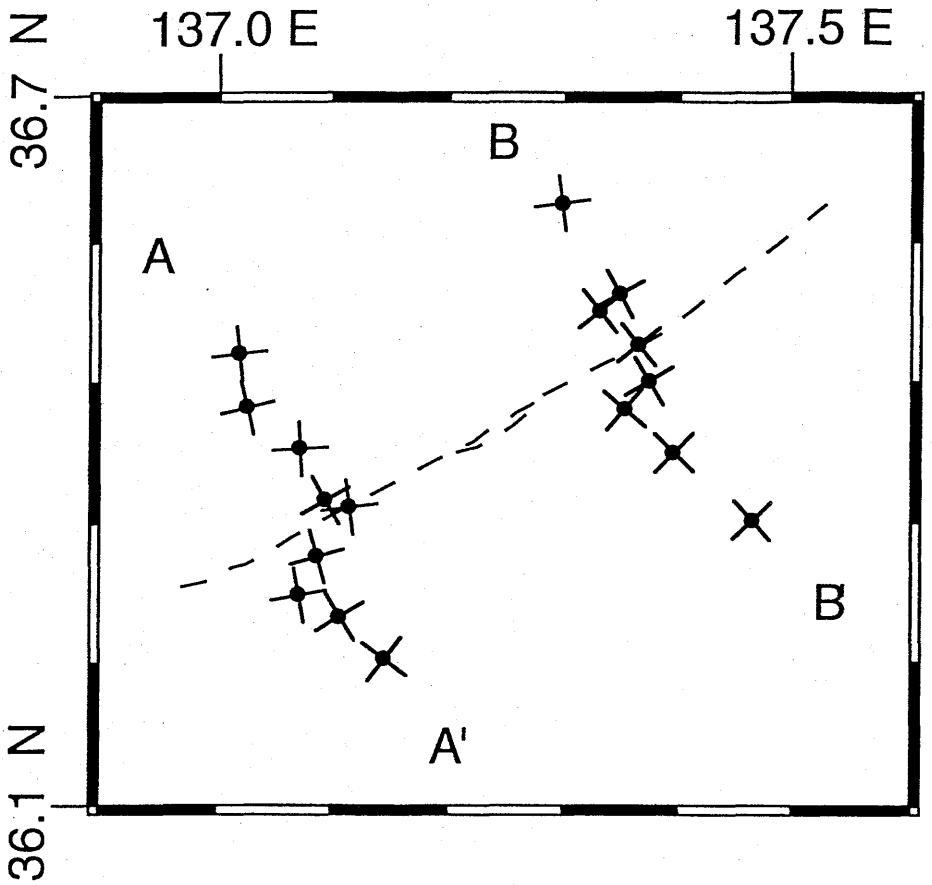

Fig. 2

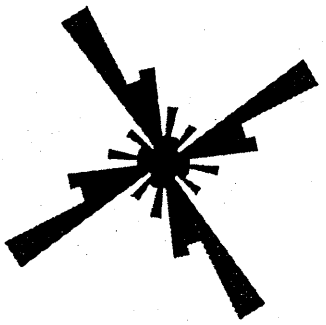

100 - 10 Hz

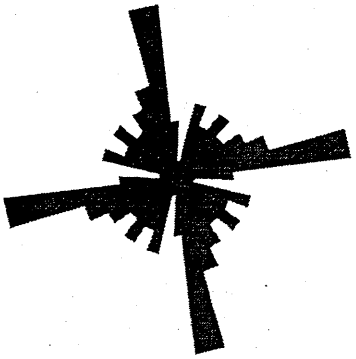

0.1 - 0.01 Hz

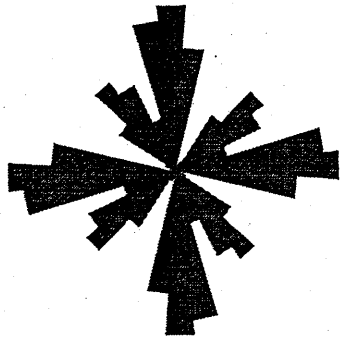

10 - 1 Hz

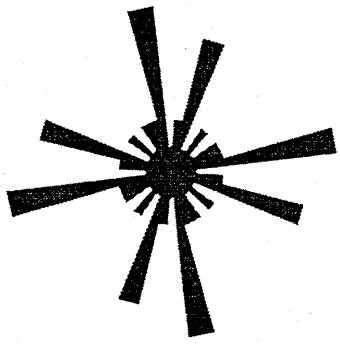

0.01 - 0.0005 Hz

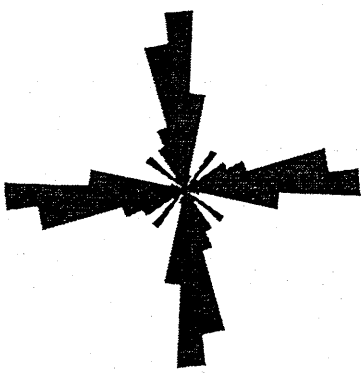

1 - 0.1 Hz

Profile AA'

Fig. 3(a)

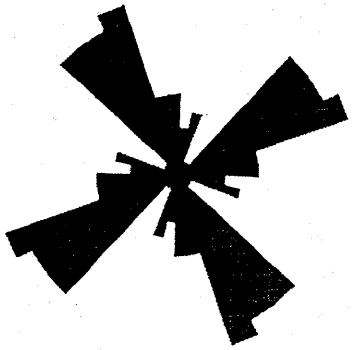

100 - 10 Hz

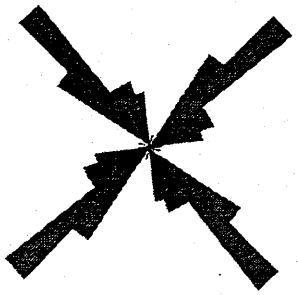

0.1 - 0.01 Hz

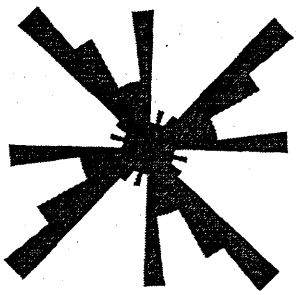

10 - 1 Hz

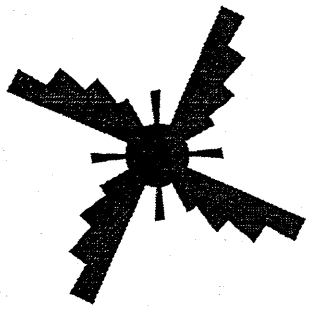

0.01 - 0.0005 Hz

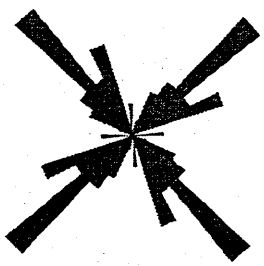

1 - 0.1 Hz

Profile BB'

Fig. 3(b)

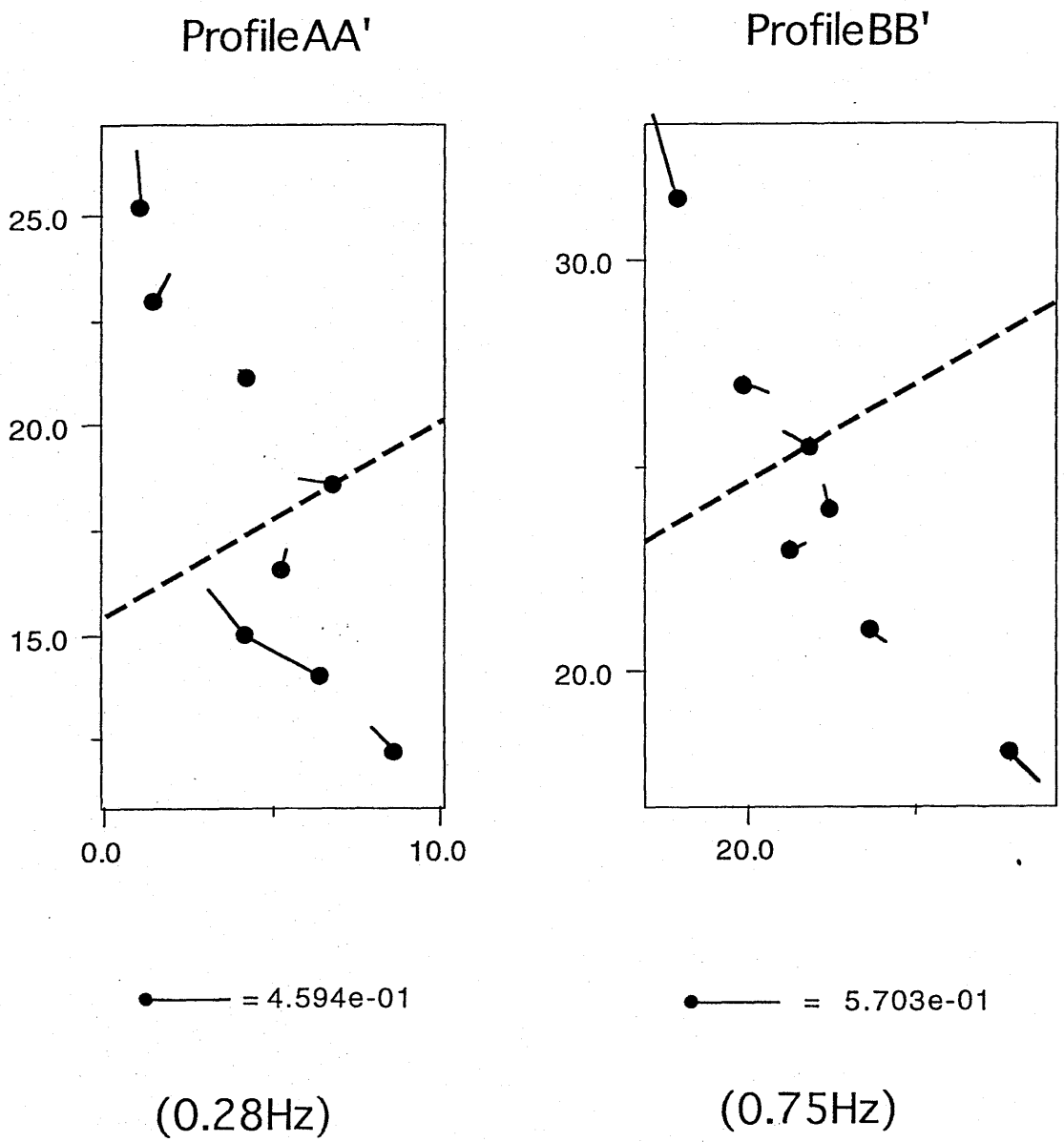
ProfileAA'
25.0
20.0
15.0
0.0
10.0
= 4.594e-01
(0.28Hz)
ProfileBB'
30.0
20.0
20.0
= 5.703e-01
(0.75Hz)

Fig. 4

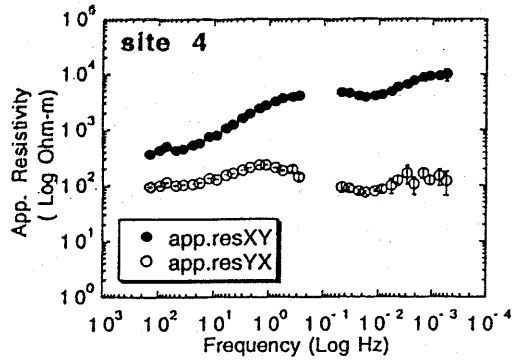
site 4
app.resXY
app.resYX
App. Resistivity (Log Ohm-m)
Frequency (Log Hz)

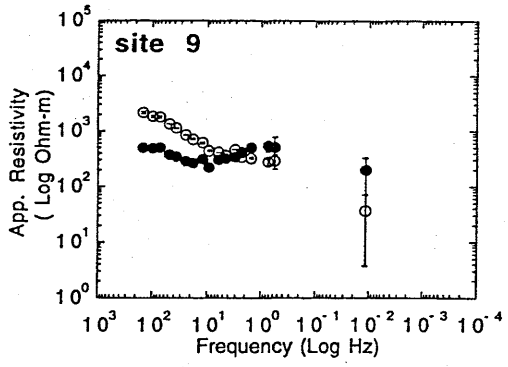
site 9
App. Resistivity (Log Ohm-m)
Frequency (Log Hz)

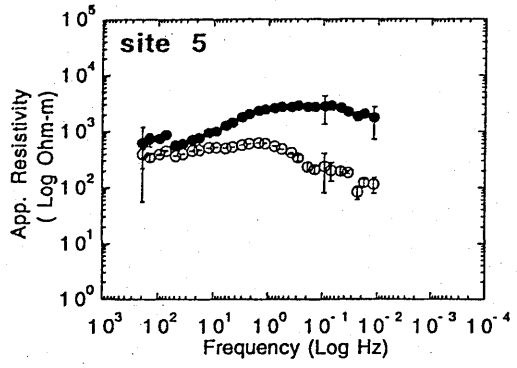
site 5
App. Resistivity (Log Ohm-m)
Frequency (Log Hz)

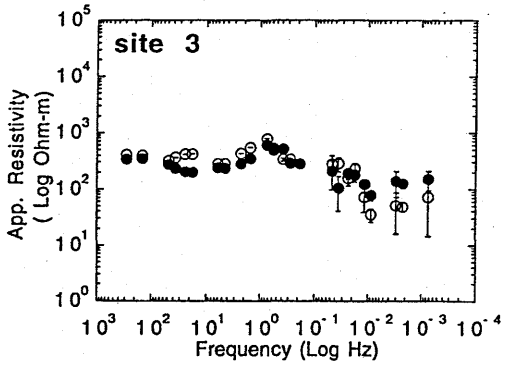
site 3
App. Resistivity (Log Ohm-m)
Frequency (Log Hz)

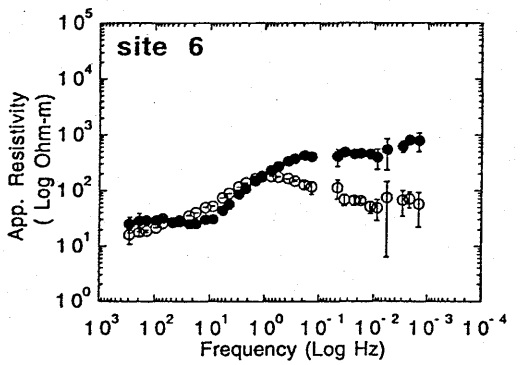
site 6
App. Resistivity (Log Ohm-m)
Frequency (Log Hz)

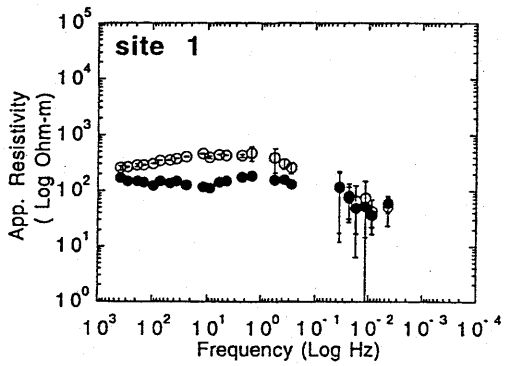
site 1
App. Resistivity (Log Ohm-m)
Frequency (Log Hz)

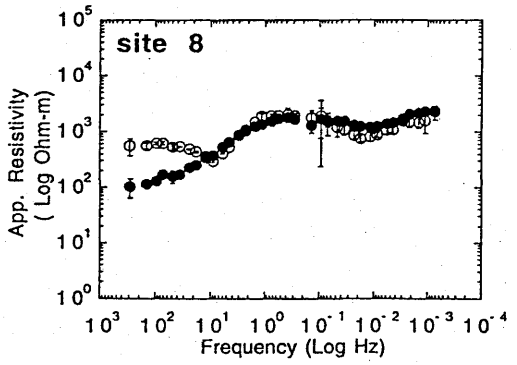
site 8
App. Resistivity (Log Ohm-m)
Frequency (Log Hz)

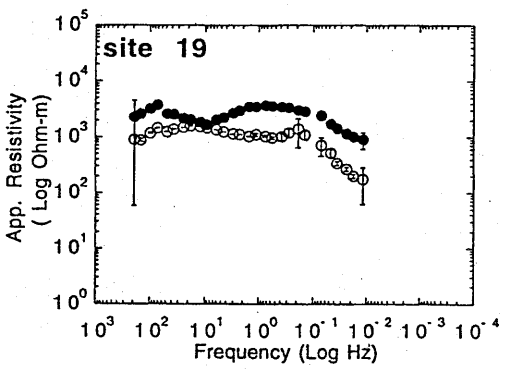
site 19
App. Resistivity (Log Ohm-m)
Frequency (Log Hz)

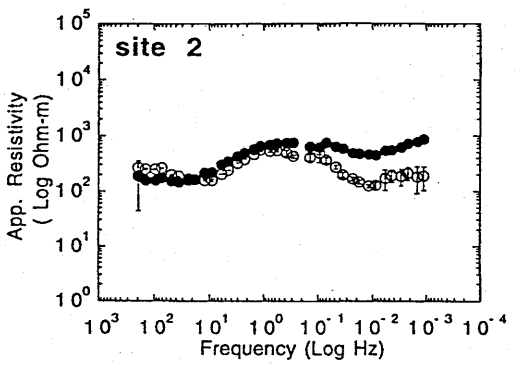
site 2
App. Resistivity (Log Ohm-m)
Frequency (Log Hz)

Fig. 5(a)

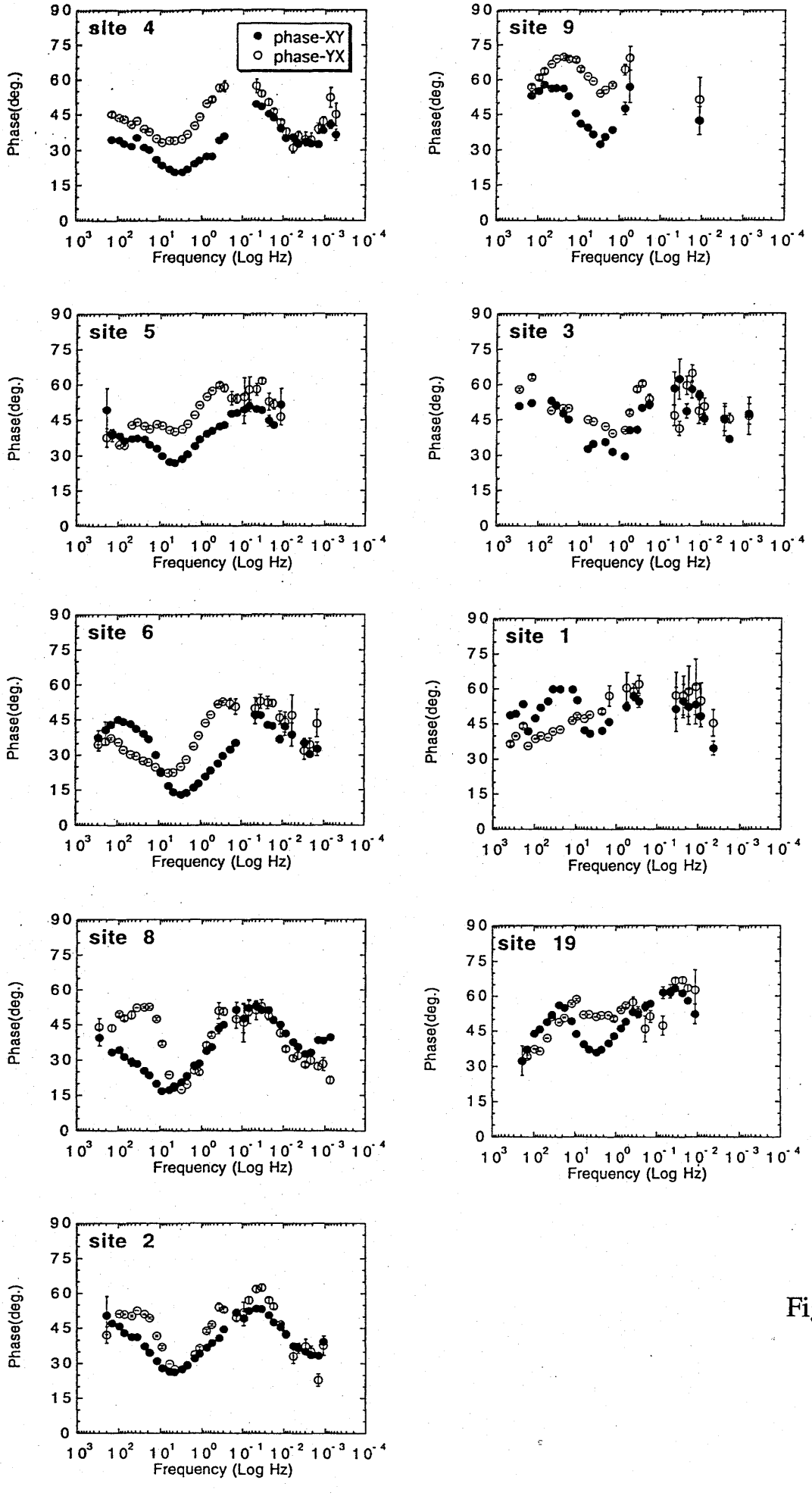
site 4
phase-XY
phase-YX
site 9
site 5
site 3
site 6
site 1
site 8
site 19
site 2
Phase(deg.)
Frequency (Log Hz)

Fig. 5(b)

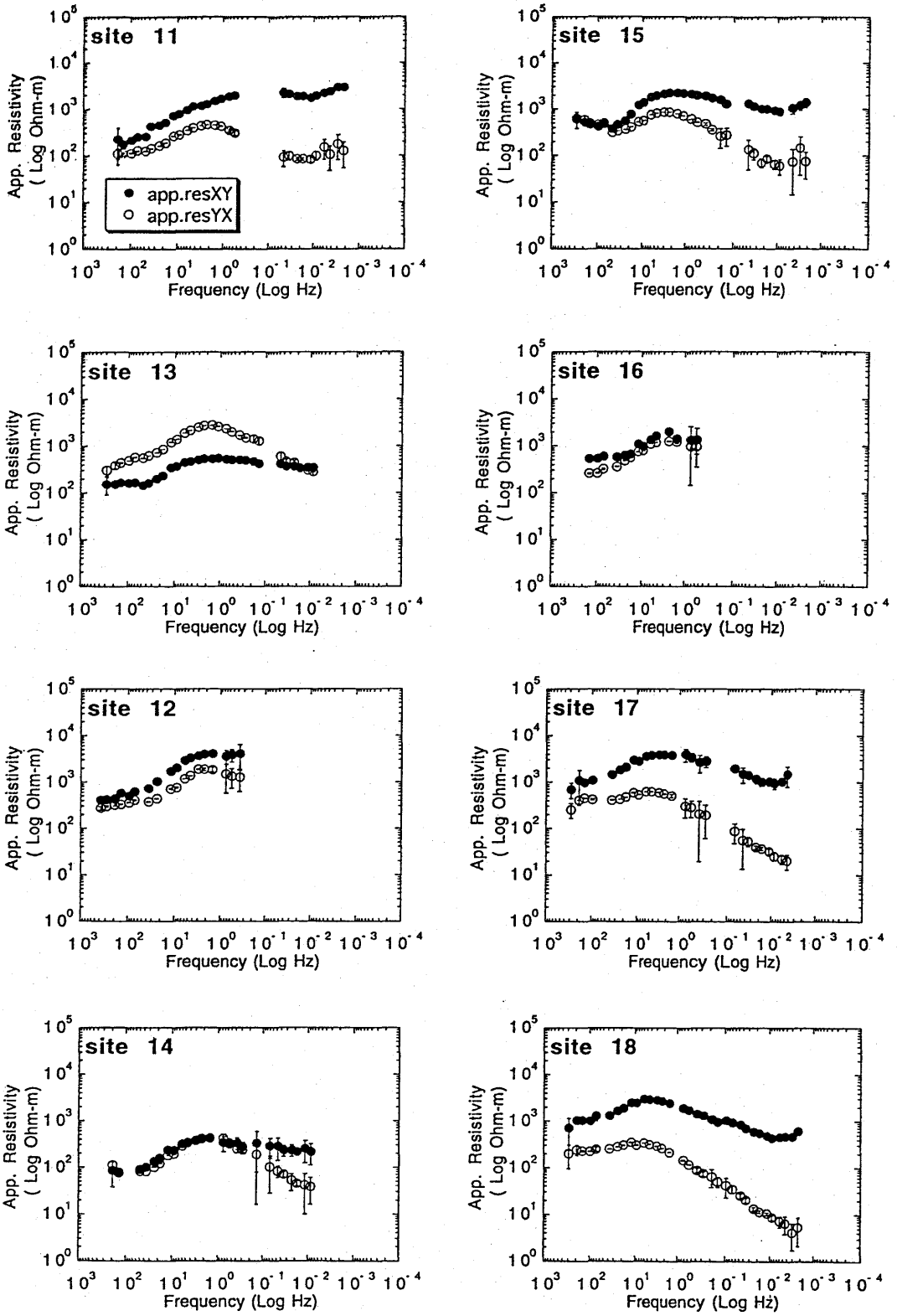
site 11
app.resXY
app.resYX
site 15
site 13
site 16
site 12
site 17
site 14
site 18
App. Resistivity (Log Ohm-m)
Frequency (Log Hz)

Fig.6(a)

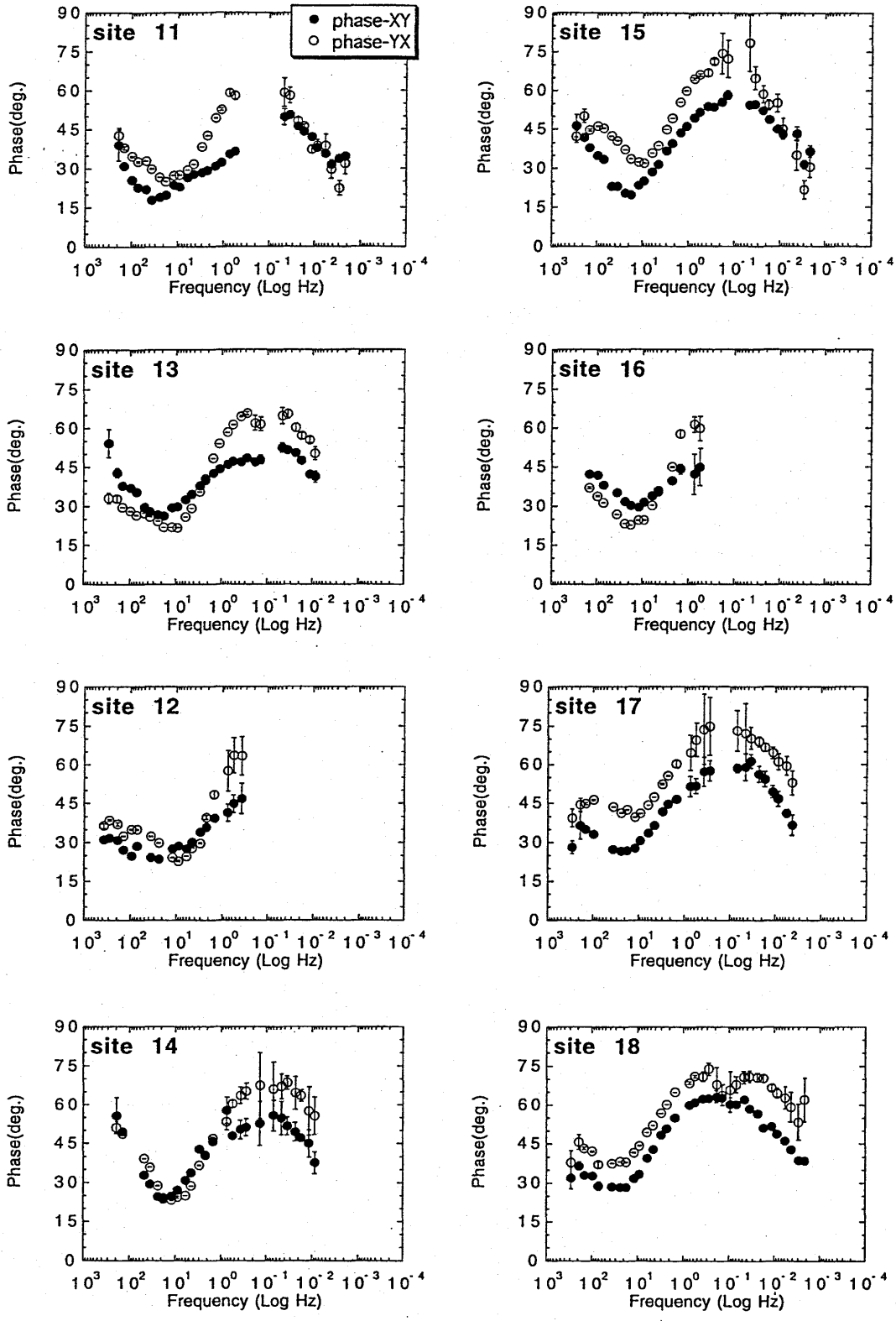
site 11
phase-XY
phase-YX
site 15
site 13
site 16
site 12
site 17
site 14
site 18
Phase(deg.)
Frequency (Log Hz)

Fig.6(b)

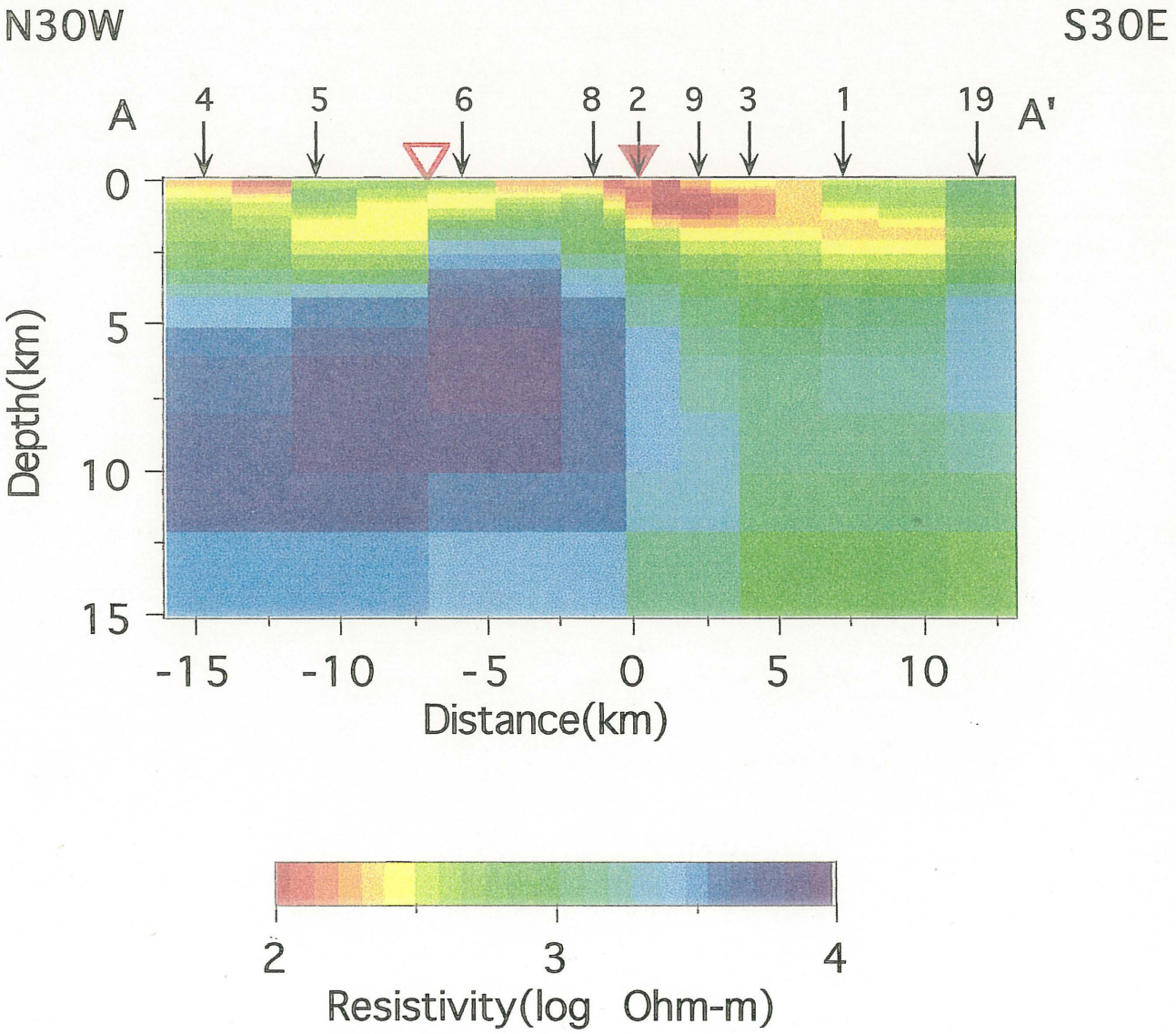
N30W
S30E
A
A'
4
5
6
8
2
9
3
1
19
0
5
10
15
Depth(km)
-15
-10
-5
0
5
10
Distance(km)
2
3
4
Resistivity(log Ohm-m)

Fig. 7

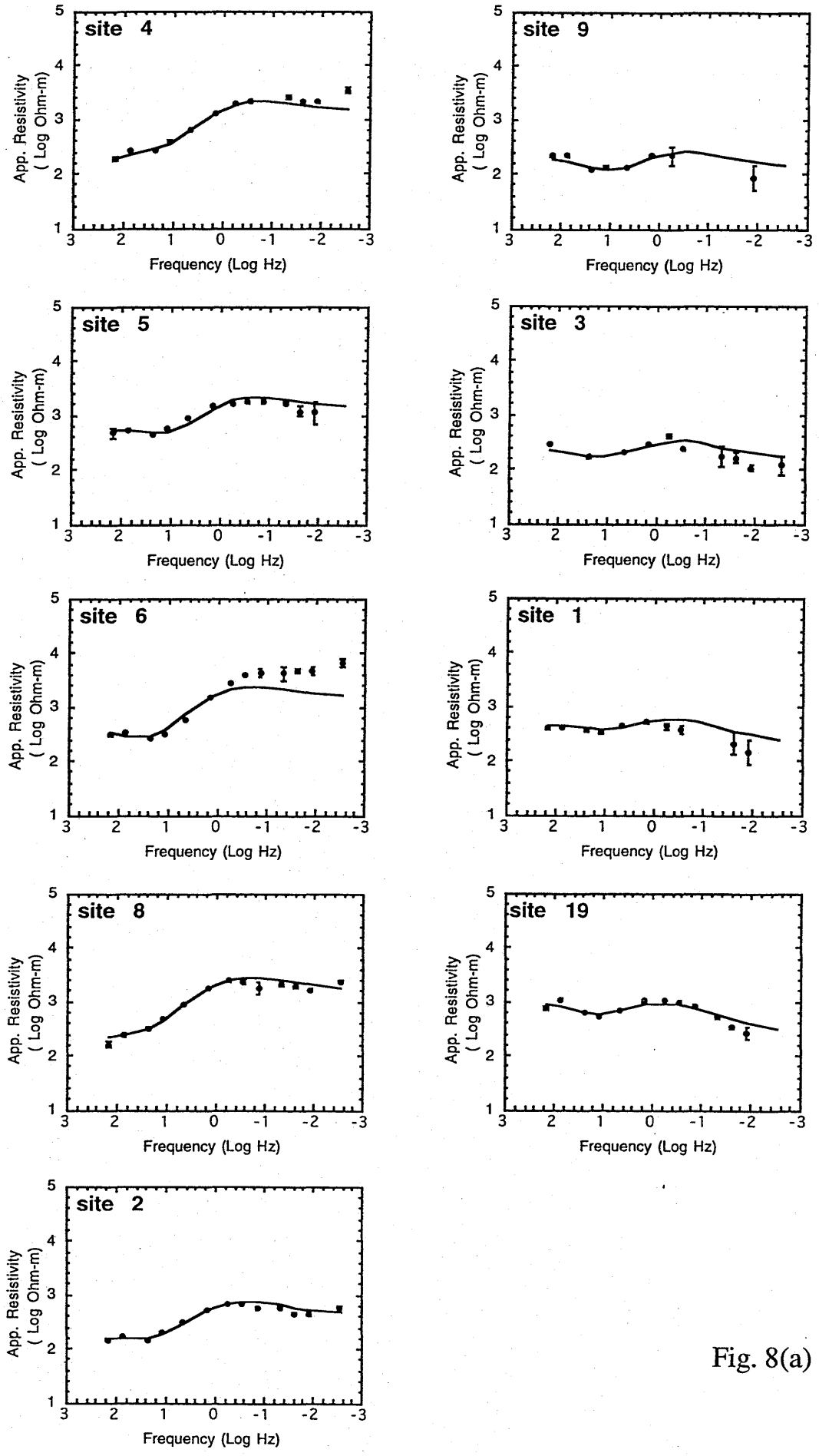
site 4
site 9
site 5
site 3
site 6
site 1
site 8
site 19
site 2
App. Resistivity (Log Ohm-m)
Frequency (Log Hz)
5
4
3
2
1
3
2
1
0
-1
-2
-3

Fig. 8(a)

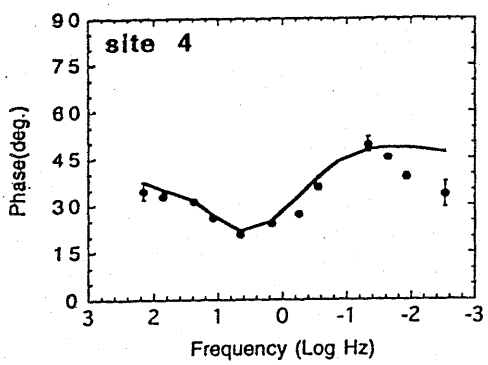
site 4
Phase(deg.)
Frequency (Log Hz)

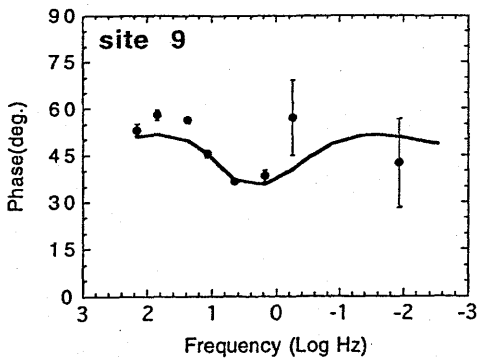
site 9
Phase(deg.)
Frequency (Log Hz)

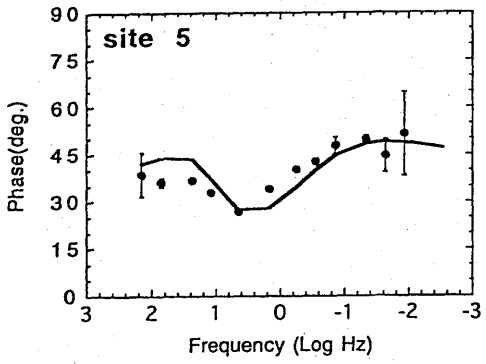
site 5
Phase(deg.)
Frequency (Log Hz)

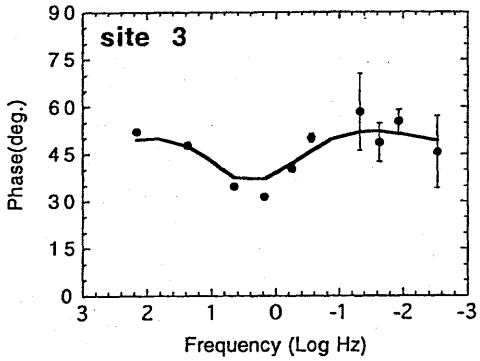
site 3
Phase(deg.)
Frequency (Log Hz)

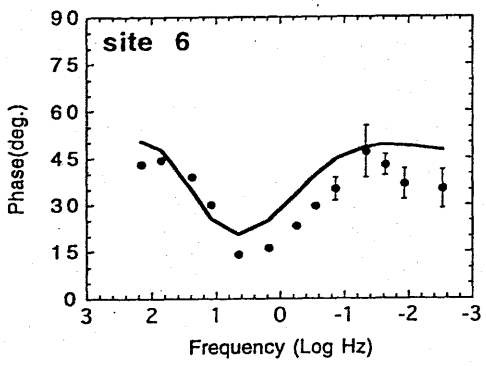
site 6
Phase(deg.)
Frequency (Log Hz)

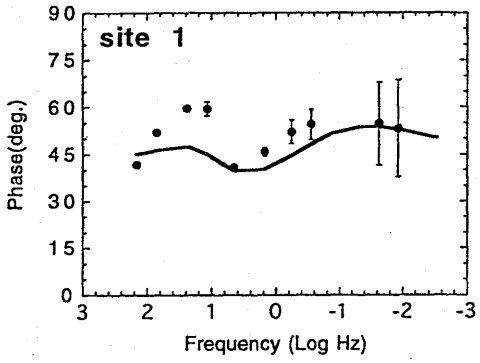
site 1
Phase(deg.)
Frequency (Log Hz)

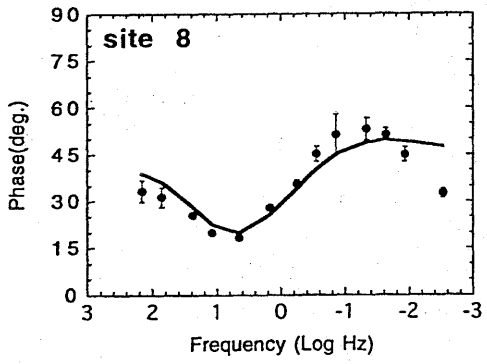
site 8
Phase(deg.)
Frequency (Log Hz)

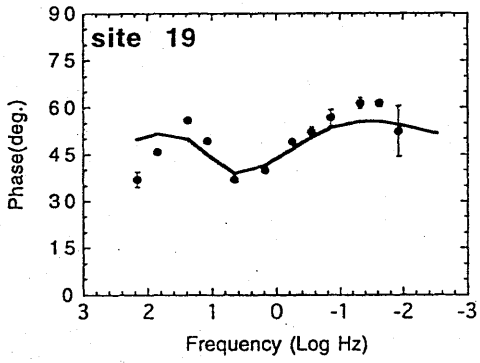
site 19
Phase(deg.)
Frequency (Log Hz)

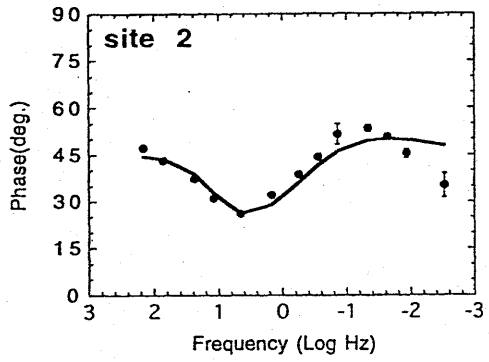
site 2
Phase(deg.)
Frequency (Log Hz)

Fig. 8(b)

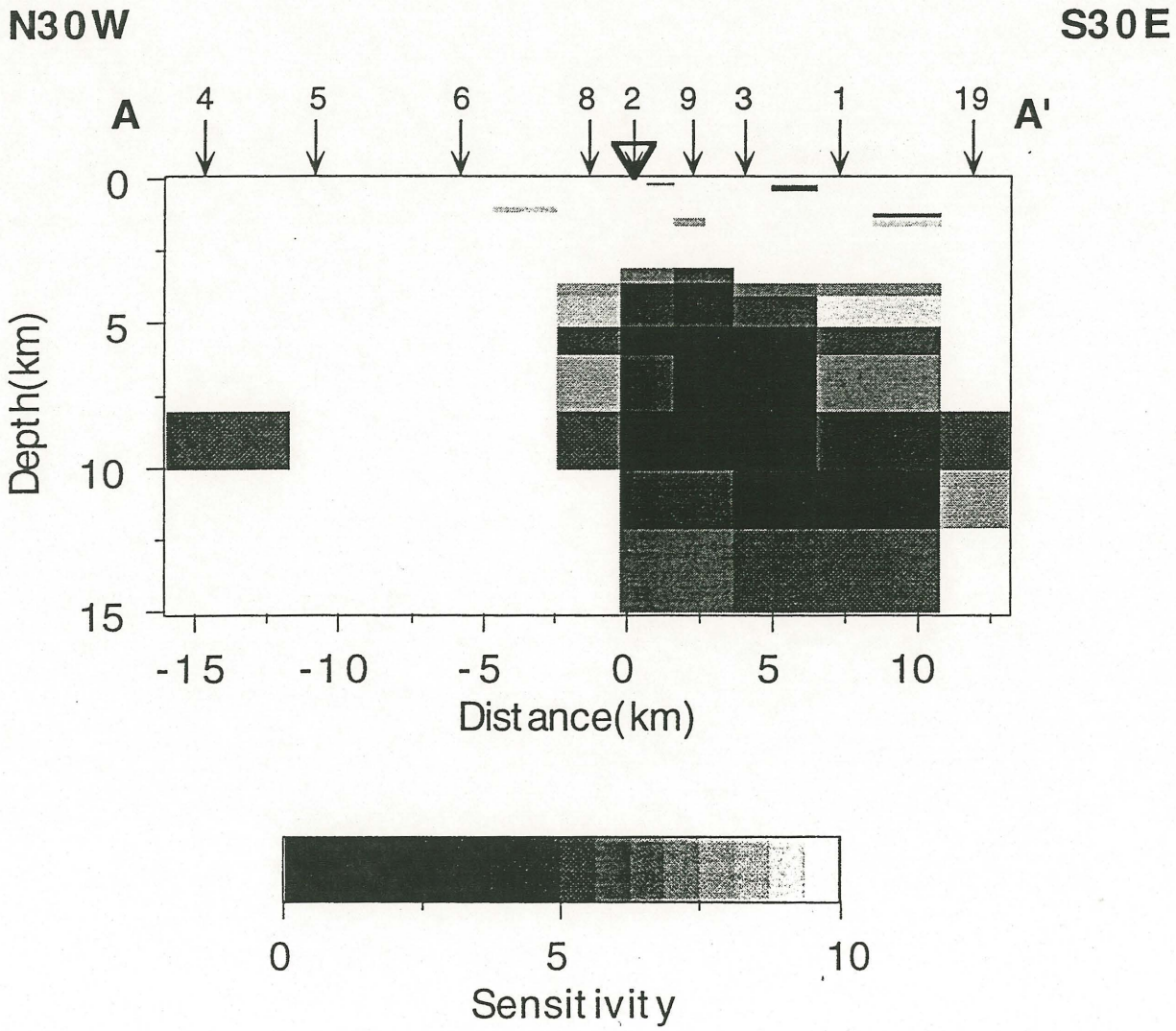
N30W
S30E
A
A'
4
5
6
8
2
9
3
1
19
0
5
10
15
Depth(km)
-15
-10
-5
0
5
10
Distance(km)
0
5
10
Sensitivity

Fig. 9

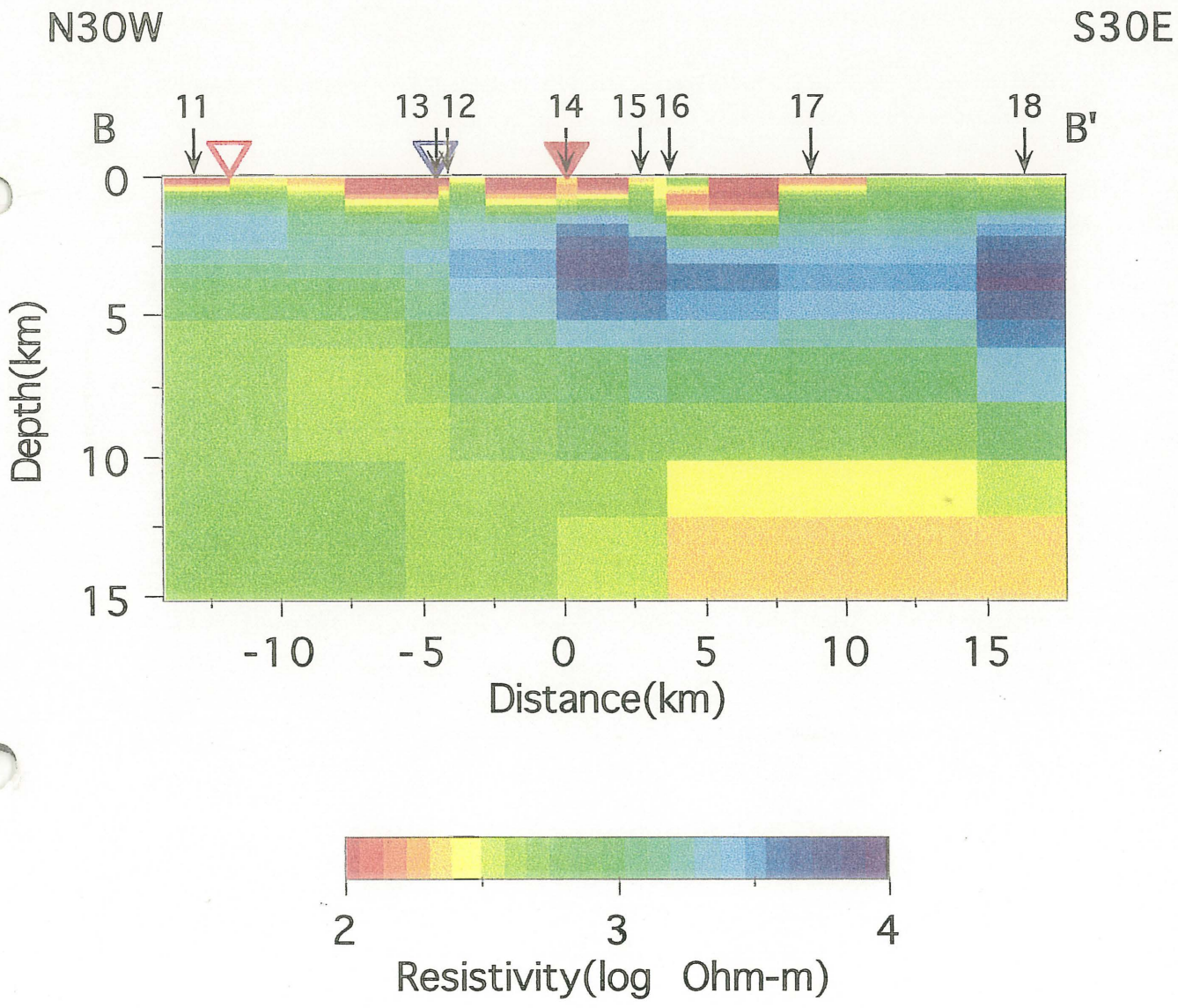
N30W
S30E
B
B'
11
13
12
14
15
16
17
18
0
5
10
15
Depth(km)
-10
-5
0
5
10
15
Distance(km)
2
3
4
Resistivity(log Ohm-m)

Fig. 10

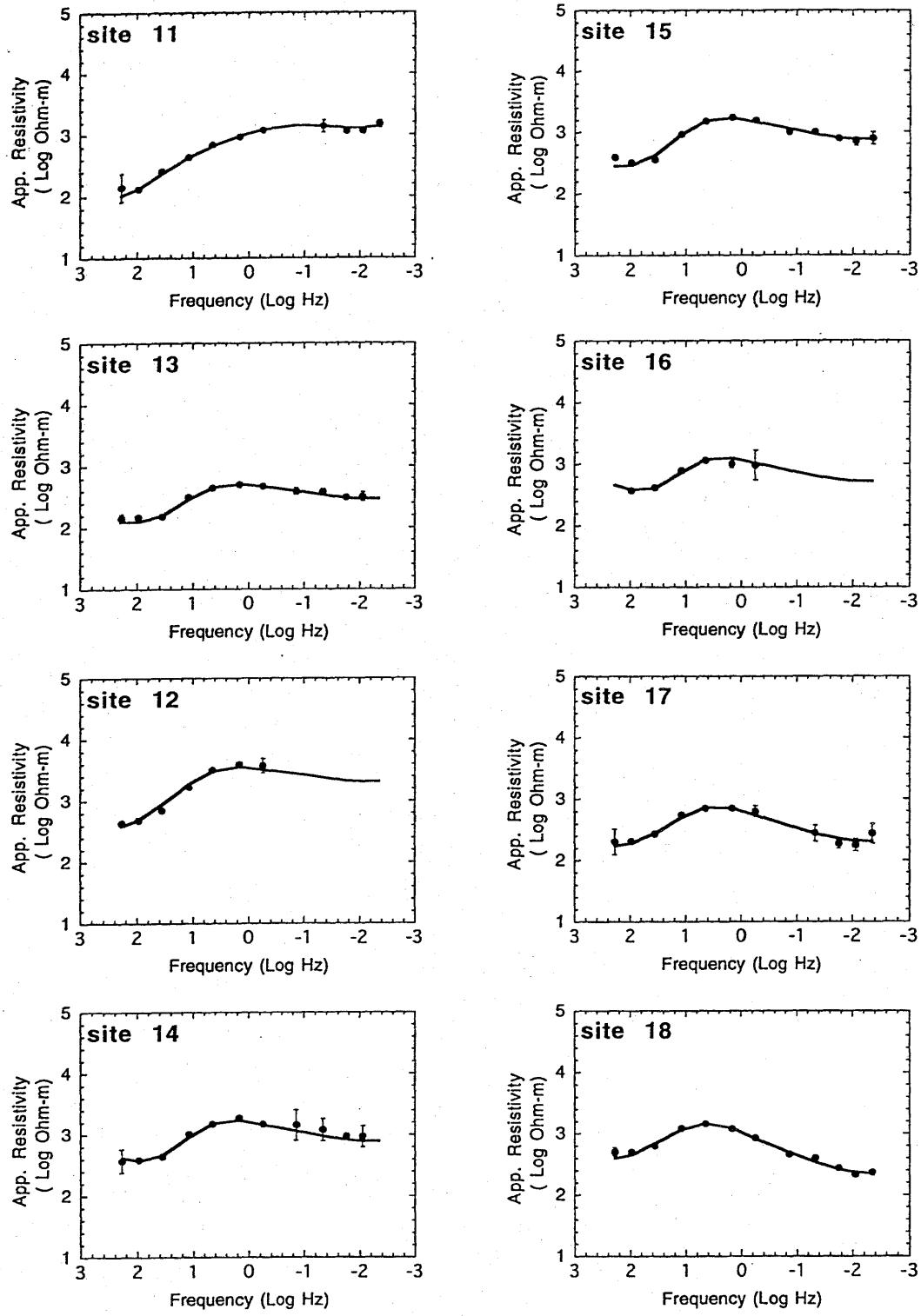
site 11
site 15
site 13
site 16
site 12
site 17
site 14
site 18
App. Resistivity (Log Ohm-m)
Frequency (Log Hz)
5
4
3
2
1
3
2
1
0
-1
-2
-3

Fig. 11(a)

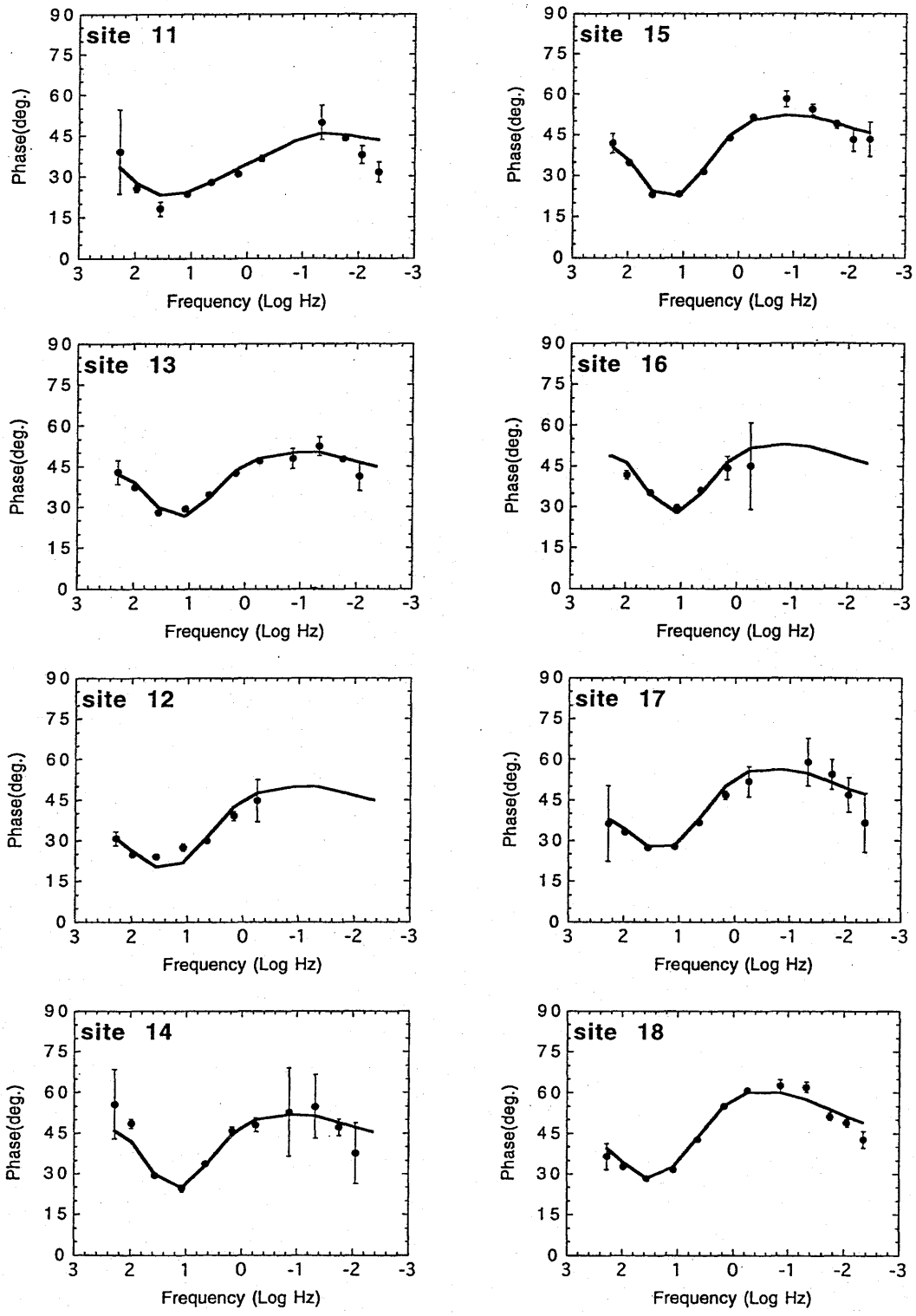
site 11
site 15
site 13
site 16
site 12
site 17
site 14
site 18
Phase(deg.)
Frequency (Log Hz)
90
75
60
45
30
15
0
3
2
1
0
-1
-2
-3

Fig. 11(b)

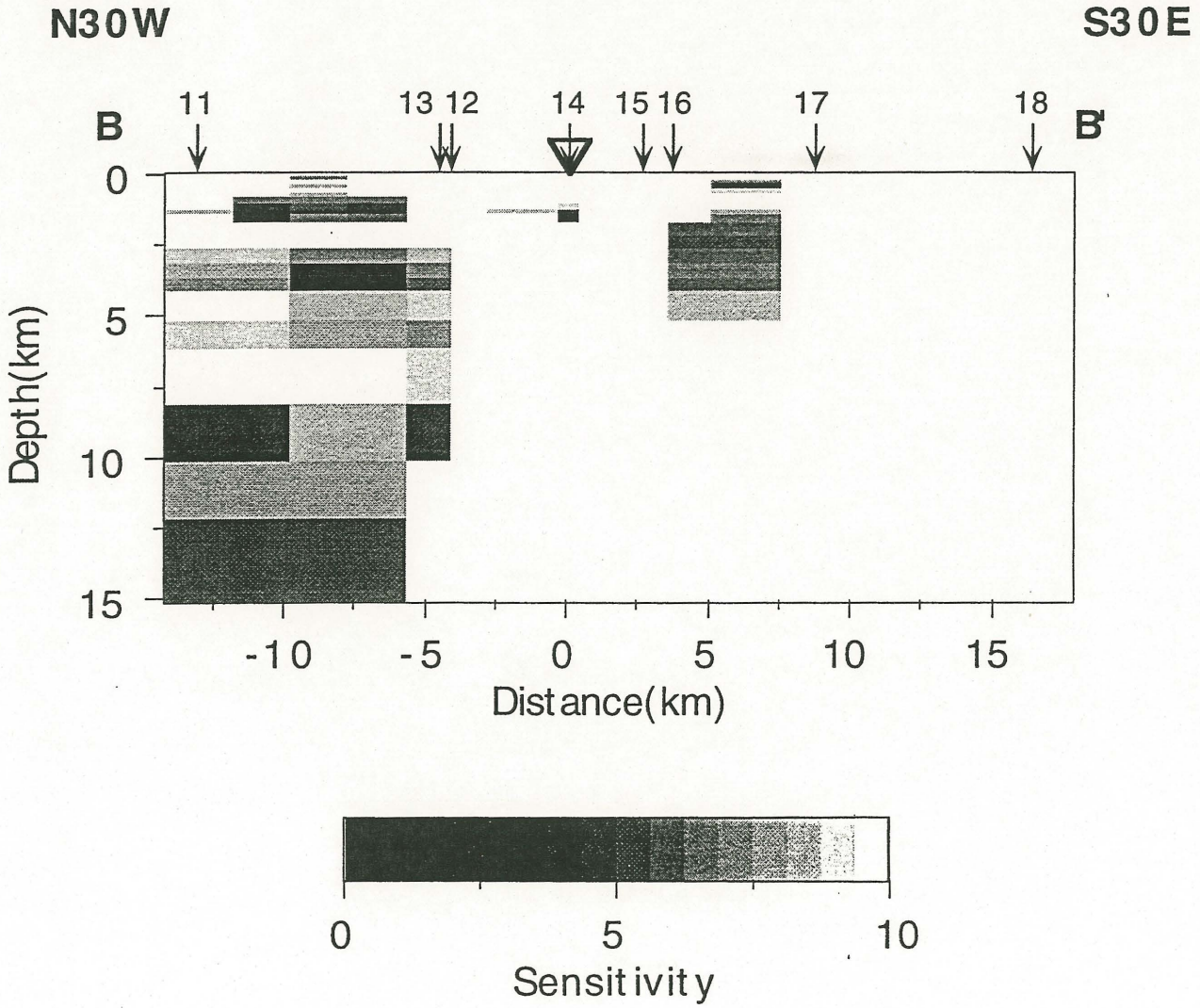
N30W
S30E
B
B'
11
13
12
14
15
16
17
18
0
5
10
15
Depth(km)
-10
-5
0
5
10
15
Distance(km)
0
5
10
Sensitivity

Fig. 12

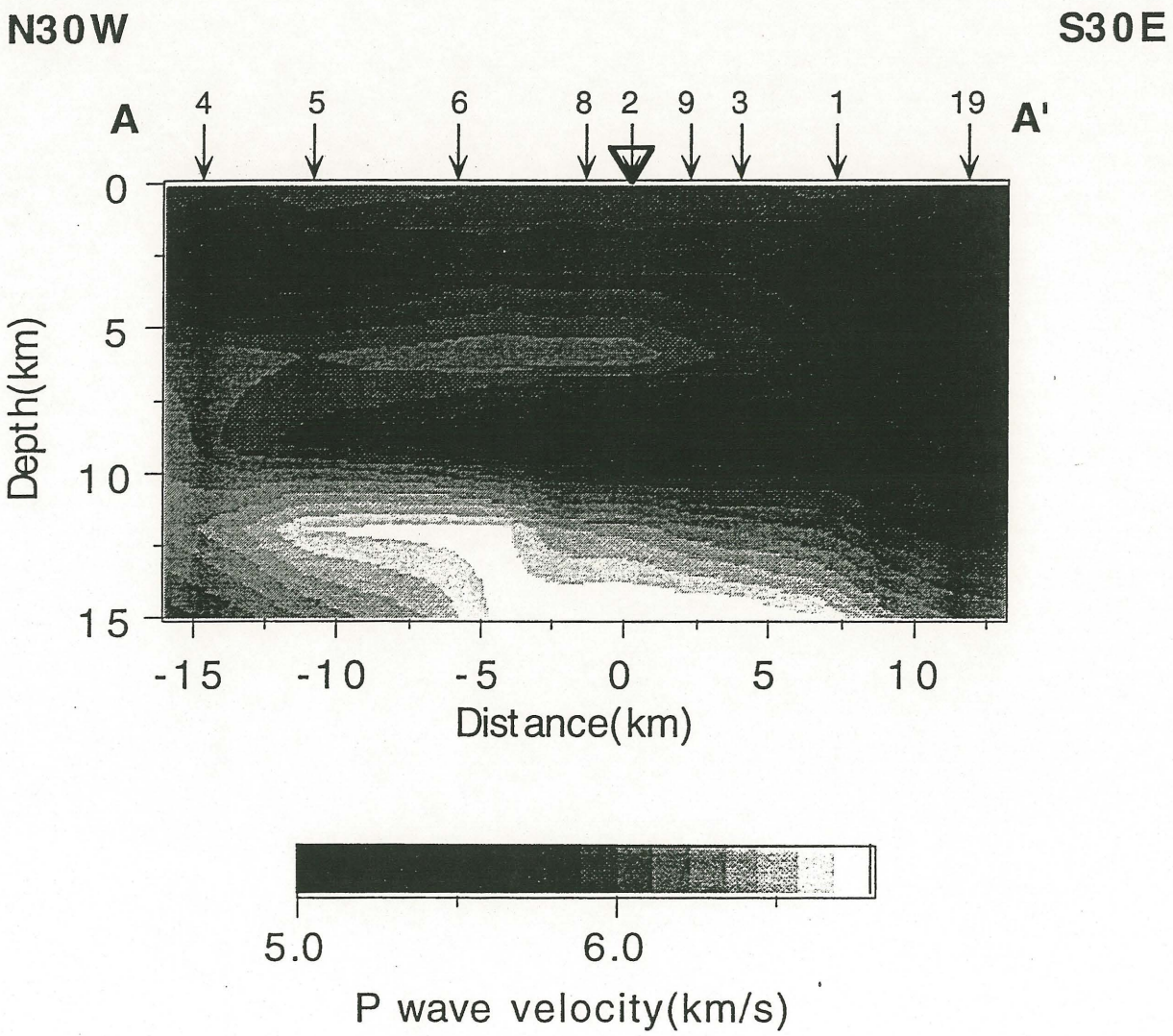
N30W
S30E
A
A'
4
5
6
8
2
9
3
1
19
0
5
10
15
Depth(km)
-15
-10
-5
0
5
10
Distance(km)
5.0
6.0
P wave velocity(km/s)

Fig. 13

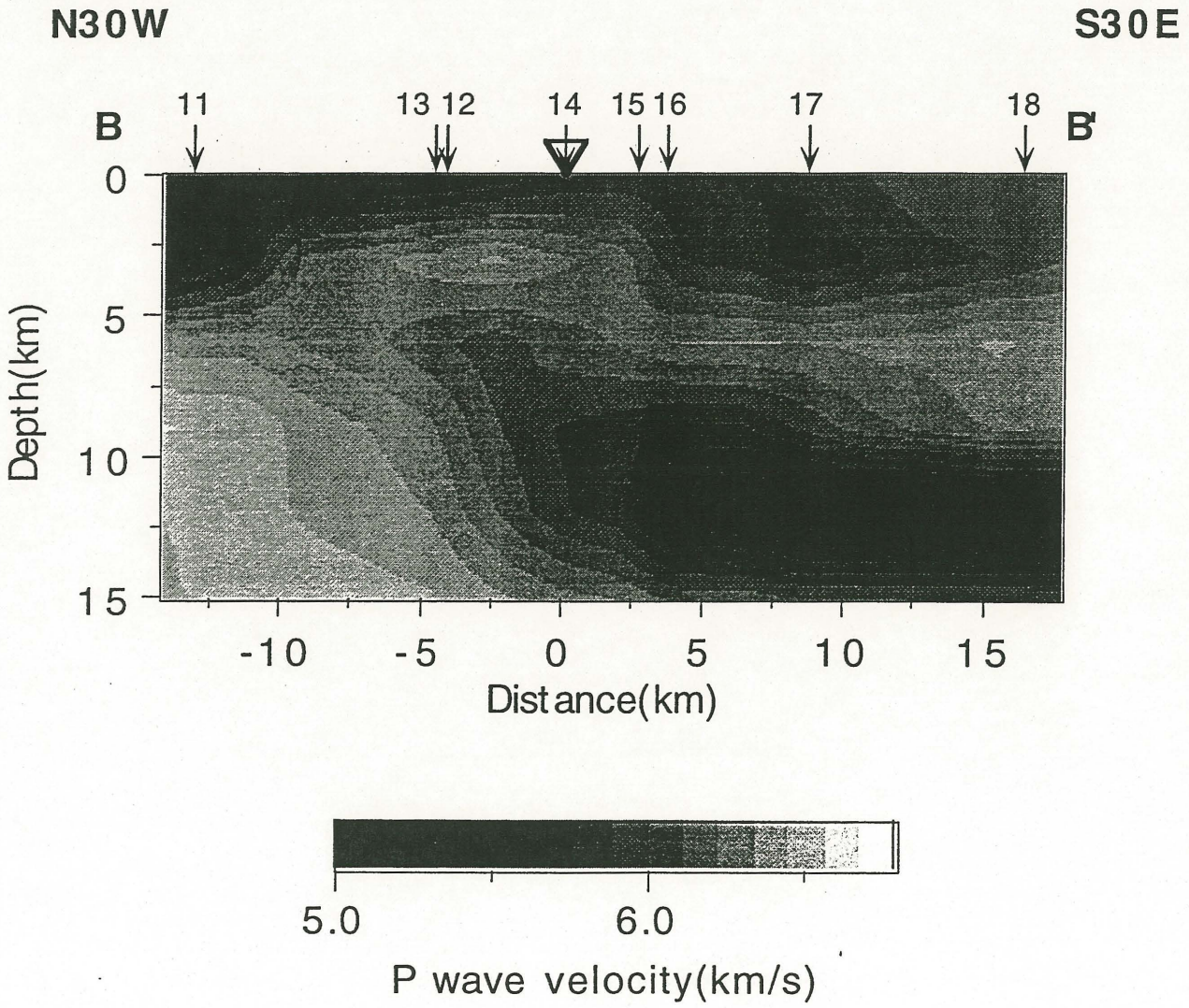
N30W
S30E
B
B'
11
13
12
14
15
16
17
18
0
5
10
15
Depth(km)
-10
-5
0
5
10
15
Distance(km)
5.0
6.0
P wave velocity(km/s)

Fig. 14

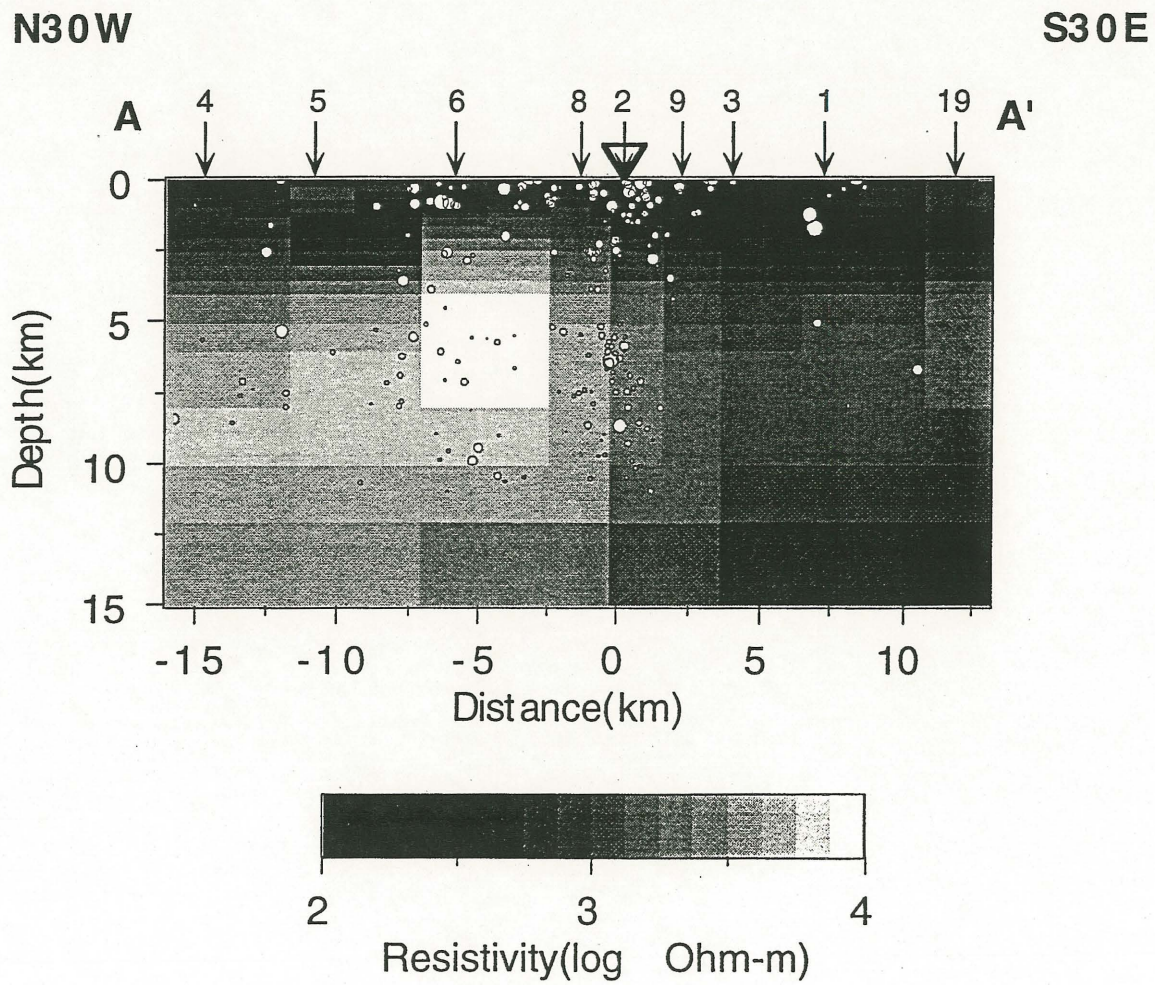
N30W
S30E
A
A'
4
5
6
8
2
9
3
1
19
0
5
10
15
Depth(km)
-15
-10
-5
0
5
10
Distance(km)
2
3
4
Resistivity(log Ohm-m)

Fig. 15

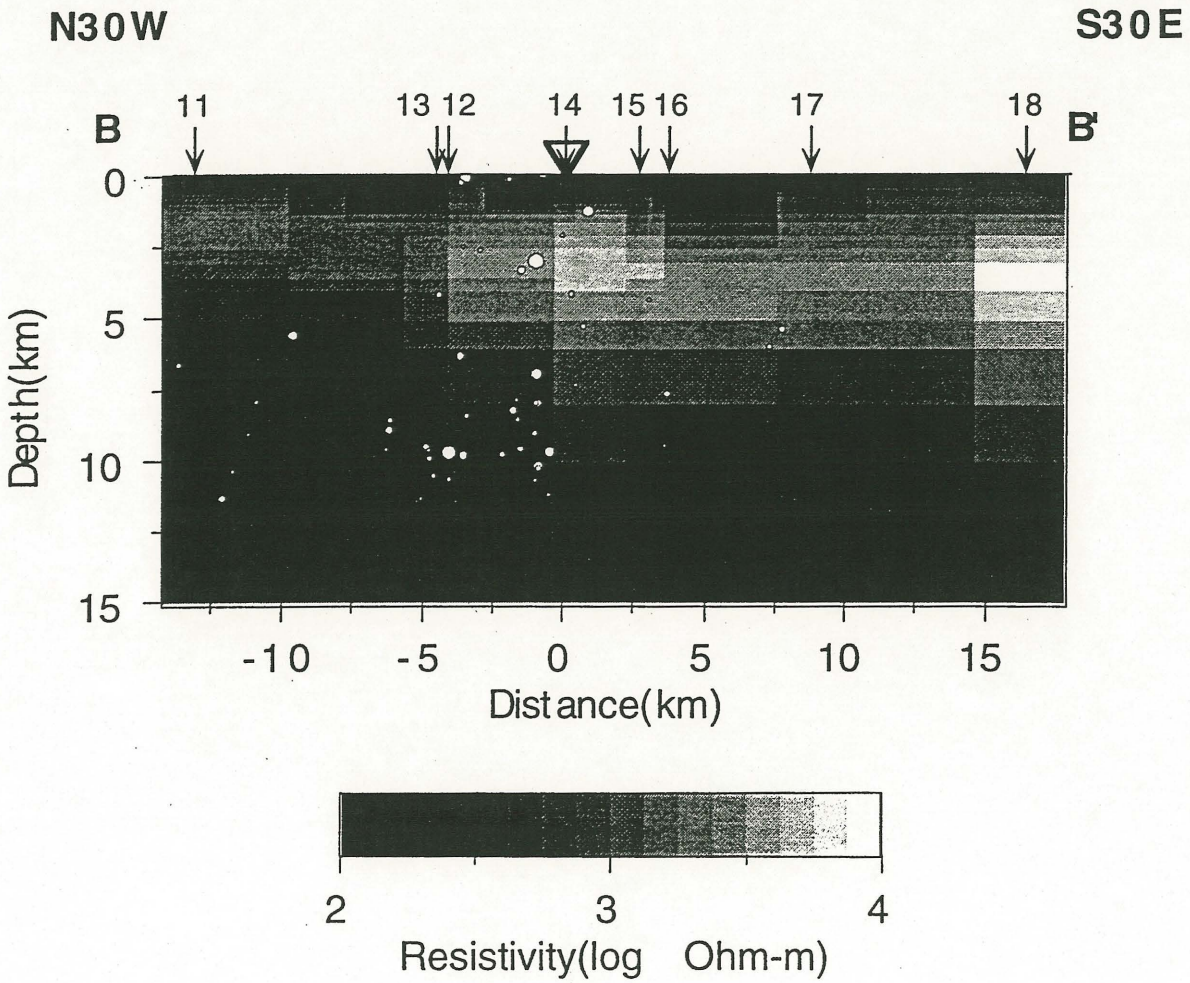
N30W
S30E
B
B'
11
13
12
14
15
16
17
18
0
5
10
15
Depth(km)
-10
-5
0
5
10
15
Distance(km)
2
3
4
Resistivity(log Ohm-m)

Fig. 16

参考論文1

The Electrical Structure across the Median Tectonic Line in East Shikoku, southwest Japan

Tadanori Goto[1], Satoru Yamaguchi[2], Norihiko Sumitomo[1] and Katsumi Yaskawa[3]

[1]Research Center for Earthquake Prediction, Disaster Prevention Research Institute, Kyoto University, Gokasho, Uji, Kyoto 611, Japan.
[2]Department of Earth and Planetary Sciences, Faculty of Science, Kobe University, Nada, Kobe 657, Japan
[3]Osaka College, Hirao, Mihara, Osaka 587, Japan
(Received ; Revised ; Accepted)

Abstract

The Median Tectonic Line (MTL) is one of the longest tectonic lines in Japan with the lateral movement and is deeply concerned with the tectonic evolution of the southwest Japan. In order to investigate the subsurface shape of the MTL and the subsurface structure around the MTL, we carried out the magnetotelluric sounding and the geomagnetic depth sounding across the MTL in the northeastern Shikoku district, southwest Japan. We estimated the resistivity model at the depth from the surface to 10 km which explain the observed apparent resistivities and phases. The most remarkable feature of the resistivity model is the existence of the north dipping boundary of resistivity corresponding with the MTL on the surface. This resistivity boundary also corresponds with a boundary of other geophysical properties. We conclude that the MTL has a north dipping at the depth from the surface to 5 km at least. The north dipping of the MTL may be concerned with the development of the initial MTL as a horizontal shear zone.

1. Introduction

Electrical resistivity soundings around active faults give us important information about their subsurface geometries such as width and depth of fracture zones. The reason is that low resistivity zones so far have been often found along active faults (e.g. Electromagnetic Research Group for the the Active Fault, 1982, 1983; Handa and Sumitomo, 1985; Jones et al.,1992; Ogawa et al., 1994b). Resistivity of a central part of the low resistivity zone is typically smaller than one order of magnitude relative to the surrounding areas due to a lot of water involved in the fracture zones which were formed by fault motions (Handa and Sumitomo ,1985) or / and due to organic carbon or graphite formed by the upwelling of deeply penetrating surface water in the fault zone (Jones et al., 1992).

Besides, investigation of the resistivity structures around the active fault is also important because faults are sometimes localized at geological boundaries and are recognized as sharp resistivity boundaries. One typical example is the resistivity structure around the Hidaka main thrust in the northern part of Japan (Ogawa et al., 1994a), and another example is seen in the San Andreas and the Sargent fault (Eberhart-Phillips et al, 1990). Along these faults, conductive sedimentary rocks possibly comes in contact with a resistive metamorphic or mafic intrusive rocks.

The Median Tectonic Line (MTL) is one of the longest tectonic lines in Japan with a length of about 1000 km (Fig. 1a) and is clearly recognizable by viewing the topography. A simplified geological map of the Shikoku district is shown in Fig. 1b. Two different Cretaceous metamorphic belts are in contact along the MTL; the Ryoke high - T and low - P metamorphic rocks and the Sambagawa high - P and low - T metamorphic rocks (Kimura et al., 1991). It is generally accepted that a large amount of material between the two belts has been removed along the MTL because their contrasting metamorphic conditions show that they could not have formed adjacent to one another.

The investigation of the resistivity structure around the MTL is important to discuss the subsurface geometry of the MTL and the surrounding crustal structure, which is deeply involved with the fault motions of the MTL and the structural developments of southwest Japan. The regional resistivity structure in Shikoku district has been summarized by Shiozaki(1994). However, the target of these previous studies was the investigation of the regional crustal structure in a wide area of Shikoku district so that the resistivity structures obtained do not have enough resolutions to employ in discussion of the subsurface shape of the MTL. The purpose of this study is to investigate the fine resistivity structure around the MTL in order to discuss its subsurface geometry.

The subsurface structure of the MTL has not yet been elucidated and has been vaguely accepted as being subvertical because of the sharpness of the lineament and the large lateral displacements compared with the vertical ones (e.g. Okada, 1980). But recently, some geophysical studies across the MTL (Ohno et al., 1989; Iseki et al., 1990; Kashihara, 1992; Yusa et al., 1992; Yoshikawa et al., 1992; and Ito et al., 1996) have been carried out. The results of the surveys indicate the possibility that the MTL has a gentle north dip angle near the surface. Unfortunately, these geophysical studies were independently carried out and the areas studied did not overlap each other. Therefore, in this study, we have selected a surveying area close to the survey line of a previous seismic reflection study (Ito et al., 1996). We applied the magnetotellutic (MT) method to the area studied, constructed the resistivity structure around the MTL and discuss the subsurface geometry of the MTL while comparing our resistivity structures with other geophysical studies.

2. Observations

We selected northeast Shikoku as the surveying area where Ito et al. (1996) carried out their seismic reflection and gravity surveys. Their survey line, our observed sites and the geological map are shown in Fig. 2. In this area, the MTL has the strike of about N80 ° E. On the northern side of the MTL, the Izumi group is distributed in a long and narrow sedimentary basin and mainly consists of thick turbiditic alternations of sandstone and shale in the Cretaceous (Kimura et al., 1991). To the north of the Izumi group, the Ryoke belt, which mainly consists of granites, is spread. The Sambagawa belt is situated along the southern side of the MTL with a width of about 20 km.

MT soundings were carried out in 1992 across the MTL and its surrounding area (Fig. 2). The following four MT soundings were made in order to cover a wide frequency range: the Very Low Frequency Magneto-Telluric (VLF-MT), the Audio frequency Magneto-Telluric (AMT), the Extremely Low Frequency Magneto-Telluric (ELF-MT) and the Ultra Low Frequency Magneto-Telluric (ULF-MT) soundings. We observed the horizontal magnetic and electric fields at each site, and estimated impedance tensors with the method developed by Vozoff (1972). We also observed the vertical magnetic field at a number of sites at the same time to carry out geomagnetic depth soundings (GDS) at these sites.

The VLF-MT (17.4kHz) soundings were carried out at 33 sites (Fig. 2) to determine the resistivity distribution near the surface. The source of the VLF signal was artificially emitted from about 300 km east of the area studied. The magnetic field at each site was polarized in about the N-S direction, thus obtaining the scalar apparent resistivity and phase difference between magnetic and electric fields.

The AMT soundings were carried out at sites 20, 23, 27 and 31 (Fig. 2). The natural fluctuations of the horizontal magnetic and electric fields were measured at 12 logarithmically equispaced frequencies between 8700Hz and 4.2Hz. We directly calculated the Fourier coefficients of the electric and magnetic fields with the synchronous detectors at each frequency. After that, we selected good data sections based on a criterion of having 0.6 of high multiple coherency (Bendat and Piersol, 1971) between magnetic and electric fields. We then calculated impedance tensors, apparent resistivities and phases. Unfortunately, we were not able to obtain any good sections with high multiple coherency at site 20 because of severe artificial noise.

The ELF-MT soundings were carried out at 20 sites whose locations are shown in Fig. 2. We analyzed four modes of the Schumann resonance phenomena: 7.8, 13.9, 20.4 and 26.6Hz. The MT impedance tensors were calculated only from manually selected time series data to remove the noisy sections.

The ULF-MT soundings, with frequencies ranging from 0.2Hz to 0.01Hz, were carried out at sites 20, 23, 27, 31 and 41 (Fig. 2). We recorded successive time series data of two electric and three magnetic components for about 5 days at each site with a 1Hz sampling rate. In order to obtain the MT parameters precisely, first, we selected time

series data showing high correlation between the magnetic and electric field by eye. Secondly, we divided the selected time series data into subsections with 1024 data points and adopted good subsections selected by a criterion of the high multiple coherency between magnetic and electric fields exceeding 0.6 and low ordinary coherency (Bendat and Piersol, 1971) between two horizontal magnetic fields below 0.4. Finally, the MT impedance tensors were calculated from the good subsections selected above. In these sites, we tried GDS and estimated the induction arrows (Schmucker, 1970) from the same good data sections of the ULF-MT soundings. Unfortunately, sufficient data for the analyses were not obtained at site 31 because of the instrumental accidents by a typhoon.

Most of the impedances finally obtained by the AMT, ELF-MT and ULF-MT soundings showed the high multiple coherencies beyond 0.6 between electric and magnetic fields and the low ordinary coherencies below 0.4 between two horizontal magnetic fields. But about 32% of all the impedances did not pass our criteria as the multiple coherency was higher than 0.6 and the magnetic coherency lower than 0.4. We considered that the tensor impedance with a high magnetic coherence is not stable and the impedance with a low multiple coherence is disturbed by strong artificial noises. We, therefore, did not include such unwanted impedance values in following discussions. Most of the impedances passing the above criteria show low skewness values (Swift, 1967) below 0.4. This low value of skewness supports the resistivity structure beneath the studied area having regionally 1- or 2-dimensional structure. However, about 21% of the passed impedances showed skewness larger than 0.4 and / or indicate unrealistic phase values in two dimensional cases (under 0° or over 90°). We suppose that such MT impedances with large skewness or unrealistic phase were affected locally by 3-dimensional resistivity structures. In this study, we accepted resistivity structure as being approximately 2-dimensional and neglected MT impedances with a skewness larger than 0.4 or an unrealistic phase. As a result, about 61% of the observed impedances were available to elucidate the resistivity structure around the MTL.

3. Results of MT soundings and GDS

The apparent resistivities and the phases obtained from the VLF-MT soundings were plotted against distances from the MTL in Fig. 3. In this study, phase means the phase difference between the electric field and magnetic field. We can see that apparent resistivities have almost similar values and the phases have similar values less than 45° through the measuring line. The average apparent resistivity and phase are $86\,\Omega$m and 38 $^\circ$, respectively.

The results of the ELF-MT soundings are shown in Fig. 4. We show apparent resistivities and phases at 7.8Hz only. The two apparent resistivities indicated in Fig. 4a, ρ xy and ρ yx, were calculated from the two orthogonal components of the electric fields directed toward N10° W and N80° E, respectively. The two phases (ϕ xy and ϕ yx) in

Fig. 4b were also calculated from the same electric fields. The profile of apparent resistivities and phases at other frequencies in the ELF band has similar tendencies to those at 7.8Hz. Two obvious features can be recognized in the phase profiles from Fig. 4b. First, both ϕ xy and ϕ yx were generally larger than 45° in the section between the MTL and a distance of about 8 km north of the MTL. Secondly, on the north side of the MTL, we can see both phase values gradually decreasing with distance from the MTL. Additionally, a gradual increasing of ρ yx to the north along the measuring line is recognizable in Fig. 4a.

Next, we show the curves of apparent resistivity and phase at the frequencies ranging from 17.4kHz to 0.01Hz (100sec) at sites 20, 23, 27, 31 and 41 in Fig. 5. We carried out 3 or 4 kinds of MT soundings as almost every site. Four characteristics are recognizable in Fig. 5. First, the apparent resistivity (ρ yx) at site 41 shows a minimum value of about 10 Ωm at 0.1Hz and increases up to about 100 Ωm as the frequency decreases. Secondly, the ρ yx curve at site 27 shows a minimum value of about 30 Ωm at 0.1Hz and increases up to about 100 Ωm as the frequency decreases. It seems that concave patterns of the apparent resistivity (ρ yx) curves around 0.1Hz become vague as the site goes northward. Thirdly, the apparent resistivities (both ρ xy and ρ yx) become large as the frequency decreases in the range lower than 0.1 Hz at all sites. Finally, the splitting of two apparent resistivities (ρ xy and ρ yx) curves is remarkable at frequencies lower than 1Hz at sites 23, 27 and 41.

In order to determine the strike of the resistivity structure around the target area, Swift's principal axes (Swift, 1967) and the induction arrows at each site were determined. Both the induction arrow and the averaged direction of the principal axes in the frequency range from 0.1Hz to 0.03Hz are shown in Fig. 6a, with the rose diagram of the directions of the principal axes at 7.8Hz shown in Fig. 6b. It is considered that the principal axes in this region show N-S or E-W directions and are approximately parallel or perpendicular to the strike of the MTL. The induction arrows as shown in Fig. 6a have almost SSE directions which are also roughly perpendicular to the regional geological strike. The directions of the principal axes and the induction arrows led us to conclude that the resistivity structure around the area is approximately 2-dimensional. The low skewness values (< 0.4) described above supported this approximation. Note that the induction arrows show the largest value at site 23, on the northern side of the MTL, and has the smallest value at site 41 which is on the southern side of the MTL.

According to the results from the MT sounding and the GDS, we are able to summarize the qualitative features about the resistivity structure around the studied area as follows. First, the outermost layer in the area studied is approximately of equal resistivity and is more conductive than the underlying layer on the basis of the profiles of apparent resistivities and low phases at 17.4kHz. The change of resistivity occurs at a depth of some tens of meters judging from the skin depth. Secondly, a conductive layer underlies the northern area of the MTL. The existence of this conductive layer is inferred from high

phase values in the ELF band and low apparent resistivity values around 0.1Hz near the MTL. We also inferred that the top depth of this conductive layer becomes deeper with the increment of the distances from the MTL because, in the ELF band, the phases became lower and the apparent resistivities became larger at the sites situated north over the MTL than at those near the MTL. Moreover, it is possible to say that this conductive zone becomes thinner while going to the north from the MTL because the concave pattern of the apparent resistivity curves around 0.1Hz gradually became vague at sites situated north over the MTL. The approximate top depth of this conductive zone was judged to be about a few or several kilometers from its corresponding skin depth. The directions of the induction arrows also support the existence of this conductive zone, that is, the induction arrows were directed southward at the northern site of the MTL and became smaller at the southern site of the MTL. Finally, we estimated that a deep resistive layer may underlie our target area because of an increase of the apparent resistivities at frequencies lower than 0.1 Hz.

4. Model analyses and their result

We estimated a 2-dimensional (2D) resistivity model around the MTL. We used the apparent resistivities and phases at the frequencies ranging from 17.4kHz to 0.01Hz in constructing the 2D-model. The finite element method described by Rodi (1976), modified by Ogawa (1988), was used for the calculation of the 2D MT responses. The width and depth of the 2D model in this study were assumed to be 1800 km and 900 km, respectively. The 2D model involved 46 horizontal $\times$17 vertical elements, parallelogram in shape to express the topographical relief. Smaller elements were arranged near the surface and the boundaries of resistivity. We took the Pacific Ocean and the Seto Inland Sea (Fig. 1) into consideration in the 2D model. The resistivity of sea water was specified to be 0.25 Ω m. In 2D modeling, it is important to determine the strike of the 2D model. In this study, we adopted the strike of 2D models as N80° E because all of the observed principal axes are approximately parallel or perpendicular to the MTL and induction arrows are also perpendicular to the strike of the MTL and the regional geological structures. We express ρ xy and ϕ xy as the apparent resistivity and the phase of TM mode and ρ yx and ϕ yx as the TE mode, respectively.

We gave several constraints to the 2D resistivity model of the target area. The first constraint is that a resistivity boundary corresponding to the MTL on the surface exists. The second constraint is that another resistivity boundary exists, corresponding to the geological boundary between the Izumi group and the Ryoke belt. As shown below, we changed the dipping angles of these boundaries to find the best-fit model. We also assumed that, in principle, the resistivity is constant within the area sectioned by these resistivity boundaries. The initial resistivities for this 2D model were given from the result of 1D modeling analyses using the Bostick inversion (Bostick, 1977) at sites 23, 27 and 31

as shown in Fig. 7, which were derived from the observed responses at frequencies higher than 1Hz. Considering that the skin depth at the lowest frequency observed may correspond to the depth of the mantle which is highly conductive, we assumed resistivities at the depths from 100 km to 400 km as 50 Ω m and from 400 km to 900 km as 1 Ω m after Utada (1987).

We changed the parameters of the 2D model about sixty times by trial and error, and looked for the best-fit model. The model chosen is shown in Fig. 8. We calculated the response functions from this model and have shown them together with observed values in Figs. 9 and 10. This best-fit model requires a north-dipping resistivity boundary which continues from the surface position of the MTL to the northern interior, with dipping angle of about 30° . The north dipping is well able to explain the observed features such as the phases at 7.8 - 26.6Hz decreasing as distance from the MTL increases, while the apparent resistivities at the same frequencies increase on the north side of the MTL. The best-fit model, in addition, has other features. First, a conductive block (10 Ω m) exists at the depths shallower than about 5 km beneath the southern portion of the target area. This conductive block is necessary to explain the observed low apparent resistivity (ρ yx) around 0.1Hz at site 41, large phases at 7.8 - 26.6Hz and qualitative features as the induction arrow. Secondly, a resistive layer (10k Ω m) underlies this conductive block in order to fit the increase in observed apparent resistivity (ρ xy) at the frequencies lower than 0.1Hz. Thirdly, The top of the resistive layer changes its depths from 5 km to 1 km with the distance from the MTL. This feature is necessary to account for the observed splitting of apparent resistivity curves at sites 27 and 41. However, the splitting of the calculated apparent resistivity curves at site 27 still remain unelucidated. Although local 3D resistivity disturbances may explain such a splitting, we are not able to make such a complex model in this study because of data in sufficient to discuss the fine resistivity structures across the MTL.

In order to confirm the supposition that the resistivity boundary inclines northward, continuing from the surface position of the MTL to the interior, we calculated the responses from simplified 2D models with the various dipping angles of the boundary and compared them with the observed responses at the frequencies between 7.8Hz and 26.6Hz. The 2D models are shown in Fig. 11a in which a flat surface with a dipping resistivity boundary is assumed. The calculated TM phases (ϕ xy) at 7.8Hz and 20.4Hz which are most sensitive to the dipping angle are shown in Fig. 11b and the root mean square (RMS) errors are also shown in Fig. 11c. We found that 30° is the most suitable dipping angle of this boundary for 7.8Hz and 15° for 20.4Hz. Accordingly, we concluded that the north dipping boundary of 15 - 30° instead of being vertical is required for explaining the observed phases and apparent resistivities. Additionally, we changed the dipping angle of the boundary below 5 km depth using the best-fit model and compared the calculated responses from the model with the observed responses at other frequencies. These 2D

models, however, have similar RMS errors because our site and the observed frequency range probably are not sensitive to such changes of the dipping angle. We concluded that the north dipping resistivity boundary continues up to a depth of several kilometers.

We also examined the robustness of the conductive (10 Ω m) zone below the target area by changing its bottom depth and shape. The 2D models used in the following sensitivity test were based on the best-fit model (Fig. 8). First, we calculated the responses from the 2D models with various bottom depths of the conductive zone shown in Fig. 12a and compared them to the observed responses at the frequencies ranging from 17.4kHz to 0.01Hz. We show the RMS errors corresponding to these 2D models in Fig. 12b. We conclude that the conductive zone extends up to about 3 km in depth. Secondly, we similarly tested the robustness of the bottom shapes of the conductive zone with the various bottom shapes shown in Fig. 13a and show their RMS errors in Fig. 13b. We conclude that the bottom of the conductive zone comes close to the surface as it goes southward from the MTL.

5. Discussion

One of the most remarkable feature in our best-fit resistivity model is that the north dipping resistivity boundary, corresponding to the MTL on the surface, exists. According to our model, this boundary can be traced to depths of several kilometers and has the north dipping angle of 15° - 30° . Along the almost same measuring line, Ito et al. (1996) carried out seismic reflection and gravity surveys, the results of which helped us to interpret our resistivity structure. The profile is shown in Fig. 2. Ito showed that north dipping reflectors can be traced almost continuously from the surface position of the MTL to about 5.5 km depth (R1 and R1' in Fig. 14). The dip angle of the reflectors is about 20 ° from the surface to about 900m depth (reflector R1) and another reflector exists with an angle of 40 - 50° , from about 1.5 km depth to about 5.5 km depth (reflector R1'). They also constructed a density distribution model which has a different density boundary continuing from the surface trace of the MTL to the interior. Ito concluded that the north dipping boundary of density agreeable with reflector R1 and R1' is preferable to a vertical boundary. It is noteworthy that the north dipping resistivity boundary in our model, which is derived from EM surveys only, is approximately coincident with the north dipping seismic reflector and the density boundary. On the basis of this coincidence, we supposed that the north dipping material boundary continues from the surface location of the MTL to about 5 km depth and this boundary possibly indicates the subsurface shape of the MTL.

A conductive zone(10 Ω m) underlying in the south of the MTL is possibly related to the Sambagawa belt. A similar conductive zone was recognized in the central part of the Sambagawa belt along another survey line by Shiozaki(1994). What produced such a conductive zone? We suggest that this conductive zone is due to graphite in the Sambagawa metamorphic rocks. Recently, films of solid carbon on grain boundaries such

as graphite have been proposed as one of the important conduction mechanisms in the crust and the upper mantle on the basis of the laboratory measurements (Duba and Shankland, 1982; Duba et al., 1988) and field observations (e.g. Stanley, 1989). In our target area, most Sambagawa rock belongs to the Besshi nappe complex, which mainly consists of graphitic metapelite and greenstones of various types with minor amounts of chert and marbles (Takasu et al., 1994). Metapelite and greenstones which are mostly metamorphosed from mudstone usually include layered graphite along their schistosity (Hashimoto,1987). Our implication is supported by the high resistivity value of the other Sambagawa metamorphic rock with lower content of graphite. In the Ikeda area, about 40 km west from the target area (Fig. 1), the Oboke nappe complex in which Sambagawa metamorphic rock is distributed, is composed of thick psammitic schist formation (Takasu et al., 1994). Psammitic schist, whose origin is mostly sandstone, maintains the original sand-grain texture (Hashimoto, 1987) and likely contains not much layered graphite. Handa et al. (1981) and Shimoizumi et al. (1988) applied the ELF-MT soundings in the Sambagawa belt around the Ikeda area and they showed high apparent resistivity values beyond 1kΩ m at the ELF band which are quite larger than the values obtained on the Sambagawa belt in our target area. The Oboke nappe complex is distributed near their sites and underlies the surrounding area with a low dip-angle (Kenzan Research Group, 1984), and probably exists at a shallow depth underlying their target area. We suppose that the different values of resistivity in the two areas reflect the difference of the content of graphite in the Sambagawa metamorphic rocks, supporting our conjecture that graphite is a major cause of the conductive zone in our model. However other conduction mechanisms such as pore fluids (e.g. Shankland and Ander, 1983) also may be involved in our conductive zone.

A resistive layer of 10kΩm exists beneath the conductive zone of 10Ωm in the south of the MTL. Its depth is greater than 1 - 5 km (See Fig.8). There is no reasonable explanation for the existence of this layer. However, other geophysical studies show that the boundaries exist at a similar depth beneath the Sambagawa belt. Ito observed weak seismic reflectors at 4.5 - 6 km depth beneath the south of the MTL (R2 in Fig. 14). Kimura et al. (1992) indicated that the top depth of the seismic zone beneath the Sambagawa belt is about 3 km deep in east Shikoku. Ohno et al. (1989) and Ohno (pers. comm.) described a density boundary at depths of about 2 km in west and central Shikoku. These reflectors, the gap of the seismicity and the density boundary roughly correspond to the top boundary of the electrically resistive layer. This correspondence suggests the existence of a sharp material boundary at 1 - 5 km depth beneath the Sambagawa belt. In our study, the high resistivity layer may consist of metamorphic rocks with little graphite such as the Oboke nappe complex or mafic intrusive rocks. We can conclude, at least, that the zone at the depth from 5 km to 10 km beneath the target area have less pore fluid or less conductive minerals such as graphite than the overlying layers.

The north dipping structure of the MTL inferred from the present resistivity model is not in harmony with the recent strike-slip fault motions of the MTL (e.g. Okada, 1980; Ichikawa, 1980) and the tectonic stress fields in Shikoku derived from seismicity (Kimura et al., 1992). On the other hand, our result rather supports the geological view that the north dipping MTL may have developed under a compressive stress perpendicular to the strike of the MTL in an early stage. Ohtomo (1993), Yamamoto (1994) and other geologists described that the mylonite zone in the southern margin of the Ryoke belt was originally formed with a flat-lying configuration and they infer the formation of the initial MTL as a horizontal shear zone.

6. Conclusion

We carried out four kinds of MT measurement across the MTL and along the survey line of the seismic reflection study by Ito et al.(1996). The apparent resistivities, impedance phases and other electromagnetic responses were observed at frequencies ranging from about 10 kHz to 100 sec. We constructed the 2-dimensional resistivity structure across the MTL using the observed responses. It is acknowledged that in the most suitable resistivity structure, the north dipping resistivity boundary corresponds with the MTL on the surface and separates the southern conductive zone from the northern resistive one. The north dipping resistivity boundary corresponds to the seismic reflector reported by Ito. We conclude that the north dipping resistivity boundary represents the MTL beneath the surface and that the conductive zone consists of the Sambagawa metamorphic rock. The north dipping MTL is not due to the recent fault motion of the MTL, but it may have been caused by the large horizontal displacement perpendicular to the MTL which occurred in the initial stage of the formation of the MTL. We could not delineate the processes of the development of the MTL in this study. However, extensive EM surveys, that is, a more spatial density, a wider frequency and a longer profile will be required.

7. Acknowledgment

We would like to thank Tanio Ito and Nobuhiro Isezaki in Chiba Univ. for their helpful advice. We had useful discussions with many members of the Faculty of Science, Kobe Univ., especially Yo-ichiro Otofuji, Takao Miyata, Masayuki Hyodo and Hirokazu Maekawa. We thank Yasuo Ogawa of the Geological Survey of Japan for providing the programs for the MT-forward analysis. Special acknowledgment goes to Tohru Mogi of Kyushu Univ. and Masashi Shimoizumi of Kita-Kyushu Polytechnic College for their instrumental assistance in the AMT soundings. Koji Kashihara and Hiroyuki Hotani contributed to the field work. This study was partly supported by the Japanese Ministry of Education, Science and Culture (grant-in-aid 03402017).

References

Bendat J. S. and A. G. Piersol, Random data: Analysis and measurement procedures, Wiley-Interscience, New York, 1971

Bostick, F. X., A simple almost exact method of MT analysis., Workshop on Electrical Methods in Geothermal Exploration, U.S. Geol. Surv., Contract No. 14080001-8-359, 1977

Duba, A. G., E. Huenges, G. Nover and G. Will, Impedance of black shale from Munsterland 1 borehole: an anomalously good conductor?, Geophys. J., 94, 413-419, 1988

Duba, A. G. and T. J. Shankland, Free carbon & electrical conductivity in the earth's mantle, Geophys. Res. Lett., 9, 1271-1274, 1982

Eberhart-Phillips, D., V. F. Labson, W. D., Stanley, A. J. Michael and B. D. Rodriguez, Preliminary velocity and resistivity models of the Loma Prieta earthquake region, Geophys. Res. Lett., 17, 1235-1238, 1990

Electromagnetic Research Group for the Active Fault, Low electrical resistivity along an active fault, the Yamasaki fault, J. Geomag. Geoelectr., 34, 103-127, 1982

Electromagnetic Research Group for the Active Fault, Electrical resistivity structure of the Tanna and the Ukihashi faults, Bull. Earthq. Res. Inst., 58, 265-286, 1983 (Japanese with English abstract)

Handa, S. and N. Sumitomo, The geoelectric structure of the Yamasaki and the Hanaori faults, southwest Japan, J. Geomag. Geoelectr., 37, 93-106, 1985

Handa, S. and O. Tamada, Observation of earth resistivity at Median Tectonic Line - Application of ELF-MT method to northeastern Shikoku district -, Tsukumo Earth Sci.,16, 1-5, 1981 (in Japanese)

Hashimoto, M., Metamorphic rocks in Japan, Iwanami Shoten, Publishers, Japan, 1987 (in Japanese)

Ichikawa, K., Geohistory of the Median Tectonic Line of southwest Japan, Mem. Geol. Soc. Jap., 18, 187-212, 1980

Iseki, S., H. Shima, S. Imamura and J. H. Mims, Middle scale structure exploration by several kinds of electrical exploration - A study of the Median Tectonic Line in Wakayama Prefecture, Program Abstr. Fall. Meet. Soc. Explor. Geophys. Jap., 318-321,1990 (in Japanese)

Ito, T. et al., Geophysical exploration of the subsurface structure of the Median Tectonic Line, East Shikoku, Japan., J. Geol. Soc. Jap., 102, 346-360, 1996 (in Japanese with English abstract)

Jones, A. G., R. D. Kurtz, D. E. Boerner, J. A. Craven, G. W. McNeice, D. I. Gough, J. M. DeLaurier and R. G. Ellis, Electromagnetic constraints on strike-slip fault geometry - The Fraser River fault system, Geology, 20, 561-564, 1992

Kashihara, K., Analyses of the electrical resistivity structure around the MTL in northern Kii peninsula, Japan, by the magnetotelluric sounding method, Master Thesis, Kobe Univ., 1992(in Japanese) **

Kenzan Research Group, Stratigraphy and geologic structure of the Sambagawa metamorphic belt in the Oboke area, central Shikoku, Japan, Earth Sci. (Chikyu Kagaku), 38, 53-63, 1984 (in Japanese with English abstract)

Kimura, S. and K. Okano, A seismological examination of the Median Tectonic Line and its surrounding area in Shikoku, Southwest Japan, Mem. Geol. Soc. Jap., 40, 187-195, 1992 (in Japanese with English abstract)

Kimura, T., I. Hayami and S. Yoshida, Geology of Japan, 287pp, University of Tokyo press, Tokyo, Japan, 1991

Ogawa, Y., FORTRAN program codes for two-dimensional magnetotelluric forward and inverse analyses, Open-file Report. Geol. Surv. Jap., No. 59, 96pp, 1988

Ogawa, Y., Y. Nishida and M. Makino, A collision boundary imaged by magnetotellurics, Hidaka Mountains, central Hokkaido, Japan, J. Geophys. Res., 99, 22373-22388, 1994a

Ogawa, Y., M. Uyeshima, Y. Honkura, H. Utada and S. Koyama, Audio-frequency magnetotelluric imaging of an active strike-slip fault, J. Geomag. Geoelectr., 46, 403-408, 1994b

Ohno, I., K. Takaichi, Y. Endo, R. Goto, A. Takahashi, M. Ishii, S. Okada, Y. Saiki, E. Ohtani and M. Kato, Gravity survey in northwestern Shikoku, Japan, and subsurface structure of the Median Tectonic Line, J. Phys. Earth, 37, 385-400, 1989

Ohtomo, Y., Origin of the Median Tectonic Line, J. Sci. Hiroshima Univ., Ser. C, 9, 611-669, 1993

Okada, A., Quaternary faulting along the Median Tectonic Line of southwest Japan, Mem. Geol. Soc. Jap., 18, 79-108, 1980

Rodi, W. L., A technique for improving the accuracy of finite element solutions for magnetotelluric data, Geophys. J. R. astr. Soc., 44, 483-506, 1976

Schmucker. U., Anomalies of geomagnetic variations in the southern United States, Bull. Scripps Inst. Oceanogr., 13, 165pp, Univ. Calif. Press, Berkeley and Los Angeles, 1970

Shankland, T. J. and M. E. Ander, Electrical conductivity, temperatures, and fluids in the Lower Crust, J. Geophys. Res., 88, 9475-9484, 1983

Shimoizumi, M. and T. Kitamura, Electromagnetic structure around the Median Tectonic Line in central Shikoku, Proc. Conductivity Anomaly Symp., 128-133, 1988 (in Japanese) **

Shiozaki, I., The study of the electrical resistivity structures beneath the Chugoku and Shikoku district, Ph.D. Thesis , Kobe Univ.,1994 (in Japanese)**

Stanley, W. D., Comparison of geoelectrical / tectonic models for suture zones in the western U.S.A and eastern Europe: are black shales a possible source of high conductivities?, Phys. Earth Planet. Inter., 53, 228-238, 1989

Swift, C. M., A magnetotelluric investigation of an electrical conductivity anomaly in the southwestern United States, Ph.D. Thesis, M.I.T., 211pp, 1967

Takasu, A., S. R. Wallis, S. Banno and R. D. Dallmeyer, Evolution of the Sambagawa metamorphic belt, Japan, Lithos, 33, 119-133, 1994

Utada, H., A direct inversion method for two-dimensional modeling in the geomagnetic induction problem, Ph.D. Thesis, Univ. of Tokyo, 409pp, 1987

Vozoff, K., The magnetotelluric method in the Exploration of sedimentary basins, Geophysics, 37, 98-141, 1972

Yamamoto, H., Kinematics of mylonitic rocks along the Median Tectonic Line, Akaishi Range, central Japan, J. Struct. Geol., 16, 61-70, 1994

Yoshikawa, S., Y. Iwasaki, T. Ikawa and H. Yokota, Geological structure of the MTL in west Wakayama by reflection seismic study, Mem. Geol. Soc. Jap., 40, 177-186, 1992 (Japanese with English abstract)

Yusa, Y., K. Takemura, K. Kitaoka, K. Kamiyama, S. Horie, I. Nakagawa, Y. Kobayashi, A. Kubotera, Y. Sudo, T. Ikawa and M. Asada, Subsurface structure of Beppu Bay (Kyushu, Japan) by seismic reflection and gravity survey, Zisin 2nd ser., 45, 199-212, 1992 (in Japanese with English abstract)

** Titles are translated in English by the author T.G.

Figure Captions

Fig. 1. Simplified Geological map in Southwest Japan(a) and Shikoku district(b). MTL means the Median Tectonic Line. TTL and ISTL are the other large tectonic lines, namely, Tanakura Tectonic Line and Itoigawa Shizuoka Tectonic Line, respectively.

Fig. 2. Locations of magnetotelluric stations (triangles, VLF-MT only; circles, VLF and ELF-MT; lozenges, VLF, ELF and ULF-MT; rectangles with station number, VLF, ELF, ULF-MT and AMT) and geological map. The solid and dashed line indicates the location of the MTL. The survey line of the seismic reflection survey (Ito et. al., 1996) are also indicated (dashed-dot line).

Fig. 3. Apparent resistivity and phase at 17.4kHz along the profile.

Fig. 4. Apparent resistivity and phase profiles at 7.8Hz along the profile with 95% random error. Rectangles and circles are calculated from the electric field directed toward N10W and N80E, respectively.

Fig. 5. Apparent resistivity and phase obtained at sites 20, 23, 27, 41 and 31 where the ULF-MT is carried out. Open and Closed circle are calculated from the electric field directed toward N10W and N80E, respectively.

Fig. 6. (a) Mean directions of the Induction arrows (real part, arrows) and the principle axes(gray bars) in the frequency range from 0.1Hz to 0.03Hz. 95% errors of the induction arrows are also indicated at the foot of the arrow. (b) Histogram of the directions of the principal axes at 7.8Hz

Fig. 7. One-dimensional resistivity model obtained by the Bostick inversion.

Fig. 8. The most suitable two-dimensional resistivity model across the MTL. The arrow means the surface location of the MTL, and smaller arrows mean the location of sites.

Fig. 9. Observed apparent resistivities and phases of Both TE and TM mode(circles), and calculated responses(lines) along the profile at 7.8Hz and 20.4Hz.

Fig. 10. Observed apparent resistivities and phases of Both TE(open circles) and TM mode(solid circles), and calculated responses(TE, solid line; TM, dashed line) in

the frequency range from 10kHz to 0.01Hz.

Fig. 11. (a) A simplified resistivity model for testing the sensitivity of the dipping resistivity boundary corresponding to the MTL on the surface. (b) Observed TM phases(circles) and calculated phases(lines) from the resistivity models with various dipping angles. (c) RMS misfits of the apparent resistivity(circles) and the phase(rectangular) against the various dipping angles of the resistivity boundary.

Fig. 12. (a) A resistivity model for testing the sensitivity of the thickness of the conductive zone beneath the southern are of the MTL. (b) RMS misfits of the apparent resistivity(circles) and the phase(rectangular) against the various depths of the bottom of the conductive zone.

Fig. 13. (a) A resistivity model for testing the sensitivity of the shape of the boundary between 10ohm-m zone and 10K ohm-m. the conductive zone beneath the southern are of the MTL. (b) RMS misfits of the apparent resistivity(circles) and the phase(rectangular) against the various shapes of the bottom of the conductive zone.

Fig. 14. The seismic depth section obtained by the seismic reflection survey (Ito et al., 1996).

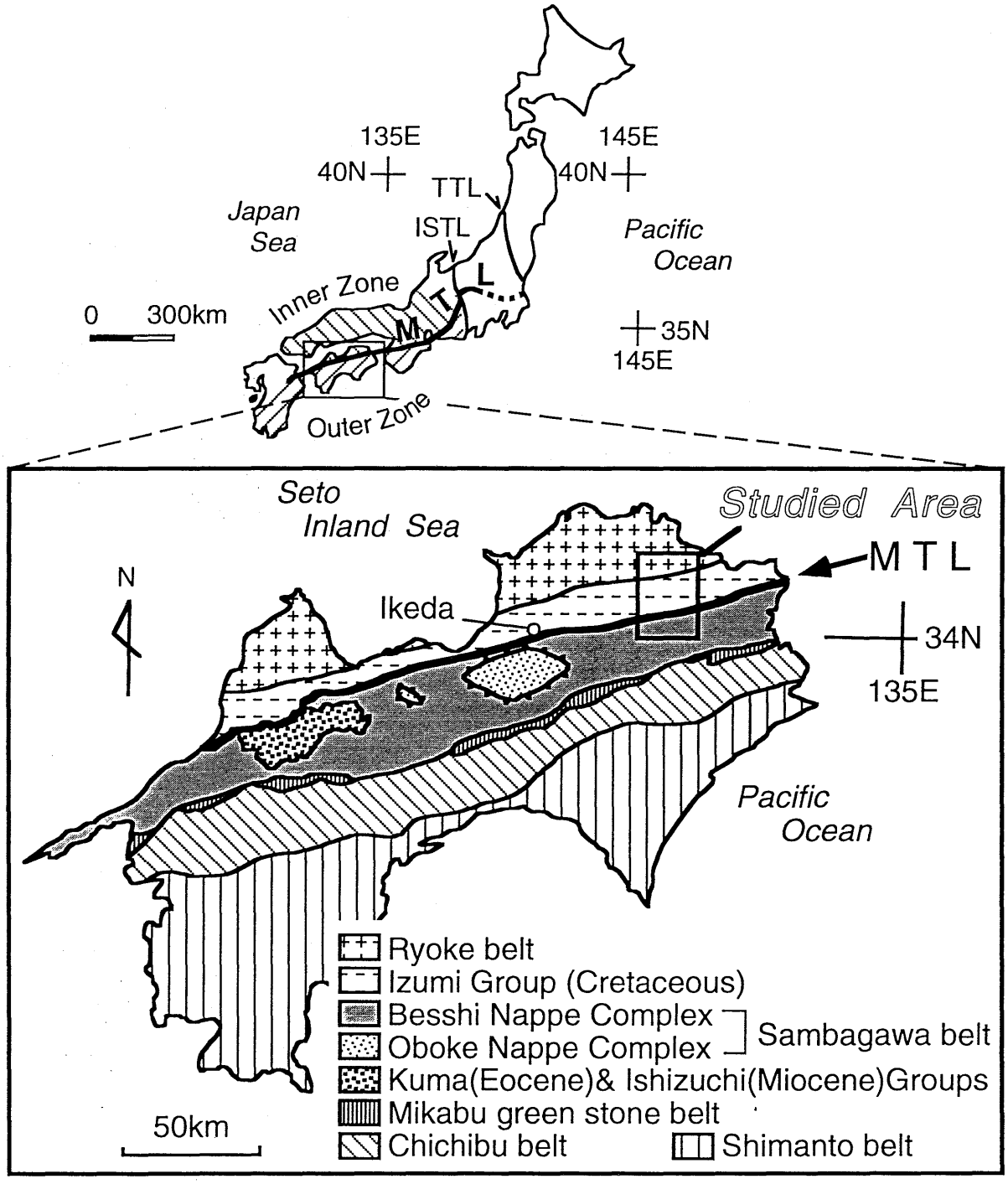

Fig.1 (T. Goto et al.)

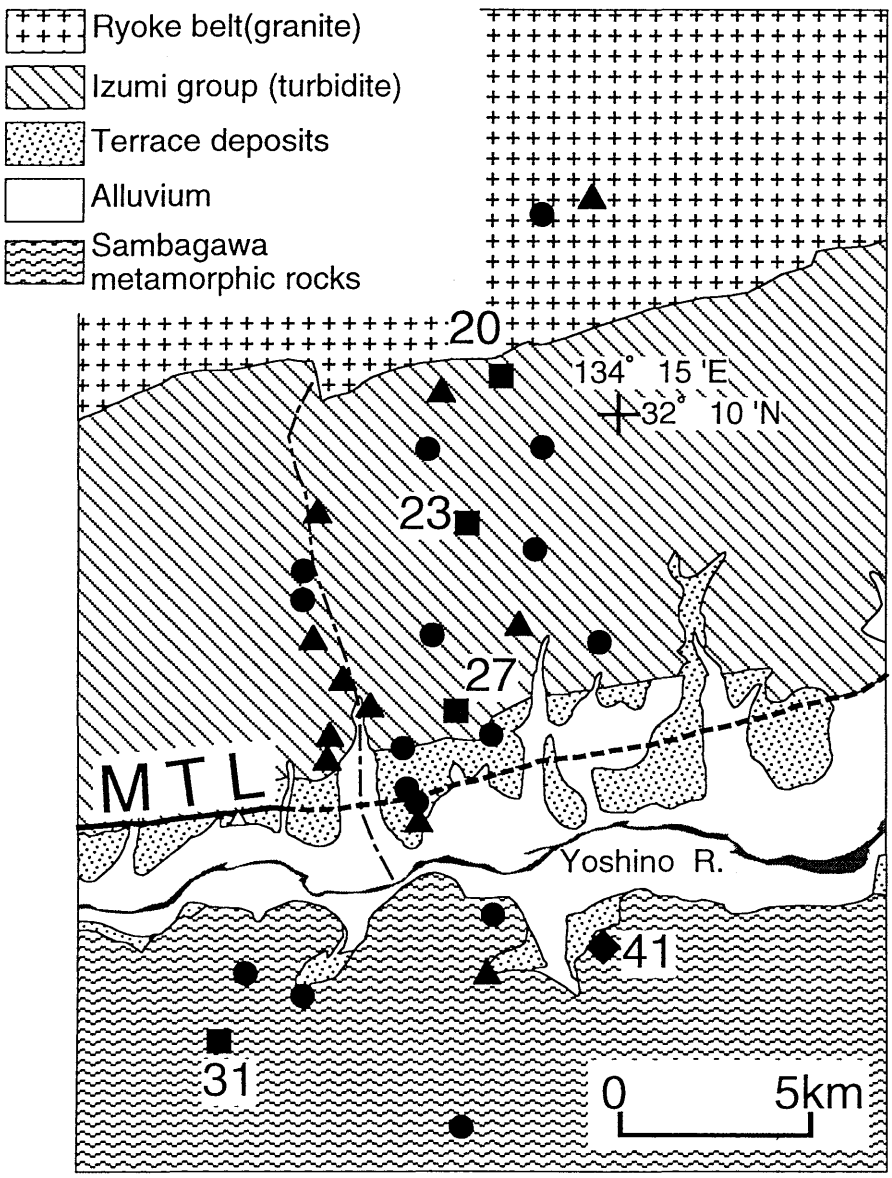

Fig.2 (T. Goto et al.)

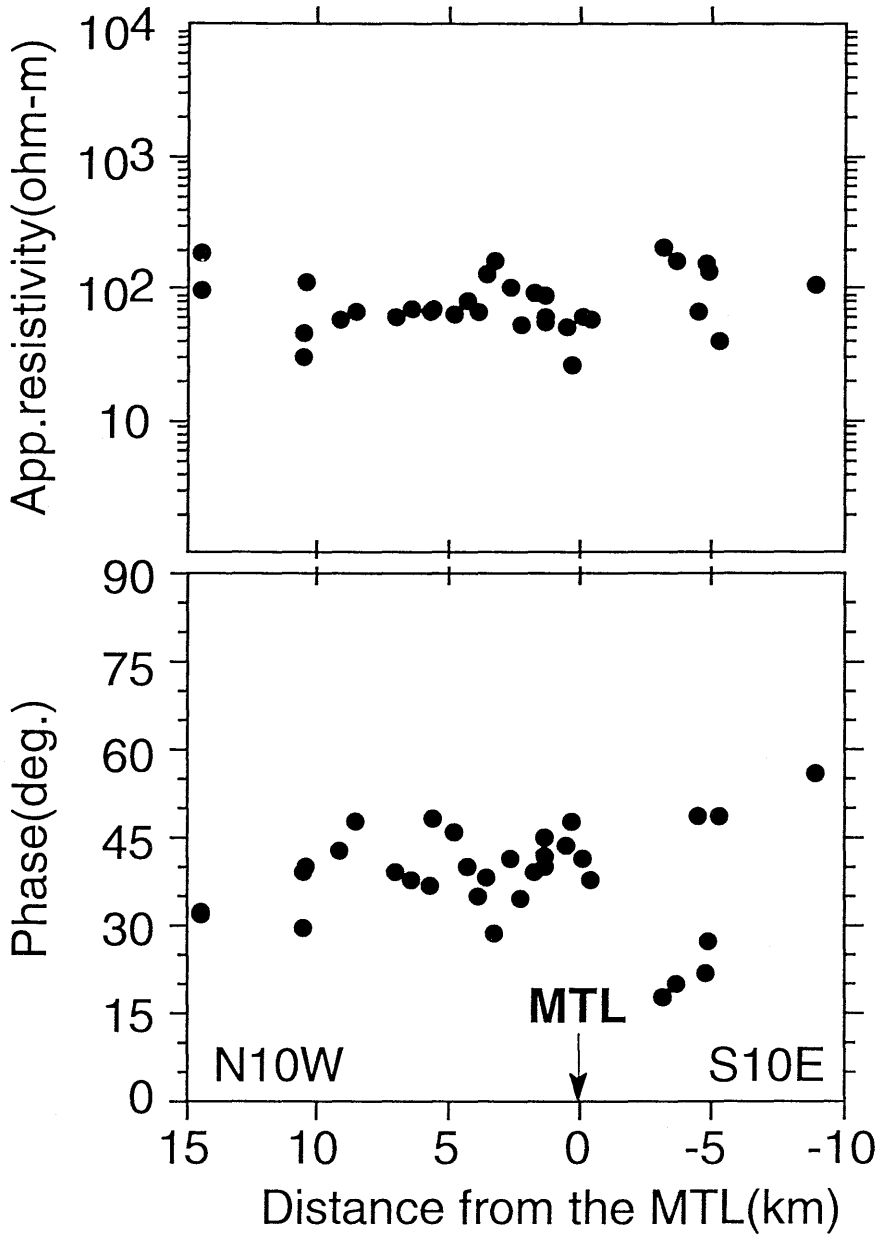

Fig.3 (T. Goto et al.)

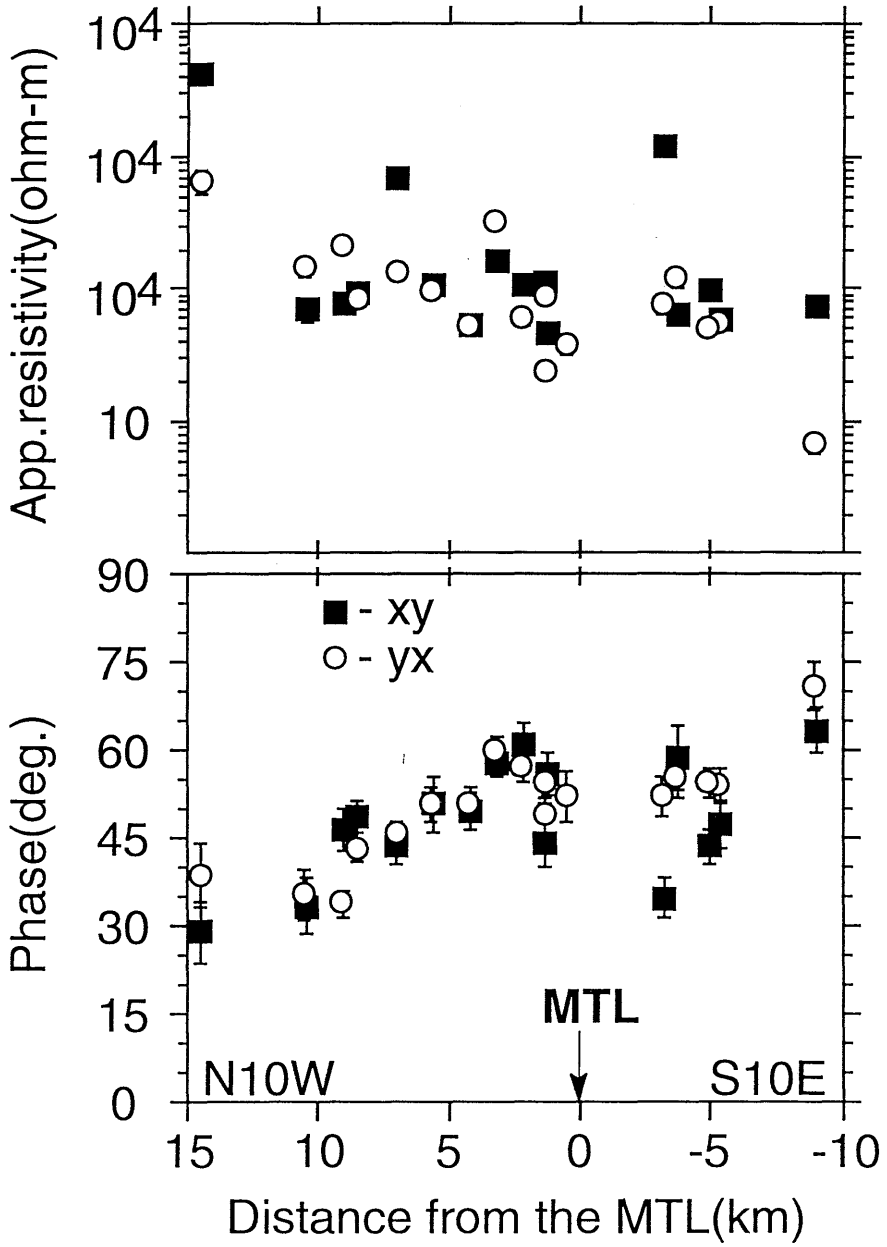

Fig.4 (T. Goto et al.)

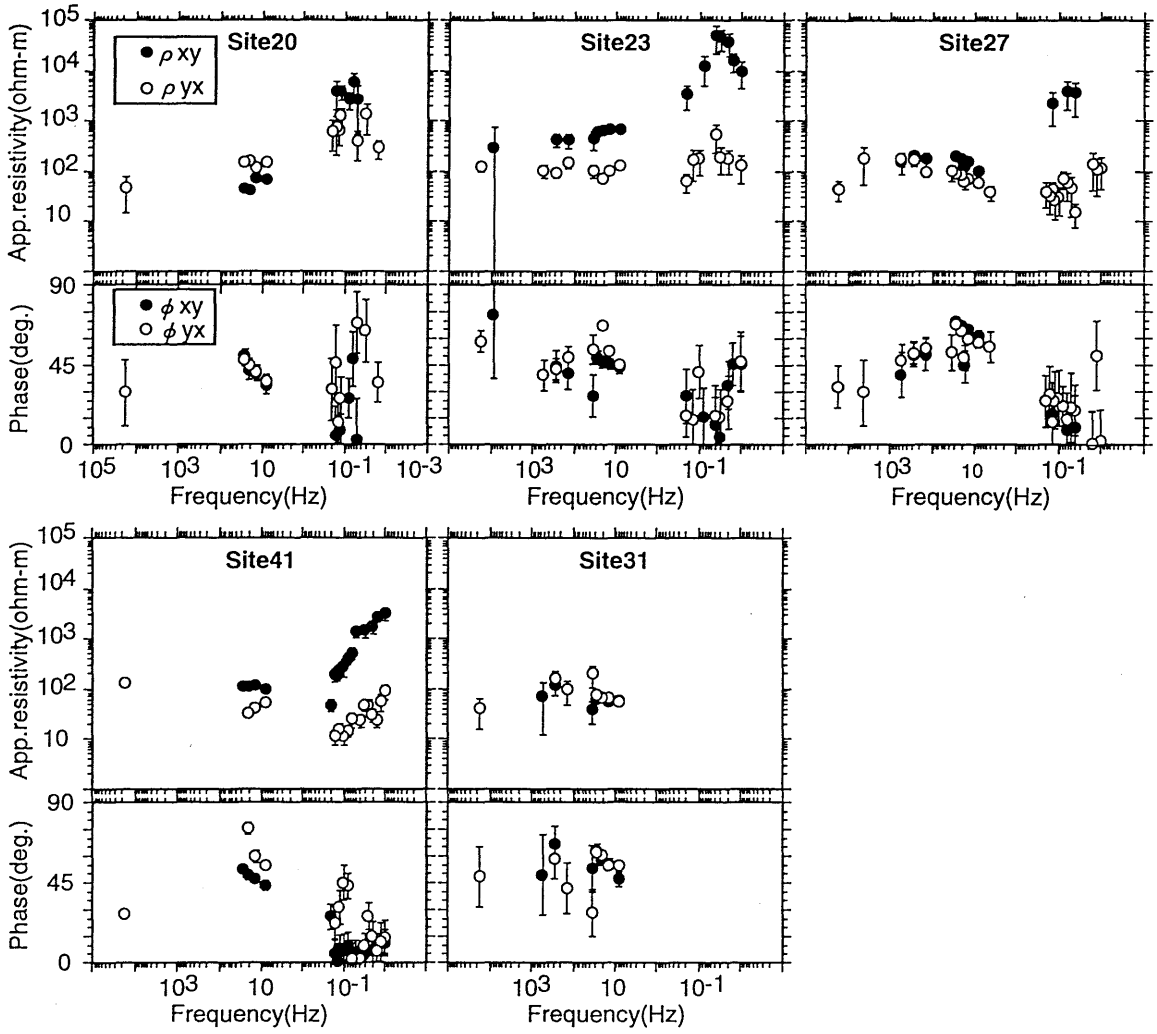

Fig.5 (T. Goto et al.)

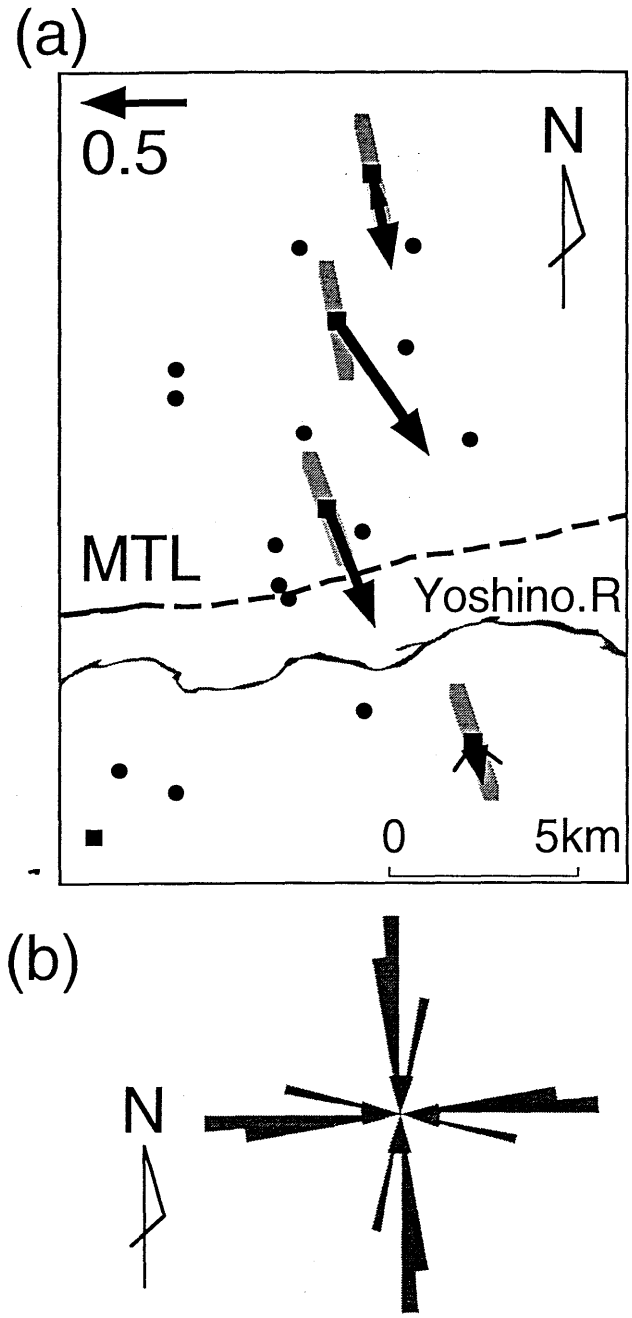

Fig.6 (T. Goto et al.)

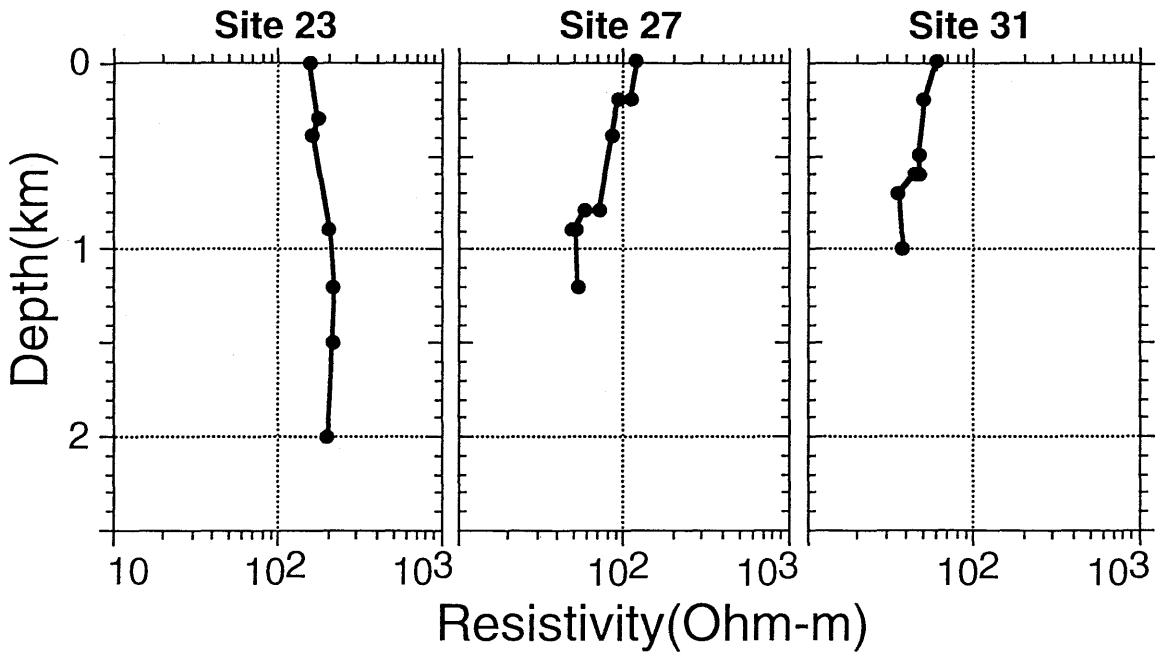

Fig.7 (T. Goto et al.)

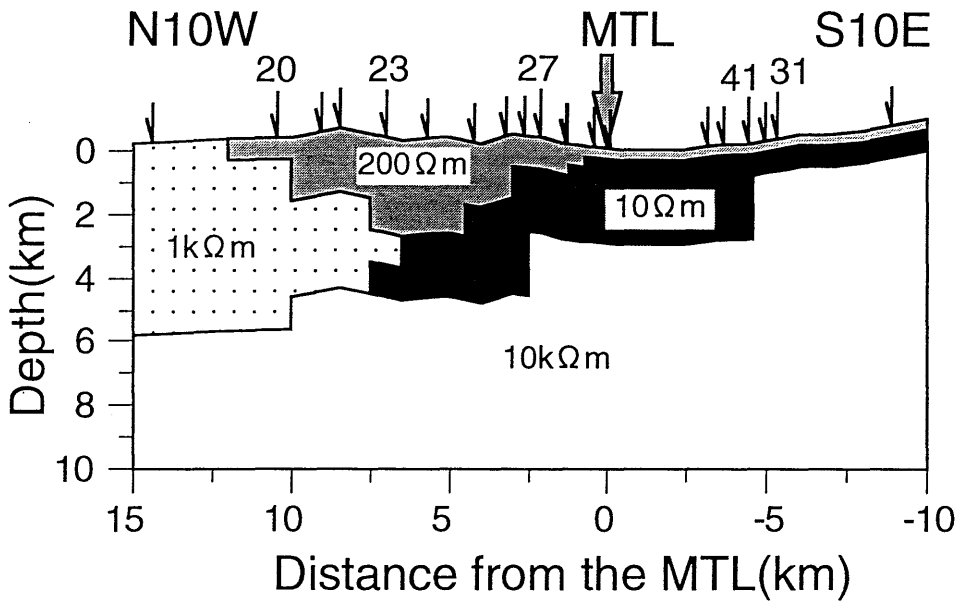

Fig.8 (T. Goto et al.)

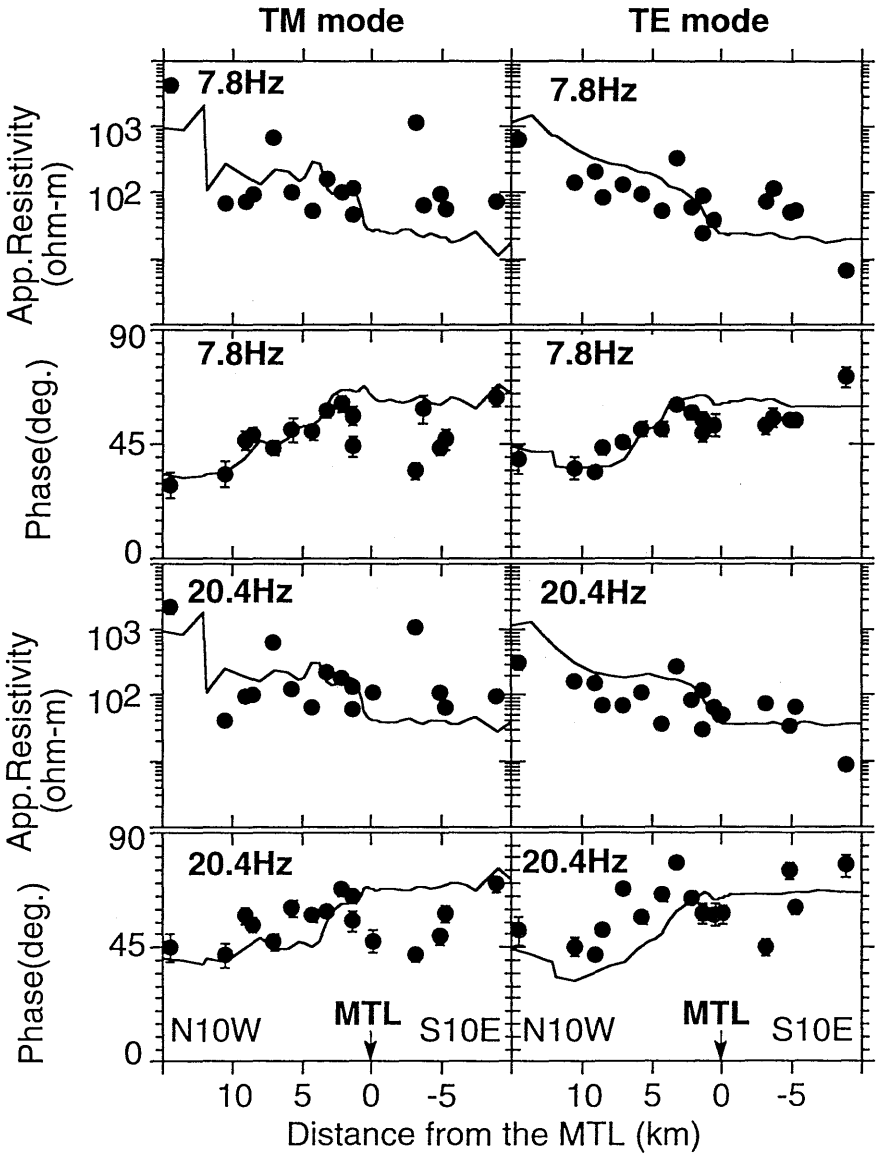

Fig.9 (T. Goto et al.)

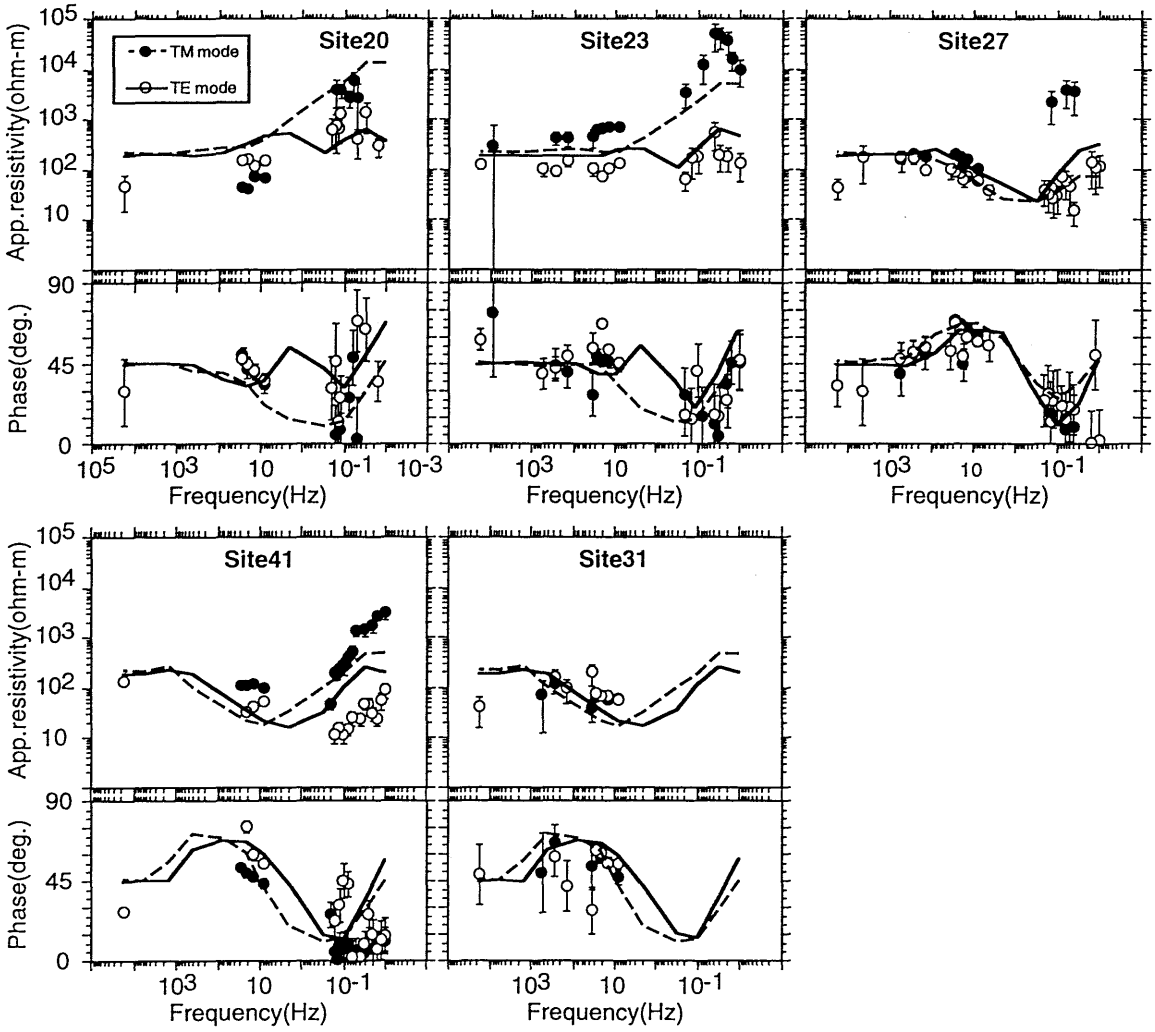

Fig.10 (T. Goto et al.)

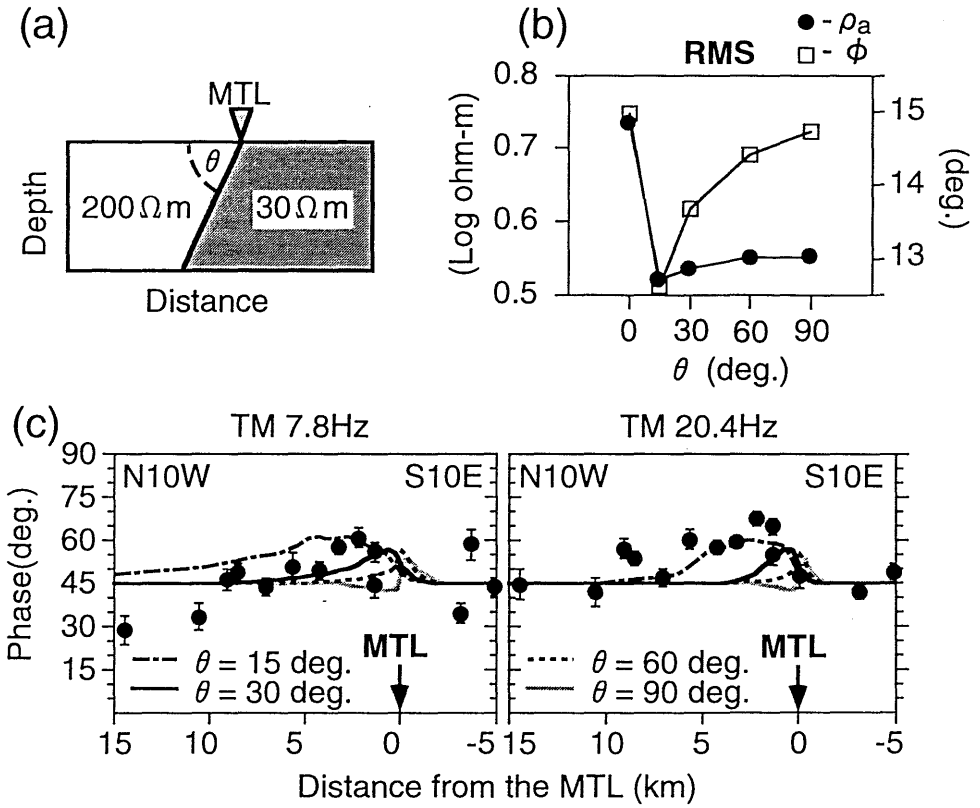

Fig.1 1 (T. Goto et al.)

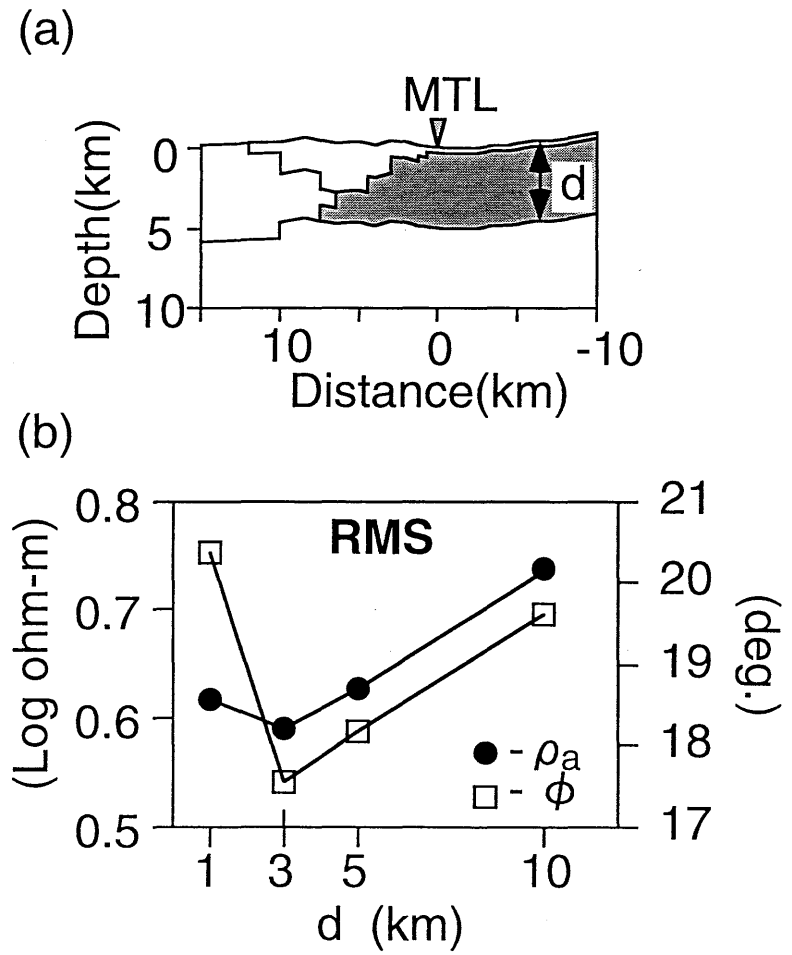

Fig.1 2 (T. Goto et al.)

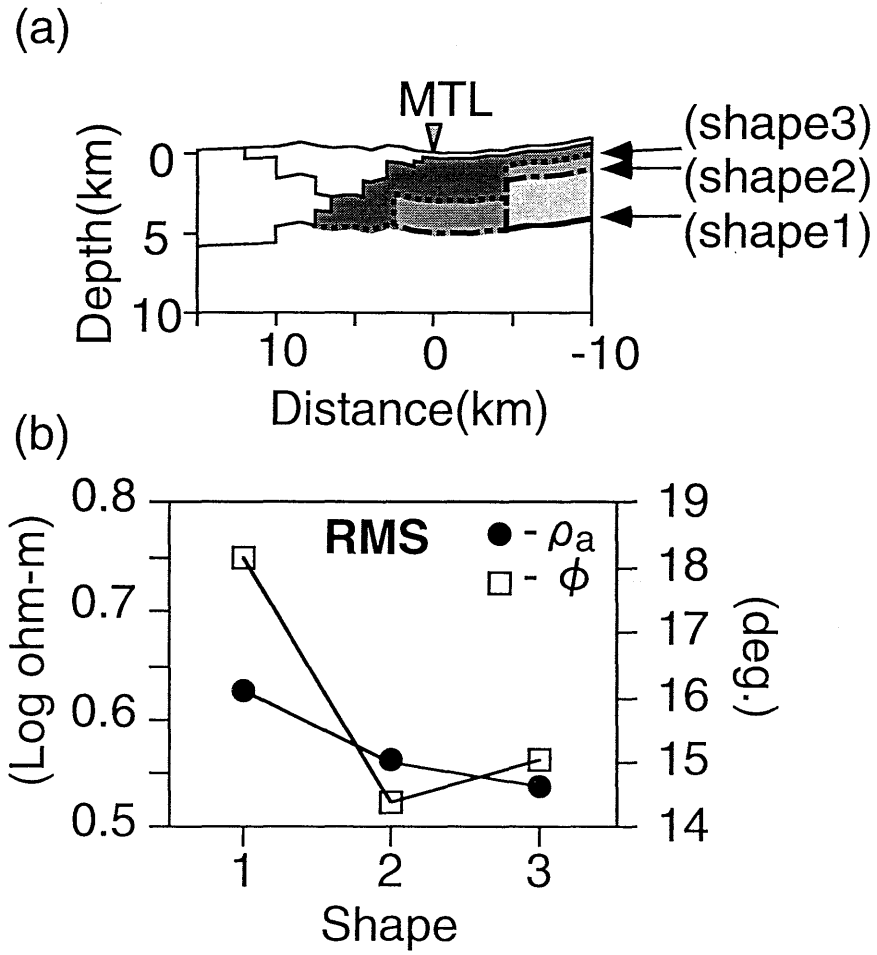

Fig.1 3 (T. Goto et al.)